UNIVERSITE DE LIEGE

FACULTE DE MEDECINE VETERINAIRE

DEPARTEMENT DES SCIENCES CLINIQUES DES ANIMAUX DE COMPAGNIE

SERVICE DE MEDECINE INTERNE DES ANIMAUX DE COMPAGNIE

Investigation par séquençage ARN à cellule unique des altérations cellulaires dans la fibrose pulmonaire idiopathique et le carcinome pulmonaire du chien et identification de nouveaux marqueurs cellulaires et outils de diagnostic

Single-cell RNA sequencing investigation of cellular alterations in canine idiopathic pulmonary fibrosis and pulmonary carcinoma and identification of novel cellular markers and diagnostic tools

Elodie RIZZOLI

THESE PRESENTEE EN VUE DE L'OBTENTION DU GRADE DE DOCTORAT EN SCIENCES VETERINAIRES

ANNEE ACADEMIQUE 2024-2025

Acknowledgments

First and foremost, I would like to express my deepest gratitude to Professor Cécile Clercx, my main supervisor, for her exceptional support throughout this journey. Cécile, your limitless motivation, endless stream of ideas, and unwavering optimism have consistently driven this project forward. Your encouragement extended far beyond the confines of this thesis, as you have supported even my future aspirations with the same enthusiasm and belief. Your deep understanding, compassion, and kindness carried me through both the highlights and challenges of this PhD. I am profoundly grateful for your guidance, trust, and continued presence at every key moment of this journey.

To Professor Thomas Marichal, my co-supervisor, thank you for your invaluable source of scientific insight and support. Your thoughtful advice, sharp scientific perspective, and continuous encouragement were instrumental in shaping this work. Your trust made me feel supported and inspired, even in moments of doubt. I am sincerely thankful for your mentorship and kindness throughout these years.

To Professor Elodie Roels, thank you for joining the team, first as a member of my thesis committee and eventually as a supervisor. Your earlier research laid the foundation for this project, particularly through your dedication to patient recruitment and long-term sample collection, and your advice and perspective significantly enriched this work.

To Professor Ellen Puré, member of my thesis committee, thank you for your valuable scientific input and for warmly welcoming me during my stay at UPenn.

To the members of the thesis jury, Professors Gianluca Matteoli (KU Leuven), Antoine Froidure (UCLouvain), Bénédicte Machiels, Didier Cataldo, Roland Hustinx, and Guy Jerusalem (ULiège), thank you for accepting to evaluate my work and for your thoughtful suggestions, which contributed to improving the manuscript. I am also grateful to the president of the jury, Professor Charlotte Sandersen, for her kind and supportive role in the process.

My warmest thanks to the Fund for Scientific Research – FNRS for granting me the funding that enabled this project.

I also wish to warmly thank all those who contributed, directly or indirectly, to the completion of this work:

To the "Westie team": Géraldine, thank you for your immense involvement in the project, through countless acquisitions and interpretations of CT scans, as well as your help with PET scan interpretation. Your support, availability, and enthusiasm for our projects were invaluable. Alexandru, thank you for your unwavering motivation, serenity, and availability during all anesthetic procedures. Thanks to your expertise and calm, every patient made it through safely, and your commitment to our projects never wavered. Anne-Christine and Margaux, thank you for carrying out numerous echocardiographic examinations on Westies, even when images were challenging to acquire or read, but you always came through. Aline, thank you for your prior research work and sample collection that made this project possible and for your advice. Arnaud, my PhD teammate from year two, thank you for your constant support and readiness to help during these last three years. Beyond research, you greatly contributed to the establishment of my houseplant collection – though now that I'm moving, I'm unsure whether to thank or blame you! Gaëlle, my PhD teammate from this year, your presence during the most difficult year was invaluable, especially in helping with Westie recruitment and follow-ups. Thank you for also becoming my walking Ettinger.

I would like to thank the pathology department of the Faculty of Veterinary Medicine, particularly Professor Mutien-Marie Garigliany for providing numerous histopathological diagnoses on my request and for spending time reviewing slides with me. Your expertise, enthusiasm for collaborative projects, and availability were truly appreciated. Constance, thank you for your help with QuPath. Mazarine, thank you for your assistance with immunohistochemistry. Michaël, thank you for your technical skills, your responsiveness to my endless requests to prepare countless slides, and for your moral support as well.

To the Immunophysiology Laboratory at GIGA, thank you all for your warm welcome and invaluable advice during times of uncertainty. Pierre, thank you for the hours spent together optimizing ELISA protocols, always with a good spirit. Valentine, your unwavering support and your presence made lab hours far more pleasant, and your bench and pipettes might just have brought luck to this project.

To the GIGA Genomics platform – Latifa, Manon, and Emilie – thank you for always managing to process my samples for scRNA-seq with incredibly short notice, occasionally during holidays or even weekends.

To the GIGA Bioinformatics platform – David and Arnaud – thank you for your assistance in R scripting and for your guidance in analyzing the scRNA-seq data.

To Professor Nadia Withofs, thank you for your kindness, encouragement, and unwavering support, as well as for your warm welcome at ICAB. I also extend my thanks to the rest of the Nuclear Medicine and Oncological Imaging division team for their kindness and support during my short internship.

To the team of the GIGA Cyclotron Research Centre – Thibault, Mohamed, Sylvestre, and Christian – thank you for your enthusiastic collaboration and your availability, including many long hours spent imaging dogs on weekends. Your commitment and expertise contributed greatly to this project.

To the members of Ellen Puré's laboratory at the University of Pennsylvania – especially Yue, Leslie, and Pranidhi – thank you for your kind welcome and help with immunohistochemistry during and after my time in Philadelphia.

To Dr. Laurence Fievez, thank you for your help with scRNA-seq experiments and protocol optimization.

To Dr. Véra Pirlet, thank you for your guidance in radioprotection and your valuable advice on our nuclear medicine projects.

To the Internal Medicine service, all the assistants, residents, and senior clinicians of MIPA, including those in cardiology, oncology, and dermatology, thank you for your presence and for your generous advice throughout the years, but also for many shared restaurants and congresses. Charlotte, thank you for always welcoming me so kindly in oncology consultations. I'm also grateful to the consultation assistants, particularly Kim, for managing tons of samples with professionalism and patience.

To the Imaging Department, residents and assistants, thank you for your many CT scan interpretations (including unrequested incidental findings!) and your good spirit, it was always a pleasure to visit imaging. To Laurie and Noémie, thank you for your assistance with CT acquisitions.

I would like to thank the Surgical Oncology Unit, particularly Annick and Stéphanie, for performing lung lobectomies and sharing surgical specimens for this study.

To all other members of the Department of Companion Animal Clinical Science I have crossed paths with during these four years, especially fellow PhD students (I hope you'll keep our little monthly meetings alive!) and the administrative staff, thank you for making the experience more enjoyable and collaborative.

I extend my warmest gratitude to all the Westie owners who entrusted me with the care of their dogs for this study, and to their referring veterinarians. Your participation was essential not only to this thesis but also to future research into this disease. Special thanks to Nahya, Lula, James, Jock, Barry, Fizz, House Music, Shiva, Lola, Doly, Idriss, Jamie, Flopy, Charlie, Iola, Eyden, Gladys, Fanchon, Vanille, Mona, Lisa, Lilly, Scotty, and Ella.

To the many vet students who joined me in Westie consultations, sometimes during difficult moments, thank you for your help and presence.

Finally, I would like to thank those closest to me. Pierre-Emmanuel, you experienced every high and low of this thesis as if it were your own. Thank you for your love and patience. To my parents and to my sister Céline, thank you for always supporting me. Special thanks to Félicien, who understood better than anyone what I was going through. Eléonore, thank you for your unwavering support at each step of the journey.

And a special thought goes to Fergie, my own Westie, who was the very reason this journey began. Thankfully, at 15 years old today, she never had to contribute any data to this study.

Abbreviations

6MWD	6-min walked distance
6MWT	6-minute walk test
^{18}F	Fluorine-18
[^{18}F]FDG	[^{18}F]fluorodeoxyglucose
[^{18}F]FLT	[^{18}F]fluorothymidine
[^{18}F]FMISO	[^{18}F]fluoromisonidazole
[^{18}F]NaF	[^{18}F]sodium fluoride
^{68}Ga	Gallium-68
ACP5	acid phosphatase 5, tartrate resistant
AE	acute exacerbation
AM	alveolar macrophages
BALF	bronchoalveolar lavage fluid
BSA	bovine serum albumin
CAF	cancer-associated fibroblast
CAR	chimeric antigen receptor
CCBE1	collagen and calcium binding EGF domains 1
CCL2	C-C motif chemokine ligand 2
CCN3	cellular communication network factor 3
CCRL2	C-C chemokine receptor-like 2
cDC1	myeloid/conventional dendritic cell 1
cDC2	myeloid/conventional dendritic cell 2
cDNA	complementary DNA
CIPF	canine idiopathic pulmonary fibrosis
COL23A1	collagen type XXIII alpha 1 chain
CPFS7	cleavage and polyadenylation specific factor 7
CT	computed tomography
CTHRC1	collagen triple helix repeat containing 1
CTSK	cathepsin K
Cu-ATSM	copper(ii) diacetyl-di(n^4-methylthiosemicarbazone)
CXCL8	C-X-C motif chemokine ligand 8

CXCL14	C-X-C motif chemokine ligand 14
DAD	diffuse alveolar damage
DC	dendritic cells
DDIT3	DNA damage inducible transcript 3
DEGs	differentially expressed genes
DPBS	Dulbecco's phosphate-buffered saline
EGFR	epidermal growth factor receptor
ELISA	enzyme-linked immunosorbent assay
EMT	epithelial to mesenchymal transition
EPT	endpoint titer
ET1	endothelin-1
FAP	fibroblast activation protein
FAPI	fibroblast activation protein inhibitor
FN1	fibronectin 1
FNA	fine needle aspiration
GGO	ground glass opacities
GO	gene ontology
HLCA	human lung cell atlas
HE	hematoxylin and eosin
HMCN1	hemicentin-1
HU	Hounsfield unit
HYAL1	hyaluronidase 1
Iba1	ionized calcium-binding adapter molecule 1
IFN	interferon
IgA	immunoglobulin a
IgKC	immunoglobulin kappa
IHC	immunohistochemistry
ILD	interstitial lung disease
IM	interstitial macrophages
IPF	idiopathic pulmonary fibrosis
KL-6	Krebs von den Lungen-6
LTBP	latent TGF-β1 binding protein

MATN4	matrillin 4
MED13L	mediator complex subunit 13L
MMP	matrix metalloproteinase
MST	median survival time
NK	natural killer
NSCLC	non-small cell lung cancer
NTRK2	neurotrophic receptor tyrosine kinase 2
PIIINP	procollagen type iii amino terminal propeptide
P(A-a)O_2	alveolar-arterial oxygen gradient
PAC	pulmonary adenocarcinoma
PaO2	arterial partial pressure in oxygen
PBS	phosphate-buffered saline
PCR	polymerase chain reaction
PD-1	programmed cell death protein 1
PD-L1	programmed death-ligand 1
PET	positron emission tomography
PET/CT	positron emission tomography combined with computed tomography
PH	pulmonary hypertension
P-Smad2/3	phosphorylated smad2/3
RBC	rank-biserial correlation
ROI	region of interest
RT-PCR	reverse transcriptase polymerase chain reaction
SAA1	serum amyloid a 1
SBRT	stereotactic body radiation therapy
scRNA-seq	single-cell RNA sequencing
SDHAF2	succinate dehydrogenase complex assembly factor 2
SP-A	surfactant protein a
SPP1	secreted phosphoprotein 1 / osteopontin
STRA6	signaling receptor and transporter of retinol
SUV	standardized uptake value
SUVmax	maximal standardized uptake value
SUVmean	mean standardized uptake value

TAM	tumor-associated macrophage
TAV	total active volume
TBA	total bile acid
TGF	transforming growth factor
TGFβR1	type I TGF-β receptors
THBS1	thrombospondin-1
TLV	total lung volume
TBR	target-to-background ratio
TTF-1	thyroid transcription factor-1
UIP	usual interstitial pneumonia
UMAP	uniform manifold approximation and projection
UMI	unique molecular identifier
WHWT	West Highland white terrier

Résumé - Abstract

Résumé

La fibrose pulmonaire idiopathique canine (CIPF) est une maladie pulmonaire interstitielle progressive caractérisée par une accumulation anormale de collagène dans l'interstitium pulmonaire, conduisant à une insuffisance respiratoire. Cette maladie de cause inconnue touche principalement les chiens âgés de race West Highland white terrier (WHWT). Elle ressemble à la fibrose pulmonaire idiopathique (IPF) humaine, une condition associée à un r9023490isque accru de cancer pulmonaire, ce qui aggrave le pronostic. Chez les chiens, le cancer pulmonaire primaire, comme l'adénocarcinome pulmonaire (PAC), présente également un mauvais pronostic aux stades avancés et semble plus fréquent chez les WHWTs atteints de CIPF, compliquant davantage le traitement. Malgré les progrès dans la caractérisation moléculaire de la CIPF, de nombreux aspects de sa pathobiologie restent inconnus. À ce jour, la CIPF est incurable et sa progression difficilement prévisible. Cela souligne un besoin en nouvelles cibles thérapeutiques, ainsi qu'en marqueurs diagnostiques et pronostiques fiables. De même, une meilleure compréhension de la pathobiologie du cancer pulmonaire canin est essentielle pour développer de nouvelles options thérapeutiques.

Cette thèse visait à explorer les altérations moléculaires et cellulaires dans la CIPF et le PAC canin afin d'identifier de nouveaux biomarqueurs et des cibles thérapeutiques potentielles. La première étape a consisté à générer un atlas de séquençage ARN à cellule unique (scRNA-seq) à partir de biopsies pulmonaires saines de chiens. Cette carte moléculaire comprenait plus de 26 000 cellules et a révélé 46 sous-populations distinctes, réparties entre les compartiments immunitaire, mésenchymateux, épithélial et endothélial. Des cellules rares et spécialisées, telles que des lymphocytes T non conventionnels et des cellules de Schwann, ont été identifiées, et les populations de fibroblastes ont montré une hétérogénéité marquée avec des indications d'un potentiel rôle immuno-régulateur. L'intégration avec des données humaines a montré de fortes similarités, confirmant le chien comme modèle pertinent en recherche respiratoire.

Les altérations moléculaires dans le PAC ont ensuite été explorées par scRNA-seq sur des biopsies de trois tumeurs primaires. Comparés à l'atlas sain, les fibroblastes associés aux cancers présentaient une forte surexpression de gènes impliqués dans la transition épithélio-mésenchymateuse et l'angiogenèse, comme fibroblast activation protein (*FAP*) et collagen triple helix repeat containing 1 (*CTHRC1*). Les macrophages associés aux tumeurs exprimaient des marqueurs possiblement liés à l'évasion immunitaire, comme l'ostéopontine (*SPP1*). D'autres altérations d'expression génique ont été observées dans les cellules épithéliales, endothéliales, lymphoïdes et musculaires. Enfin, la présence de fibroblastes CTHRC1+ et de macrophages SPP1+ dans les tumeurs a été confirmée spatialement par microscopie en immunofluorescence. Cette

étude souligne l'hétérogénéité cellulaire et moléculaire du PAC et suggère de nouvelles pistes de biomarqueurs et de cibles thérapeutiques.

Une analyse scRNA-seq préliminaire a été menée sur des tissus pulmonaires atteints de CIPF. Bien que reposant sur un nombre limité d'échantillons, elle a fourni des résultats notables, notamment la surexpression de FAP dans les fibroblastes et de SPP1 dans les macrophages. Cette étude constitue une première caractérisation à l'échelle cellulaire du tissu pulmonaire atteint de CIPF, mettant en évidence des cibles moléculaires potentielles. L'inclusion d'échantillons additionnels sera essentielle pour confirmer ces résultats et identifier d'autres altérations liées à la maladie.

Une étude de l'expression de FAP par immunohistochimie montré que FAP était absente dans les tissus sains mais fortement exprimée par les fibroblastes associés aux cancers dans les biopsies de PAC, et par les fibroblastes dans les zones de fibrose active dans les biopsies pulmonaires de CIPF. L'expression de FAP était fortement corrélée à l'activité de la fibrose et, dans une moindre mesure, à sa sévérité. Ces résultats établissent FAP comme un marqueur robuste de l'activité fibrotique dans les poumons atteints de CIPF. Bien que les concentrations plasmatiques de FAP aient été significativement plus faibles chez les chiens atteints, la pertinence clinique de cette observation reste incertaine. L'étude a donc révélé le potentiel de FAP comme marqueur diagnostique et cible thérapeutique dans la CIPF et le PAC.

Enfin, afin de développer une méthode non invasive de détection de l'expression de FAP in vivo, une étude pilote a évalué la faisabilité et la sécurité de l'imagerie par tomographie par émission de positons au [^{18}F]FAPI-74 combinée à la tomodensitométrie ([^{18}F]FAPI-74 PET/CT) chez des chiens sains et chez des WHWT atteints de CIPF. La procédure d'imagerie a été bien tolérée et a révélé une captation accrue du traceur dans les poumons atteints de CIPF par rapport aux témoins sains. Une élimination hépatobiliaire et urinaire a été observée, avec une captation modérée dans le tractus gastro-intestinal. Ces résultats suggèrent que l'imagerie PET/CT au [^{18}F]FAPI-74 est une méthode prometteuse et non invasive pour détecter et monitorer l'activité de la fibrose dans la CIPF.

Cette thèse approfondit notre compréhension du poumon du chien en combinant transcriptomique unicellulaire et imagerie moléculaire. Elle fournit le premier atlas à échelle cellulaire du poumon sain de chien, établissant une référence pour les recherches futures. Dans les contextes pathologiques, elle met en évidence des altérations moléculaires clés dans le PAC et la CIPF. FAP émerge comme un marqueur prometteur de processus fibrotiques et néoplasiques, avec des applications thérapeutiques et diagnostiques potentielles, telle que l'imagerie PET/CT au [^{18}F]FAPI-74.

Summary

Canine idiopathic pulmonary fibrosis (CIPF) is a progressive interstitial lung disease characterized by abnormal collagen accumulation in the lung interstitium, leading to respiratory failure. The disease primarily affects aging West Highland white terriers and is of unknown origin. It shares similarities with human idiopathic pulmonary fibrosis (IPF), a condition often associated with an increased risk of developing lung cancer, which worsens prognosis. In dogs, primary lung cancer such as pulmonary adenocarcinoma (PAC) similarly carries a poor prognosis at advanced stages and may be more prevalent in WHWTs with CIPF, further complicating treatment strategies. Despite advances in molecular characterization of CIPF, much remains unknown regarding its pathobiology. At present, CIPF is incurable, and predicting its progression is challenging. This highlights an urgent need for novel therapeutic targets and reliable diagnostic or prognostic markers. Similarly, deeper insights into the pathobiology of canine lung cancer are essential to guide the development of new treatment options.

This thesis aimed to explore the molecular and cellular alterations CIPF and canine PAC with the aim of identifying new biomarkers and potential therapeutic targets. The first step involved the generation of a single-cell RNA sequencing (scRNA-seq) atlas from healthy canine lung biopsies. This comprehensive molecular map included over 26,000 cells and uncovered 46 transcriptionally distinct subpopulations across immune, mesenchymal, epithelial, and endothelial compartments. Rare and specialized cells, such as unconventional T cells and Schwann cells, were identified, and fibroblast populations showed significant heterogeneity with indications of immune-regulatory potential. Cross-species integration with human lung data revealed strong transcriptional parallels, validating the dog as a relevant translational model for respiratory disease research.

Building on this foundation, molecular alterations in PAC were investigated using scRNA-seq on biopsies from three primary tumors. Compared with the healthy atlas, cancer-associated fibroblasts in PAC displayed strong upregulation of genes involved in epithelial-to-mesenchymal transition and angiogenesis, such as fibroblast activation protein (*FAP)* and collagen triple helix repeat containing 1 (*CTHRC1)*. Tumor-associated macrophages expressed markers possibly linked to immune evasion, such as osteopontin *(SPP1)*. Additional gene expression changes were observed across epithelial, endothelial, lymphoid, and muscle cells. Finally, the presence of $CTHRC1^{+}$ fibroblasts and $SPP1^{+}$ macrophages within tumors was demonstrated spatially using immunofluorescence microscopy. This study emphasizes the cellular and molecular heterogeneity of PAC and suggests new avenues for biomarkers and therapeutic targets.

In parallel, a preliminary single-cell transcriptomic analysis was conducted on CIPF-affected lung tissue. This study, though based on a small number of samples, offered notable findings including the overexpression of *FAP* in fibroblasts and *SPP1* in macrophages. This preliminary study provides an early single-cell characterization of CIPF lung tissue, revealing potential molecular targets. Expanding the sample size in future research will be crucial to confirm these findings and identify additional disease-related changes.

FAP expression was investigated in CIPF-affected lung and in PAC biopsies. This study demonstrated that FAP expression was absent in healthy lung tissue but strongly expressed by cancer-associated fibroblasts in PAC and by fibroblasts in areas of active fibrosis in CIPF. Importantly, FAP expression correlated strongly with fibrosis activity and, to a lesser extent, with severity. These findings, validated through both visual scoring and digital image analysis, established FAP as a robust marker of fibrotic activity in CIPF lungs. Although plasmatic FAP concentrations were found to be significantly lower in affected dogs, the clinical relevance of this finding remains uncertain. Nonetheless, the study emphasized the potential of FAP for diagnostic and therapeutic strategies in dogs affected by CIPF and/or PAC.

Finally, we aim to develop a noninvasive method of detecting FAP expression in vivo. A pilot study assessed the feasibility and safety of [^{18}F]FAPI-74 positron emission tomography combined with computed tomography (PET/CT) imaging in both healthy dogs and WHWTs diagnosed with CIPF. The imaging procedure was well tolerated and revealed significantly increased tracer uptake in CIPF-affected lungs compared with healthy controls. Biodistribution data indicated hepatobiliary and urinary clearance, with moderate gastrointestinal uptake. These results suggest that [^{18}F]FAPI-74 PET/CT is a promising, noninvasive method to detect and monitor active fibrotic processes in CIPF.

This thesis deepens our understanding of canine lung biology by combining single-cell transcriptomics and molecular imaging to study both healthy and diseased states. It provides the first single-cell atlas of the healthy canine lung, establishing a critical reference for future investigations. In disease contexts, it reveals key molecular alterations in canine PAC and CIPF. FAP emerged as a promising marker of fibrotic and neoplastic processes, with potential diagnostic and therapeutic applications. The successful use of [^{18}F]FAPI-74 PET/CT imaging in dogs with CIPF demonstrates a feasible, noninvasive approach to monitor fibrotic activity in vivo.

General preamble

General preamble

This work focuses on two chronic lung diseases that spontaneously occur in old dogs. The first is canine idiopathic pulmonary fibrosis (CIPF), which affects predominantly West Highland white terriers (WHWTs), and consists of a progressive accumulation of collagen by activated fibroblasts, leading to respiratory insufficiency. Fibrosis is a pathological process closely interconnected with carcinogenesis. In humans, idiopathic pulmonary fibrosis (IPF), a comparable disease, is associated with an increased risk of lung cancer. Canine lung cancer, which also carries a poor prognosis in its advanced stages and may present a higher risk in dogs with CIPF, will be the other focus of this work.

Previous studies have expanded our understanding of CIPF, including advances in the molecular characterization of the disease. However, its etiology and pathobiology remain incompletely understood. CIPF is incurable, and its progression is difficult to predict. Therefore, there is a need for new therapeutic targets, as well as diagnostic and prognostic markers. In canine lung cancer, a better understanding of pathobiology could support the development of novel therapies, particularly important for advanced-stage disease, where treatment options are limited.

In the introduction, we will review the current knowledge about CIPF and canine lung cancer. We will also introduce two major techniques that are used in this work, single-cell mRNA sequencing (scRNA-seq) and positron emission tomography (PET).

Introduction

1 Canine idiopathic pulmonary fibrosis

1.1 Generalities

Canine idiopathic pulmonary fibrosis (CIPF) was comprehensively described for the first time by Corcoran in 1999 (Corcoran et al., 1999a), as a disease characterized by chronic fibrosis of the lung interstitium of unknown cause, occurring predominantly in West Highland white terriers (WHWTs). In such disease, an aberrant deposition of collagen fibrils occurs in the interstitium, increasing the extracellular matrix and expanding the interstitium, separating the capillary endothelial cell from the alveolar epithelium (Norris et al., 2005).

The name canine idiopathic pulmonary fibrosis was first introduced in 2005 by Johnson et al. and has been adopted due to its similarities with a human disease, idiopathic pulmonary fibrosis (IPF) (Johnson et al., 2005; Heikkilä-Laurila and Rajamäki, 2014; Clercx et al., 2018; Laurila and Rajamäki, 2020a). Other terms have been used to refer to the same clinical entity : chronic pulmonary disease (Corcoran et al., 1999a, 2011; Schober and Baade, 2006), chronic idiopathic pulmonary fibrosis (Lobetti et al., 2001; Webb and Armstrong, 2002), idiopathic pulmonary fibrosis (Norris et al., 2002; Heikkilä et al., 2011) and interstitial lung disease (Norris et al., 2005).

In cats and dogs, interstitial lung diseases (ILDs) are classified as either idiopathic interstitial pneumonias, ILDs of known cause or miscellaneous ILDs (Reinero, 2019a, 2019b). Idiopathic interstitial pneumonias comprise sporadic fibrotic ILD, familial fibrotic ILD, acute interstitial pneumonia, non-specific interstitial pneumonia, lymphocytic interstitial pneumonia, cryptogenic organizing pneumonia and other idiopathic interstitial pneumonias (Reinero, 2019a). To date, CIPF is the best described ILD affecting dogs, and consists of a chronic, progressive, familial fibrotic ILD of unknown cause, occurring mainly in old WHWTs (Heikkilä et al., 2011; Clercx et al., 2018; Reinero, 2019a; Laurila and Rajamäki, 2020a).

The canine disease presents differences with the human clinical entity IPF, but also shares many similarities (Syrjä et al., 2013; Clercx et al., 2018). Furthermore, the spontaneous occurrence in dogs and the similar environmental conditions of humans and dogs make CIPF an appealing model of IPF (Clercx et al., 2018; Barnes et al., 2019).

The prevalence of CIPF is currently unknown. This is due to the difficulty in diagnosing CIPF accurately, the possibility of misdiagnosis, and the lack of inventory of the general population of WHWTs (Clercx et al., 2018; Laurila and Rajamäki, 2020a). In 2018, a questionnaire-based survey among 420 WHWT owners revealed that 138 (33%) had been affected with CIPF during the course of

their lives (Roels et al., 2018). A recent study in WHWTs under veterinary care in the United Kingdom reported that lower respiratory tract diseases had an overall prevalence of 2.2% and accounted for 10.2% of deaths, making them one of the leading causes of death in WHWTs (O'Neill et al., 2019).

1.2 Etiology and risk factors

The etiology of CIPF is currently unknown. Since WHWTs present a strong predisposition for CIPF, a genetic background is highly suspected (Clercx et al., 2018). Additionally, having a genetic relationship with another WHWT affected with CIPF appears to increase the risk of developing CIPF (Roels et al., 2018). A genome wide association study in WHWTs identified genetic variants associated with CIPF in regions coding for the cleavage and polyadenylation specific factor 7 (*CPFS7*) and the succinate dehydrogenase complex assembly factor 2 (*SDHAF2*) genes (Piras et al., 2020). However, the diagnosis was self-reported by dog owners and no other clinical information was available for this study, which raises concerns about the accuracy of the diagnoses (Piras et al., 2020).

However, not all senior WHWTs develop CIPF, which suggests that other factors contribute to the onset or the progression of the disease (Roels et al., 2018). Environmental risk factors were identified in a questionnaire-based survey, such as living in an old house, absence of a ventilation system and frequent grooming in dedicated facilities (Roels et al., 2018).

In recent studies, microaspirations secondary to gastroesophageal reflux were found to be associated with CIPF and could also constitute a factor predisposing WHWTs to the disease (Määttä et al., 2018; Kouki et al., 2023). In humans, microaspirations of gastric acid are believed to induce repetitive alveolar damages, and would cause an aberrant wound healing in susceptible patients, leading to lung fibrosis (Caminati et al., 2019; Alfaro and Robalo Cordeiro, 2020). In dogs with CIPF, salivary total bile acids (TBA) and bronchoalveolar lavage fluid (BALF) TBA are higher than in healthy dogs (Määttä et al., 2018; Kouki et al., 2023), indicating that WHWTs affected by CIPF may present a higher occurrence of microaspirations. However, BALF TBA was also higher in healthy WHWTs compared to healthy Beagle dogs (Määttä et al., 2018). Another study failed to provide clear evidence of occult gastrointestinal aspiration as no protein markers indicative of reflux aspiration (such as pepsin or trefoil factor 1) were identified by quantitative proteomic analysis of BALF (Maher et al., 2022).

Infectious etiologies have been widely studied and mostly ruled out. Lung parasites (such as *Angiostrongylus vasorum*) infections are frequently excluded during the diagnostic work up of CIPF (Heikkilä et al., 2011; Roels et al., 2017). As pan-fungal polymerase chain reaction (PCR) test equally

amplified fungal DNA in lung biopsies from WHWTs affected with CIPF and from control dogs, active fungal infection does not seem to be associated with CIPF (Roels et al., 2022). However, a serological assay revealed a significantly higher proportion of positive precipitin reactions in the serum from CIPF-affected dogs compared with controls, indicating an increased prevalence of environmental fungal exposure in dogs with CIPF (Roels et al., 2022). This may suggest a lung sensitization to inhaled fungal allergens, but should be explored by further investigation (Roels et al., 2022).

In humans, horses and rodents, some forms of pulmonary fibrosis were shown to be associated with gammaherpesvirus infections (Williams, 2014). Therefore, it was also investigated in CIPF, but the results suggested it was unlikely, since herpesvirus DNA polymerase could not be amplified by PCR from any lung neither blood samples from WHWTs affected with CIPF and from control dogs (Roels et al., 2016).

Bacterial infections are an unlikely cause of CIPF. In WHWTs with or without CIPF, the bacterial load in BALF was not different and the lung microbiota was quite similar (Fastrès et al., 2020c). However, differences in the lung microbiota were identified between WHWTs (with and without CIPF) and dogs from other domestic breeds. In the lung microbiota of WHWTs, 6 genera were more abundant, including Brochothrix, Curvibacter, Pseudarcicella, Flavobacteriaceae genus, Rhodoluna and Limnohabitans (Fastrès et al., 2020c). Most of these bacteria preferentially contaminate food or water, which can be ingested by dogs. The higher risk of microaspirations secondary to gastroesophageal reflux in WHWTs compared to other breeds is a possible explanation of these microbiota differences (Määttä et al., 2018; Fastrès et al., 2020c). The Flavobacteriaceae family and the Curvibacter genera have a potential pathogenic role and could potentially activate the immune system, alter the airway epithelium and induce or perpetuate airway inflammation (Fastrès et al., 2020c). The aforementioned differences might serve as predisposing factors to CIPF.

1.3 Pathogenesis

The pathogenesis of CIPF is not completely understood. The current hypothesis is that repetitive insults to the distal lung parenchyma lead to an aberrant wound healing process, causing excessive accumulation of extracellular matrix in the pulmonary interstitium (Lilja-Maula et al., 2015; Laurila and Rajamäki, 2020a). Figure 1 summarizes the current hypotheses regarding the etiology and pathogenesis of CIPF.

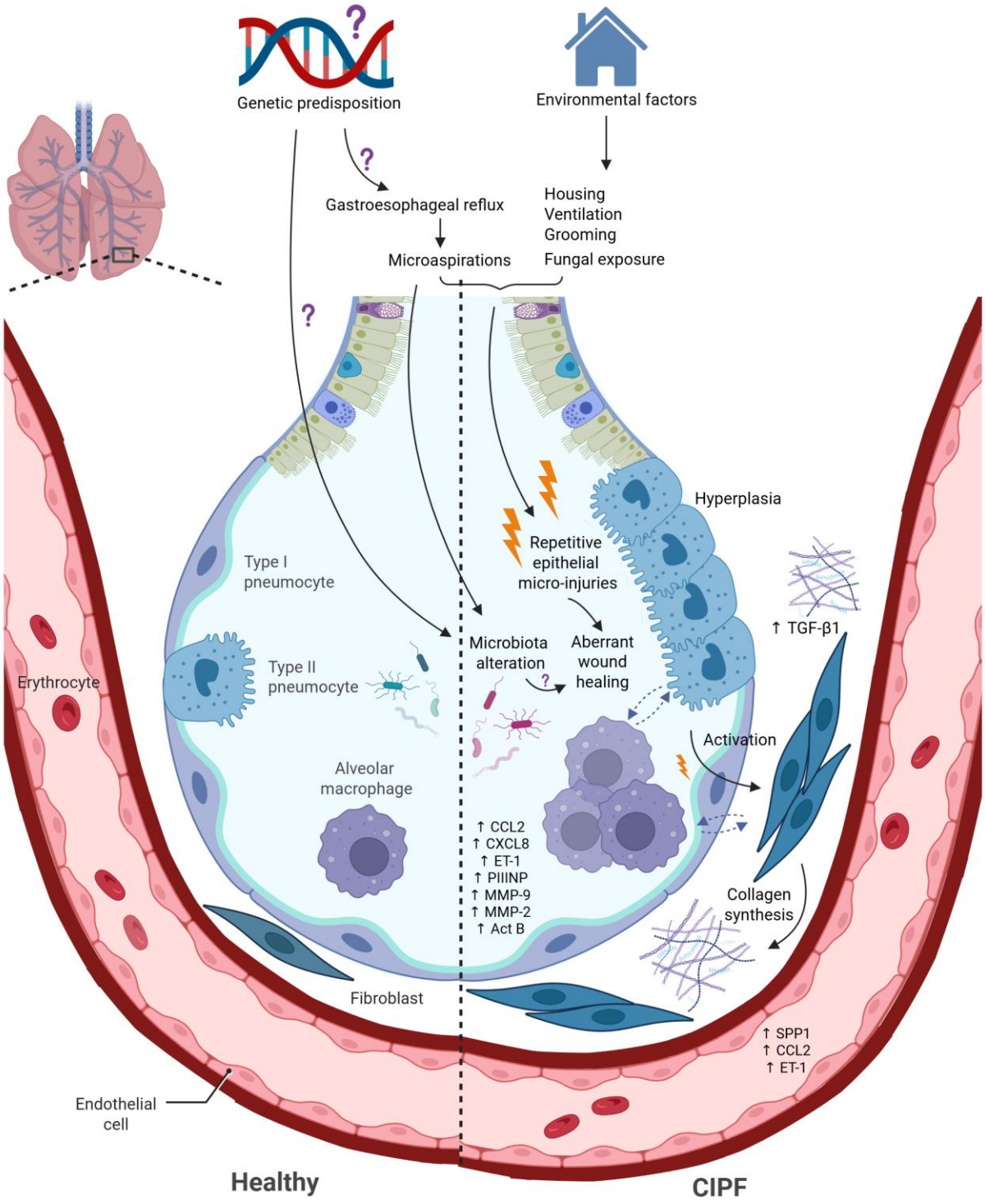

Figure 1 (created in https://BioRender.com)**.** Current hypotheses regarding canine idiopathic pulmonary fibrosis (CIPF) etiology and pathogenesis. CIPF is highly suspected to have a genetic background, although genetic factors have not been identified yet (Clercx et al., 2018; Roels et al., 2018). Dogs from the West Highland white terrier breed, the predisposed breed, have a higher rate of gastroesophageal reflux, potentially causing microaspirations (Määttä et al., 2018; Kouki et al., 2023), as well as differences in lung microbiota (Fastrès et al., 2020c) compared with dogs from other breeds, which may contribute to the

disease. Environmental factors have been identified as well, including living in older housing, lack of ventilation system, frequent grooming (Roels et al., 2018) and increased fungal exposure (Roels et al., 2022). Subsequent repetitive epithelial micro-injuries, with the possible contribution of a potentially pathogenic lung microbiota, lead to an aberrant wound healing process (Krafft et al., 2014; L. Lilja-Maula et al., 2014; Fastrès et al., 2020c). This abnormal healing response is mainly characterized by type II pneumocyte hyperplasia, alveolar macrophage expansion (Heikkilä et al., 2011; Syrjä et al., 2013), aberrant activation of transforming growth factor (TGF)-β1 (Krafft et al., 2014; L. Lilja-Maula et al., 2014), activation of fibroblasts and excessive extracellular matrix deposition in the lung interstitium (Norris et al., 2005; Syrjä et al., 2013). Some biomarkers are elevated in affected dogs and may contribute to the disease pathogenesis, including osteopontin (SPP1), C-C motif chemokine ligand 2 (CCL2) and endothelin-1 (ET-1) in the serum, and CCL2, chemokine (C-X-C motif) ligand 8 (CXCL8), ET-1, procollagen type III amino terminal propeptide (PIIINP), matrix metalloproteinase (MMP)-2 and MMP-9 and activin B (Act B) in the bronchoalveolar lavage fluid (Krafft et al., 2011, 2013a; Heikkilä et al., 2013; Elodie Roels et al., 2015b; Lilja-Maula et al., 2015; Määttä et al., 2021; Niinikoski et al., 2022; Fastrès et al., 2023).

Human IPF is now widely recognized as an epithelium-driven disease, where repetitive alveolar epithelial micro-injuries in susceptible individuals, namely aged individuals with genetic predispositions and environmental exposures, trigger an abnormal wound healing response. This dysfunctional repair process leads to the development and progression of lung fibrosis (Sgalla et al., 2018; Selman and Pardo, 2020).

In dogs, it is believed that repeated alveolar epithelial injuries lead to aberrant activation of transforming growth factor (TGF)-β (Lilja-Maula et al., 2015). The TGF-β1 signaling, regulatory and activation pathways have been studied and appear altered in CIPF. A difference in TGF-β1 mRNA was not identified by quantitative reverse transcriptase-PCR (RT-PCR) between CIPF and control lung biopsies, but a strong diffuse expression of the TGF-β1 protein was observed in the fibrous matrix in areas of pulmonary fibrosis in all dogs affected by CIPF (Krafft et al., 2014). Type I TGF-β receptors (TGFβR1) were not observed in the fibrotic tissue, but a high immunoreactivity was observed in alveolar epithelial cells, especially hyperplastic pneumocytes (Krafft et al., 2014). Increased TGF-β1 signaling activity was identified in the altered alveolar epithelium in CIPF through the observation of a high phosphorylated Smad2/3 (P-Smad2/3) immunoreactivity by immunohistochemistry (IHC), which was absent in healthy lungs (Krafft et al., 2014; L. Lilja-Maula et al., 2014). TGF-β1 storage and regulation appear altered in CIPF, as an increased expression of latent TGF-β1 binding protein (LTBP)-1 was observed by IHC in peribronchial, perivascular and altered alveolar epithelium areas (L. Lilja-Maula et al., 2014), and a decreased expression of LTBP-4 was quantified by RT-PCR (Krafft et al., 2014). Thrombospondin-1 (THBS1), a protein involved in TGF-β1 activation, had an significantly

increased gene expression in CIPF lung biopsies, compared with control lungs (Krafft et al., 2014). Finally, while serum TGF-β1 concentration was not different between WHWTs affected with CIPF and healthy WHWTs, it was higher in breeds predisposed to CIPF compared with non-predisposed ones, which might partly explain the breed susceptibility to CIPF (Krafft et al., 2014).

C-C motif chemokine ligand 2 (CCL2) and chemokine (C-X-C motif) ligand 8 (CXCL8) or interleukin-8, appear to be involved in the pathogenesis of CIPF. CCL2, a monocyte chemoattractant, is involved in human IPF and has a profibrotic effect by activating fibroblasts, upregulating TGF-β1 and stimulating collagen synthesis (Sgalla et al., 2018; Selman and Pardo, 2020; S. Liu et al., 2023). Research in humans has shown that CXCL8 could contribute to the development of pulmonary fibrosis by promoting the proliferation, differentiation and migration of mesenchymal progenitor cells, and by inducing the migration of macrophages to the fibroblastic foci (Yang et al., 2018; She et al., 2021). In dogs, a first study using RT-PCR identified an overexpression of CCL2 and CXCL8 mRNA in CIPF lung biopsies compared with control lung biopsies (Krafft et al., 2013a). A more recent study with better age-matched samples did not find any significant differences in mRNA expression of CCL2 and CXCL8 and their respective receptors CCR2 and CXCR2. However, CCL2 and CXCL8 immunohistochemical labelling was observed in bronchial epithelial cells and occasional hyperplastic alveolar epithelial cells in CIPF lung biopsies, while being absent in healthy lungs (Roels et al., 2015b). Additional CXCL8 immunoreactivity was observed in some alveolar macrophages in one out of four CIPF lung biopsies (Roels et al., 2015b).

The role of activins, proteins belonging to the TGF-β superfamily and carrying an important role in inflammation and fibrosis, was also investigated in the pathogenesis of CIPF (Lilja-Maula et al., 2015). During the course of the disease, an acute worsening of unknown cause, called acute exacerbation (AE), can occur and is often fatal (Lilja-Maula et al., 2015). Microscopically, it is characterized by diffuse alveolar damage (DAD). In WHWTs with CIPF and in dogs from other breeds with acute respiratory distress syndrome, activin B showed strong expression in the altered alveolar epithelium (Lilja-Maula et al., 2015). Activin B could be measured in the BALF of WHWTs with CIPF, particularly in dogs experiencing AE, but was absent in the BALF of healthy WHWTs. These findings indicate that activin B may play a role in the pathobiology of CIPF and could serve as a marker of alveolar epithelial damage (Lilja-Maula et al., 2015).

In dogs affected with CIPF, no altered systemic hemostatic, fibrinolytic or inflammatory state could be identified in comparison with control WHWTs (Roels et al., 2019). Platelet count and plasma fibrinogen concentration exceeded the upper reference limit in nearly half of the WHWTs studied,

regardless of disease status, suggesting they may act as predisposing factors or reflect normal biological variation in this breed (Roels et al., 2019).

Recent studies have focused on the role of alveolar macrophages in the pathogenesis of CIPF. Pro-fibrotic macrophages have been identified in the BALF of WHWTs with CIPF, by comparison with healthy WHWTs. Those macrophage express osteopontin 1 (SPP1), which is believed to be involved in the pathogenesis of CIPF (Fastrès et al., 2023).

1.4 Clinical presentation

CIPF predominantly affects WHWTs (Clercx et al., 2018; Laurila and Rajamäki, 2020a). Idiopathic pulmonary fibrosis has been sporadically described in dogs from other breeds such as Staffordshire bull terriers (Corcoran et al., 1999b; Lobetti et al., 2001; Norris et al., 2002), Cairn terriers (Corcoran et al., 1999a; Johnson et al., 2005), Bull terriers (Lobetti et al., 2001), Scottish terriers (Krafft et al., 2013a). However, it is unknown if the disease described in those other breeds is exactly the same as in WHWTs (Heikkilä et al., 2011; Clercx et al., 2018; Laurila and Rajamäki, 2020a).

CIPF mostly occurs in old adults ; with a median age at diagnosis of 9 to 13 years and a range of 5 to 15 years (Corcoran et al., 1999a; Heikkilä et al., 2011; Corcoran et al., 2011; Thierry et al., 2017; Roels et al., 2017, 2019; Holopainen et al., 2019). However, very rare cases as young as 3 years old have been reported (Johnson et al., 2005; Schober and Baade, 2006). A sex predisposition was never identified (Clercx et al., 2018; Laurila and Rajamäki, 2020a).

CIPF develops slowly and usually deteriorates progressively over months to years (Corcoran et al., 1999a). The most common clinical signs are cough and exercise intolerance (Corcoran et al., 1999a; Johnson et al., 2005; Heikkilä et al., 2011; Corcoran et al., 2011; Thierry et al., 2017; Roels et al., 2017, 2019). Other possible clinical signs include tachypnea at rest or during mild exercise, restrictive dyspnea with frequent abdominal breathing pattern, cyanosis (as in Figure 2) and syncope (Corcoran et al., 1999a, 2011; Johnson et al., 2005; Heikkilä et al., 2011; Thierry et al., 2017; Roels et al., 2017, 2019). Most dogs stay bright and alert thanks to adaptation to slowly developing respiratory insufficiency (Corcoran et al., 1999a, 2011; Heikkilä et al., 2011).

Figure 2 (extracted from http://caninepulmonaryfibrosis.uliege.be)**.** Cyanosis visible on the tongue of a WHWT affected by CIPF.

Before diagnosis, median duration of clinical signs varies from 3 to 13 months (Corcoran et al., 1999a, 2011; Heikkilä et al., 2011; Roels et al., 2017; Thierry et al., 2017; Holopainen et al., 2019). In mild or moderate cases, the dog owners often attribute the clinical signs to the normal aging process and remain unaware of the deterioration of the respiratory function (Corcoran et al., 1999a).

On lung auscultation, diffuse inspiratory pulmonary crackles can be heard in most dogs (Corcoran et al., 1999a, 2011; Johnson et al., 2005; Heikkilä et al., 2011; Roels et al., 2017; Thierry et al., 2017). However, they might not be audible in case of shallow, tachypneic breathing in severely affected dogs (Heikkilä et al., 2011). Inspiratory crackles can sometime be audible through the mouth, without a stethoscope (Heikkilä et al., 2011). A fraction of dogs affected by CIPF develops secondary arterial pulmonary hypertension (PH) which can lead to a significant secondary tricuspid reflux and a low-grade, right-sided, systolic murmur (Laurila and Rajamäki, 2020a).

1.5 Diagnosis

The diagnosis of CIPF relies on signalment, clinical signs, diagnostic imaging, and exclusion of other diseases causing similar clinical signs. A complete diagnostic work-up includes history assessment, clinical examination, hematological and serum biochemical analyses, arterial blood gas assessment, 6-minute walk test, echocardiography, thoracic computed tomography, bronchoscopy and BALF analysis. A definitive diagnosis of CIPF requires confirmation by histopathological examination (Clercx et al., 2018; Laurila and Rajamäki, 2020a).

1.5.1 6-minute walk test

The 6-minute walk test (6MWT) assesses the distance walked by a dog within 6 minutes of time, which is called the "6-min walked distance" (6MWD). It is a well-tolerated noninvasive test used to evaluate exercise intolerance and one of the only two pulmonary function tests available in dogs (Clercx et al., 2018; Laurila and Rajamäki, 2020a). Lilja-Maula et al. demonstrated that WHWTs affected with CIPF walk a significantly shorter median 6MWD, 398 m (range 273–519 m), compared with healthy controls, 492 m (420–568 m) (L. I. O. Lilja-Maula et al., 2014). Other studies reported comparable median 6MWD (350 to 378 m) in WHWTs affected with CIPF (Roels et al., 2019, 2017). During the follow-up of CIPF, 4 out of 5 WHWTs had a reduced 6MWD 9 to 11 months after the first 6MWT (L. I. O. Lilja-Maula et al., 2014). The 6MWD was also positively moderately correlated with the arterial partial pressure in oxygen (PaO_2) (L. I. O. Lilja-Maula et al., 2014). Therefore, repeated 6MWT can be used to monitor exercise intolerance over time and thus the progression of CIPF (Laurila and Rajamäki, 2020a).

1.5.2 Arterial blood gas analysis

Analysis of arterial blood gases is the second pulmonary function test available in dogs (Clercx, Fastrès and Roels, 2018; Laurila and Rajamäki, 2020). WHWTs with CIPF present moderate (80-60 mmHg) to severe (lower than 60mmHg) hypoxemia, with a median PaO_2 ranging from 58.9 to 65.5 mmHg in WHWTs with CIPF, compared with 96.1 to 99.1 mmHg in healthy dogs . WHWTs with CIPF also present a significantly increased alveolar-arterial oxygen gradient ($P(A\text{-}a)O_2$), with a median value of 50.1 mmHg (range 28.0–84.7), compared with 17.5 (range 10.7–26.8) in healthy dogs (Corcoran et al., 1999a; Heikkilä et al., 2011). During the follow-up of WHWTs with IPF, some authors observed a significant decrease in PaO_2 and increase in $P(A\text{-}a)O_2$ (L. I. O. Lilja-Maula et al., 2014). Arterial blood gas analysis may thus reflect disease severity and progression in case of repeated measures (L. I. O. Lilja-Maula et al., 2014).

1.5.3 Hematology and serum biochemistry

Hematology and biochemistry analysis are often unremarkable in CIPF-affected WHWTs and are usually performed to rule out other causes of exercise intolerance or comorbidities (Corcoran et al., 1999a; Johnson et al., 2005; Clercx et al., 2018; Laurila and Rajamäki, 2020a). For an unknown reason, dogs affected with CIPF, as humans with IPF, do not commonly present polycythemia (Laurila and Rajamäki, 2020a). Serum alkaline phosphate and platelet counts are frequently increased above reference ranges in both healthy and CIPF-affected WHWTs, without significant differences between CIPF and controls (Johnson et al., 2005; Heikkilä et al., 2011; Corcoran et al., 2011; E. Roels et al.,

2015; Roels et al., 2019; Thierry et al., 2017). This may represent a physiological specificity of the breed.

Studies in human IPF patients have shown increased platelet reactivity, suggesting a potential role in the disease through the release of pro-fibrotic mediators such as TGF-β1 and platelet derived growth factor (Crooks et al., 2014). While platelet reactivity has not been studied in dogs, a similar mechanism could explain why breeds with naturally high platelet counts may have an increased predisposition to lung fibrosis.

1.5.4 Echocardiography

Cardiac ultrasound is performed to rule out primary cardiac diseases and to assess the presence of secondary pulmonary arterial hypertension (Clercx, Fastrès and Roels, 2018; Laurila and Rajamäki, 2020). Echocardiographic signs of PH were documented in a high proportion of WHWTs affected with CIPF, from 44 to 67.9% of cases, according to different studies (Schober and Baade, 2006; Heikkilä et al., 2011; Roels et al., 2021, 2024; Fastrès et al., 2023). In the absence of cardiac catheterization, pulmonary arterial pressure is most commonly estimated using the peak velocity of the tricuspid regurgitation jet (Thierry et al., 2017; Clercx et al., 2018; Reinero et al., 2020). For PH evaluation, and for establishing the probability of PH, other echocardiographic measurements are also used such as the right ventricle and atrium sizes, the systolic flattening of the interventricular septum, the pulmonary artery diameter to aortic diameter ratio, the pulmonary artery flow profile, the caudal vena cava size, the acceleration time to ejection time ratio of the pulmonary artery flow, the right pulmonary artery distensibility index and the right pulmonary vein to pulmonary artery ratio (Schober and Baade, 2006; Reinero et al., 2020; Roels et al., 2021).

No association was identified between the presence of moderate to severe PH and survival in WHWTs with CIPF (Roels et al., 2021). This was most likely due to subsequent treatment of PH-suffering WHWTs with sildenafil and regular follow-ups (Roels et al., 2021). Sildenafil, given in cases of pre-capillary PH, improves exercise intolerance and quality of life, mitigates the progression of specific echocardiographic parameters related to PH, and could improve survival (Brown et al., 2010; Jaffey et al., 2019; Johnson and Stern, 2020; Roels et al., 2024). This highlights the importance of PH detection and regular echocardiographic follow-ups in CIPF.

1.5.5 Diagnostic imaging

Thoracic radiography findings are neither specific no sensitive for CIPF, but are useful for exclusion of other lung diseases, such as neoplasia (Laurila and Rajamäki, 2020a). The most common

finding on thoracic radiographs in dogs affected with CIPF is a generalized, mild to severe, interstitial to bronchointerstitial pattern (Corcoran et al., 1999a; Johnson et al., 2005; Heikkilä et al., 2011; Thierry et al., 2017), as illustrated in Figure 3. Some dogs may present patchy alveolar opacities with indistinct margins (Heikkilä et al., 2011). Right-sided cardiomegaly is sometimes observed (Corcoran et al., 1999a; Johnson et al., 2005). However, healthy senior WHWTs might also present mild bronchial or bronchointerstitial patterns on thoracic radiographs (Heikkilä et al., 2011), which could impair the detection of early fibrosis. Additionally, the thick skin of WHWTs complicates the interpretation of subtle findings (Laurila and Rajamäki, 2020a).

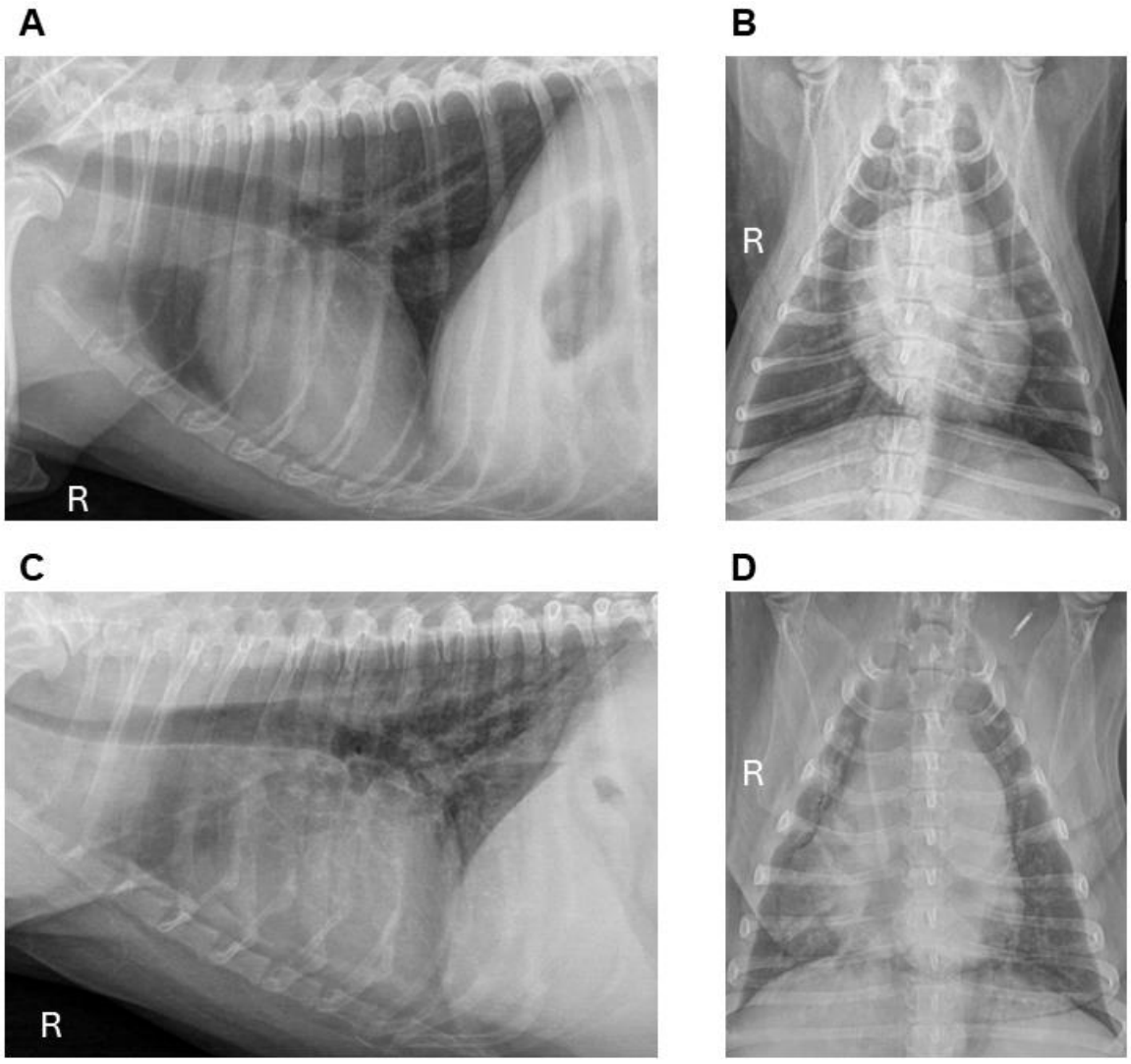

Figure 3. Above, thoracic radiographs of a 7-year-old West Highland white terrier (WHWT) free of lung disease in (A) right lateral view and (B) ventro-dorsal view. Below, thoracic radiographs of a 14-year-old WHWT affected by canine idiopathic pulmonary fibrosis in (C) right lateral view and (D) ventro-dorsal view, showing severe diffuse broncho-interstitial opacities in the lungs, as well as a collapse of the cervical and cranial

thoracic trachea. Images were obtained from the diagnostic imaging department of Teaching Veterinary Hospital of the University of Liège.

Nowadays, thoracic high resolution computed tomography (CT) plays an essential role in the diagnostic work-up of CIPF. The most common CT finding in CIPF is ground glass opacities (GGO), described with varying degrees in all dogs and in all disease stages (Johnson et al., 2005; Corcoran et al., 2011; Heikkilä et al., 2011; Roels et al., 2017; Thierry et al., 2017; Holopainen et al., 2019). GGO is defined as an increased attenuation with preservation of the bronchial and vascular margins (Bankier et al., 2024). Other findings include mosaic attenuation pattern (patchwork of regions of differing attenuation), parenchymal bands, subpleural lines, subpleural interstitial thickening, peribronchovascular interstitial thickening, consolidations, nodules, traction bronchiectasis (bronchial dilatation with thickened, irregular bronchial walls) and honeycombing (subpleural cystic airspaces) (Johnson et al., 2005; Corcoran et al., 2011; Heikkilä et al., 2011; Roels et al., 2017; Thierry et al., 2017; Holopainen et al., 2019). Some of these features are illustrated in Figure 4. Honeycombing, a severe reticular pattern which is a major feature of human IPF, is a rare CT finding in CIPF and mild degrees were identified only in severe cases (Johnson et al., 2005; Corcoran et al., 2011; Roels et al., 2017; Thierry et al., 2017). In one study, the dorsocaudal lung lobes seemed predominantly affected by CIPF lesions, but this has not been confirmed by other studies yet (Heikkilä et al., 2011; Thierry et al., 2017). In WHWTs exempt from CIPF, thoracic high resolution CT may reveal mild localized ground-glass opacity (Roels et al., 2017, 2019).

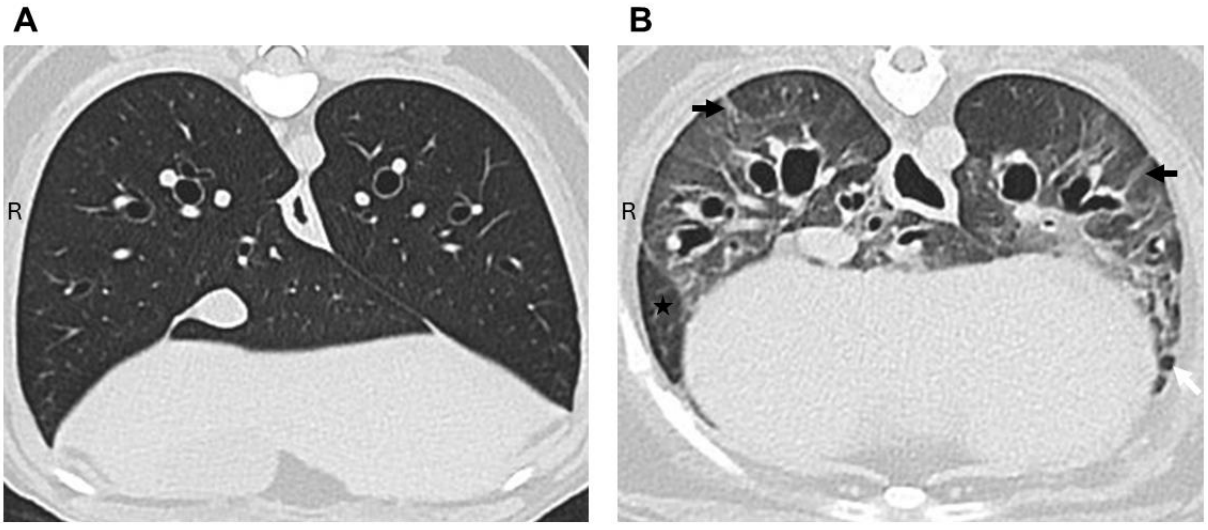

Figure 4. Representative computed tomography transverse image in lung window and in inspiratory phase, of a (A) 10-year-old West Highland white terrier exempt from lung disease and (B) a 14-year-old West Highland white terrier affected by canine idiopathic pulmonary fibrosis, showing diffuse ground glass

opacities with a mosaic attenuation pattern (black star), parenchymal bands (black arrows), peribronchovascular interstitial thickening, bronchiectasis and honeycombing (white arrow). Images were obtained from the diagnostic imaging department of Teaching Veterinary Hospital of the University of Liège.

The median Hounsfield unit (HU) values, characterizing lung attenuation, was significantly higher in WHWTs affected with CIPF compared with healthy controls (Heikkilä et al., 2011; Thierry et al., 2017; Holopainen et al., 2019). The most recent studies reported median lung attenuation of -495 to -563 HU in WHWTs with CIPF, and -708 to -761 HU in healthy dogs (Thierry et al., 2017; Holopainen et al., 2019). In one study, a low cut-off value of -702 HU classified dogs as being affected with CIPF with a false positive rate of 7% and a sensitivity of 97% (Thierry et al., 2017).

In one study, the CT abnormalities observed in WHWTs affected with CIPF allowed the attribution of a CT score, which showed a moderate positive correlation with the clinical score, and a moderate negative correlation with survival time. WHWTs with mild lesions on CT are thus more likely to be less severely affected and to survive longer, and CT findings might be prognostic factors (Thierry et al., 2017).

In some severely CIPF-affected dogs, general anesthesia may be contraindicated. In these cases, CT images may be acquired faster and more safely without general anesthesia, using only physical restraint, with or without minimal chemical restraint with butorphanol (Roels et al., 2017; Holopainen et al., 2019). A transparent positioning device, such as the modified VetMousetrap™, can be used for physical restraint in awake animals (Holopainen et al., 2019). Performing CT under sedation only provides adequate image quality for the assessment of the lesions associated with CIPF (Holopainen et al., 2019). In a study comparing acquisitions under sedation and general anesthesia, the identification of lesions such as consolidations, nodules, parenchymal and subpleural bands, bronchial wall thickening, and bronchiectasis did not differ between acquisitions (Roels et al., 2017). However, the extent of GGO and the identification and grading of mosaic attenuation patterns differed significantly between acquisitions (Roels et al., 2017). Furthermore, the inability to acquire images during specific phases of respiration may lead to artifacts caused by underinflation during expiration or motion-related artifacts (Holopainen et al., 2019). Those differences should be taken into account when acquiring CT images without general anesthesia.

A recent study showed that computed tomography angiography could also be used to assess PH (Soliveres et al., 2021). WHWTs CIPF had higher pulmonary trunk to aorta diameter ratio compared to healthy WHWTs. In WHWTs with PH, pulmonary trunk diameter was higher than in

WHWTs without PH, and a cutoff value of 13.8mm could be used to diagnose PH in WHWTs with CIPF with a sensitivity of 90% and a specificity of 87% (Soliveres et al., 2021).

1.5.6 Bronchoscopy and bronchoalveolar lavage fluid analysis

Bronchoscopy and BALF analysis findings are not specific for CIPF but are useful to rule out an infectious disease process or airway diseases (Clercx et al., 2018; Laurila and Rajamäki, 2020a). Careful planning of anesthesia and oxygen supplementation before, during, and after the procedure are recommended, especially in severely hypoxemic dogs (Laurila and Rajamäki, 2020a).

In some WHWTs with CIPF, bronchoscopy can reveal bronchial mucosal irregularity, tracheal collapse, mild to moderate amount of bronchial mucus, mild bronchiectasis and bronchomalacia (Corcoran et al., 1999a; Johnson et al., 2005; Heikkilä et al., 2011; Roels et al., 2017). A high proportion of WHWTs affected with CIPF has signs of chronic bronchitis on bronchoscopy (Johnson et al., 2005; Corcoran et al., 2011; Thierry et al., 2017). These bronchoscopy findings are not specific for CIPF. Most findings may be attributed to concurrent chronic bronchitis, which is frequent in terriers (Corcoran et al., 1999a, 2011), or to old age (Heikkilä et al., 2011; Mercier et al., 2011).

BALF analysis in WHWTs affected with CIPF can reveal a moderate increase in total cell count, increased total macrophages and increased total neutrophils (Corcoran et al., 1999a, 2011; Heikkilä et al., 2011; Roels et al., 2017; Thierry et al., 2017). An increase in total mast cells, and a decrease in the percentage of lymphocytes were also described (Heikkilä et al., 2011). In one study, total cell count correlated negatively with PaO_2 (Heikkilä et al., 2011). Culture of BALF should reveal no bacterial growth (Heikkilä et al., 2011).

1.5.7 Histopathological features

The definitive diagnosis of CIPF requires histopathology (Heikkilä et al., 2011; Clercx et al., 2018). In case of suspicion of CIPF, surgical ante-mortem lung biopsies are not usually obtained due to the invasiveness of the procedure and the questionable benefit in the absence of a CIPF-specific therapy (Johnson et al., 2005; Clercx et al., 2018; Laurila and Rajamäki, 2020a). In view of the spatial heterogeneity of CIPF lung lesions, biopsy samples obtained focally may not be representative of the disease process (Clercx et al., 2018).

In CIPF, lung histopathology reveals a mild to moderate diffuse mature interstitial fibrosis with multifocal areas of more severe, less mature and more cellular fibrosis in subpleural or peribronchial areas (Syrjä et al., 2013; Thierry et al., 2017). Areas of mature fibrosis are characterized

by either diffuse or multifocal moderate to severe thickening of the lung interstitium by accumulation of dense, sparsely cellular, fibrous matrix (Figure 5A and 5C) (Heikkilä et al., 2011). Analysis of the composition of the extracellular matrix in CIPF lung biopsies revealed that the thickening of alveolar septa was caused by an accumulation of type I and, more predominantly, type III collagen fibrils (Norris et al., 2005). The elastin and alpha-smooth muscle actin contents and distributions were not different from control biopsies (Norris et al., 2005). Inflammatory changes affecting the lung parenchyma are not always described, but mild to moderate lymphoplasmacytic interstitial inflammation can occur (Heikkilä et al., 2011; Syrjä et al., 2013; Thierry et al., 2017).

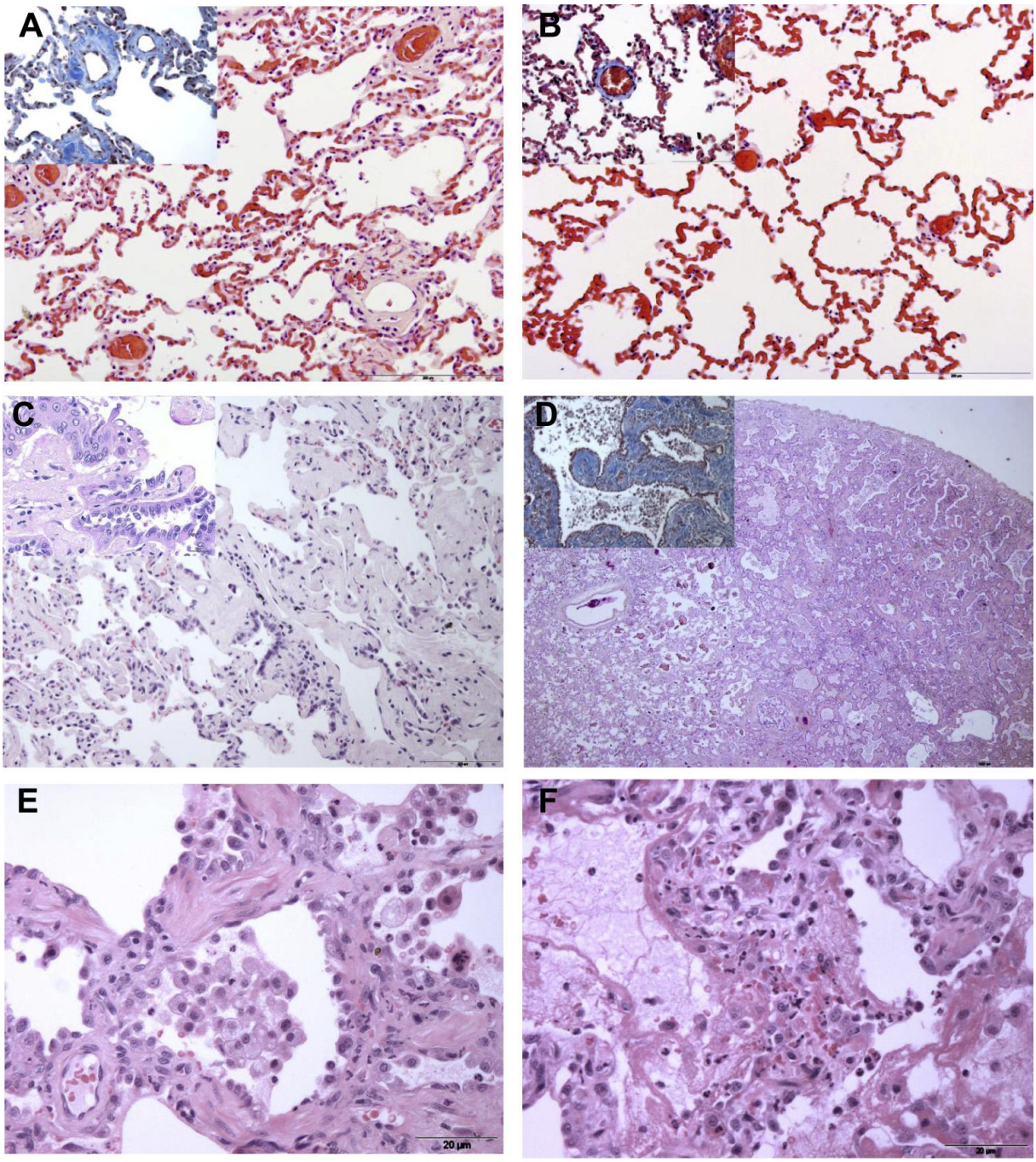

Figure 5 (extracted from Syrjä et al., 2013). Histopathological features of CIPF in WHWTs. (A) Mild diffuse mature interstitial fibrosis. Hematoxylin and eosin (HE). Bar, 200 mm. Inset: perivascular concentric fibrosis. Masson's trichrome. (B) Lung histology of a control WHWT. HE. Bar, 200 mm. Inset: vessel of a control WHWT. Masson's trichrome. (C) Transition from mild diffuse fibrosis on the left, to a focus of accentuated disease, with severe interstitial fibrosis on the right. HE. Bar, 200 mm. Inset: Type 2 pneumocyte hyperplasia and squamous metaplasia of the alveolar epithelium. (D) Subpleural area of severe interstitial fibrosis and honeycombing. HE. Bar, 1 mm. Inset: cystic fibrotic airspace within areas of honeycombing. Masson's trichrome. (E) Interstitial smooth muscle metaplasia, desquamating alveolar macrophages and type 2

pneumocyte hyperplasia within the severe fibrotic areas. HE. Bar, 20 mm. (F) Acute alveolar damage with hyaline membrane formation. HE. Bar, 20 mm.

Multifocal areas of severe and active fibrosis are characterized by a diffuse presence of myofibroblasts in alveolar interstitium as well as profound alveolar epithelial and luminal changes and occasional honeycombing (Figure 5D) (Heikkilä et al., 2011; Syrjä et al., 2013). Epithelial changes include type 2 pneumocyte atypia and hyperplasia, as well as epithelial pseudostratification and squamous metaplasia of the peribronchiolar alveolar epithelium (Figure 5C, inset) (Heikkilä et al., 2011; Syrjä et al., 2013; Thierry et al., 2017). Luminal changes include a mild to moderate accumulation of foamy alveolar macrophages (Figure 5E), with occasional multinucleated giant cells (Heikkilä et al., 2011; Syrjä et al., 2013; Thierry et al., 2017). Diffuse alveolar damage, characterized by hyaline membranes lining the alveolar luminal wall (Figure 5F), can be seen in some cases, particularly in lung biopsies from WHWTs undergoing AE and being euthanized because of acute dyspnea (Syrjä et al., 2013; Lilja-Maula et al., 2015).

In comparison with human diseases, areas of diffuse mature fibrosis resembles nonspecific interstitial pneumonia pattern, found in hypersensitivity pneumonitis, while patchy areas of accentuation resemble usual interstitial pneumonia (UIP), the histopathological pattern of human IPF (Syrjä et al., 2013; Raghu et al., 2022a). Fibroblastic foci, a hallmark of human IPF consisting of prominent interstitial foci of fibroblasts and myofibroblasts within a myxoid matrix, have never been described in dogs (Norris et al., 2005; Heikkilä et al., 2011; Syrjä et al., 2013; Raghu et al., 2022a).

1.5.8 Biomarkers

Research of diagnostic and prognostic biomarkers for CIPF have been extensively performed through both screening and targeted approaches (Clercx et al., 2018). Although none are currently routinely used in veterinary practice, some appear promising.

The following biomarkers were increased in WHWTs with CIPF compared with healthy WHWTs: SPP1 in serum (Fastrès et al., 2023), CCL2 in serum (Krafft et al., 2013a; Elodie Roels et al., 2015b; Niinikoski et al., 2022) and in BALF (Elodie Roels et al., 2015b), endothelin-1 (ET-1) in serum and in BALF (Krafft et al., 2011), CXCL8 in BALF (Elodie Roels et al., 2015b), procollagen type III amino terminal propeptide (PIIINP) in BALF (Heikkilä et al., 2013), BALF matrix metalloproteinase (MMP)-2 and MMP-9 (Määttä et al., 2021) and BALF activin B most notably if they had concurrent AE or DAD (Lilja-Maula et al., 2015).

A few biomakers are also able to differentiate WHWTs with CIPF from dogs with chronic bronchitis : serum and BALF ET-1 (Krafft et al., 2011), BALF PIIINP (Heikkilä et al., 2013), serum MMP7, BALF MMP-9, and BALF MMP-2 (Määttä et al., 2021). Serum ET-1, serum MMP7 and BALF MMP2 are also able to discriminate between CIPF and eosinophilic bronchopneumopathy (Krafft et al., 2011; Määttä et al., 2021).

Some biomarkers, increased in healthy WHWTs compared with other healthy dogs from non CIPF-predisposed breeds, may thus be related to the breed predisposition to CIPF: serum and BALF SPP1 (Fastrès et al., 2023), serum CCL2 (E. Roels et al., 2015; Niinikoski et al., 2022), serum CXCL8 (E. Roels et al., 2015), serum TGF- β1 (Krafft et al., 2014) and serum Krebs Von den Lungen-6 (KL-6) (Fastrès et al., 2018). Fibronectin 1 (FN1) in serum (Fastrès et al., 2023) and vascular endothelial growth factor A in BALF (Niinikoski et al., 2022) were both decreased in healthy WHWTs compared to healthy dogs from other breeds.

A few biomarkers may also have a prognostic value. High serum CCL2 at the time of diagnosis of CIPF was shown to be negatively associated with survival time (Elodie Roels et al., 2015a), while in dogs affected by CIPF and severe hypoxemia ($PaO_2 \leq 60$ mmHg), serum pro-MMP-7 activity was associated with an increased risk of death (Määttä et al., 2021).

1.6 Treatment

To this date, there is no curative treatment for CIPF (Clercx et al., 2018; Laurila and Rajamäki, 2020a). Indeed, the effect of specific anti-fibrotic treatment in WHWTs with CIPF has not been documented yet. In human medicine, two anti-fibrotic drugs are approved for the treatment of IPF, nintedanib and pirfenidone. Both drugs were shown to decrease pulmonary function decline of IPF patients, thus slowing disease progression and improving survival (Glassberg, 2019; Raghu et al., 2022a). However, none of these treatments stop the progression of IPF or reverse the fibrotic changes. Unfortunately, in toxicologic studies for drug approval, nintedanib, an antifibrotic and anti-inflammatory tyrosine kinase inhibitor, was shown to cause severe gastro-intestinal toxicity in dogs, even at a low dose (European Medicines Agency, 2015; Raghu et al., 2022a). Pirfenidone is an antifibrotic agent with antioxidant, anti-inflammatory and antiproliferative properties (Raghu et al., 2022a). The safety profile of pirfenidone in dogs and its use is CIPF treatment has never been documented (Clercx et al., 2018; Laurila and Rajamäki, 2020a). Pirfenidone is very expensive and some authors calculated that treating a WHWT with CIPF would cost 12 to 17 euros per day (estimation made in July 2019) (Laurila and Rajamäki, 2020a).

Therefore, the treatment of CIPF currently consists of alleviating clinical signs and improving quality of life by suppressing cough and treating comorbidities such as PH or secondary infections (Clercx et al., 2018; Laurila and Rajamäki, 2020a). Oral or inhaled corticosteroids are commonly used to relieve cough, especially in dogs with concurrent bronchial changes, but do not seem to improve lung function (Corcoran et al., 1999a; Clercx et al., 2018; Laurila and Rajamäki, 2020a). Theophylline, which causes mild bronchodilation, enhances mucociliary clearance and increases contractility of the diaphragm, has also been recommended in association with corticosteroids (Corcoran et al., 1999a; Laurila and Rajamäki, 2020). The use of antitussives should be considered if the cough is irritating (Heikkilä-Laurila and Rajamäki, 2014). However, none of these treatments appear to fully alleviate clinical signs.

WHWTs affected with CIPF and secondary PH are treated with sildenafil, a phosphodiesterase-5 inhibitor, which improves exercise intolerance and quality of life, mitigates the progression of specific echocardiographic parameters related to PH, and could improve survival of dogs with pre-capillary PH. Indeed, in a study in dogs with PH, exercise tolerance, measured by mean activity count per minute, and quality of life scores were significantly higher in dogs treated with sildenafil compared with dogs receiving placebo (Brown et al., 2010). In dogs with PH secondary to respiratory disease, quality of life scores significantly improved after one month of treatment with sildenafil (Johnson and Stern, 2020). In dogs with PH secondary to respiratory disease and/or hypoxia, sildenafil treatment was associated with improved survival (Jaffey et al., 2019). Sildenafil treatment was also suspected to improve survival in a study in WHWTs affected with CIPF (Roels et al., 2021). Very recently, it was shown that sildenafil may mitigate the progression of PH-related echocardiographic changes in WHWTs with CIPF and PH (Roels et al., 2024).

In case of acute worsening of respiratory function during the course of CIPF, a possible etiology (e.g. bacterial pneumonia) should be investigated and treated appropriately (Laurila and Rajamäki, 2020a). Unfortunately, the cause may stay undetermined. In human IPF, a sudden and rapid decline in lung function without an identifiable cause is called an acute exacerbation (AE) and is associated with a high mortality rate (Collard et al., 2016). In humans, current guidelines advise treatment of AE with corticosteroids (Raghu et al., 2022a).

Although a beneficial effect has never documented, the use of proton pump inhibitors or histamine-2 receptor blockers has been advocated by some authors due to the increased rate of microaspirations in WHWTs (Määttä et al., 2018; Laurila and Rajamäki, 2020a; Kouki et al., 2023). In

human IPF, the current guidelines advise against treating IPF patients exempt from gastroesophageal reflux symptoms with antiacid medication (Raghu et al., 2022a).

Other general recommendations include keeping routine daily walks (unless the dog shows signs of exhaustion) and improving air quality (Laurila and Rajamäki, 2020a; Reinero et al., 2020). Weight loss is also recommended for obese patients to increase thoracic wall compliance and decrease extrathoracic and intra-abdominal adipose tissue (Reinero et al., 2020). Additionally, using a harness instead of a neck collar can help reduce the stimulus for coughing (Reinero et al., 2020).

1.7 Prognosis

The prognosis of CIPF is poor. Since there is not effective anti-fibrotic treatment, CIPF causes progressive respiratory insufficiency leading to death or euthanasia (Clercx et al., 2018; Laurila and Rajamäki, 2020a). Reported median survival times (MST) stand between 15.5 and 32 months (range 2-51 months) from the onset of clinical signs, and between 7 and 11 months (range 0-40 months) from diagnosis (Corcoran et al., 1999a; L. I. O. Lilja-Maula et al., 2014; Thierry et al., 2017). Potential prognostic factors are sparse. Serum CCL2 concentrations above 700 pg/mL in WHWTs affected with CIPF were significantly associated with worse survival (Elodie Roels et al., 2015a). The severity of CT abnormalities observed in WHWTs affected with CIPF was negatively associated with survival time (Thierry et al., 2017). Other clinical factors collected at the time of diagnosis such as PaO_2, $PaCO_2$, $P(A\text{-}a)O_2$ or serum ET-1 concentration could not be identified as prognostic factors (L. I. O. Lilja-Maula et al., 2014). The absence of prognostic biomarkers, combined with the variability in individual disease progression, makes the prediction of disease progression in WHWTs with CIPF particularly challenging (Clercx et al., 2018; Laurila and Rajamäki, 2020a).

1.8 Idiopathic pulmonary fibrosis in humans

Humans can also be affected by fibrotic interstitial pneumonias of unknown cause. The most prevalent and severe is IPF and affects older adults, particularly men. It causes progressive respiratory insufficiency and carries a poor prognosis, with MST of 3 to 5 years (Fernández Pérez et al., 2010; Salisbury et al., 2017; Raghu et al., 2022a). IPF is defined by the histological characteristics of usual interstitial pneumonia (UIP), which includes patchy dense fibrosis, architectural distortion with destructive scarring and/or honeycombing, primarily affecting the subpleural and paraseptal parenchyma, along with the presence of fibroblast foci (Hochhegger et al., 2019; Raghu et al., 2022a). To date, research in human IPF identified several occupational and environment risk factors such as

metal dust, wood dust, pesticide, occupational history of farming or agriculture and smoking (Park et al., 2021).

1.9 Lung cancer as a comorbidity

Lung cancer is a frequent comorbidity in humans affected by IPF. The prevalence of lung cancer in patients with IPF ranges from 2.7% to 48% and is significantly higher than in the general population (Tomassetti et al., 2015; Ballester et al., 2019; Kewalramani et al., 2022). Lung cancer and IPF share common risk factors and pathobiological mechanisms, and IPF increases the risk of lung cancer by 7 to 20% (Ballester et al., 2019; Kewalramani et al., 2022). The occurrence of lung cancer in patients affected by IPF negatively impacts survival and creates specific challenges in management (Tomassetti et al., 2015; Kewalramani et al., 2022). Patients with concurrent IPF and lung cancer undergoing therapy with surgery, radiotherapy, chemotherapy or immune checkpoint inhibitors therapy have an increased risk of complications, such as AE, radiation pneumonitis, immune-mediated pneumonitis, than patients affected with lung cancer alone (Kewalramani et al., 2022).

In cats, coincident pulmonary neoplasia was reported in 6 over 23 cats with a tentative diagnosis idiopathic pulmonary fibrosis (Cohn et al., 2004). Although published data is missing from the literature, other authors studying CIPF report they observed cases of concurrent pulmonary carcinoma and believe lung cancer is also associated with CIPF in WHWTs (Laurila and Rajamäki, 2020a). In our cohort of WHWTs affected by CIPF, primary lung cancer was strongly suspected or confirmed in 7% of cases (unpublished data). Besides, genetic variants recently associated with CIPF in the gene CPSF7 were also associated with lung adenocarcinoma in humans (Piras et al., 2020).

2 Canine lung cancer

2.1 Epidemiology and etiology

Primary pulmonary neoplasia is relatively rare in dogs, with an incidence at necropsy of less than 1% (Wilson, 2016; Rebhun and Culp, 2020). It affects dogs of old age, without apparent sex predisposition (Ogilvie et al., 1989; McPhetridge et al., 2021). Large breed dogs are overrepresented, particularly Boxers, Labrador Retrievers, Dobermans, Australian Shepherds, Irish Setters and Bernese mountain dogs (Ogilvie et al., 1989; Rebhun and Culp, 2020; Lee et al., 2020; McPhetridge et al., 2021). Bernese mountain dogs, but also Miniature Schnauzers are overrepresented among cases of primary pulmonary histiocytic sarcoma (Marlowe et al., 2018; McPhetridge et al., 2021).

So far, no strong direct association has been identified between lung cancer and environmental factors such as passive smoke exposure (Reif et al., 1992). However, an increased risk of lung cancer was identified in dogs which had high amounts of anthracosis, which is the accumulation in lungs of black dust matter due to inhalation of polluted air (Bettini et al., 2010). Interestingly, it was shown that dogs chronically passively exposed to cigarette smoke have increased BALF macrophage and lymphocyte population, in addition to anthracosis in macrophage cytoplasm (Roza and Viegas, 2007).

2.2 Clinical presentation

In 25 to 37% of cases, dogs are asymptomatic and lung neoplasia is discovered incidentally (Ogilvie et al., 1989; McNiel et al., 1997; Marlowe et al., 2018; Rose and Worley, 2020; McPhetridge et al., 2021). The most common clinical sign is dry cough (Ogilvie et al., 1989; McNiel et al., 1997; Marlowe et al., 2018; McPhetridge et al., 2021). Other possible symptoms include dyspnea, tachypnea, lethargy, hyporexia, weight loss, hemoptysis, exercise intolerance and even lameness, when paraneoplastic hypertrophic osteopathy or bone metastasis are present (Ogilvie et al., 1989; McNiel et al., 1997; Marlowe et al., 2018; McPhetridge et al., 2021). Other paraneoplastic syndromes such as hypercalcemia, fever and secretion of adrenocorticotropic hormone have been described in dogs, as well as in humans (Ogilvie et al., 1989). On lung auscultation, in case of pleural effusion, lung and heart sounds may be muffled (McNiel et al., 1997; McPhetridge et al., 2021). Abdominal effusion can be found too, due to vena cava compression as part of the Budd-Chiari syndrome secondary to lung neoplasia (McPhetridge et al., 2021).

2.3 Diagnosis

2.3.1 Thoracic imaging

Most primary lung tumors are diagnosed by thoracic radiography (Ogilvie et al., 1989; McNiel et al., 1997) , which is widely available in veterinary practice and does not require general anesthesia. Most commonly, a well-circumscribed solitary mass is found in the periphery of a caudal lung lobe (Marolf et al., 2011). The distinction of pulmonary and mediastinal masses by thoracic radiography can sometimes be challenging. A study estimated an overall agreement of 61.3% between thoracic radiography and CT to differentiate pulmonary from mediastinal masses (Ruby et al., 2020).

CT is now widely used for diagnosis and staging of pulmonary neoplasia in dogs, as illustrated by Figure 6. In a study characterizing CT findings or primary lung tumors, including 17 primary carcinomas and 2 primary sarcomas, all were bronchocentric in origin with internal air

bronchograms (Marolf et al., 2011). Most lung tumors were solitary, well circumscribed, and with mild to moderate heterogeneous contrast enhancement (Marolf et al., 2011). Primary pulmonary neoplasia appears to be more commonly located in caudal lobes rather than cranial lobes (McPhetridge et al., 2021; Treggiari et al., 2025). CT was shown to identify pulmonary metastasis in 17.6 to 26% of dogs and distant metastasis in 0.9% (Marolf et al., 2011; McPhetridge et al., 2021). Overall, CT appears better at detecting small lung nodules than thoracic radiography (Nemanic et al., 2006; Alexander et al., 2012; Armbrust et al., 2012).

Figure 6. Computed tomography transverse image in lung window, of a 12-year-old Griffon affected by primary pulmonary adenocarcinoma (black arrow) in the right caudal lobe. Images were obtained from the diagnostic imaging department of Teaching Veterinary Hospital of the University of Liège.

CT is also useful and more sensitive than radiography to identify tracheobronchial lymph node metastasis (Paoloni et al., 2006). Tracheobronchial lymph node diameter, heterogeneity and ring contrast enhancement patterns on CT were significantly correlated to metastatic disease (Ballegeer et al., 2010). In dogs with primary pulmonary neoplasia, CT has a high specificity (70–100%) but variable sensitivity (50–83%) in detecting tracheobronchial lymph node metastasis, with positive predictive value ranging from 53.2% to 100% and negative predictive value from 71.9% to 89% (Paoloni et al., 2006; Rose and Worley, 2020; McPhetridge et al., 2021).

Thoracic ultrasound can also be used to detect neoplastic lesions, which mostly appear homogeneously hypoechoic, often with smooth, echogenic borders (Larson, 2009; Reichle and Wisner, 2000). Thoracic ultrasound has a low sensitivity, to thoracic radiography, to detect lung

nodules (Pacholec et al., 2021; Rick et al., 2019). However, ultrasound is particularly useful to perform ultrasound-guided fine needle aspiration (FNA) or biopsies (Reichle and Wisner, 2000).

2.3.2 Cytology

FNA of pulmonary masses is commonly performed to obtain rapidly and non-invasively a cytological diagnosis. In a recent study, FNA accurately indicated a diagnosis of neoplasia in 75.6% of the cases of primary pulmonary neoplasia (McPhetridge et al., 2021). It is usually performed under sedation with ultrasound guidance, but CT or fluoroscopic guidance can also be achieved (Wood et al., 1998; Zekas et al., 2005; Jacob, 2024).

2.3.3 Histopathology

Histopathology on lung biopsies before lung lobectomy is not commonly performed due to its invasive nature and its questionable clinical relevance (Marcinowska et al., 2025). Pretreatment lung biopsies can be obtained by core needle biopsy, bronchoscopy, keyhole incision with staple application, and thoracoscopy (Bauer, 2000; Norris et al., 2002; Wormser et al., 2014; Zekas et al., 2005).

The most prevalent histological type of primary pulmonary neoplasia is pulmonary carcinoma, with adenocarcinoma (illustrated by Figure 7) being more common than squamous cell carcinoma (Ogilvie et al., 1989; Bettini et al., 2010; McPhetridge et al., 2021; Treggiari et al., 2025). Next in prevalence are sarcomas, primarily primary pulmonary histiocytic sarcoma, and more rarely fibrosarcoma and chondrosarcoma. Other tumor types include adenomas, pulmonary neuroendocrine tumors, and rarer neoplasms such as plasmacytomas and carcinosarcomas (Bettini et al., 2010; McPhetridge et al., 2021). Pulmonary nodules associated with metastatic non-pulmonary malignant neoplasms are most commonly attributed to hemangiosarcoma, osteosarcoma, histiocytic sarcoma, soft tissue sarcoma, adenocarcinoma, melanoma, lymphoma, or mast cell tumor (Lamb et al., 2019).

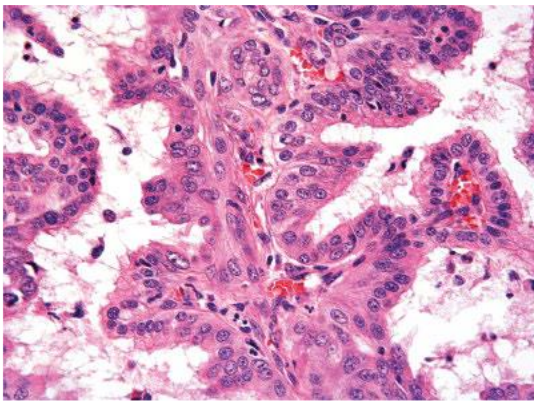

Figure 7 (extracted from Wilson, 2016). Photomicrograph of a canine primary pulmonary adenocarcinoma with a papillary growth pattern.

2.3.4 Molecular markers

Differentiating primary lung carcinomas from metastases of another type of carcinoma can be challenging (Marcinowska et al., 2025). Therefore, molecular markers play a valuable role in the diagnosis and prognostication of canine pulmonary cancers. Thyroid transcription factor-1 (TTF-1) has been identified as a highly specific and moderately sensitive marker for canine primary lung carcinomas, aiding in distinguishing them from metastatic tumors, with the exception of thyroid carcinomas which also express TTF-1 (Ramos-Vara et al., 2005; Bettini et al., 2009). Additionally, surfactant protein A (SP-A) and napsin A have been recognized as useful markers to diagnose and differentiate pulmonary carcinomas from metastatic tumors, with SP-A showing the highest sensitivity and specificity. SP-A immunoreactivity is absent in nonpulmonary tumors, making it a highly specific diagnostic tool (Beck et al., 2017). Regarding pulmonary histiocytic sarcomas, they are usually confirmed with a positive anti-CD18 staining by IHC (Marlowe et al., 2018).

Beyond diagnostic markers, molecular profiling has highlighted potential therapeutic targets in canine pulmonary cancers. Overexpression of epidermal growth factor receptor (EGFR) has been associated with a poor prognosis and linked to environmental factors such as air pollution (Sabattini et al., 2014). Additionally, tyrosine kinase receptors, including platelet-derived growth factor receptor α and anaplastic lymphoma kinase tyrosine receptor, have been found to have increased expression and phosphorylation in canine pulmonary adenocarcinoma (PAC). However, EGFR expression and phosphorylation were not significantly elevated compared to normal lung tissue, and no activating EGFR mutations were detected in exons 18–21 (Mariotti et al., 2014). Furthermore, HER2 (ERBB2) mutations have been identified in 38% of canine PAC. These mutations result in constitutive activation of oncogenic signaling pathways and increased sensitivity to HER2

inhibitors such as lapatinib and neratinib (Lorch et al., 2019). HER2 expression was also confirmed by IHC in 69% of canine primary lung cancers, suggesting its potential as a therapeutic target for HER2-directed treatments (Yoshimoto et al., 2020).

Tumor-associated macrophages, particularly the M2 polarization marked by CD204 expression, have also been linked to poorer prognosis and tumor progression in canine PAC. High $CD204^{+}$ macrophage levels are associated with lung metastasis and shorter overall survival in affected dogs (Yokota et al., 2023). These findings underscore the potential for targeted therapies in canine lung cancers and highlight the need for further research into the molecular underpinnings of these tumors.

2.4 Treatment, outcome and prognosis

2.4.1 Surgery

The current treatment of choice for a primary pulmonary neoplasia is lung lobectomy (Marlowe et al., 2018; Lee et al., 2020; McPhetridge et al., 2021). A complete lobectomy is achieved in the majority of cases, although cases of partial lobectomy are described (McPhetridge et al., 2021). Recent studies documented occurrences of intraoperative complications of 11.8%, postoperative complications of 12.4-20.6% and mortality within 14 days of surgery of 5.9% (McPhetridge et al., 2021; Treggiari et al., 2025). Lung lobectomy is typically conducted through thoracotomy; however, for small tumors, it can also be performed using video-assisted thoracoscopic surgery with comparable short-term outcomes (Mayhew et al., 2013; Bleakley et al., 2015; Rose and Worley, 2020).

Post-lobectomy outcomes significantly vary based on histological tumor type. Recent studies report MST of 370–399 days for primary pulmonary carcinoma, 300 – 374 days for primary pulmonary histiocytic sarcoma and 498 days for pulmonary neuroendocrine tumors in dogs surviving at least 15 days after surgery (Marlowe et al., 2018; Lee et al., 2020; McPhetridge et al., 2021). Median disease-free interval were 344 days for pulmonary carcinoma, 253 days for primary histiocytic sarcoma and 347 days for neuroendocrine tumors (McPhetridge et al., 2021).

For primary pulmonary carcinoma, a Canine Lung Carcinoma Stage Classification system (Table 1) was recently established, adapted from the human lung cancer stage classification (Lee et al., 2020). This staging system is prognostic for survival after surgical resection of primary pulmonary carcinoma, with survival time significantly decreasing as stage increases. Reported MST are, for dogs surviving the postoperative period, 663 – 952 days for stage 1, 389 – 658 days for stage 2, 158 – 361 days for stage 3 and 52 – 273 days for stage 4 (Lee et al., 2020; McPhetridge et al., 2021). Another

recent study has also validated the prognostic value of this staging system for PAC in small breed-dogs (Ichimata et al., 2023). Given the critical role of accurate lymph node assessment in staging and prognosis, surgical removal or biopsy is strongly recommended, irrespective of lymph node appearance on preoperative CT (McPhetridge et al., 2021).

Table 1. Canine lung carcinoma stage classification (from Lee et al., 2020).

T	Size (cm)	Solitary vs multiple nodules	Organ invasion
T1	≤3	Solitary	None
T2	>3 to ≤5	Solitary	Visceral pleura, main bronchi (not carina)
T3	>5 to ≤7	Separate nodule(s) in same lobe	Chest wall, pericardium, phrenic nerve
T4	>7	Separate nodule(s) in ipsilateral lung lobe(s)	Mediastinum, diaphragm, heart, great vessels, recurrent laryngeal nerve, carina, trachea, esophagus, spine
N			
N0	No lymph node metastasis		
N1	Ipsilateral tracheobronchial lymph node		
N2	Distant lymph node metastases		
M			
M0	No distant metastasis		
M1	Malignant effusion, contralateral lung lobe metastasis, extra-thoracic metastasis		
Stage			
Stage 1	T1, N0, M0		
Stage 2	T2, N0, M0; T3, N0, M0; T1-2, N1, M0		
Stage 3	T4, N0, M0; T3-4, N1, M0; T1-4, N2, M0		
Stage 4	T1-4, N1-2, M1		

In addition to tumor stage, several prognostic factors were identified to negatively impact survival times of dogs with primary pulmonary neoplasia. Primary tumor size over 5 cm, incomplete surgical margins, increased mitotic count, high histological grade and poor differentiation, intrathoracic lymph node metastasis, distant metastasis and pleural effusion at diagnosis were associated with shorter survival times (McNiel et al., 1997; Marlowe et al., 2018; Lee et al., 2020; Rose and Worley, 2020; McPhetridge et al., 2021; Treggiari et al., 2025). The presence of clinical signs at diagnosis, however, was inconsistently associated with decreased survival (McNiel et al., 1997; Marlowe et al., 2018; Lee et al., 2020; McPhetridge et al., 2021).

2.4.2 Chemotherapy

The therapeutic benefits of postoperative adjuvant chemotherapy remain uncertain. So far, no study has demonstrated a significant survival benefit of postoperative maximum tolerated dose chemotherapy with any type of primary pulmonary neoplasia, despite multiple studies in relatively

large cohorts of dogs (Lee et al., 2020; Rose and Worley, 2020; McPhetridge et al., 2021; Treggiari et al., 2025). In a recent studies in dogs with pulmonary carcinoma, 37-40% received chemotherapy postoperatively, most commonly single-agent vinorelbine (49-50%), followed by single-agent carboplatin (12-27%) and alternating agents (Lee et al., 2020; McPhetridge et al., 2021). Disease-free intervals did not differ significantly between dogs treated with surgery alone and those receiving adjuvant chemotherapy, nor did MST when dogs were classified by stage (Lee et al., 2020; Rose and Worley, 2020; McPhetridge et al., 2021). Regarding tyrosine kinase inhibitors, in a retrospective study with 22 dogs with PAC, MST were significantly longer in dogs receiving postoperative adjuvant toceranib phosphate treatment (191 days) compared with dogs treated with surgery alone (145 days), indicating a potential benefit, despite the short survival times reported in this study (Yamazaki et al., 2020).

In a recent retrospective study, vinorelbine as a first-line treatment for dogs with stage IV primary pulmonary carcinoma achieved an 80% partial response rate, with a median time to progression of 88 days and a MST of 100 days, while demonstrating a favorable toxicity profile (Rinaldi et al., 2023). In dogs with advanced (T3 or N1 or M1) primary pulmonary carcinoma, metronomic chemotherapy as sole treatment (with low-dose cyclophosphamide, piroxicam and thalidomide) significantly prolonged time to progression (172 days) and survival time (139 days) compared to surgery, maximum-tolerated dose chemotherapy, or no oncologic treatment, while also improving quality of life without notable toxicity, suggesting it as a viable therapeutic alternative (Polton et al., 2018).

The vast majority of dogs with primary pulmonary histiocytic sarcoma receive postoperative adjuvant chemotherapy, most commonly single-agent lomustine, and the number of dogs undergoing surgery alone is too small to make meaningful comparisons about survival (Marlowe et al., 2018; McPhetridge et al., 2021). Measurable responses were observed in dogs with primary pulmonary histiocytic sarcoma treated with chemotherapy alone; however, their survival was shorter compared to those undergoing lobectomy (Marlowe et al., 2018).

2.4.3 Radiotherapy

Radiotherapy has emerged as a promising alternative or adjunct to surgery for treating primary lung cancer in dogs, particularly when immediate surgical intervention is not feasible. Hypofractionated radiotherapy has demonstrated efficacy in tumor size reduction, with six out of nine dogs with solitary PAC showing partial response, allowing for subsequent surgical resection in most cases (Kawabe et al., 2019). While radiation-induced toxicity was observed, it was generally self-

limiting or manageable with anti-inflammatory treatment (Kawabe et al., 2019). Additionally, stereotactic body radiation therapy (SBRT) has been evaluated for local tumor control in canine pulmonary carcinomas, all stages together, demonstrating a MST of 343 days, with 38% of patients surviving beyond one year (Martin et al., 2023). SBRT was well tolerated, with relatively low rates of acute and late lung toxicities, and it provided complete or partial tumor responses in over half of the cases (Martin et al., 2023). These findings suggest that radiotherapy, whether as a neoadjuvant to surgery or as a primary treatment, can be a viable and effective option for managing canine lung cancer, potentially improving survival outcomes in advanced-stage cases.

In conclusion, unresectable or metastatic primary pulmonary cancer poses a significant therapeutic challenge and carries a poor prognosis. Therefore, a better understanding of primary lung cancer pathobiology in dogs is warranted to develop new treatment strategies.

2.5 Lung cancer in humans

Lung cancer is the leading cause of cancer-related morbidity and mortality around the globe. Non-small cell lung cancer occurs most frequently, and accounts for more than 80% of all cases, while small cell lung cancer represents about 15% of cases (Siegel et al., 2023, 2024). Smoking is by far the leading cause of lung cancer, and is associated with all types of lung cancer (Siegel et al., 2023). Additional risk factors include second-hand smoke, asbestos, radon, and other environmental, genetic and dietary variables (Malhotra et al., 2016). Smoking prevalence has declined, but reports indicate a raising proportion of lung cancers in never-smoker patients, especially among women and in younger age categories (Pelosof et al., 2017; LoPiccolo et al., 2024).

Lung cancer is often diagnosed at an advanced stage. Indeed, the disease tends to progress silently until it is far advanced. Moreover, patients may experience substantial delays at each step in the process of diagnosis, from the development of symptoms to the beginning of the treatment (Ellis and Vandermeer, 2011). Early diagnosis is associated with a better prognosis. Screening, diagnosis and staging are made through imaging (chest radiographs, CT, magnetic resonance imaging and positron emission tomography), breath analysis, and tissue procurement for analysis and molecular testing (Remon et al., 2021; Fan et al., 2024).

Treatment of early stages include surgical resection, adjuvant chemotherapy, and osimertinib in patients with EGFR mutations. Unresectable cases are treated with radiotherapy, chemotherapy, immunotherapy and targeted therapies (Meyer et al., 2024). In the last years, the use of programmed cell death protein 1 (PD-1)/ programmed death-ligand 1 (PD-L1) immune checkpoint

inhibitors have dramatically improved outcomes in lung cancer (Liu et al., 2021; Reck et al., 2022). They are now widely used, at different stages of the disease (Lahiri et al., 2023).

3 Single-cell mRNA sequencing

3.1 Objectives

Single-cell mRNA sequencing (scRNA-seq) enables high-throughput, high-resolution transcriptomic analysis by profiling the transcriptome of individual cells within a biological sample, thereby capturing cellular diversity with unprecedented detail (Fastrès et al., 2020a).

Before the advent of single-cell transcriptomic analysis, bulk RNA sequencing was widely used to study gene expression across entire cell populations. However, this approach averaged gene expression levels, limiting the ability to assess cellular heterogeneity (Hwang et al., 2018). Similarly, conventional flow cytometry techniques for cell characterization were constrained by the number of detectable markers and required prior knowledge for cell identification (Salomon et al., 2019).

In recent years, scRNA-seq has emerged as a powerful tool to overcome these limitations, enabling unbiased, high-resolution exploration of cellular biology at the microscopic level (Hedlund and Deng, 2018). scRNA-seq has thus allowed us to identify novel cell types and states, as well as to decipher the molecular mechanisms governing tissue function in both health and disease (Salomon et al., 2019). It has also provided critical insights into tissue cellular composition (Hedlund and Deng, 2018; Salomon et al., 2019). This technology has been extensively applied to investigate cellular heterogeneity across various tissues, conditions, and time points (Hedlund and Deng, 2018; Papalexi and Satija, 2018; Salomon et al., 2019).

While scRNA-seq remains in its early stages for non-traditional animal models, its application in the canine respiratory system has already been validated for identifying and characterizing cellular subpopulations in BALF from both healthy individuals and those with canine idiopathic pulmonary fibrosis (Fastrès et al., 2020a, 2020b). However, since BALF analysis captures only a fraction of lung cells, it provides limited insight into the broader cellular landscape of the lung.

In human research, comprehensive lung cell atlases have been established, offering invaluable references for studying lung diseases (Travaglini et al., 2020; Sikkema et al., 2023; Madissoon et al., 2023). In contrast, a detailed molecular characterization of all cell types in canine lung tissue has yet to be undertaken. A thorough understanding of canine lung cell biology is essential for unravelling the cellular and molecular mechanisms driving parenchymal lung diseases.

Investigating cell subpopulation differences between healthy and diseased dogs could enhance our knowledge of disease pathogenesis and pave the way for novel therapeutic approaches.

3.2 Methods

Droplet-based scRNA-seq is a powerful technique that enables high-throughput transcriptomic analysis of individual cells with cost and time efficiency (Macosko et al., 2015; Zheng et al., 2017; Salomon et al., 2019; Chen et al., 2019). This method encapsulates single cells along with barcoded beads into water-in-oil droplets within a microfluidic system, ensuring that each droplet contains a single cell and a uniquely barcoded bead (Macosko et al., 2015; Zheng et al., 2017). Systems like the 10X Genomics Chromium platform can rapidly generate thousands of these droplets, also known as gel beads in emulsion (Zheng et al., 2017; Salomon et al., 2019). Each bead is coated with oligonucleotides carrying sequencing adapters, a unique cell barcode for cell identification, a unique molecular identifier (UMI) to track individual transcripts, and a poly-d(T) sequence for capturing polyadenylated mRNA (Macosko et al., 2015; Zheng et al., 2017; Salomon et al., 2019). Upon encapsulation, cells are lysed, and reverse transcription incorporates the cell barcode and UMI into the complementary DNA (cDNA). The emulsion is then broken, and all cDNA molecules undergo PCR amplification before library preparation and sequencing (Zheng et al., 2017). The resulting data are processed into a gene-cell matrix, where the number of unique transcripts per gene in each cell is recorded. By clustering cells with similar transcriptomic profiles, researchers can identify distinct cell populations and differentially expressed genes (DEGs), which provide insights into biological functions and differences between conditions (Macosko et al., 2015; Zheng et al., 2017; Stuart and Satija, 2019).

3.3 Limitations

Despite its advantages, droplet-based scRNA-seq has several limitations that must be considered to ensure high-quality data. One major challenge is the requirement for fresh samples that need rapid processing to minimize transcriptomic alterations after collection, as degraded or dead cells can release RNA into the suspension, leading to artifacts in gene expression profiles (Zheng et al., 2017; Salomon et al., 2019). Although the speed and efficiency of droplet-based methods help reduce such contamination, doublet formation, where two cells are co-encapsulated into the same droplet, remains a concern, potentially leading to misinterpretation of cellular identity. Reducing cell and bead concentrations can lower doublet rates, but this increases waste and cost by reducing droplet occupancy (Salomon et al., 2019; Chen et al., 2019). Quality control measures, such as filtering out cells with abnormal read counts or high mitochondrial gene expression, are essential to

detect and remove dead cells, broken cells, and doublets (Chen et al., 2019). Another limitation is the low capture efficiency of transcripts; in platforms like the 10X Genomics Chromium system, only about 50% of input cells are successfully encapsulated with a barcoded bead, and only 10-20% of cellular transcripts are captured and reverse transcribed (Zheng et al., 2017; Hwang et al., 2018). This inefficiency can lead to the underrepresentation of rare cell types and the failure to detect lowly expressed genes (See et al., 2018; Chen et al., 2019). Finally, in species with incomplete genome annotation, such as dogs, interpreting scRNA-seq data presents an additional challenge. A low mapping ratio of reads due to incomplete reference genomes can hinder transcript identification and limit biological insights derived from the data (Chen et al., 2019).

4 Fibroblast activation protein

4.1 Function

Fibroblast activation protein (FAP), also known as seprase, is a transmembrane serine protease with both dipeptidyl peptidase activity and endopeptidase activities (Christiansen et al., 2007). Its dipeptidyl peptidase activity cleaves neuropeptide Y, peptide YY, substance P and brain natriuretic peptide 32 (Keane et al., 2011) while its endopeptidase function contributes to extracellular matrix remodeling by cleaving denatured type I collagen (Christiansen et al., 2007). A soluble circulating form of FAP, known as antiplasmin-cleaving enzyme, enhances inhibition of plasmin by converting α2-antiplasmin into a more active form, thereby reducing fibrinolysis and promoting tissue scarring (Lee et al., 2004). A third known substrate of endopeptidase activity is fibroblast growth factor 21 (Dunshee et al., 2016). FAP may also exert non-enzymatic activities, as catalytically inactive FAP has been shown to induce biological effects, potentially through acting on intracellular signaling via beta-integrins (Huang et al., 2011; Lv et al., 2016).

4.2 Expression

4.2.1 Development and health

FAP is typically absent in normal tissues but is upregulated in areas of active tissue remodeling. Its expression has been observed during amphibian metamorphosis (e.g., tail resorption), throughout murine development in cartilage and intercostal muscles, and in mammalian wound healing and scar formation (Fitzgerald and Weiner, 2020). Low basal levels of FAP are detectable in healthy adult mice skeletal muscle, bone marrow, adipose tissue, skin and

pancreas , as well as in human adipose tissue, liver and plasma (Roberts et al., 2013; Keane et al., 2014; Fitzgerald and Weiner, 2020).

4.2.2 Disease

FAP is highly expressed in pathological processes involving intense extracellular matrix remodeling. In human IPF, FAP is strongly expressed by fibroblasts in fibroblastic foci and in the fibrotic lung interstitium, and is positively correlated with the severity of fibrosis (Acharya et al., 2006; P. Yang et al., 2023). In dogs, FAP gene overexpression has been observed in post-mortem lung biopsies from WHWTs affected by CIPF, as determined by microarray analysis and quantitative RT-PCR (Krafft et al., 2013b). FAP is overexpressed in other fibrotic conditions, including liver fibrosis (Levy et al., 2002), skin keloids (Dienus et al., 2010) intestinal strictures associated with Crohn's disease (Rovedatti et al., 2011), as well as in non-fibrotic diseases such as osteoarthritis, rheumatoid arthritis (Milner et al., 2006; Bauer et al., 2006), atherosclerosis (Brokopp et al., 2011), myocardial infarction (Tillmanns et al., 2015), and various autoimmune and metabolic disorders (Zhen et al., 2016). In dogs, FAP expression has been detected in experimentally induced atrial fibrillation (Li et al., 2023).

FAP is markedly upregulated in a wide range of cancers and is expressed in over 90% of human carcinomas, including non-small-cell lung carcinoma (Liao et al., 2013; Kilvaer et al., 2015; Shi et al., 2020). In dogs, FAP overexpression has been identified in the stroma of mast cell tumors (Giuliano et al., 2017) and mammary carcinomas (Ettlin et al., 2017). Although primarily localized to cancer-associated fibroblasts, FAP expression is also occasionally reported in immune cells (Arnold et al., 2014), endothelial cells (Iwasa et al., 2003), and epithelial tumor cells (Iwasa et al., 2003; Shi et al., 2020). In human lung cancer and other solid tumors, high stromal FAP expression is associated with increased local invasion, lymph node metastasis rates, and reduced overall survival (Liao et al., 2013; Liu et al., 2015; Fitzgerald and Weiner, 2020; Shi et al., 2020). Mechanistically, FAP is believed to enhance proliferation, migration and invasion of tumor cells through remodeling of the extracellular matrix, regulation of intracellular signaling, promotion of angiogenesis and epithelial-to-mesenchymal transition, anti-tumor immunity suppression, stem cell promotion and therapy resistance (Hamson et al., 2014; Puré and Blomberg, 2018; Fitzgerald and Weiner, 2020).

5 Positron emission tomography

5.1 Current veterinary practice

Positron emission tomography (PET) imaging, often combined with computed tomography (PET/CT), is gaining popularity in veterinary medicine for clinical and research applications (LeBlanc and Morandi, 2014; LeBlanc and Peremans, 2014; Randall, 2016). Although veterinary facilities are rarely equipped with PET or PET/CT, collaborations with human medical facilities allow imaging veterinary patients (LeBlanc and Morandi, 2014).

The most common radiotracer used for PET imaging is [^{18}F]fluorodeoxyglucose ([^{18}F]FDG), which is used mainly on oncological patients to detect lesions with high glucose metabolism, so neoplastic lesions (LeBlanc and Peremans, 2014; Randall, 2016; Maitz et al., 2022). Other PET radiotracers used for veterinary clinical use or clinical research include [^{18}F]fluorothymidine ([^{18}F]FLT), which detects DNA synthesis and thus cell proliferation, [^{18}F]sodium fluoride ([^{18}F]NaF), which highlights osteoblastic activity, thus bone lesions, and [^{18}F]fluoromisonidazole ([^{18}F]FMISO) and Copper(II) diacetyl-di(*N*^{4}-methylthiosemicarbazone) (Cu-ATSM), which both reveal tumor hypoxia (LeBlanc and Peremans, 2014; Randall, 2016; Maitz et al., 2022). PET imaging providing metabolic information, often combined with CT providing precise anatomic localization, constitutes an excellent diagnostic and staging technique (LeBlanc and Peremans, 2014; Randall, 2016; Maitz et al., 2022).

The use of positron emission tomography (PET) with [^{18}F]FDG has been described in dogs with lung cancer but is not routinely adopted in veterinary clinical practice (Kim et al., 2014; Seiler et al., 2015).

5.2 New modalities in development

New tracers for PET are currently being developed in human medicine, mainly for oncologic diseases but also for ILDs. Since FAP is a marker of activated fibroblasts in human IPF (Acharya et al., 2006; P. Yang et al., 2023), new FAP-targeted imaging techniques have been developed for the non-invasive assessment of fibrotic ILDs, including IPF. A FAP inhibitor (FAPI) is radiolabeled with Gallium-68 (^{68}Ga) or Fluorine-18 (^{18}F) and is used as a radiotracer for PET/CT (Röhrich et al., 2022; P. Yang et al., 2023; Mori et al., 2024; Hotta et al., 2024). Such tracer thus specifically labels FAP-positive activated fibroblasts in vivo (P. Yang et al., 2023). Recent studies showed an elevated tracer uptake in IPF (Röhrich et al., 2022; P. Yang et al., 2023; Mori et al., 2024; Hotta et al., 2024). While some studies showed a correlation between the uptake and CT lesions (Röhrich et al., 2022; Mori et al., 2024; Hotta

et al., 2024), the extent of the uptake was significantly positively correlated to biomarker KL-6 serum concentration (P. Yang et al., 2023) and negatively correlated to pulmonary function tests (P. Yang et al., 2023; Mori et al., 2024), thus reflecting the severity of ILD. The uptake was also positively correlated with immunohistochemical FAP expression, which was concentrated in fibrotic foci, indicating active fibrogenesis (Hotta et al., 2024). FAP-targeted PET/CT imaging could be reliably used to noninvasively monitor the abundance and distribution of activated fibroblasts in various types of ILDs including IPF (P. Yang et al., 2023), and thus to predict disease progression (Mori et al., 2024).

Given that FAP is highly expressed in cancer-associated fibroblasts, FAP-targeted PET imaging has emerged as a promising diagnostic tool for lung cancer staging and treatment planning, offering advantages over conventional [^{18}F]FDG PET imaging (Dendl et al., 2021). Several studies have demonstrated the high tumor uptake and contrast of FAP-specific PET tracers, such as [^{68}Ga]FAPI and [^{18}F]FAPI derivatives, in lung cancer (Kratochwil et al., 2019; Giesel et al., 2021; Röhrich et al., 2022; Wei et al., 2022, 2023). FAPI PET/CT has even demonstrated superior diagnostic performance over FDG PET/CT in lung cancer, offering higher sensitivity, specificity, and accuracy for metastasis detection while providing a lower radiation burden (Giesel et al., 2021; Wei et al., 2022, 2023). Its enhanced ability to detect metastatic lesions make it a more reliable imaging modality for staging and treatment planning. Additionally, the application of [^{68}Ga]FAPI PET/CT in fibrotic interstitial lung diseases, which are often associated with lung cancer, has shown promising results in distinguishing fibrotic lesions from malignancies (Röhrich et al., 2022).

[^{18}F]FAPI PET/CT has been used in a proof-of-concept study in experimentally induced atrial fibrillation in experimental dogs. They showed an increased uptake of [^{18}F]FAPI in the right atrium of beagles with atrial fibrillation. However, only the heart was imaged, and no data on biodistribution, bioelimination was published (Li et al., 2023). [^{18}F]FAPI PET/CT has never been used to investigate FAP expression in vivo in canine lungs.

Objectives

Canine idiopathic pulmonary fibrosis (CIPF), consisting of a progressive accumulation of collagen in the lung interstitium of unknown cause, leads to respiratory insufficiency (Clercx et al., 2018; Laurila and Rajamäki, 2020a). Humans affected by idiopathic pulmonary fibrosis (IPF) have an increased risk of lung cancer, which shares common risk factors and pathobiological mechanisms with IPF (Tomassetti et al., 2015; Ballester et al., 2019; Kewalramani et al., 2022). The simultaneous occurrence of IPF and lung cancer worsens prognosis and poses significant therapeutic challenges (Tomassetti et al., 2015; Kewalramani et al., 2022). In dogs, primary lung cancer also carries a poor prognosis in its advanced stages (Lee et al., 2020; McPhetridge et al., 2021; Treggiari et al., 2025) and appears more prevalent in West Highland white terriers (WHWTs) affected by CIPF, in which therapeutic management becomes even more challenging.

Although previous studies have advanced our understanding of CIPF, including regarding the molecular characterization (Fastrès et al., 2020b), the etiology and pathogenesis of the disease remain only partially understood. CIPF is currently incurable, and its progression is often hardly unpredictable (Clercx et al., 2018; Laurila and Rajamäki, 2020a). Therefore, there is a need for novel therapeutic targets, as well as reliable diagnostic and prognostic markers. Similarly, in canine lung cancer, deeper insights into disease pathobiology could drive the development of new treatment strategies, particularly needed for advanced-stage disease.

1. Identification of novel cellular markers and therapeutic targets

Thus, this thesis aimed to enhance understanding of the pathobiology and to discover new cellular markers of CIPF and canine pulmonary adenocarcinoma (PAC) by exploring the molecular alterations occurring in lung cells within both diseases.

The first study aimed to create a molecular atlas of healthy lung cells in dogs by performing single-cell RNA sequencing (scRNA-seq) in healthy lung biopsies, to provide a reference for further investigations of lung cell subpopulations in lung diseases. Then, the second study focused on characterizing the molecular alterations occurring in cells from PAC biopsies, aiming to identify new biomarkers and therapeutic targets in an unbiased manner. To strengthen the scRNA-seq findings, which lack spatial context, we also aimed to validate specific markers of interest using immunostaining techniques. Finally, the third study aimed to characterize the molecular alterations occurring in cells from lung tissue biopsies collected from CIPF-affected WHWTs.

2. Investigation of fibroblast activation protein in CIPF and PAC

The fourth study of this thesis focuses on the expression of fibroblast activation protein (FAP) in WHWTs affected by CIPF and in PAC. In humans, FAP is a membrane protein expressed in the stroma of non-small-cell lung carcinoma (Liao et al., 2013; Shi et al., 2020) and in activated fibroblasts in IPF (Acharya et al., 2006; P. Yang et al., 2023). Therefore, we aimed to characterize FAP expression by immunohistochemistry in biopsies from healthy lungs, CIPF-affected lungs and PAC, and to investigate potential correlations with fibrosis severity and activity using both visual and digital quantitative analyses. In this fourth study, we also aimed to assess the potential of plasmatic FAP as a biomarker of CIPF using an enzyme-linked immunosorbent assay.

3. Development of a new FAP-based diagnostic and monitoring tool

FAP has emerged as a cellular marker of active fibrosis in CIPF-affected lung tissue. In humans, FAP-targeted PET/CT is increasingly being explored for interstitial lung diseases such as IPF, emerging as a promising non-invasive tool for monitoring disease progression and treatment response (Röhrich et al., 2022; Yang et al., 2023; Hotta et al., 2024; Mori et al., 2024). In human lung cancer, it also constitutes a highly promising diagnostic technique for lung cancer staging and treatment planning (Giesel et al., 2021; Röhrich et al., 2022; Wei et al., 2022, 2023).

Therefore, the fifth study aimed to assess the safety and feasibility of [^{18}F]FAPI-74 PET combined with CT in dogs, and to determine whether this approach enables in vivo detection of FAP expression in the lungs of dogs affected by CIPF, in comparison with healthy controls. This noninvasive imaging tool could facilitate monitoring of FAP expression, and thus of fibrosis activity, representing a promising method for diagnosing CIPF and assessing disease progression.

Experimental section

Experimental section

Study 1:

A single cell RNA sequencing atlas of the healthy canine lung:

a foundation for comparative studies

Preamble

scRNA-seq offers unprecedented insight into tissue cellular complexity, allowing for the identification of diverse cell types and their gene expression profiles. While comprehensive atlases of human lung cells, as well as canine BALF cells, have been published, the cellular and molecular landscape of the healthy canine lung remains largely unexplored. Given the growing recognition of dogs as relevant models for human lung diseases, owing to shared genetics, physiological features, and environmental exposures, as well as spontaneous disease occurrences, building a detailed map of canine lung cell types is valuable for both veterinary and translational research.

Using droplet-based scRNA-seq, we analyzed 26,278 cells derived from fresh healthy lung biopsies of four dogs. Samples included both post-mortem and tumor-adjacent non-affected tissues. After quality control, data integration, and clustering using Seurat, we identified 46 transcriptionally distinct cell populations spanning all major lung tissue compartments: immune (23 clusters), mesenchymal (13), epithelial (5), and endothelial (5). Our findings revealed a high degree of cellular diversity. Among mesenchymal cells, we identified six distinct fibroblast clusters, some of which expressed genes involved in immune regulation and inflammatory signaling. The immune compartment was particularly rich, with high-resolution identification of macrophage, monocyte, dendritic cell, and lymphoid subsets, including rare populations such as γδ T cells. Notably, $CCL13^{+}$ macrophages may represent interstitial macrophages, absent in previous studies focusing on BALF. Epithelial and endothelial cells were clearly distinguishable based on canonical markers and showed strong conservation with known human cell types. Integration of our dataset with the Human Lung Cell Atlas (HLCA) revealed a high degree of transcriptional homology between canine and human lung cells across all compartments.

Overall, this study provides the first single-cell atlas of the healthy canine lung, revealing rich cellular heterogeneity and novel markers and greatly expanding our understanding of lung cellular composition and gene expression in dogs. These findings lay a crucial molecular foundation for future investigations into lung diseases in dogs and support the utility of dogs as translational models for pulmonary research.

Experimental section

Study 1:

A single-cell RNA sequencing atlas of the healthy canine lung: a foundation for comparative studies

Frontiers in Immunology *16:1501603*

Elodie Rizzoli, Laurence Fievez, Aline Fastrès, Elodie Roels, Thomas Marichal, Cécile Clercx

Abstract

Single-cell RNA sequencing (scRNA-seq) can be used to resolve the cellular and molecular heterogeneity within a tissue by identifying cell populations with an unprecedented granularity along with their transcriptional signatures. Yet, the single cell gene expression profiles of cell populations in the healthy canine lung tissue remain unexplored and such analysis could reveal novel cell populations or markers lacking in dogs and facilitate comparisons with lung diseases. Using fresh healthy lung biopsies from four dogs, we conducted droplet-based scRNA-seq on 26,278 cells. We characterized 46 transcriptionally distinct cell subpopulations across all lung tissue compartments including 23 immune, 13 mesenchymal, five epithelial and five endothelial cell subpopulations. Of note, we captured rare cells such as unconventional T cells or Schwann cells. Differential gene expression profiles identified specific markers across all cell subpopulations. Fibroblasts clusters exhibited a marked transcriptional heterogeneity, some of which might exert immune regulatory functions. Finally, the integration of canine lung cells with an annotated human lung atlas highlighted many similarities in gene expression profiles between species. This study thus provides an extensive molecular cell atlas of the healthy canine lung, expanding our knowledge of lung cell diversity in dogs, and providing the molecular foundation for investigating lung cell identities and functions in canine lung diseases. Besides, the occurrence of spontaneous lung diseases in pet dogs, with phenotypes closely resembling those in humans, may provide a relevant model for advancing research into human lung diseases.

Introduction

Single-cell mRNA sequencing (scRNA-seq) enables high throughput and high-resolution transcriptomic analysis of the heterogeneity of cells within a population by profiling the transcriptome of each cell constituting a biological sample (Fastrès et al., 2020a). Extensive cell atlases of the human lung have been published and serve as highly valuable references for the analysis of diseased lung (Travaglini et al., 2020; Madissoon et al., 2023; Sikkema et al., 2023). Although scRNA-seq is still in its premises in non-conventional animal model species, it has already been validated in dogs for the identification and characterization of cellular subpopulations in the bronchoalveolar lavage fluid (BALF) of healthy dogs and dogs affected with canine idiopathic pulmonary fibrosis (Fastrès et al., 2020a, 2020b). However, analyzing BALF provides information over only a subset of lung cells and to date, the molecular state of all cells in canine lung tissue has not been investigated yet. A deep understanding of canine lung cell biology is crucial to decipher alterations occurring in parenchymal lung diseases. Such comparisons of cell subpopulations between healthy and diseased dogs should lead to a better understanding of the pathophysiology of lung diseases, which is of interest in the perspective of finding new treatment strategies.

Moreover, the canine species is increasingly recognized as a relevant species to understand human diseases. Indeed, dogs and humans share genetic, anatomical and physiological similarities, similar immune system and immune responses and the same environment and exposures (Paoloni and Khanna, 2007, 2008; Hytönen and Lohi, 2016; Dow, 2019; Chow et al., 2024). The similarities between the human and canine genomes are stronger than between human and mouse for many gene families including those related to cancer for instance (Paoloni and Khanna, 2008). Besides lung cancer (Lee et al., 2020), dogs can spontaneously develop other lung diseases, such as idiopathic pulmonary fibrosis (Clercx et al., 2018; Barnes et al., 2019) and pulmonary embolism (Johnson et al., 1999), that share features with human conditions, providing thus a model of spontaneously occurring disease. Although pet dogs would never replace experimental mouse models for preclinical mechanistic studies (Dow, 2019), studying the molecular foundations of pulmonary diseases in dogs would provide valuable complementary insights into the pathophysiology of spontaneous diseases.

Accordingly, the aim of the present study was to generate an extensive molecular cell atlas of the healthy canine lung using scRNA-seq and to establish gene expression profiles of all lung cells. Such atlas would provide foundation for investigating disease-related heterogeneity at single cell level.

Material and methods

1. Sample collection

Healthy canine lung tissues were collected either from dogs euthanized for reasons unrelated to this study, or from healthy regions of lung lobes resected for solitary lung tumors, ensuring a margin of at least 2 cm from the visible tumor edge. All dogs were privately-owned. Samples were collected with informed owner consent and under the local Animal Ethics Committee approval (#20-2245). In each dog, one parenchymal lung biopsy was collected directly after death or lobectomy and transported in HBSS (Gibco) containing 5% v/v of FBS (Gibco) on ice for immediate processing. Histopathological evaluation confirmed that the biopsy site was free of lung disease.

2. Sample preparation

Each lung sample underwent mechanical dissociation with razor blades and was suspended in HBSS + 5% FBS with collagenase A (1 mg/mL; Sigma) and DNase I (0.05 mg/mL; Roche) before incubation at 37°C for 45 min. The cells were then filtered through a 70 µm cell strainer (BD Falcon) and resuspended in PBS (Biowest) containing 10 mM EDTA (Merck Millipore). Red blood cells were lysed as needed with a lysis buffer containing 0.15 M NH4Cl, 0.01 M KHCO3 and 0.1 mM EDTA at pH 7.5. The final cell suspension contained between 500 and 1000 cells/µL in PBS containing 0.04% of BSA (Sigma) and 0.2 U/µL of RNase inhibitor (Roche). Final cell viability was assessed by trypan blue staining and considered acceptable above 70 percent.

3. Library preparation and sequencing

Approximatively 10,000 cells from each lung sample were loaded in a Chromium Controller or Chromium iX instrument (10x Genomics, Pleasanton, CA) and encapsuled with unique barcoded primers using the drop-sequencing method according to manufacturer's instructions. Emulsion breakage, cDNA amplification and libraries construction were performed using Chromium Single Cell 3′ reagent kit v2 (10x Genomics) according to manufacturer's instructions. Libraries were sequenced with a NextSeq500 system (Illumina, San Diego, CA) with a target of 20,000 reads per cell, which resulted in relatively low saturation (34.1, 55.0, 46.8 and 52.8 percent) but turned out to be sufficient to effectively delineate cell types. Raw sequencing data files (.bcl) were converted to FASTQ format using bcl2fastq v2.20.0.422 (Illumina) and Cell Ranger software version 9.0.0 (10x Genomics) was utilized for aligning sequencing reads in FASTQ files to the dog reference

transcriptome (CanFam3.1), filtering, counting unique molecular identifiers, and generating gene-barcode matrices.

4. Data filtering, integration and clustering

Filtered gene expression matrices were analyzed using Seurat R package version 4.3 (http://satijalab.org/seurat/). Beforehand, each sample was individually processed to eliminate doublets, low-quality or dying cells. Genes expressed in less than 10 cells were excluded, as well as cells expressing less than 200 genes or having more than 20 percent reads assigned to mitochondrial genes. Cell clusters co-expressing distinct canonical markers from two or more tissue compartments were considered as doublets and removed from the datasets. After combining datasets, each sample was normalized with SCTransform, regressing out the effects of the percentage of mitochondrial reads and of the cell cycle score, calculated with the "CellCycleScoring" function. Integration of individual samples was performed using normalized values from SCTransform and the top 3000 variables genes as anchors for canonical correlation analysis. Principal component analysis was used to perform linear dimension reduction and an elbow plot was used to determine the number of principal component analysis dimensions to select. Clustering was performed using the Louvain-graph-based algorithm in R and visualized by non-linear dimensional reduction using uniform manifold approximation and projection (UMAP) plots. Ideal clustering resolution was determined using the package clustree (Zappia and Oshlack, 2018). The following clustering parameters were used for the integrated dataset: res = 2.8, dims = 100, min.dist = 0.3. Each cluster was assigned to a tissue compartment using their expression of canonical marker genes (*EPCAM* for epithelial, *PTPRC* for immune, *PECAM1* for endothelial cells, the rest being mesenchymal cells). Each compartment was individualized, and integration and clustering were repeated in each subset as described above. The following dimension reduction and clustering parameters were used for final cell subsets; muscle: res = 0.9, dims = 15, min.dist = 0.35; fibroblasts: res = 0.7, dims = 5, min.dist = 0.35; myeloid: res = 1.8, dims = 60, min.dist = 0.35; lymphoid: res = 1.5, dims = 50, min.dist = 0.35; epithelial: res = 0.7, dims = 8, min.dist = 0.35; endothelial: res = 0.8, dims = 12, min.dist = 0.35. Cell cluster identities were determined based on their expression of canonical markers genes described in the literature and their lists of differentially expressed genes (DEGs).

5. Differential gene expression analysis

The FindAllMarkers function (with Wilcoxon rank sum test adjusted for multiple testing with Bonferroni correction) was used to identify DEGs across clusters. Only DEGs with adjusted $P<0.05$

were considered. When possible, differential expression analysis was also performed using DESeq2 after pseudobulk conversion (Love et al., 2014). Pseudobulk approach was used to compare cell clusters with limited heterogeneity and with at least 15 cells in each sample. DEGs with an adjusted $P < 0.05$ and a log2(fold change) > 0.58 were considered statistically significant. Using lists of significant positive DEGs, gene ontology (GO) analyses for biological processes were performed with the GO Consortium website (https://geneontology.org/; released on 2024/11/03). GO analyses were performed using Fisher's Exact test and Bonferroni correction for multiple testing. Statistically significant enrichments were then selected according to their biological relevance.

6. Data visualization

Clustering was visualized using uniform manifold approximation and projection (UMAP) plots. Gene expression was visualized using feature plots, violin plots and dot plots using SCTransform normalized counts. The absence of cancer cells in lung samples adjacent to a focal tumor was further validated by comparing the expression of growth factor receptor genes (*EGFR* and *ERBB2*) and proliferation marker genes (*PCNA* and *MKI67*) in split feature plots after downsampling the data to obtain equal cell numbers depicted in the feature plot for each condition.

7. Human lung homology analysis

A fully annotated healthy human lung dataset was obtained from the integrated Human Lung Cell Atlas (HLCA) core, which combines 584 944 healthy lung cells from 107 individuals, re-annotated to generate a consensus cell type reference (Sikkema et al., 2023). The lung parenchyma subset of the HLCA core was selected and downsampled to 50,000 cells to facilitate Seurat object management. The gene symbols from the human dataset were converted from human to canine using the convert_orthologs() function from the orthogene package (Schilder and Skene, 2022). The human and canine datasets were merged, normalized with SCTransform and integrated into one object using the same integration workflow as above. Cell type homologies between species were evaluated using an approach adopted from Ammons et al. (Ammons et al., 2023, 2024): The prefix 'can' or 'hu_' was added to canine and human cell type annotations, and hierarchical clustering was performed using the hclust() function with method set to "complete".

Results

1. Study sample summary

Healthy lung tissue biopsies were collected from four different dogs. Two post-mortem biopsies originated from dogs exempt from lung disease and two originated from the unaffected lung tissue adjacent to a focal primary pulmonary adenocarcinoma. Three biopsies were collected from the periphery of the right caudal lobe and one was collected from the periphery of the right cranial lobe. There were two female and two male dogs; two Pointers, one Cocker and one Beagle crossbreed. They were aged from 5 to 10 years (median 7 years) and weighed from 12 to 30 kg (median 18.8 kg). All samples were confirmed to be free of lung disease by histopathology.

2. Four lung tissue compartments are individualized

After tissue dissociation, scRNA-seq was performed on each sample. A total of 26,278 cells sequenced at a depth of 26,900 mean reads per cell passed quality control. A summary of sequencing and mapping quality control metrics for each sample is available in Table 1. After integration of samples in Seurat, four major lung tissue compartments were identified thanks to canonical markers expression (Figure 1A-D). The expression of *EPCAM* allowed the identification of epithelial cells, *PECAM1* (coding for CD31) of endothelial cells, *PTPRC* (coding for CD45) of immune cells, and cells expressing neither *EPCAM*, *PECAM1*, nor *PTPRC* were identified as mesenchymal cells (Habermann et al., 2020; Travaglini et al., 2020). Each individual sample contributed to all four tissue compartments without overt batch effect (Figure 1E-F). Subsequently, each compartment was individualized and re-clustering was performed within each subset.

Table 1. Summary of sequencing and mapping quality control metrics for each sample.

	g 1	**g 2**	**g 3**	**g 4**
nber of cells passing quality control	9	1	6	2
uencing saturation, %	.	)	3	3
ds mapped confidently to genome, %	5	5	3	.
ds mapped confidently to transcriptome, %	3	4	2	)
lian genes/cell	58		62	06
lian unique molecular identifier counts/cell	.0	79	30	71
al genes detected	455	372	019	335

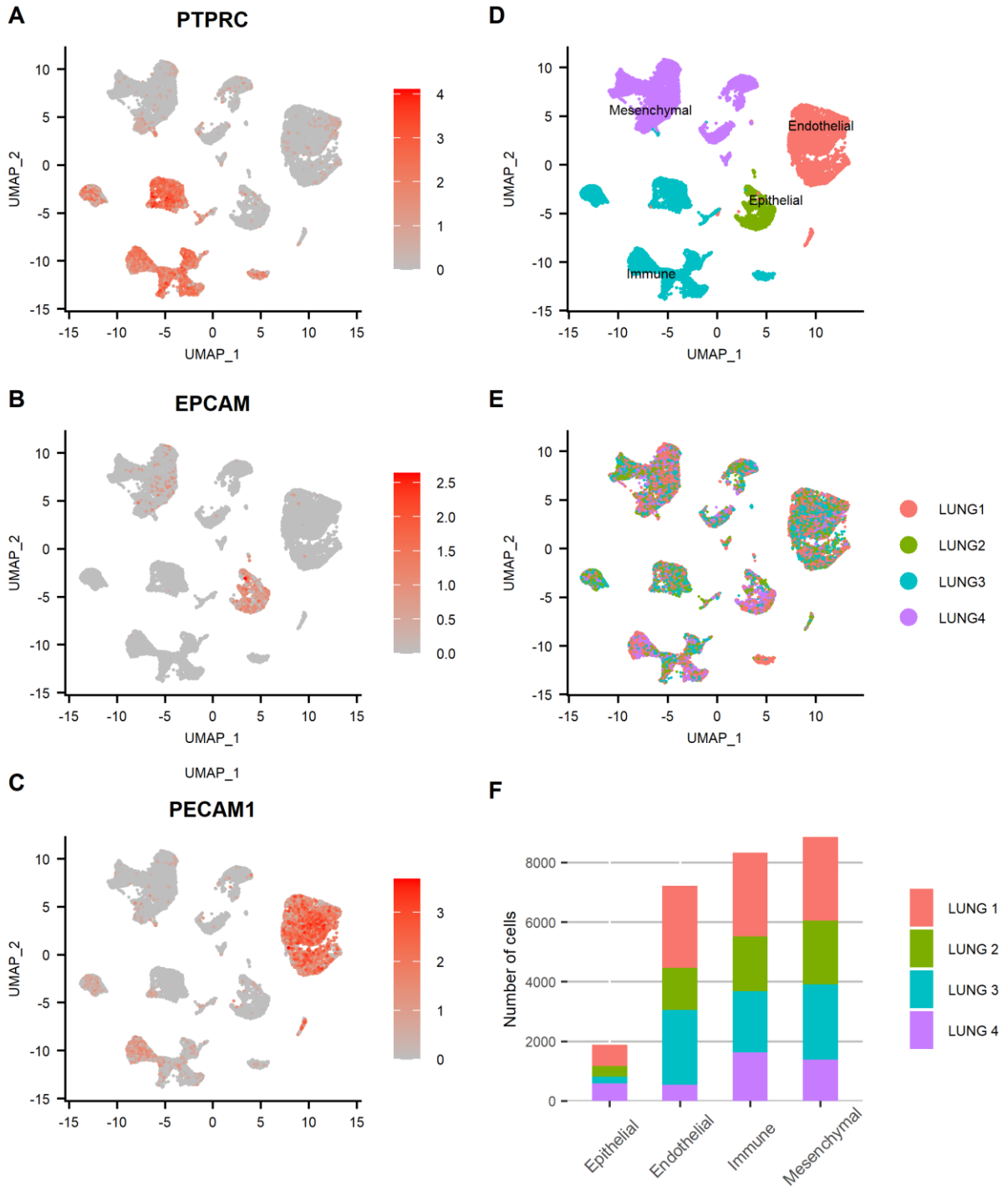

Figure 1. Four major lung tissue compartments were identified and evenly distributed among lung samples. (A-C) Feature plots representing the normalized expression of canonical markers used to discriminate lung tissue compartments (*PTPRC*: immune, *EPCAM*: epithelial, *PECAM1*: endothelial, other cells: mesenchymal). Color scales represent the expression level of each gene. UMAP representation of the cells of all lung samples annotated by (D) tissue compartment and (E) sample origin. (F) Bar plot showing the relative contribution of each sample to each tissue compartment.

3. Lung mesenchymal cells include muscle cells, fibroblasts and Schwann cells

The gene expression profiles of mesenchymal cells allowed their characterization into three sub-groups (Figure 2): muscle cells (expressing genes of contractility such as *ACTA2*, *TAGLN*, *MYH11*), fibroblasts (overexpressing genes coding for collagens such as *COL1A1* and matrix proteins) and Schwann cells (specifically expressing markers such as *SCN7A*, *NRXN1*, *CDH19* and *NCAM1*) (Tsukui et al., 2020; Narvaez Del Pilar et al., 2022; Madissoon et al., 2023). GO analysis based on Schwann cells DEGs revealed an enrichment in 'axonogenesis' and 'myelination' processes (detailed lists of enriched biological processes from all performed GO analyses are provided in Supplementary Table 1).

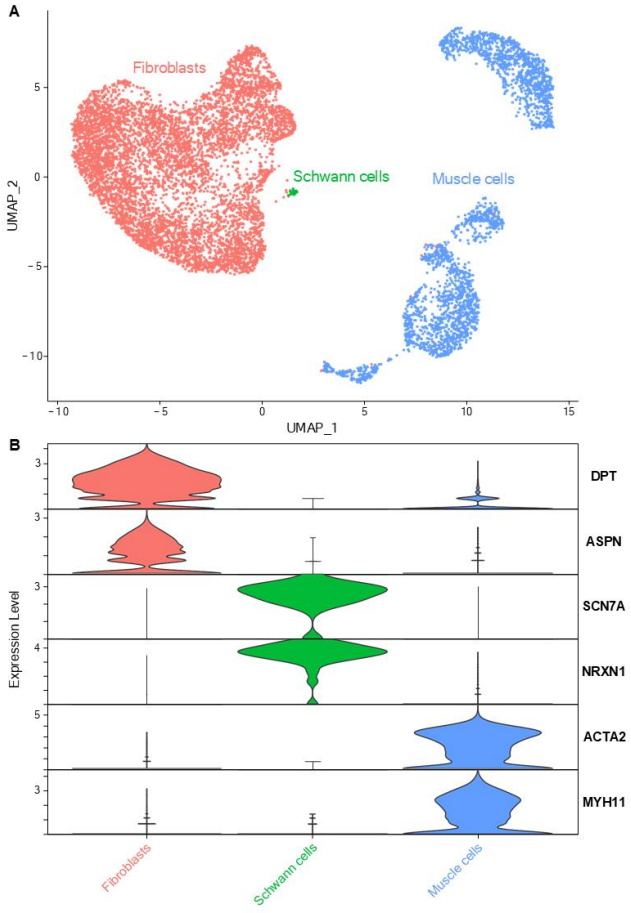

Figure 2. Lung mesenchymal cells. (A) UMAP representation of the three main mesenchymal cell types: fibroblasts, Schwann cells and smooth muscle cells. (B) Violin plots depicting the specific expression of key genes associated with each main cell type.

4. Lung fibroblast clusters exhibit a marked heterogeneity

Subclustering and analysis of fibroblasts allowed identification of six transcriptionally distinct clusters (Figure 3). The complete list of DEGs of each fibroblast cluster versus all other fibroblasts are provided in Supplementary Table 2. In accordance to the 3-axis classification for mesenchymal cells described in the literature (Narvaez Del Pilar et al., 2022), fibroblasts were annotated as either adventitial (proximal, located in the bronchovascular bundle) or alveolar (distal) fibroblasts.

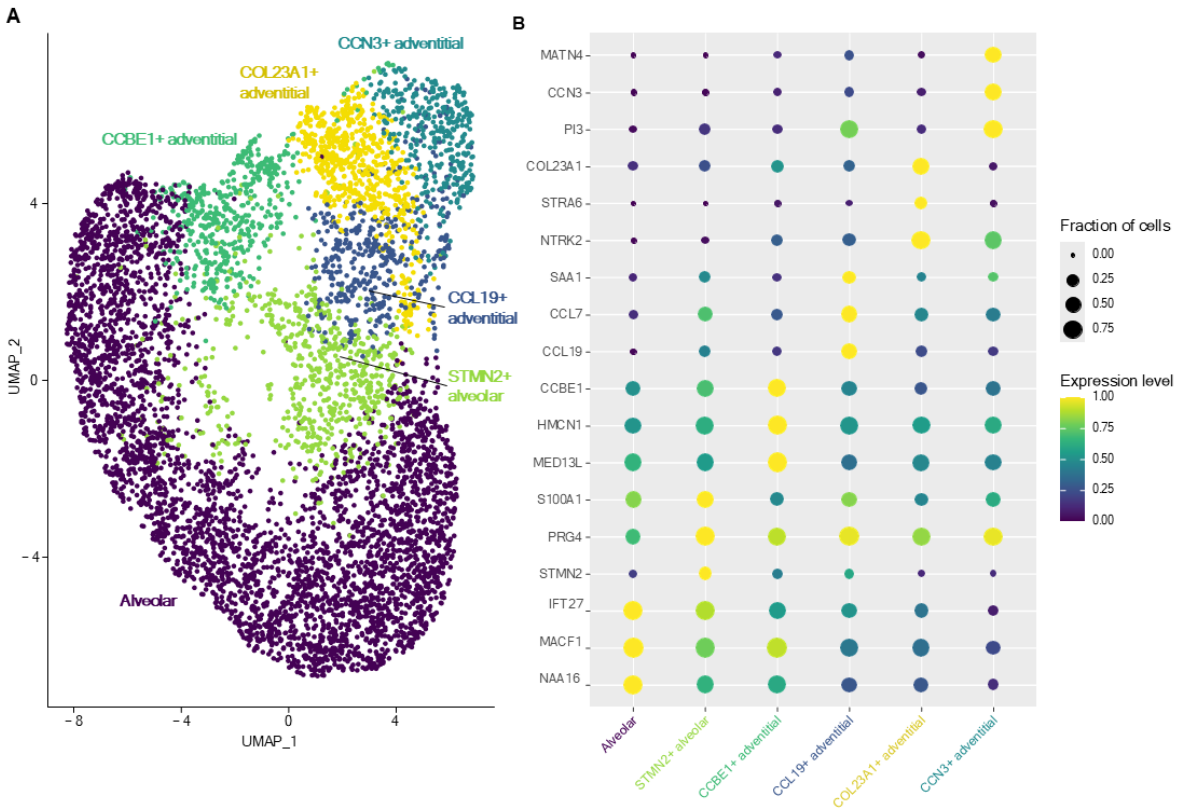

Figure 3. Lung fibroblasts. (A) UMAP representation of the six distinct fibroblasts clusters identified in canine healthy lungs. (B) Dot plot representing the specific expression of markers by different fibroblasts clusters.

Alveolar fibroblasts were annotated based on their overexpression of *COL13A1*, *WNT2*, *NPNT, FGFR4* and *GPC3* (Travaglini et al., 2020; Tsukui et al., 2020; Narvaez Del Pilar et al., 2022). One cluster of alveolar fibroblasts, referred to as '*STMN2*$^{+}$ alveolar fibroblasts' clustered separately from other alveolar fibroblasts. This cluster overexpressed genes such as *STMN2, PRG4, IL33, COL6A6* as well as cytokine and chemokine genes such as *CCL19*, *CXCL12*, *CCL7* and compared with alveolar fibroblasts, GO analysis revealed an enrichment in 'cytokine-mediated signaling pathway', 'inflammatory response' and 'positive regulation of cell population proliferation' (Table 2; Supplementary Table 1).

Table 2. Gene ontology analysis of the transcriptomic profiles of fibroblasts clusters.

Cluster	Biological process	Gene set	Upregulated	Expected	Fold enrichment	P-value
'*STMN2*$^+$ adventitial fibroblasts'	cytokine-mediated signalling pathway	295	11	1.11	9.9	9.40E-05
	regulation of inflammatory response	235	8	0.89	9.04	1.99E-02
	inflammatory response	304	9	1.15	7.86	1.46E-02
	positive regulation of cell population proliferation	547	12	2.06	5.82	6.30E-03
	regulation of cell migration	626	12	2.36	5.09	2.55E-02
'*CCL19*$^+$ adventitial fibroblasts'	leukocyte proliferation	86	10	1.18	8.47	1.98E-03
	cytokine-mediated signalling pathway	295	24	4.05	5.92	2.23E-08
	inflammatory response	304	20	4.18	4.79	6.05E-05
	regulation of inflammatory response	235	14	3.23	4.34	3.42E-02
	positive regulation of immune system process	678	33	9.31	3.54	2.22E-06
	regulation of cytokine production	502	23	6.89	3.34	3.55E-03
	immune system process	1516	51	20.82	2.45	1.70E-05
'*CCN3*$^+$ adventitial fibroblasts'	regulation of cell migration	626	41	15.43	2.66	1.03E-04
	positive regulation of cell population proliferation	547	34	13.49	2.52	6.00E-03
	regulation of transport	950	48	23.42	2.05	1.87E-02
	nervous system development	1414	68	34.86	1.95	7.41E-04
	tissue development	1170	56	28.85	1.94	1.52E-02
	regulation of developmental process	1511	68	37.25	1.83	1.10E-02
'*COL23A1*$^+$ adventitial fibroblasts'	positive regulation of cell migration	369	22	5.49	4.01	2.75E-04
	animal organ morphogenesis	671	28	9.98	2.8	6.87E-03
	regulation of cell population proliferation	972	37	14.46	2.56	1.14E-03
'*CCBE1*$^+$ adventitial fibroblasts'	circulatory system development	612	57	29.13	1.96	1.08E-02
	tube development	584	54	27.79	1.94	2.78E-02
	regulation of developmental process	1511	128	71.91	1.78	1.01E-06
	regulation of cell population proliferation	972	78	46.26	1.69	4.37E-02
	anatomical structure morphogenesis	1527	112	72.68	1.54	3.13E-02

Analyses were performed using lists of significant (P<0.05) positive differentially expressed genes between '*STMN2*$^+$ alveolar fibroblasts' and other alveolar fibroblasts, and between clusters of adventitial fibroblasts versus all other fibroblasts. 'Gene set' indicates the number of genes in the gene set, 'Upregulated' the number of genes from the gene set that are upregulated in the cluster, 'Expected' the number of genes from the gene set expected to be present if there is no enrichment.

Adventitial fibroblasts (overexpressing *COL14A1, GLI1* and *DCN*) (Tsukui et al., 2020; Narvaez Del Pilar et al., 2022) were divided into four clusters, named after their most specific marker. '*CCL19*$^{+}$ adventitial fibroblasts' overexpressed cytokine and chemokine genes (*CCL19, CCL7*), serum amyloid A1 (*SAA1*), fibroblast activation protein (*FAP*) and, compared with all other fibroblasts, GO analyses revealed significant enrichment in transcripts involved in inflammatory response and regulation of leukocyte proliferation (Table 2; Supplementary Table 1). '*CCN3*$^{+}$ adventitial fibroblasts' overexpressed cellular communication network factor 3 (*CCN3*), matrillin 4 (*MATN4*) and also *FAP*, while GO analyses identified biological processes such as 'regulation of cell migration', 'positive regulation of cell population proliferation' and 'regulation of developmental process' as significantly overrepresented (Table 2; Supplementary Table 1). '*COL23A1*$^{+}$ adventitial fibroblasts' overexpressed CXC motif chemokine ligand 14 (*CXCL14*), neurotrophic receptor tyrosine kinase 2 (*NTRK2*), signaling receptor and transporter of retinol (*STRA6*) as well as collagen type XXIII alpha 1 chain (*COL23A1*) and biological processes such as 'positive regulation of cell migration' and 'animal organ morphogenesis' were enriched in GO analyses (Table 2; Supplementary Table 1). The last cluster of adventitial fibroblasts, '*CCBE1*$^{+}$ adventitial fibroblasts', overexpressing mediator complex subunit 13L (*MED13L*), hemicentin-1 (*HMCN1*) and collagen and calcium binding EGF domains 1 (*CCBE1*), also had an increased expression of transcripts associated with morphogenesis processes such as 'circulatory system development', 'tube development' and 'regulation of developmental process' (Table 2; Supplementary Table 1). In summary, lung fibroblasts exhibited heterogeneity in transcriptional profiles, possibly reflecting substantial functional diversity.

5. Lung smooth muscle cells divide into airway and vascular axis

Smooth muscle cells were divided into six different cell subpopulations (Figure 4), each defined by specific DEGs compared with all other muscle cells (Supplementary Table 3). They were classified according to the two remaining axis of mesenchymal cells : airway and vascular axis (Narvaez Del Pilar et al., 2022). Airway axis was constituted, proximally to distally, by airway smooth muscle cells (overexpressing *ACTC1*) and by peribronchial myofibroblasts (overexpressing *SOSTDC1* and *FGF18*) (Narvaez Del Pilar et al., 2022; Madissoon et al., 2023). Vascular axis (*NOTCH3*$^{+}$) was composed of, proximally to distally, vascular smooth muscle cells and two clusters of pericytes, which exhibited lower expression of contractility genes (e.g. *ACTA2*, *TAGLN*, *MYH11*) (Travaglini et al., 2020; Tsukui et al., 2020; Narvaez Del Pilar et al., 2022). DEGs of the largest (*POSTN*, *FAM162B*, *HIGD1B*) and of the smallest pericyte cluster (*APOA1*, *ADRA2A*, *RGS16*, *COL12A1*, *CLU*) were previously described as markers of pericytes from the pulmonary and systemic circulation, respectively

(Madissoon et al., 2023). The remaining cluster expressed both markers of smooth muscle cells (*ACTA2*, *MYH11*) and fibroblasts (*DPT*, *ASPN*, collagens) and was thus annotated as 'myofibroblasts' (Habermann et al., 2020; Travaglini et al., 2020).

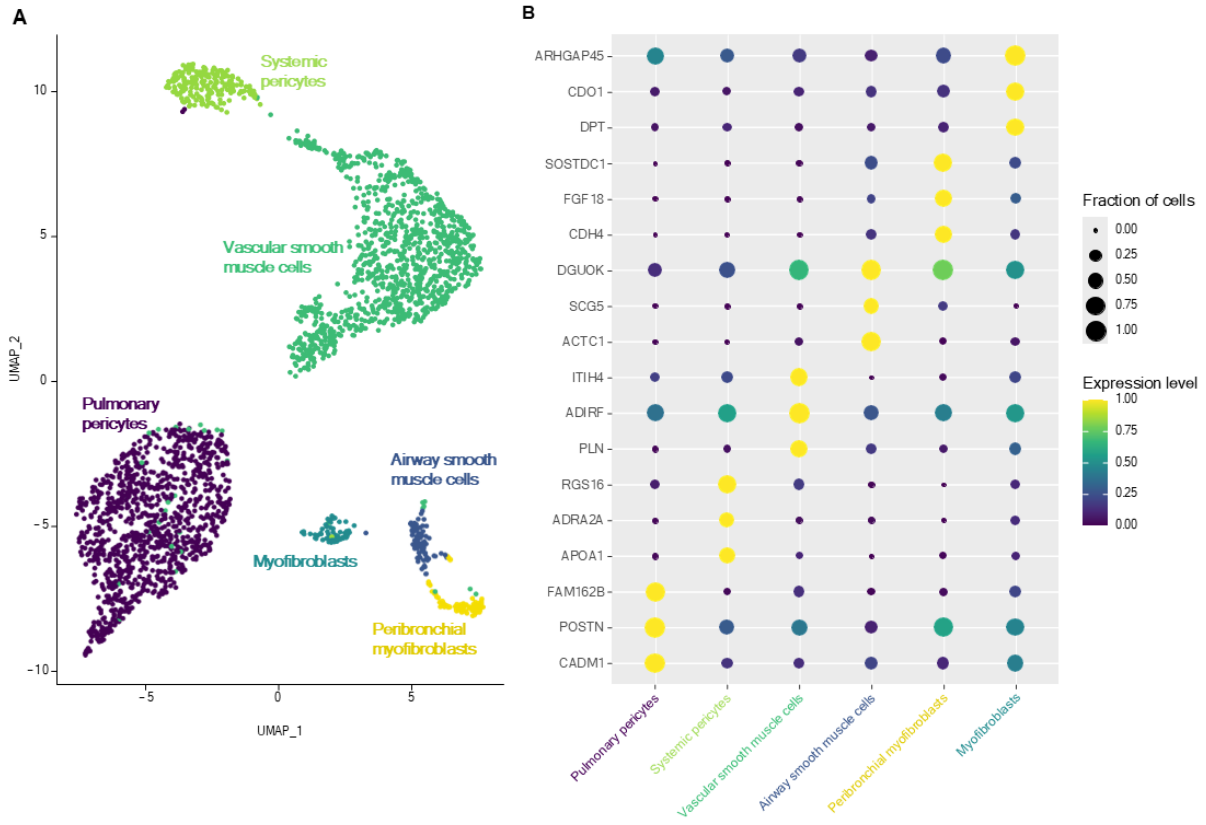

Figure 4. Lung smooth muscle cells. (A) UMAP representation of the six smooth muscle cell subtypes. (B) Dot plot representing the specific expression of muscle cell subtypes markers.

6. Lung immune cells are identified with high resolution

Lung immune cells were divided into myeloid and lymphoid cells, which were individualized for re-clustering to increase resolution. Myeloid cells were constituted of 13 subpopulations (Figure 5A and C; Supplementary Table 4), including seven clusters of macrophages and monocytes, four clusters of dendritic cells (DC), in addition to neutrophils and mast cells.

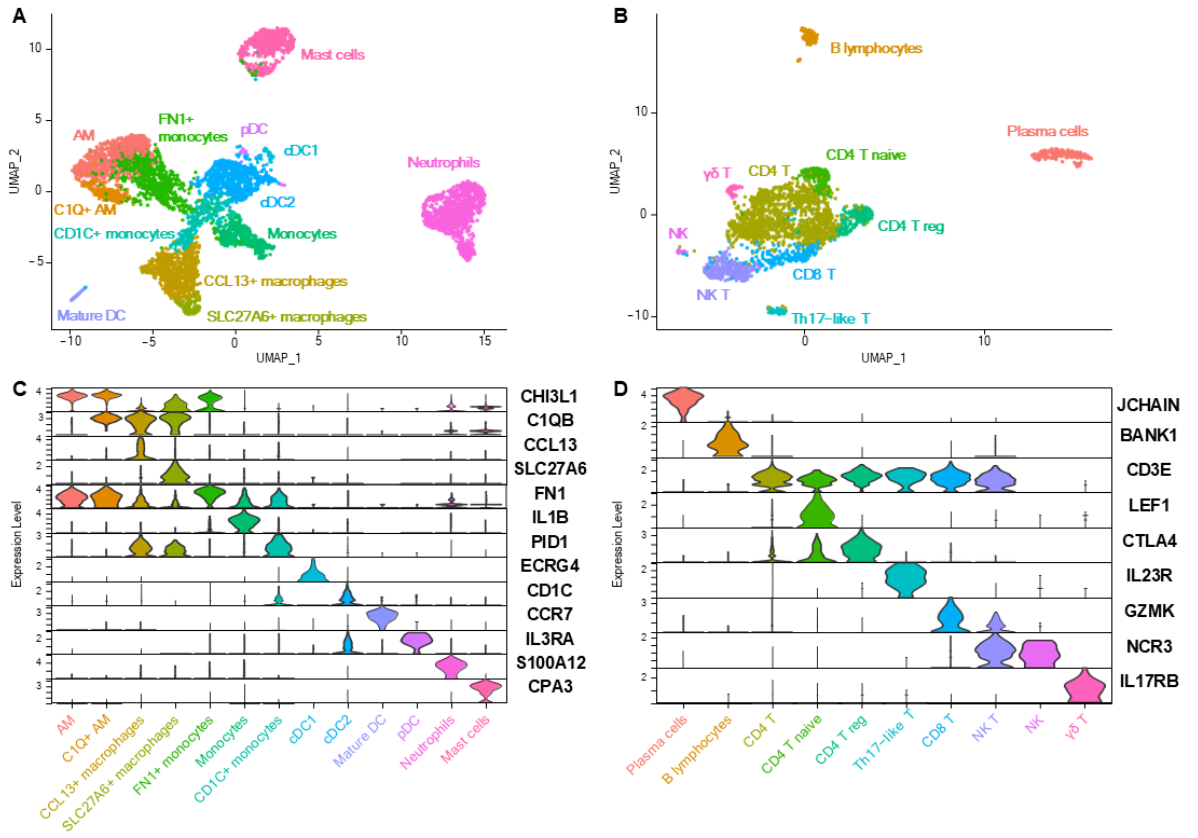

Figure 5. Lung immune cells. (A) UMAP representation of the 13 distinct myeloid cell clusters. (B) UMAP representation of the 10 distinct lymphoid cell subtypes. (C-D) Violin plots depicting the expression of key markers for each immune cell subtype.

Two clusters of alveolar macrophages (AM) were identified based on their overexpression of, among others, *MARCO*, *SIGLEC1* and *PPARG* (Patel and Metcalf, 2018; Fastrès et al., 2020a; Madissoon et al., 2023; Sikkema et al., 2023). The smaller AM cluster differed from the main cluster in its expression of genes of the complement component subunits (*C1QA, C1QB, C1QC*). Another macrophage cluster, named '*CCL13*$^{+}$ macrophages' overexpressed complement genes, cytokines and chemokines such as *CCL13*, *CCL14* and *CX3CX1,* as well as *STAB1, F13A1* and *LYVE1*. GO analyses based on DEGs between *CCL13*$^{+}$ macrophages and AM (Supplementary Table 5) identified enriched biological processes such as 'endocytosis', 'leukocyte chemotaxis', 'positive regulation of macromolecule metabolic process' (Table 3; Supplementary Table 1). '*SLC27A6*$^{+}$ macrophages' shared markers with '*CCL13*$^{+}$ macrophages' while DEGs compared with the latter (*SLC27A6*, *GPNMB*, *CTSK*, *DHDH*, *APOE*; Supplementary Table 5) revealed through GO analysis an enrichment in 'regulation of amyloid-beta clearance', 'positive regulation of endocytosis', 'negative regulation of protein metabolic process' (Table 3; Supplementary Table 1). Macrophage clusters seemed to exhibit a degree of overlap between gene expression profiles, especially regarding the expression of

MRC1, C1QA, C1QB, C1QC, as in humans, and as opposed to mice, in which the expression of those genes are restricted to one macrophage cluster (Zilionis et al., 2019).

Table 3. Gene ontology analysis of the transcriptomic profiles of specific monocytes or macrophages clusters.

Cluster	Biological process	Gene set	Upregulated	Expected	Fold enrichment	P-value
'*CCL13*$^+$ macrophages'	leukocyte chemotaxis	85	14	2.69	5.2	2.90E-03
	endocytosis	348	36	11.02	3.27	3.43E-06
	leukocyte differentiation	282	27	8.93	3.02	2.46E-03
	regulation of cell activation	400	31	12.67	2.45	4.83E-02
	positive regulation of immune system process	678	50	21.47	2.33	2.37E-04
	positive regulation of macromolecule metabolic process	2026	100	64.15	1.56	4.72E-02
'*SLC27A6*$^+$ macrophages'	regulation of amyloid-beta clearance	8	3	0.03	86.41	2.99E-02
	positive regulation of endocytosis	101	6	0.44	13.69	3.53E-02
	negative regulation of protein metabolic process	288	9	1.25	7.2	3.08E-02
'*FN1*$^+$ monocytes'	antigen processing and presentation of exogenous peptide antigen via MHC class II	24	8	0.26	31.07	6.74E-07
	peptide antigen assembly with MHC protein complex	19	5	0.2	24.53	9.59E-03
	positive regulation of endocytosis	101	9	1.08	8.3	9.77E-03
	regulation of cell activation	400	16	4.29	3.73	4.97E-02
	protein catabolic process	638	23	6.85	3.36	2.91E-03
'*CD1C*$^+$ monocytes'	peptide antigen assembly with MHC class II protein complex	15	5	0.18	28.53	3.91E-03
	antigen processing and presentation of exogenous peptide antigen via MHC class II	24	6	0.28	21.4	1.85E-03
	adaptive immune response	248	14	2.9	4.83	9.75E-03
	regulation of immune response	650	23	7.59	3.03	1.76E-02
	positive regulation of immune system process	678	23	7.92	2.9	3.53E-02

Analyses were performed using lists of significant (P<0.05) positive differentially expressed genes between '*CCL13*$^+$ macrophages' and 'Alveolar macrophages', between '*SLC27A6*$^+$ macrophages' and '*CCL13*$^+$ macrophages', between '*FN1*$^+$ monocytes' and 'Monocytes' and between '*CD1C*$^+$ monocytes' and 'Monocytes'. 'Gene set' indicates the number of genes in the gene set, 'Upregulated' the number of genes from the gene set that are upregulated in the cluster, 'Expected' the number of genes from the gene set expected to be present if there is no enrichment. MHC: major histocompatibility complex.

Monocytes overexpressed *IL1B*, *IL1A, EREG, VCAN* and *MAFB* (Schyns et al., 2019; Fastrès et al., 2020a). '*FN1*$^{+}$ monocytes', compared with other monocytes, overexpressed genes (such as *APOC1, C1QC, LMNA, HLA-DQB2*, *DLA-DRA*, *MRC1*; Supplementary Table 5) enriched in biological processes related to 'antigen processing and presentation', 'regulation of endocytosis' and 'protein catabolic process' (Table 3; Supplementary Table 1). '*CD1C*$^{+}$ monocytes', compared with other monocytes, overexpressed genes (such as *PKIB, MRC1, HLA-DBQ2, DLA-DQA1, FCER1A* ; Supplementary Table 5) enriched in biological processes related to 'antigen processing and presentation', 'adaptive immune response' and 'regulation of immune response' (Table 3; Supplementary Table 1) and might represent a transitional state towards DC or monocyte-derived DC.

Four different types of DC were identified based on their expression profiles: plasmacytoid DC, mature DC, myeloid/conventional DC 1 (cDC1), and myeloid/conventional DC 2 (cDC2) (Patel and Metcalf, 2018; Fastrès et al., 2020a; Madissoon et al., 2023; Ammons et al., 2023, 2024). Among notable genes, *IDO1*, an immunotherapy target expressed by mature DC, is also expressed by human DC, while being expressed at very low levels in mouse DC (Zilionis et al., 2019; Guo et al., 2023). Neutrophils were recognizable thanks to their overexpression of *S100A12* or *SELL* (Fastrès et al., 2020a; Ammons et al., 2023) and mast cells expressed very specific markers such as *KIT*, *CPA3* or *MS4A2* (Fastrès et al., 2020a; Habermann et al., 2020; Travaglini et al., 2020). No eosinophils nor basophils were identified.

Lymphoid cells were also characterized with a very high resolution, allowing the profiling of 10 cell clusters (Figure 5B and D; Supplementary Table 6). The expression of *CD3E* allowed the discrimination of T lymphocytes from other lymphoid cells (Fastrès et al., 2020a; Travaglini et al., 2020). Besides the main group of *CD4*$^{+}$ T cells (expressing *CD4*, *IL7R*, *THY1*), three additional *CD4*$^{+}$ T subpopulations could be further discriminated and classified as naïve T cells (expressing *CCR7*, *LEF1*, *SELL*), regulatory T cells (with higher expression of *CTLA4* and *TNFRSF4*) and Th17-like T cells (expressing genes of Th17-associated proteins *IL23R*, *IL17A, CCR6* and *RORA*) (Travaglini et al., 2020; Eschke et al., 2023; Ammons et al., 2023). *CD8A*$^{+}$ T cells comprised *CD8*$^{+}$ cytotoxic T cells (expressing cytokines and cytotoxicity-associated markers such as granzyme and killer cell lectin-like receptor genes) and natural killer (NK) T cells (expressing *NCR3* in addition to other genes of proteins associated with cytotoxicity) (Travaglini et al., 2020; Eschke et al., 2023; Ammons et al., 2023). A last cluster of T cells was identified as 'γδ T cells' (overexpressing *IL17RB* and *GATA3*) (Ammons et al., 2023). A small cluster of NK cells (negative for *CD3E* but expressing *NFKBID*, *NCR3*, *KLRK1*, *CD96*) was

also identified (Habermann et al., 2020; Gingrich et al., 2021; Ammons et al., 2023). Forming two distant clusters, B lymphocytes (*FCRLA*$^{+}$) and plasma cells (*JCHAIN*$^{+}$) were present as well (Travaglini et al., 2020; Fastrès et al., 2020a; Habermann et al., 2020; Madissoon et al., 2023).

7. Epithelial and endothelial cells markers cluster according to canonical cell types

Lung epithelial cells clustered into five different cell types, and each exhibited their own transcriptional profile (Figure 6A and B; Supplementary Table 7). Conservatively to human data (Travaglini et al., 2020; Habermann et al., 2020; Madissoon et al., 2023), canine lung epithelial cells spread into alveolar type 2 cells (overexpressing genes of surfactant proteins and napsin A protein, the latter being used as a lung carcinoma marker in dogs), alveolar type 1 cells (expressing *AGER*), secretory cells (expressing *SCGB1A1*, *MUC5B*), basal cells (expressing *KRT14* and transcription factor *TP63*) and ciliated cells (expressing *CAPS*, *FOXJ1*, *CCDC78*, *HYDIN*). The expression levels of growth factor receptor genes (*EGFR* and *ERBB2*) and proliferation marker genes (*PCNA* and *MKI67*) in epithelial cells were not significantly higher in unaffected lung samples adjacent to a focal tumor compared with samples originating from healthy lungs (Supplementary Figure 1). Moreover, enrichment analysis did neither reveal cancer-associated genes (Supplementary Table 8) nor enrichment in cancer-associated biological processes (Supplementary Table 1) in epithelial cells from unaffected tumor-adjacent lung samples as compared to those from lung samples of dogs exempt of lung disease.

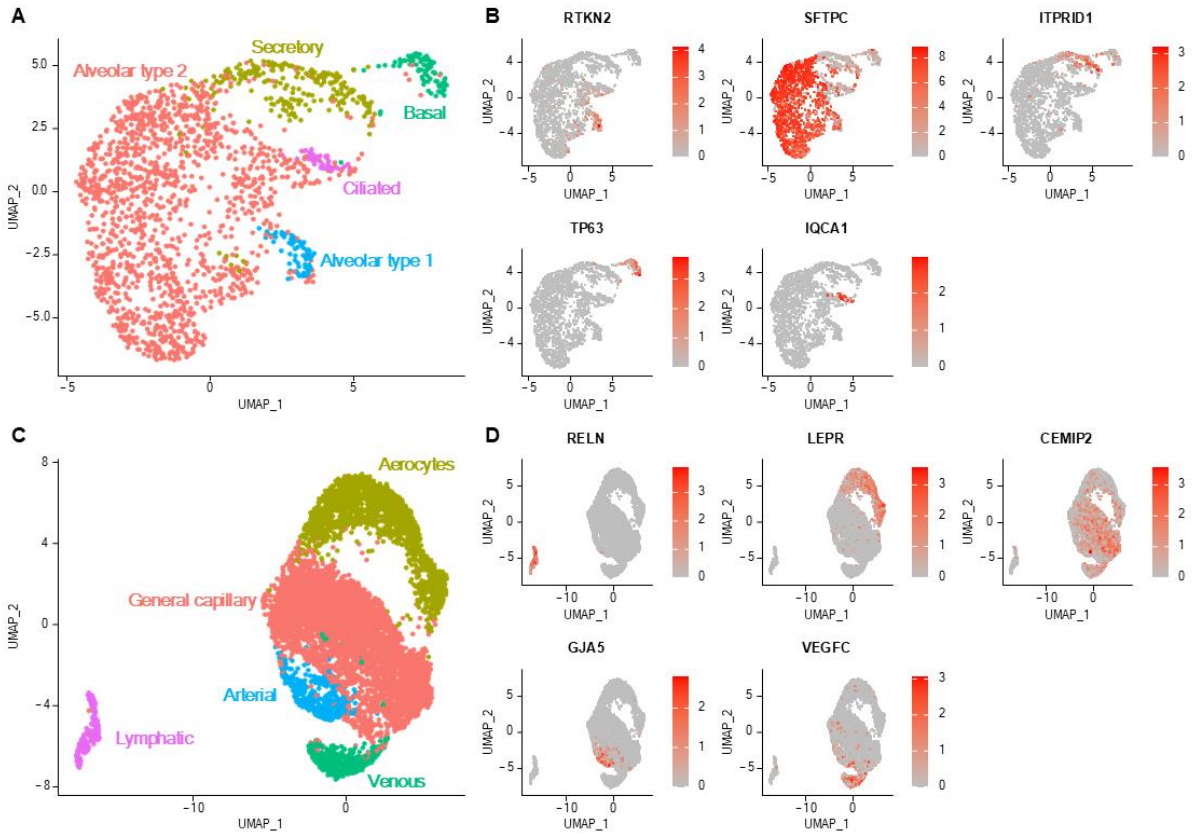

Figure 6. Lung epithelial and endothelial cells. (A) UMAP representation of the five distinct epithelial cell subtypes. (B) Feature plots depicting the normalized expression level of specific markers for each epithelial cell type. Color scales represent the expression level of each gene. (C) UMAP representation of the five distinct endothelial cell subtypes. (D) Feature plots depicting the normalized expression level (red color scale) of specific markers for each endothelial cell type.

Lung endothelial cells were distributed into five cell clusters (Figure 6C and D; Supplementary Table 9). Lymphatic endothelial cells were distinguished from vascular endothelial cells with their low expression of *VWF* (a vascular endothelial cell marker) and their overexpression of specific markers (including *PDPN* and *PROX1*) (Travaglini et al., 2020; Schupp et al., 2021). Vascular endothelial cells were divided into endothelial cells constituting capillaries of the pulmonary circulation, namely aerocytes (also exhibiting low *VWF* expression), capillaries of the general circulation (general capillary endothelial cells), arteries (with comparatively higher *GJA5* and *BMX* expression) and veins (higher *ACKR1* expression) (Travaglini et al., 2020; Schupp et al., 2021).

8. Summary of canine lung cell transcriptional diversity

By combining all cell compartments, a total of 46 different cell clusters were identified, constituting an extensive atlas of canine lung cells. A summary of transcriptional signatures of each of the 46 cell clusters is provided in Table 4 and complete lists of DEGs of one cell cluster versus all

other lung cells are reported in Supplementary Table 10. The contribution of each lung sample to every cell cluster is documented as raw counts (Supplementary Table 11) and percentages (Supplementary Figure 2). Overall, all four samples contributed to nearly every lung cell cluster, enhancing the cellular diversity of the single-cell atlas. Notable exceptions were mast cells, with 87 percent originating from Lung 1 despite being present in all samples; Schwann cells, with 94 percent derived from Lung 3 and none detected in Lung 4 (which provided the lowest total number of cells), and ciliated cells, which were absent from Lung 2.

Table 4. Summary of the transcriptional signatures of canine lung cells.

Cell type	Markers
Mesenchymal cells	
Schwann cells	*NRXN1, CDH19, SCN7A, SNCA, NTNG1, NRN1, MPZ*
Muscle cells	***ACTA2, TAGLN, MYH11***
Pericytes (pulmonary circulation)	*CADM1, POSTN, FAM162B, F3, SLC4A4, ENPP2, HIGD1B, PAG1*
Pericytes (systemic circulation)	*APOA1, ADRA2A, PDE1A, COL12A1, IL33, ADGRF5, RGS16*
Vascular smooth muscle cells	*PLN, ADIRF, DSTN, ITIH4, FAM13C, DGUOK, MAP1B, FABP3*
Airway smooth muscle cells	*ACTC1, SCG5, SEMA3C, NWD2, CACNA2D3, MT3, TENM1*
Peribronchial myofibroblasts	*CDH4, CCBE1, FGF18, MFAP5, SOSTDC1, ADAMTS6, EPHA7, SMOC2*
Myofibroblasts	*NKAIN3, CADM2, COL6A5, C3, PTPRD, DPT, ADRA1A, GPM6B*
Fibroblasts	***COL1A1***
Alveolar fibroblasts	*NAA16, MACF1, SPECC1L, IFT27, VEGFD, NPNT, ASPN*
STMN2$^+$ alveolar fibroblasts	*STMN2, PRG4, IL33, COL6A6, CCL7, CCBE1, S100A1*
CCBE1$^+$ adventitial fibroblasts	*MED13L, HMCN1, SETBP1, CCBE1, ZFPM2, COL6A6, XYLT1*
CCL19$^+$ adventitial fibroblasts	*PI3, CCL19, CCL7, FAP, F3, NFKBIA, SAA1, CXCL12*
CCN3$^+$ adventitial fibroblasts	*PI3, CCN3, RIT2, MATN4, PCOLCE2, SMOC2, GPC6, RBP4*
COL23A1$^+$ adventitial fibroblasts	*AQP1, NRTK2, LAMA2, LSP1, STRA6, SNF385D, COL23A1, PLCL1*
Immune cells	***PTPRC***
Myeloid immune cells	
Alveolar macrophages (AM)	*CHI3L1, CPNE6, CLU, GDE1, CDC42EP3, BPI, MARCO, PPARG*
C1Q$^+$ AM	*C1QB, C1QC, C1QA, RDH16, CHI3L1, CPNE6, MARCO, PPARG*
CCL13$^+$ macrophages	*CCL13, C1QC, STAB1, PID1, F13A1, PLTP, CCL14, CCL8, C1QA*
SLC27A6$^+$ macrophages	*SLC27A6, PLTP, TREM2, MMP2, CTSK, STAB1, DHDH, GPNMB*
Monocytes	*IL1B, EREG, IL37, SNAI1, VCAN, SERPINB2, IL1A, CCL3, MAFB*
FN1$^+$ monocytes	*FN1, SMPDL3A, LMNA, RBP4, GLDN, IL1A, MAFB, APOC1*
CD1C$^+$ monocytes	*PID1, IL1RN, IL1R1, ATF3, MMP12, LYZ, MAFB, CD1C*
Myeloid/conventional DC 1	*CLNK, ECRG4, CLEC1B, HOOK1, DOCK5, DLA-DOA, CADM1, IRF8*
Myeloid/conventional DC 2	*PKIB, NAPSA, NCAM2, NR4A2, DLA-DOA, TRABD2A, PPM1J, CD1C*
Mature DC	*CCR7, SLC22A23, SLCO5A1, IDO1, PLEKHG1, FSCN1, IL4I1, CD40*
Plasmacytoid dendritic cells (DC)	*GPHA2, SHANK2, IL3RA, SPATA6, IGKC, HMGCS1, PPM1J, TCF4*
Neutrophils	*S100A12, S100A9(ENSCAFG00000029470), IL18BP, SAT1, CXCL8, SOD2, CD4, SELL*
Mast cells	*CPA3, MS4A2, MAGI2, CMA1, KIT, SYTL3, FCER1A, HPGDS*
Lymphoid immune cells	
CD4 T lymphocytes	*JAZF1, IL7R, S100A8, LGALS3, INPP4B, ICOS, S100A5, CD3E*
CD4 naïve T cells	*CCR7, LEF1, CTPS1, RGS10, SELL, IGF1R, TLE1, USP12*
CD4 regulatory T cells	*CTLA4, DBX2, TNFRSF4, TNFRSF18, IKZF2, LGALS3, CD28*
Th17-like T cells	*IL23R, BLK, IL1R1, CPNE8, SYNDIG1, IL1R2, IL17A, CCR6, RORA*
CD8 cytotoxic T cells	*CCL5, CCL4, GZMK, CCL3, KLRK1, CTSW, GZMB, CD8A*
Natural killer T cells	*NCR3, KLRD1, GZMB, KLRB1, GZMA, TXK, KLRK1, FASLG*
Natural killer cells	*SNCG, F2RL3, KLRB1, FCER1G, KLRK1, CRTAM, NCR3, CD96*
γδ T cells	*PTGES, PDE7B, PDE11A, IL17RB, CRLF2, IL1RL1, SLC4A4, GATA3*
B lymphocytes	*ARHGAP24, BANK1, TNFRSF13C, BCL11A, DLA-DOA, FCRLA, MS4A1, CCR7*
Plasma cells	*JCHAIN, MZB1, POU2AF1, TNFRSF17, DERL3, TXNDC5, FKBP11, RARRES2*
Epithelial cells	***EPCAM***
Alveolar type 1 cells	*RTKN2, ZNF365, SEMA6D, CAV2, CAV1, TIMP3, AGER*
Alveolar type 2 cells	*SFTPC, NAPSA, C5, LRRK2, SLC34A2, ACOXL, SFTPB, SFTPD*
Secretory cells	*ITPRID1, KCNIP4, SCGB1A1, AQP5, GPX2, CHL1, CLEC10A, NAV3*
Basal cells	*TP63, IL33, CNTNAP5, RNASE4, GABRE, CLDN1, SEMA5A, COL21A1*
Ciliated cells	*IQCA1, DCDC1, DNAH5, RIBC2, ROPN1L, CFAP126, TNNI3, MORN5*
Endothelial cells	***PECAM1***
Lymphatic endothelial cells	*RELN, NRP2, KCTD12, TSHZ2, MRC1, PROX1, LSP1, TBX1, PDPN*
Aerocytes	*LEPR, CFI, PLXNC1, CNTNAP2, KDR, EMP2, RGS6, EDNRB*
General capillary endothelial cells	*LYVE1, SPARCL1, CEMIP2, PTPRB, CADM1, CD36*
Arterial endothelial cells	*PDE3A, GJA5, BMX, BMPER, CLU, MECOM, MGP, LTBP4*
Venous endothelial cells	*VEGFC, ADGRG6, RNF144B, SELP, TIMP1, ACKR3, VCAM1, ACKR1*

9. Human lung homology analysis

The final annotated dataset combining all canine lung cell types was integrated with a single-cell reference atlas of the healthy human lung (Sikkema et al., 2023). Hierarchical clustering allowed the evaluation of cell type homologies between species. Even considering the differences in the level of final cell type annotations, canine lung cells showed a high degree of homology to human lung cells within each tissue compartment (Supplementary Figure 3). All endothelial cell types, and almost all epithelial cell types, except for basal cells, paired off 1:1 in terminal clades, suggesting a high degree of similarity. Among immune cells, canine and human mast cells, B lymphocytes, CD4 T cells, CD8 T cells, plasma cells DC1, DC2, mature (migratory) DC, alveolar macrophages also paired off 1:1 in terminal clades. Within mesenchymal cells, canine and human alveolar fibroblasts clustered together, and human adventitial fibroblasts clustered on the same clade as all four canine adventitial fibroblasts clusters. We also identified subtle differences between species. For example, canine *CD1C*$^{+}$ monocytes clustered with human DC2, which would strengthen the hypothesis that this cluster might represent a transitional state towards DC. While canine pericytes from the pulmonary circulation paired perfectly with human pericytes, canine pericytes from the systemic circulation seemed more similar to other canine and human smooth muscle cells. Additionally, canine '*STMN2*$^{+}$ alveolar fibroblasts' paired 1:1 with human peribronchial fibroblasts. Taken together, the cross-species analysis underscores the similarities in lung cell transcriptional profiles, while also drawing attention to potential differences between the two species.

Discussion

This scRNA-seq atlas of healthy canine lung identified 46 transcriptionally distinct cell clusters and provided the molecular signatures for each of them, increasing considerably our knowledge of canine lung cellular biology and diversity. Our analysis revealed six distinct fibroblasts clusters. Such heterogeneity may reflect a diversity of fibroblasts activation states and possibly various functions, as some fibroblast clusters seem involved in immune regulatory functions. Regarding immune cells, the high resolution of the present analysis allowed the identification of rarer cell types such as γδ T cells, unconventional T cells that were already described in canine peripheral blood by scRNA-seq (Ammons et al., 2023; Eschke et al., 2023). Additionally, lung smooth muscle cells, epithelial cells and endothelial cells were relatively easily identified using classification systems and markers described in humans (Travaglini et al., 2020; Schupp et al., 2021; Madissoon et al., 2023; Sikkema et al., 2023). Finally, homology analysis between canine and human lungs showed a high degree of similarity in lung cell transcriptional profiles while also highlighting potential differences.

In the literature, there is no description of single cell expression profiles of fibroblasts subsets in dogs. Indeed, in existing studies, fibroblasts are either absent, e.g. in BALF (Fastrès et al., 2020a, 2020b), or are presented as a one entity (Shi et al., 2022; Ammons et al., 2024; Manchester et al., 2024). After integration, canine alveolar and adventitial fibroblasts from our dataset mapped with human alveolar and adventitial fibroblasts, respectively, except for the cluster of '*STMN2*$^+$ alveolar fibroblasts' mapping with human and canine adventitial fibroblasts, which might suggest some continuum in fibroblasts transcriptional profiles. Interestingly, we could find particular resemblances between some fibroblast clusters present in our datasets and fibroblast subpopulations newly described in the healthy human lung (Madissoon et al., 2023). '*CCL19*$^+$ adventitial fibroblasts' shared markers (such as *CCL19* and *CXCL12*) with a fibroblast subset likely exerting immune-recruiting properties and mapped to rare immune infiltrates in the bronchus (Madissoon et al., 2023). Interestingly, '*CCL19*$^+$ adventitial fibroblasts' and '*CCN3*$^+$ adventitial fibroblasts' overexpressed fibroblast activation protein *(FAP*), a marker of activated fibroblasts and cancer-associated fibroblasts, including in canine idiopathic pulmonary fibrosis and canine lung cancer (Rizzoli et al., 2024). '*COL23A1*$^+$ adventitial fibroblasts' shared key markers (*COL15A1*, *ENTPD1*, *PLCL1*) with peribronchial fibroblasts, a subpopulation specifically localized around the airway epithelium, which is enriched in idiopathic pulmonary fibrosis and may be implicated as a key cell type in lung disease (Madissoon et al., 2023). Regarding other mesenchymal cells, the cluster of lung

pericytes from the systemic circulation shares a dozen specific markers (including *APOA1, ADRA2A, RGS16* and *ADAMTS4*) with a cluster of *APOA1*$^{+}$ smooth muscle cells described in canine arteries (Shi et al., 2022).

Although scRNA-seq studies conducted so far on different canine samples (Ammons et al., 2024, 2023; Eschke et al., 2023; Fastrès et al., 2020a, 2020b; Manchester et al., 2024) have provided valuable help, the classification of lung immune cells, especially monocyte and macrophages, remained challenging. Indeed, conventional markers arising from human and mouse studies are sometimes unhelpful for cell identification in dogs, due to incomplete annotation of the canine genome, species differences regarding transcriptome, or occasional low transcript abundance (Ammons et al., 2023). For example, *CD14* and *CD16*, often used to characterize monocyte populations, lack annotation in the reference transcriptome used in this study (CanFam3.1). In this study, alveolar macrophages shared their most statistically significant makers (including embryonic-derived AM marker *MARCO*) with the cluster of alveolar macrophages mainly populating healthy canine BALF (Fastrès et al., 2020a). *FN1*$^{+}$ monocytes shared top markers with a cluster of *MARCO*$^{-}$*FN1*$^{+}$ macrophages from canine BALF, enriched in cytokine genes, which was considered as monocyte-derived macrophages or monocytes (Fastrès et al., 2020a). In canine lungs, *FN1*$^{+}$ monocytes and '*SLC47A6*$^{+}$ macrophages both expressed *SPP1*, which is a marker of monocyte-derived macrophages in the integrated human lung cell atlas (Sikkema et al., 2023). Interestingly, *FN1*$^{+}$*SPP1*$^{+}$ monocyte-derived macrophages are believed to be involved in the pathogenesis of canine idiopathic pulmonary fibrosis (Fastrès et al., 2020b, 2023) and profibrotic *SPP1*$^{+}$ monocyte-derived macrophages were also reported in human COVID-19, pulmonary fibrosis and lung cancer (Sikkema et al., 2023). Using the overexpression of a combination of human (Patel and Metcalf, 2018; Sikkema et al., 2023) and mouse (Gibbings et al., 2017; Schyns et al., 2019; Chakarov et al., 2019; Chaudhary et al., 2022) markers (*CX3CR1, F13A1, STAB1, LYVE1, C1QA, C1QC, C1QB*), *CCL13*$^{+}$ macrophages may be classified as interstitial macrophages. Furthermore, this cluster did not match any cluster present in canine BALF, which did not contain any interstitial macrophages (Fastrès et al., 2020a, 2020b). *CCL13*$^{+}$ macrophages shared markers (*STAB1, C1QA, C1QC, C1QB, CCL7*) with macrophages identified in canine duodenum (Manchester et al., 2024), another tissue containing postnatal-derived macrophages which have a phenotype similar to interstitial macrophages in mice (Gibbings et al., 2017). Additionally, the gene expression profiles of immune cells did not allow us to discriminate lung-resident from intravascular immune cells using lung immune cell residency signatures as reported in humans (Travaglini et al., 2020), possibly because resident and circulating cells clustered together and were not distinguishable, or because we lack appropriate discriminating markers in

dogs. Additional studies with a spatial component would be highly valuable to confirm the localization of cell subpopulations in the tissue, particularly when performing comparisons with diseased tissues, to better understand the nature and localization of cells implicated in the disease pathophysiology.

This study has some limitations that warrant consideration. As only four dogs were used for this study, all cell populations from healthy canine lungs may not be fully represented. Since the cell type proportions differed between individuals, the transcriptome of some cell types may be driven primarily by one sample (e.g.: mast cells in Lung 1), suggesting that increasing the number of healthy lung samples could provide a more accurate and comprehensive representation of all lung cell transcriptomes. However, the study included dogs that were middle to old adults, representing three different breeds and sizes to approximate the diversity of healthy canine lung cell populations.

Moreover, the tissue dissociation process, an essential step in scRNA-seq, is another factor that may influence the relative proportions of cell types. While dissociation must be efficient enough to release hard-to-dissociate cells, proteolytic digestion at 37°C can be harsh on more sensitive cell types (Denisenko et al., 2020). This stress can lead to changes in gene expression, such as the upregulation of heat shock proteins, or the depletion of fragile cell populations, including epithelial cells, which may consequently be underrepresented in the final data (Denisenko et al., 2020). Hence the relative abundance of each cell type should be interpreted with caution.

Furthermore, one strength of scRNA-seq is its ability to define the gene expression profiles of diverse cell populations within a sample (Travaglini et al., 2020). However, certain cell types may remain uncaptured due to their extreme rarity or the need for specialized isolation methods (Travaglini et al., 2020). For instance, as in similar studies with lung tissue, eosinophils were absent from our dataset, likely due to their high RNase content causing rapid mRNA degradation (Fastrès et al., 2020a; Travaglini et al., 2020; Madissoon et al., 2023). Unexpectedly, mesothelial cells were not identified in our dataset due to the absence of expression of known mesothelial cell markers (*MSLN, CALB2, UPK3B, KLK11, ITLN1*). Although mesothelial cells are expected in peripheral lung samples, they still constitute a very rare cell type in single cell data, representing only 0.07 percent of all lung cells in the HLCA (Sikkema et al., 2023).

Additionally, our findings would greatly benefit from subsequent spatial validation. While scRNA-seq provides valuable transcriptional insights, it lacks spatial context, which is essential for understanding the differentiation, localization and functional roles of these cell types within the

lung microenvironment. In situ validation – whether through smFISH for RNA detection or, even more critically, protein-based approaches such as immunostaining – would offer a more comprehensive and robust picture of these subsets. Given that mRNA expression does not always correlate with protein abundance, protein-level validation would be particularly valuable. Such spatial analyses would not only refine our understanding of these clusters but also strengthen the biological interpretations of their roles and interactions within the tissue.

Lastly, because obtaining fresh, healthy lung biopsies from dogs euthanized for unrelated reasons can be challenging in a clinical setting, we included biopsies from healthy lung tissue adjacent to primary lung tumors. This approach enabled us to expand our dataset and include diverse samples, but it also warrants cautious interpretation. The presence of cancer cells in tumor-adjacent healthy lung tissues was considered unlikely based on histopathology, the lack of expression of *EGFR* and *ERBB2*, expressed in respectively 73 and 69 percent of canine primary lung cancers (Yoshimoto et al., 2020), the lack of expression of proliferation markers used to identify replicating cells, and the analysis of differentially expressed genes and of biological process enrichments. However, only a limited marker panel was used, the molecular profiles of the primary tumors are unknown, and statistical power was limited due to the small sample sizes. Additionally, field effects from nearby tumors may have influenced gene expression in adjacent healthy tissue, although healthy lung tissues were collected with a margin of at least 2 cm from the visible tumor edge, which would further minimize the risk of contamination by tumor-associated effects.

In conclusion, this study provides a comprehensive molecular cell atlas of the canine healthy lung by describing 46 transcriptionally distinct lung cell clusters along with their gene expression signatures. Such atlas will provide the molecular foundation for investigating lung cell identities, functions and interactions in canine lung diseases. Additionally, the numerous similarities observed between canine and human lung cells highlighted the potential of the canine model to provide insights into human lung diseases.

Acknowledgments

The authors gratefully thank the GIGA Genomics and Bioinformatics platform, especially David Stern and Arnaud Lavergne for their guidance in script writing and data analysis, and Latifa Karim and her team for their availability.

References

Ammons, D.T., Harris, R.A., Hopkins, L.S., Kurihara, J., Weishaar, K., Dow, S., 2023. A single-cell RNA sequencing atlas of circulating leukocytes from healthy and osteosarcoma affected dogs. Front Immunol 14, 1162700. https://doi.org/10.3389/fimmu.2023.1162700

Ammons, D.T., Hopkins, L.S., Cronise, K.E., Kurihara, J., Regan, D.P., Dow, S., 2024. Single-cell RNA sequencing reveals the cellular and molecular heterogeneity of treatment-naïve primary osteosarcoma in dogs. Commun Biol 7, 1–18. https://doi.org/10.1038/s42003-024-06182-w

Barnes, T., Brown, K.K., Corcoran, B., Glassberg, M.K., Kervitsky, D.J., Limper, A.H., McGuire, K., Williams, K., Roman, J., Comparative Biology of Pulmonary Fibrosis Group, 2019. Research in Pulmonary Fibrosis Across Species: Unleashing Discovery Through Comparative Biology. Am J Med Sci 357, 399–404. https://doi.org/10.1016/j.amjms.2019.02.005

Chakarov, S., Lim, H.Y., Tan, L., Lim, S.Y., See, P., Lum, J., Zhang, X.-M., Foo, S., Nakamizo, S., Duan, K., Kong, W.T., Gentek, R., Balachander, A., Carbajo, D., Bleriot, C., Malleret, B., Tam, J.K.C., Baig, S., Shabeer, M., Toh, S.-A.E.S., Schlitzer, A., Larbi, A., Marichal, T., Malissen, B., Chen, J., Poidinger, M., Kabashima, K., Bajenoff, M., Ng, L.G., Angeli, V., Ginhoux, F., 2019. Two distinct interstitial macrophage populations coexist across tissues in specific subtissular niches. Science 363, eaau0964. https://doi.org/10.1126/science.aau0964

Chaudhary, N., Jayaraman, A., Reinhardt, C., Campbell, J.D., Bosmann, M., 2022. A single-cell lung atlas of complement genes identifies the mesothelium and epithelium as prominent sources of extrahepatic complement proteins. Mucosal Immunol 15, 927–939. https://doi.org/10.1038/s41385-022-00534-7

Chow, L., Wheat, W., Ramirez, D., Impastato, R., Dow, S., 2024. Direct comparison of canine and human immune responses using transcriptomic and functional analyses. Sci Rep 14, 2207. https://doi.org/10.1038/s41598-023-50340-9

Clercx, C., Fastrès, A., Roels, E., 2018. Idiopathic pulmonary fibrosis in West Highland white terriers: An update. The Veterinary Journal 242, 53–58. https://doi.org/10.1016/j.tvjl.2018.10.007

Denisenko, E., Guo, B.B., Jones, M., Hou, R., de Kock, L., Lassmann, T., Poppe, D., Clément, O., Simmons, R.K., Lister, R., Forrest, A.R.R., 2020. Systematic assessment of tissue dissociation and storage biases in single-cell and single-nucleus RNA-seq workflows. Genome Biology 21, 130. https://doi.org/10.1186/s13059-020-02048-6

Dow, S., 2019. A Role for Dogs in Advancing Cancer Immunotherapy Research. Front Immunol 10, 2935. https://doi.org/10.3389/fimmu.2019.02935

Eschke, M., Moore, P.F., Chang, H., Alber, G., Keller, S.M., 2023. Canine peripheral blood TCRαβ T cell atlas: Identification of diverse subsets including CD8A+ MAIT-like cells by combined single-cell transcriptome and V(D)J repertoire analysis. Front Immunol 14, 1123366. https://doi.org/10.3389/fimmu.2023.1123366

Fastrès, A., Pirottin, D., Fievez, L., Marichal, T., Desmet, C.J., Bureau, F., Clercx, C., 2020a. Characterization of the Bronchoalveolar Lavage Fluid by Single Cell Gene Expression Analysis in Healthy Dogs: A Promising Technique. Front Immunol 11, 1707. https://doi.org/10.3389/fimmu.2020.01707

Fastrès, A., Pirottin, D., Fievez, L., Tutunaru, A.-C., Bolen, G., Merveille, A.-C., Marichal, T., Desmet, C.J., Bureau, F., Clercx, C., 2020b. Identification of Pro-Fibrotic Macrophage Populations by Single-Cell Transcriptomic Analysis in West Highland White Terriers Affected With Canine Idiopathic Pulmonary Fibrosis. Front Immunol 11, 611749. https://doi.org/10.3389/fimmu.2020.611749

Fastrès, A., Roels, E., Tutunaru, A.C., Bolen, G., Merveille, A.-C., Day, M.J., Garigliany, M.-M., Antoine, N., Clercx, C., 2023. Osteopontin and fibronectin in lung tissue, serum, and bronchoalveolar lavage fluid of dogs with idiopathic pulmonary fibrosis and control dogs. J Vet Intern Med 37, 2468–2477. https://doi.org/10.1111/jvim.16870

Gibbings, S.L., Thomas, S.M., Atif, S.M., McCubbrey, A.L., Desch, A.N., Danhorn, T., Leach, S.M., Bratton, D.L., Henson, P.M., Janssen, W.J., Jakubzick, C.V., 2017. Three Unique Interstitial Macrophages in the Murine Lung at Steady State. American Journal of Respiratory Cell and Molecular Biology 57, 66. https://doi.org/10.1165/rcmb.2016-0361OC

Gingrich, A.A., Reiter, T.E., Judge, S.J., York, D., Yanagisawa, M., Razmara, A., Sturgill, I., Basmaci, U.N., Brady, R.V., Stoffel, K., Murphy, W.J., Rebhun, R.B., Brown, C.T., Canter, R.J., 2021. Comparative Immunogenomics of Canine Natural Killer Cells as Immunotherapy Target. Front Immunol 12, 670309. https://doi.org/10.3389/fimmu.2021.670309

Guo, M., Morley, M.P., Jiang, C., Wu, Y., Li, G., Du, Y., Zhao, S., Wagner, A., Cakar, A.C., Kouril, M., Jin, K., Gaddis, N., Kitzmiller, J.A., Stewart, K., Basil, M.C., Lin, S.M., Ying, Y., Babu, A., Wikenheiser-Brokamp, K.A., Mun, K.S., Naren, A.P., Clair, G., Adkins, J.N., Pryhuber, G.S., Misra, R.S., Aronow, B.J., Tickle, T.L., Salomonis, N., Sun, X., Morrisey, E.E., Whitsett, J.A., Lin, S., Xu, Y., 2023. Guided construction of single cell reference for human and mouse lung. Nat Commun 14, 4566. https://doi.org/10.1038/s41467-023-40173-5

Habermann, A.C., Gutierrez, A.J., Bui, L.T., Yahn, S.L., Winters, N.I., Calvi, C.L., Peter, L., Chung, M.-I., Taylor, C.J., Jetter, C., Raju, L., Roberson, J., Ding, G., Wood, L., Sucre, J.M.S., Richmond, B.W., Serezani, A.P., McDonnell, W.J., Mallal, S.B., Bacchetta, M.J., Loyd, J.E., Shaver, C.M., Ware, L.B., Bremner, R., Walia, R., Blackwell, T.S., Banovich, N.E., Kropski, J.A., 2020. Single-cell RNA sequencing

reveals profibrotic roles of distinct epithelial and mesenchymal lineages in pulmonary fibrosis. Sci Adv 6, eaba1972. https://doi.org/10.1126/sciadv.aba1972

Hytönen, M.K., Lohi, H., 2016. Canine models of human rare disorders. Rare Dis 4, e1241362. https://doi.org/10.1080/21675511.2016.1241362

Johnson, L.R., Lappin, M.R., Baker, D.C., 1999. Pulmonary thromboembolism in 29 dogs: 1985-1995. J Vet Intern Med 13, 338–345. https://doi.org/10.1892/0891-6640(1999)013<0338:ptid>2.3.co;2

Lee, B.M., Clarke, D., Watson, M., Laver, T., 2020. Retrospective evaluation of a modified human lung cancer stage classification in dogs with surgically excised primary pulmonary carcinomas. Veterinary and Comparative Oncology 18, 590–598. https://doi.org/10.1111/vco.12582

Love, M.I., Huber, W., Anders, S., 2014. Moderated estimation of fold change and dispersion for RNA-seq data with DESeq2. Genome Biol 15, 550. https://doi.org/10.1186/s13059-014-0550-8

Madissoon, E., Oliver, A.J., Kleshchevnikov, V., Wilbrey-Clark, A., Polanski, K., Richoz, N., Ribeiro Orsi, A., Mamanova, L., Bolt, L., Elmentaite, R., Pett, J.P., Huang, N., Xu, C., He, P., Dabrowska, M., Pritchard, S., Tuck, L., Prigmore, E., Perera, S., Knights, A., Oszlanczi, A., Hunter, A., Vieira, S.F., Patel, M., Lindeboom, R.G.H., Campos, L.S., Matsuo, K., Nakayama, T., Yoshida, M., Worlock, K.B., Nikolić, M.Z., Georgakopoulos, N., Mahbubani, K.T., Saeb-Parsy, K., Bayraktar, O.A., Clatworthy, M.R., Stegle, O., Kumasaka, N., Teichmann, S.A., Meyer, K.B., 2023. A spatially resolved atlas of the human lung characterizes a gland-associated immune niche. Nat Genet 55, 66–77. https://doi.org/10.1038/s41588-022-01243-4

Manchester, A.C., Ammons, D.T., Lappin, M.R., Dow, S., 2024. Single cell transcriptomic analysis of the canine duodenum in chronic inflammatory enteropathy and health. Front Immunol 15, 1397590. https://doi.org/10.3389/fimmu.2024.1397590

Narvaez Del Pilar, O., Gacha Garay, M.J., Chen, J., 2022. Three-axis classification of mouse lung mesenchymal cells reveals two populations of myofibroblasts. Development 149, dev200081. https://doi.org/10.1242/dev.200081

Paoloni, M., Khanna, C., 2008. Translation of new cancer treatments from pet dogs to humans. Nat Rev Cancer 8, 147–156. https://doi.org/10.1038/nrc2273

Paoloni, M.C., Khanna, C., 2007. Comparative Oncology Today. Veterinary Clinics of North America: Small Animal Practice, State of the Art Veterinary Oncology 37, 1023–1032. https://doi.org/10.1016/j.cvsm.2007.08.003

Patel, V.I., Metcalf, J.P., 2018. Airway Macrophage and Dendritic Cell Subsets in the Resting Human Lung. Crit Rev Immunol 38, 303–331. https://doi.org/10.1615/CritRevImmunol.2018026459

Rizzoli, E., de Meeûs d'Argenteuil, C., Fastrès, A., Roels, E., Janssen, P., Puré, E., Garigliany, M.-M., Marichal, T., Clercx, C., 2024. Fibroblast activation protein is a cellular marker of fibrotic activity in canine idiopathic pulmonary fibrosis. Front Vet Sci 11, 1416124. https://doi.org/10.3389/fvets.2024.1416124

Schilder, B., Skene, N., 2022. orthogene: an R package for easy mapping of orthologous genes across hundreds of species. Bioconductor.

Schupp, J.C., Adams, T.S., Cosme, C., Raredon, M.S.B., Yuan, Y., Omote, N., Poli, S., Chioccioli, M., Rose, K.-A., Manning, E.P., Sauler, M., DeIuliis, G., Ahangari, F., Neumark, N., Habermann, A.C., Gutierrez, A.J., Bui, L.T., Lafyatis, R., Pierce, R.W., Meyer, K.B., Nawijn, M.C., Teichmann, S.A., Banovich, N.E., Kropski, J.A., Niklason, L.E., Pe'er, D., Yan, X., Homer, R.J., Rosas, I.O., Kaminski, N., 2021. Integrated Single-Cell Atlas of Endothelial Cells of the Human Lung. Circulation 144, 286–302. https://doi.org/10.1161/CIRCULATIONAHA.120.052318

Schyns, J., Bai, Q., Ruscitti, C., Radermecker, C., De Schepper, S., Chakarov, S., Farnir, F., Pirottin, D., Ginhoux, F., Boeckxstaens, G., Bureau, F., Marichal, T., 2019. Non-classical tissue monocytes and two functionally distinct populations of interstitial macrophages populate the mouse lung. Nat Commun 10, 3964. https://doi.org/10.1038/s41467-019-11843-0

Shi, X., Zhu, S., Liu, M., Stone, S.S., Rong, Y., Mao, K., Xu, X., Ma, C., Jiang, Z., Zha, Y., Yan, C., Yu, X., Wu, D., Liu, G., Mi, J., Zhao, J., Li, Y., Ding, Y., Wang, X., Zhang, Y.-B., Ji, X., 2022. Single-Cell RNA-Seq Reveals a Population of Smooth Muscle Cells Responsible for Atherogenesis. Aging Dis 13, 1939–1953. https://doi.org/10.14336/AD.2022.0313

Sikkema, L., Ramírez-Suástegui, C., Strobl, D.C., Gillett, T.E., Zappia, L., Madissoon, E., Markov, N.S., Zaragosi, L.-E., Ji, Y., Ansari, M., Arguel, M.-J., Apperloo, L., Banchero, M., Bécavin, C., Berg, M., Chichelnitskiy, E., Chung, M., Collin, A., Gay, A.C.A., Gote-Schniering, J., Hooshiar Kashani, B., Inecik, K., Jain, M., Kapellos, T.S., Kole, T.M., Leroy, S., Mayr, C.H., Oliver, A.J., von Papen, M., Peter, L., Taylor, C.J., Walzthoeni, T., Xu, C., Bui, L.T., De Donno, C., Dony, L., Faiz, A., Guo, M., Gutierrez, A.J., Heumos, L., Huang, N., Ibarra, I.L., Jackson, N.D., Kadur Lakshminarasimha Murthy, P., Lotfollahi, M., Tabib, T., Talavera-López, C., Travaglini, K.J., Wilbrey-Clark, A., Worlock, K.B., Yoshida, M., van den Berge, M., Bossé, Y., Desai, T.J., Eickelberg, O., Kaminski, N., Krasnow, M.A., Lafyatis, R., Nikolic, M.Z., Powell, J.E., Rajagopal, J., Rojas, M., Rozenblatt-Rosen, O., Seibold, M.A., Sheppard, D., Shepherd, D.P., Sin, D.D., Timens, W., Tsankov, A.M., Whitsett, J., Xu, Y., Banovich, N.E., Barbry, P., Duong, T.E., Falk, C.S., Meyer, K.B., Kropski, J.A., Pe'er, D., Schiller, H.B., Tata, P.R., Schultze, J.L., Teichmann, S.A., Misharin, A.V.,

Nawijn, M.C., Luecken, M.D., Theis, F.J., 2023. An integrated cell atlas of the lung in health and disease. Nat Med 29, 1563–1577. https://doi.org/10.1038/s41591-023-02327-2

Travaglini, K.J., Nabhan, A.N., Penland, L., Sinha, R., Gillich, A., Sit, R.V., Chang, S., Conley, S.D., Mori, Y., Seita, J., Berry, G.J., Shrager, J.B., Metzger, R.J., Kuo, C.S., Neff, N., Weissman, I.L., Quake, S.R., Krasnow, M.A., 2020. A molecular cell atlas of the human lung from single-cell RNA sequencing. Nature 587, 619–625. https://doi.org/10.1038/s41586-020-2922-4

Tsukui, T., Sun, K.-H., Wetter, J.B., Wilson-Kanamori, J.R., Hazelwood, L.A., Henderson, N.C., Adams, T.S., Schupp, J.C., Poli, S.D., Rosas, I.O., Kaminski, N., Matthay, M.A., Wolters, P.J., Sheppard, D., 2020. Collagen-producing lung cell atlas identifies multiple subsets with distinct localization and relevance to fibrosis. Nat Commun 11, 1920. https://doi.org/10.1038/s41467-020-15647-5

Yoshimoto, S., Kato, D., Kamoto, S., Yamamoto, K., Tsuboi, M., Shinada, M., Ikeda, N., Tanaka, Y., Yoshitake, R., Eto, S., Saeki, K., Chambers, J., Hashimoto, Y., Uchida, K., Nishimura, R., Nakagawa, T., 2020. Overexpression of human epidermal growth factor receptor 2 in canine primary lung cancer. Journal of Veterinary Medical Science 82, 804–808. https://doi.org/10.1292/jvms.20-0026

Zappia, L., Oshlack, A., 2018. Clustering trees: a visualization for evaluating clusterings at multiple resolutions. GigaScience 7, giy083. https://doi.org/10.1093/gigascience/giy083

Zilionis, R., Engblom, C., Pfirschke, C., Savova, V., Zemmour, D., Saatcioglu, H.D., Krishnan, I., Maroni, G., Meyerovitz, C.V., Kerwin, C.M., Choi, S., Richards, W.G., De Rienzo, A., Tenen, D.G., Bueno, R., Levantini, E., Pittet, M.J., Klein, A.M., 2019. Single-Cell Transcriptomics of Human and Mouse Lung Cancers Reveals Conserved Myeloid Populations across Individuals and Species. Immunity 50, 1317-1334.e10. https://doi.org/10.1016/j.immuni.2019.03.009

Supplemental material

The Supplementary Material for this article can be found online at: https://www.frontiersin.org/articles/10.3389/fimmu.2025.1501603/full#supplementary-material.

Raw and processed sequencing data can be found in ArrayExpress online repository (https://www.ebi.ac.uk/arrayexpress/) under the accession number E-MTAB-14296. The complete analysis code is publicly available at https://github.com/elodierizzoli/canine_lung_healthy. Any additional data requests can be made by contacting the corresponding author.

Experimental section

Study 2:

Unveiling the molecular disruptions in canine pulmonary adenocarcinoma using single-cell RNA sequencing

Preamble

In dogs, primary lung cancer of advanced stage presents a therapeutic challenge and is associated with a poor prognosis. To support the development of targeted therapies, this study explored the tumor microenvironment of canine pulmonary adenocarcinoma (PAC), the most common subtype, using scRNA-seq. By integrating data from three freshly excised PAC biopsies with a previously established scRNA-seq atlas of healthy canine lungs, the analysis identified 51 distinct cell subtypes. In PAC samples, myofibroblasts were notably overrepresented and showed upregulation of genes linked to epithelial-to-mesenchymal transition and angiogenesis, including FAP and CTHRC1. Among immune populations, mature dendritic cells were enriched, while tumor-associated macrophages (TAMs) overexpressed SPP1, potentially contributing to immune evasion. Additional gene expression changes were observed across epithelial, endothelial, lymphoid, and muscle cell populations. Immunofluorescence confirmed the presence of $CTHRC1^{+}$ cancer-associated fibroblasts and $SPP1^{+}$ TAMs within the tumor microenvironment. Overall, this study offers a single-cell resolution map of canine PAC, revealing key cellular and molecular alterations that may drive tumor progression and offering potential targets for future therapeutic approaches.

Experimental section

Study 2:

Unveiling the molecular disruptions in canine pulmonary adenocarcinoma using single-cell RNA sequencing

Unpublished

Elodie Rizzoli, Laurence Fievez, Mutien-Marie Garigliany, Thomas Marichal, Cécile Clercx

Abstract

Primary lung cancer, a prevalent disease in humans, is relatively less common in dogs. However, advanced stages pose therapeutic challenges and carry poor prognosis. A deeper understanding of the tumor microenvironment is essential to guide the development of novel treatments. In this study, we aimed to characterize the cellular landscape and gene expression profiles of canine pulmonary adenocarcinoma (PAC), the most prevalent subtype of canine primary lung cancer.

In this cross-sectional study, fresh biopsy samples were obtained from three primary PAC after surgical excision via lobectomy and processed for single-cell RNA sequencing. Datasets from PAC samples were integrated with datasets from healthy lung samples before comparison of cell type distributions and differential gene expression analysis. Immunofluorescence microscopy was used to confirm markers expression in paraffin sections.

Compared with healthy lungs, cancer-associated fibroblasts (CAFs) overexpressed genes associated with epithelial-to-mesenchymal transition and angiogenesis. Within immune cells, mature dendritic cells were overrepresented in PAC samples. Tumor-associated macrophages (TAMs) overexpressed markers possibly linked to immune evasion. Altered gene expression profiles were also identified in PAC epithelial, endothelial, lymphoid and muscle cells. With immunofluorescence microscopy, the presence of collagen triple helix repeat containing 1 (*CTHRC1*)$^+$ CAFs and osteopontin (*SPP1*)$^+$ TAMs in the tumor microenvironment was confirmed.

In conclusion, this study provides a single-cell resolution overview of the cellular and molecular heterogeneity in canine PAC, identifying alterations in the tumor microenvironment, particularly in fibroblasts and macrophages, which may contribute to the disease pathogenesis. These findings carry implications for the development of new therapeutic strategies.

Introduction

Primary pulmonary neoplasia appears to be less common in dogs than in humans, with a necropsy incidence of less than 1% (Wilson, 2016; Rebhun and Culp, 2020). Among these, pulmonary carcinoma is the most frequently diagnosed histological type, with adenocarcinoma being the most prevalent subtype (Ogilvie et al., 1989; Bettini et al., 2010; McPhetridge et al., 2021; Treggiari et al., 2025). Surgical resection via lung lobectomy remains the treatment of choice, yielding median survival times of 370 to 399 days and a median disease-free interval of 344 days in dogs surviving the postoperative period (Lee et al., 2020; McPhetridge et al., 2021). However, survival time significantly decreases with advancing disease stage (Lee et al., 2020; McPhetridge et al., 2021). To date, the benefits of postoperative adjuvant chemotherapy remain unproven (Lee et al., 2020; Rose and Worley, 2020; McPhetridge et al., 2021; Treggiari et al., 2025). As such, unresectable or metastatic primary pulmonary carcinoma presents a major therapeutic challenge and is associated with a poor prognosis, highlighting the need for a better understanding of the pathobiology of canine lung cancer to guide the development of novel therapeutic strategies.

In humans, lung cancer remains the leading cause of cancer-related morbidity and mortality. Non-small cell lung cancer (NSCLC), which includes adenocarcinoma, squamous cell carcinoma, and large cell carcinoma, accounts for more than 80% of cases (Siegel et al., 2024). In recent years, spontaneously occurring cancers in dogs have gained recognition as comparative models for human malignancies (Dow, 2019). Canine pulmonary carcinoma shares several features, including histological characteristics, with its human counterpart, supporting its relevance as a translational model (Shiota et al., 2023).

Single-cell RNA sequencing (scRNA-seq) is an emerging high-throughput technology that enables transcriptomic profiling at single-cell resolution (Fastrès et al., 2020a). This approach facilitates the unbiased identification of disease-associated cell populations and differentially expressed genes, offering potential insights into new therapeutic targets.

The aim of this study was to investigate the cellular composition and gene expression profiles of canine pulmonary adenocarcinoma (PAC) using scRNA-seq, and to compare these findings with those from healthy lung tissue.

Material and methods

1. Sample collection

Biopsies from three solitary canine primary PAC were collected immediately after complete lobectomy in client-owned dogs, with informed owner consent. In each tumor, two adjacent biopsies were obtained at the tumor edge: one was fixed in 10% neutral buffered formalin and embedded in paraffin for future histological studies, and one was immediately processed for scRNA-seq analysis. The remaining surgical specimen was submitted to a commercial diagnostic pathology laboratory for histopathological evaluation.

As controls, four healthy lung samples used to generate a scRNA-seq atlas of the healthy canine lung were included (Rizzoli et al., 2025). Those four samples were collected from client-owned dogs, either post-mortem (n=2) or from non-involved lung adjacent to solitary lung tumors (n=2) included in the present study, ensuring a margin of at least 2 cm from the visible tumor edge. All samples, including controls, were processed in the same manner.

2. Histopathology

Formalin-fixed, paraffin-embedded biopsies were cut into 5-µm sections and routinely processed for histopathological evaluation using hematoxylin and eosin (HE) staining. Diagnosis of pulmonary adenocarcinoma was confirmed and the predominant growth pattern in the biopsy was identified (Travis et al., 2011; Wilson, 2016).

3. Single-cell RNA sequencing

a. Sample preparation, library preparation and sequencing

For scRNA-seq analysis, tumor biopsies were processed following the procedure used for healthy lungs (Rizzoli et al., 2025). Briefly, fresh biopsies were transported in Hank's Balanced Salt solution (Gibco) containing 5% v/v of fetal bovine serum (Gibco) on ice for immediate processing. Each sample underwent mechanical and chemical dissociation until obtention of a suspension of single cells. Approximately 10,000 cells per sample were processed and sequenced using the 10x Genomics Chromium platform and Illumina NextSeq500, as previously described (Rizzoli et al., 2025). Sequencing reads were aligned to the dog reference transcriptome (CanFam3.1) and gene-barcode matrices were generated using Cell Ranger v9.0.0 (10x Genomics).

b. Data filtering, integration and clustering

Filtered gene expression matrices were analyzed using Seurat R package (v4.3.0) (Hao et al., 2021). Each sample underwent individual quality control to remove doublets, low-quality or dying cells. Genes expressed in fewer than 10 cells were excluded, along with cells expressing under 200 genes or over 20% mitochondrial reads. Clusters co-expressing markers from multiple tissue compartments were also identified as doublets and removed. Datasets from PAC samples were integrated with datasets from four healthy lung samples (Rizzoli et al., 2025) after SCTransform normalization, regressing out the effects of the percentage of mitochondrial reads, and canonical correlation analysis integration, using the top 3000 variable genes as integration anchors. Principal component analysis was used for linear dimensionality reduction, and an elbow plot guided the selection of principal components. Clustering was visualized using uniform manifold approximation and projection (UMAP), and optimal resolution was determined with the clustree package (Zappia and Oshlack, 2018). Each cluster was assigned to a tissue compartment using their expression of canonical marker genes (*EPCAM* for epithelial, *PTPRC* for immune, *PECAM1* for endothelial cells, the rest being mesenchymal cells) and previously assigned healthy lung cell identities. Each compartment was individualized, and integration and clustering were repeated in each subset. Cell cluster identities were determined based on previously assigned healthy lung cell identities, and the expression of known marker genes from the literature. Unsupervised cluster-derived cell types were then grouped into biologically relevant subtypes.

c. Cell abundance analysis

Cell type percentages were calculated for each sample by dividing the number of cells within a given cell type by the total number of cells within the corresponding compartment (mesenchymal, immune, epithelial, or endothelial). These percentages were compared between PAC and healthy lung samples using a two-sided Wilcoxon rank-sum exact test. Due to the limited number of samples (n = 3 PAC, n = 4 healthy), a P-value of less than 0.1 was considered statistically significant. The effect size was estimated using Rank-Biserial Correlation (RBC). All statistical analyses were performed using R software (v4.2.3). Median percentages ± interquartile range, exact P-values and RBC were reported for each group where applicable.

d. Feature visualization

Gene expression was visualized using feature plots, violin plots and dot plots using SCTransform normalized counts. Split feature plots were used to visualize gene expression between

conditions after downsampling the sample with the highest number of cells to depict equal cell numbers per condition.

e. Differential gene expression analysis

Differential gene expression analysis between PAC and healthy cell types was performed using DESeq2 method (v1.38.3) after pseudobulk conversion (Love et al., 2014). The pseudobulk approach was applied to compare cell types containing at least 10 cells per sample. Genes with an adjusted P value less than 0.05 and a log2 fold change superior to 0.58 were considered significantly differentially expressed.

f. Gene set enrichment analysis

Gene set enrichment analyses were performed using lists of significantly differentially expressed genes between PAC and healthy cell types using the enricher() function from the clusterProfiler package (v4.6.2) (Wu et al., 2021) and the 'hallmark' gene sets database from the msigdbr package (v7.5.1) (Subramanian et al., 2005). Enriched gene sets with a false discovery rate less than 0.05 and a P value less than 0.05 were considered statistically significant.

4. Immunofluorescence microscopy

Formalin-fixed paraffin-embedded 5-µm tissue sections were used for immunofluorescence microscopy. Antigen retrieval was performed by incubating slides in 10 mM sodium carbonate buffer (pH 9.0) at high temperature for 12 minutes, followed by a 15-minute cooling period. Sections were then permeabilized in phosphate-buffered saline (PBS) containing 0.5% Triton X-100 for 2 minutes at room temperature and blocked for 1.5 hours in PBS supplemented with 2% bovine serum albumin and 2% donkey serum. Slides were incubated with primary antibodies mouse anti-CTHRC1 (1:200), goat anti-Iba1 (1:200), and rabbit anti-SPP1 (1:1000) diluted in blocking buffer for 1 hour at room temperature (CTHRC1, Iba1) or overnight at 4°C (SPP1). Corresponding Alexa Fluor-conjugated donkey secondary antibodies (anti-mouse 647, anti-goat 488, anti-rabbit 568; all diluted at 1:500 in blocking buffer) were applied for 2 hours at room temperature together with DAPI (1:1000). The references of all antibodies are provided in Supplementary Material. Slides were washed in PBS with 0.05% Tween-20 between each step, mounted with ProLong Gold, and cover-slipped for imaging.

Results

1. Study samples

Table 1 summarizes clinical data regarding the cases used in the present study. Primary pulmonary adenocarcinomas were either stage I (PAC1 and PAC2) or stage II (PAC3) and all were previously untreated. Histologically, one adenocarcinoma (PAC1) had a predominant lepidic (formerly bronchioloalveolar) growth pattern and a mucinous component, one (PAC2) exhibited a papillary growth pattern and one (PAC3) exhibited an acinar growth pattern with a marked neutrophilic infiltration. Although it was not objectified in the present biopsy, histopathological analysis of the whole tumor specimen from PAC3 also revealed areas of squamous differentiation. Figure 1 illustrates representative areas of HE -stained sections of PAC cases.

Table 1. Summary of clinical data from PAC and healthy lung cases.

Case	Age	Breed	Weight (kg)	Gender	Lung lobe	Size† (cm)	Stage‡	Histopathological diagnosis
PAC 1	10	Beagle crossbreed	12.5	F	Right caudal	2.3	I (T1,N0,M0)	Adenocarcinoma, lepidic growth
PAC 2	12	Belgian Griffon	4.8	M	Right caudal	3	I (T1,N0,M0)	Adenocarcinoma, papillary growth
PAC 3	8	Cocker	12	F	Right cranial	3.5	II (T2,N1,M0)	Adenocarcinoma, acinar growth
LUNG 1	10	Beagle crossbreed	12.5	F	Right caudal	NA	NA	Healthy
LUNG 2	5	Pointer	25	M	Right caudal	NA	NA	Healthy
LUNG 3	6	Pointer	30	M	Right caudal	NA	NA	Healthy
LUNG 4	8	Cocker	12	F	Right cranial	NA	NA	Healthy

Controls used in this study were used in previously published atlas of the healthy canine lung (Rizzoli et al., 2025).
† *Size is expressed by the maximum tumor diameter based on preoperative computed tomography measurements. Staging was performed according to the Canine Lung Carcinoma Stage Classification* (Lee et al., 2020). *PAC: pulmonary adenocarcinoma; F: female; M: male; NA: not applicable.*

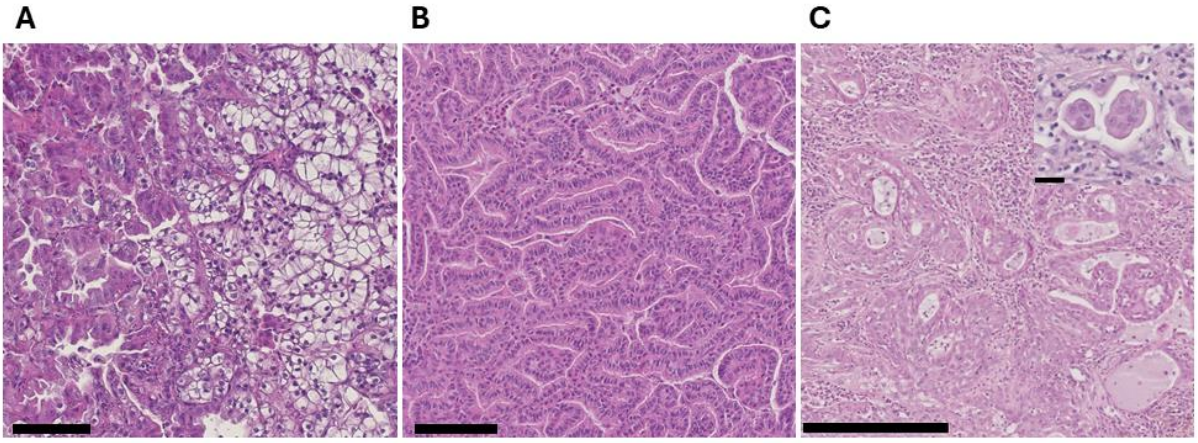

Figure 1. Representative photomicrographs of primary pulmonary adenocarcinoma biopsies with hematoxylin and eosin staining. (A) PAC1, bar: 100 µm. (B) PAC2, bar: 100 µm. (C) PAC3; bar: 250 µm; inset: multinucleated giant cells in the peritumoral stroma, bar: 25 µm.

2. Cellular and molecular heterogeneity of primary pulmonary adenocarcinoma

a. General overview

Following quality control, we obtained 26,188 cells from 4 healthy lung samples and 30,135 cells from PAC samples, sequenced to an average depth of 22,606 reads per cell (Supplementary Table 2). Final clustering provided 51 clusters including fibroblasts (6), muscle cells (4), myeloid cells (15), lymphoid cells (14), epithelial cells (7) and endothelial cells (5) (Supplementary Table 3). Comparisons of cell type proportions between conditions are detailed in Supplementary Table 4. Overrepresented biological process in PAC compares with healthy lungs are provided in Supplementary Table 5, along with the overexpressed genes included in each gene set.

b. Mesenchymal cells

Compared with all fibroblasts from healthy lungs, fibroblasts from PAC samples overexpressed genes associated with epithelial to mesenchymal transition (EMT) such as *FAP, CTHRC1, MMP3, INHBA, COL11A1, TIMP1, WNT5A, ACTA2* as well as genes involved in mitosis such as *TOP2A* and *MKI67* (Figure 2). Other enriched biological processes include hypoxia (*PFKP, STC1*), angiogenesis (*POSTN, VEGFA*), inflammatory response (*CCL17*, *IL1R1*), glycolysis (*FBP2, TGFA*), TNFα signalling (*SERPINE1, TNFAIP6*) and TGFβ signalling (*LTBP2, TGFBR1*). Among the six fibroblasts clusters, one cluster of myofibroblasts overexpressed genes associated with contractility (including *ACTA2, TPM2, MYL9*), compared to other fibroblast clusters, and was overrepresented in PAC samples (p=0.057, RBC=0.8). PAC myofibroblasts overexpressed cancer-associated fibroblasts markers such as *FAP, CTHRC1, INHBA* and *POSTN* as well as other genes involved in EMT and angiogenesis (Chen et

al., 2023). Within muscle cells (Supplementary Figure 1), pericytes from the systemic circulation were also increased in PAC (p=0.057, RBC=0.8). An enrichment in genes involved in EMT, mitosis and inflammatory response was also identified in PAC muscle cells, compared with all muscle cell clusters from healthy lungs.

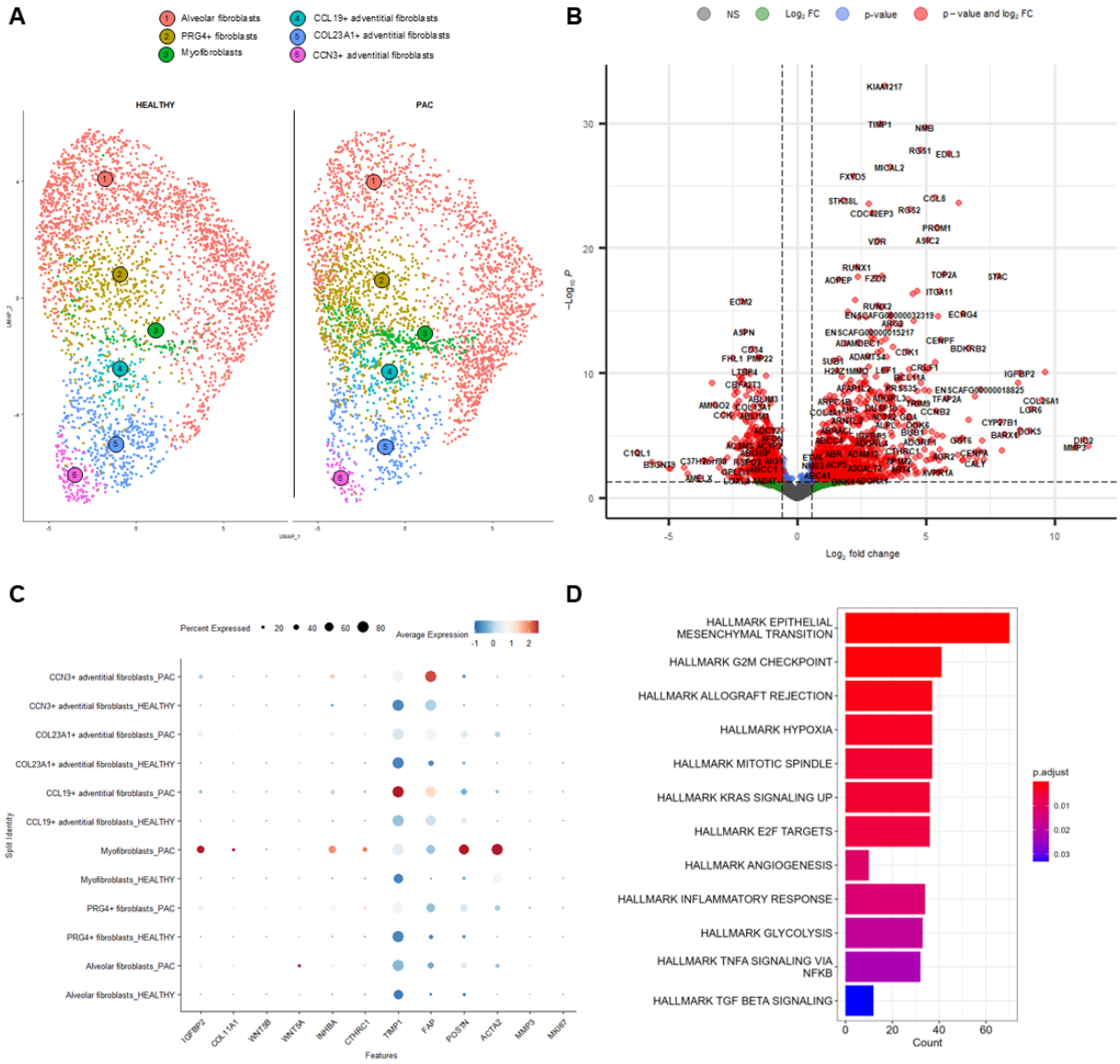

Figure 2. Cancer-associated fibroblasts changes. (A) Split UMAP plot representing fibroblast clusters in healthy lung and in PAC samples. (B) Volcano plot representing differentially expressed genes between all PAC and all healthy lung fibroblasts. (C) Split dot plot representing the normalized expression of genes in PAC and healthy lung fibroblast clusters. (D) Bar plot illustrating overrepresented biological processes in PAC fibroblasts. PAC: pulmonary adenocarcinoma. UMAP: Uniform Manifold Approximation and Projection; PAC: pulmonary adenocarcinoma.

c. Myeloid cells

Immune cells proportions, relative to the total number of cells, were increased in PAC samples (p=0.057, RBC=0.8). Within myeloid cells (Figure 3A), lung multinucleated giant cells were identified in PAC1 and PAC3, based on their expression of genes such as cathepsin K (*CTSK*), hyaluronidase 1 (*HYAL1*) and acid phosphatase 5, tartrate resistant (*ACP5*), which are markers of other multinucleated giant cells derived from hematopoietic macrophage/monocyte precursor cells, bone osteoclasts (Ammons et al., 2024). The presence of multinucleated giant cells in the peritumoral stroma of both carcinomas was confirmed by assessment of HE-stained sections (Figure 1C). Mature dendritic cells were also overrepresented in PAC samples (p=0.057, RBC=0.8).

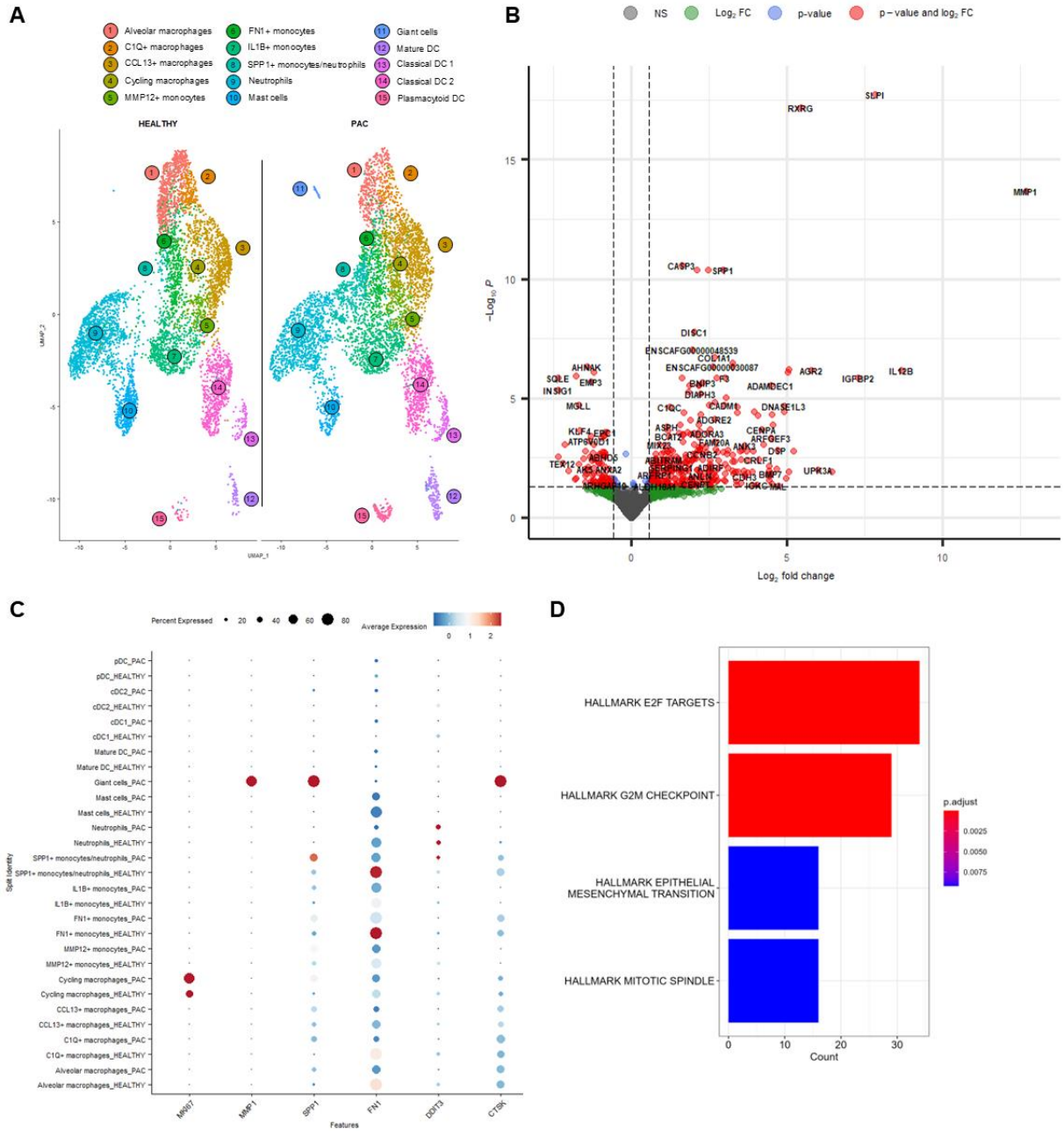

Figure 3. Cancer-associated myeloid cell changes. (A) Split UMAP plot representing myeloid cell clusters in healthy lungs and in PAC samples. (B) Volcano plot representing differentially expressed genes between all PAC and all healthy lung macrophages and monocytes. (C) Split dot plot representing the normalized expression of genes in PAC and healthy lung myeloid cell clusters. (D) Bar plot illustrating overrepresented biological processes in PAC macrophages and monocytes. PAC: pulmonary adenocarcinoma. UMAP: Uniform Manifold Approximation and Projection; PAC: pulmonary adenocarcinoma.

PAC macrophages and monocytes overexpressed genes involved in cell replication, such as *CENPA* and *KIF22*, but also genes involved in EMT such as *MMP1, IGFBP2* and *SPP1* (Figure 3B, C and D). 'SPP1^{+} monocytes/neutrophils', a cluster prominent in PAC (p=0.114, RBC=0.7), had the strongest

expression of *SPP1*, together with FN1$^+$ monocytes. It seemed to be constituted by a population of SPP1$^+$ monocytes clustering together with neutrophils originating mainly from PAC3 and overexpressing DNA Damage Inducible Transcript 3 (*DDIT3*) and C-C Chemokine receptor-like 2 (*CCRL2*), two markers of tumor-associated neutrophils (Salcher et al., 2022). PAC 'SPP1+ monocytes', compared with those from healthy lungs, overexpressed genes associated with hypoxia and mTOR signalling (*PDK1, GAPDH, TPI1*).

d. Lymphoid cells

Within lymphoid cells (Figure 4), in addition to previously described subtypes, we identified a small T cell cluster exhibiting a gene expression profile (*ISG15, OAS1, IFIT1, IFI44*) consistent with an interferon (IFN) response gene signature (Ammons et al., 2024) (IFN T cells). Another small T cell cluster had a gene expression pattern dominated by known stress-response-related genes such as heat shock proteins (*DNAJB1, HSPH1, DNAJA1*) and immediate-early genes *FOS* and *FOSB* (Denisenko et al., 2020) (Stressed T cells). Compared with all healthy lung T cells, all PAC T cells overexpressed genes enriched in mitosis processes (*PLK1, CDC20, KIF23*). PAC CD8$^+$ T cells overexpressed activation markers *TNF, TNFRSF4, TNFRSF18* and exhaustion marker *LAG3* (Tietscher et al., 2023). PAC regulatory T cells also overexpressed *TNFRSF4* and *TNFRSF18*. The overexpression of *PDCD1* (coding for immune checkpoint PD-1) in all PAC T cells (p=0.163), in PAC CD8$^+$ T cells (p=0.557) or in PAC regulatory T cells (p=0.058) was not statistically significant but was mainly present in PAC3. Finally, three clusters of plasma cells were identified and were all overrepresented in PAC samples (p=0.057, RBC=0.8), including a cluster of immunoglobulin A (IgA)$^+$ plasma cells and a cluster of immunoglobulin kappa constant (IgKC)$^+$ plasma cells.

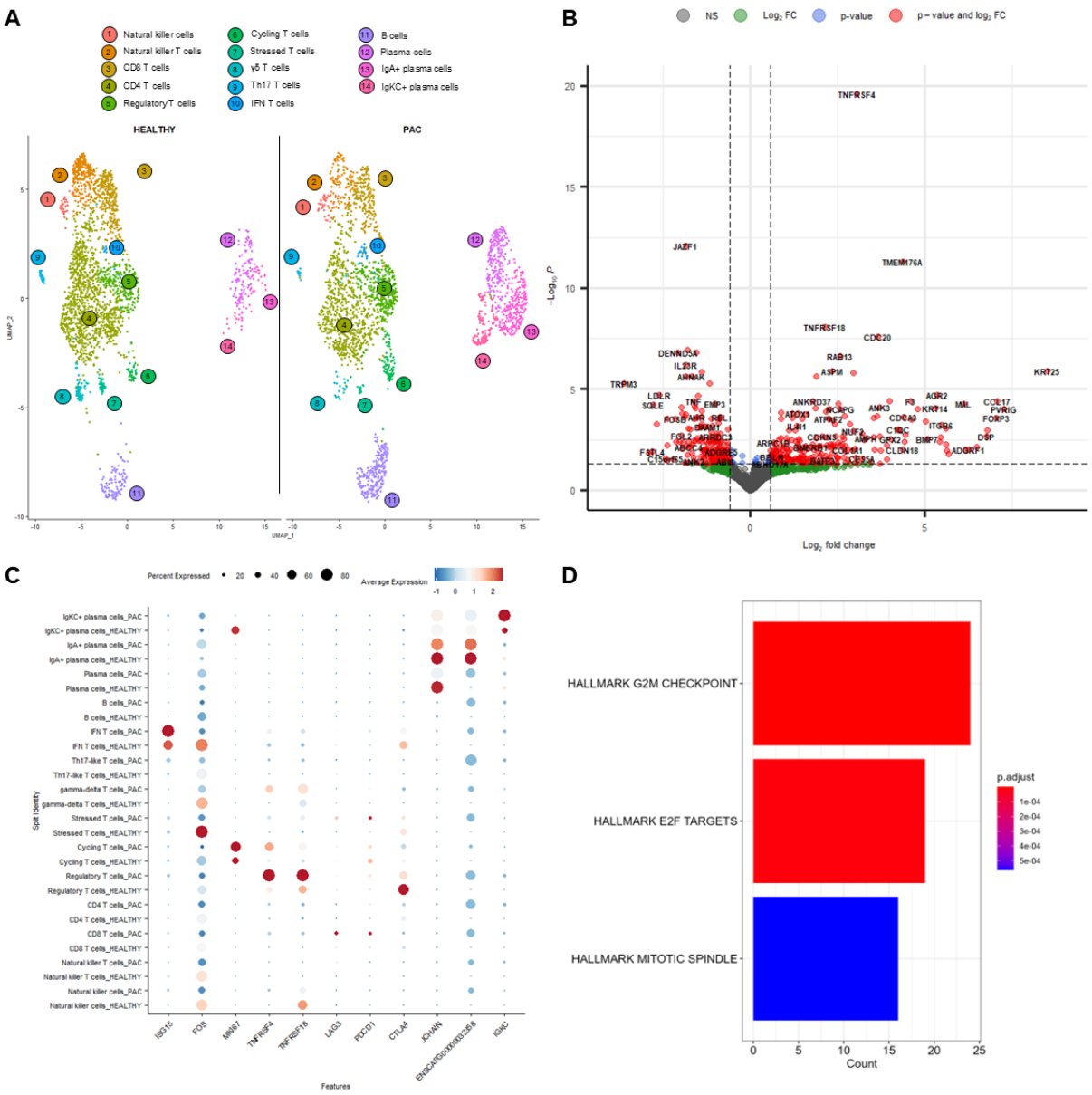

Figure 4. Cancer-associated lymphoid cell changes. (A) Split UMAP plot representing lymphoid cell clusters in healthy lung and in PAC samples. (B) Volcano plot representing differentially expressed genes between all PAC and all healthy lung T cells. (C) Split dot plot representing the normalized expression of genes in PAC and healthy lung lymphoid cell clusters. (D) Bar plot illustrating overrepresented biological processes in PAC T cells. UMAP: Uniform Manifold Approximation and Projection; PAC: pulmonary adenocarcinoma.

e. Endothelial cells

Regarding endothelial cells (Supplementary Figure 3), general capillary endothelial cells were overrepresented in PAC samples (p=0.057, RBC=0.8). While all PAC vascular endothelial cells overexpressed genes involved in EMT, general capillary endothelial cells also overexpressed genes involved in mitosis, complement response (*CCL5, CA2*), KRAS signalling (*SLPI, MMP9*), TNFα signalling

via NF-κB (*CCL5, IL6*), inflammatory response (*CCL17, CCL5*) and coagulation (*MMP9, APOA1*), hypoxia (*IGFBP3, VEGFA*) and angiogenesis (*SPP1, VEGFA*).

f. Epithelial and cancer cells

In addition to classical epithelial cell types, three cell clusters were prominent in tumor samples, expressed markers of secretory cells (*SCGB1A1, MUC1*) and cell cycle genes (*MKI67, TOP2A*) and were annotated as secretory/cancer cells (Figure 5). One cluster of cycling epithelial cells was also identified and was overrepresented in PAC samples (p=0.057, RBC=0.8). Compared with healthy cell clusters, 'Secretory/cancer cells 1' overexpressed genes associated with hypoxia (*PFKP, GADPH, TPI1*), IFN response (*IFI30, ISG15*), EMT (*TIMP1, FN1*) and cholesterol homeostasis (*ALDOC, ANTXR2*). 'Cancer cells 2' overexpressed genes associated with mitosis (*CENPF, TOP2A*), TNFα signalling via NF-κB (*CXCL10*, *AREG*, *VEGFA*), coagulation (*PRSS23, FN1*), but also EMT, hypoxia and IFN response. 'Cancer cells 3' overexpressed genes such as *SOBP, PFKP and GAPDH* but no biological process was significantly overrepresented. Epidermal growth factor receptor (*EGFR*) was significantly overexpressed by clusters of 'Secretory/Cancer Cells 1' and 'Cancer Cells 2' and was also overexpressed in all PAC epithelial cells compared with healthy epithelial cells. Compared with healthy clusters, the overexpression of *CD274* (coding for immune checkpoint PD-L1) in PAC cancer cells was not statistically significant (p=0.297), but CD274 was mainly overexpressed in PAC3.

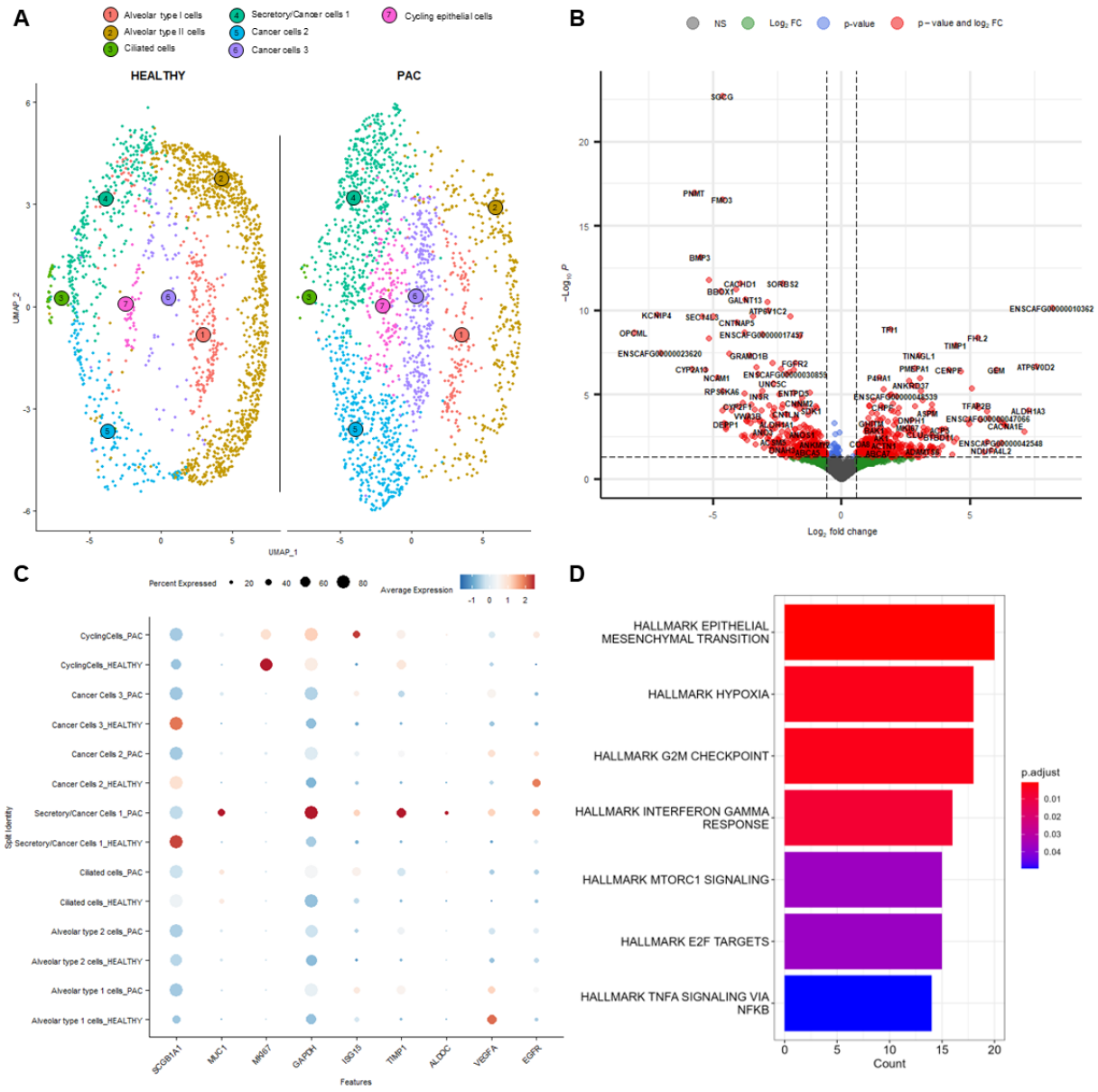

Figure 5. Cancer-associated changes in epithelial cells. (A) Split UMAP plot representing epithelial cell clusters in healthy lungs and in PAC samples. (B) Volcano plot representing differentially expressed genes between all PAC cancer cells and corresponding clusters in healthy lung samples. (C) Split dot plot representing the normalized expression of genes in PAC and healthy lung epithelial cell clusters. (D) Bar plot illustrating overrepresented biological processes in PAC cancer cells. UMAP: Uniform Manifold Approximation and Projection; PAC: pulmonary adenocarcinoma.

Among genes of protein routinely used as markers to differentiate canine pulmonary from metastatic tumors, *TTF1* and *NAPSA* (Ramos-Vara et al., 2005; Bettini et al., 2009; Beck et al., 2017) were expressed at varying levels by all clusters of PAC and healthy epithelial cells. While *NAPSA* was more specifically expressed by alveolar type 2 cells, *TTF1* was most highly expressed in PAC 'Cancer

cells 2' and PAC cycling epithelial cells. Finally, human lung adenocarcinoma marker *MUC1* (Salcher et al., 2022) was significantly overexpressed by PAC 'Secretory/cancer cells 1'.

3. In-situ investigation of CTHRC1$^+$ CAFs and SPP1$^+$ TAMs

PAC tissue sections were used to confirm the expression of cancer-associated fibroblast (CAF) marker CTHRC1 (collagen triple helix repeat containing 1) and tumor-associated macrophages (TAM) marker SPP1 (secreted phosphoprotein 1 or osteopontin) by immunofluorescence microscopy. Expression of SPP1 by TAMs was confirmed by visualizing the co-expression of SPP1 and ionized calcium-binding adapter molecule 1 (Iba1), a pan-myeloid marker (Figure 6A). The expression of CTHRC1 by CAFs was observed in stromal areas around or adjacent to tumor cells nests (Figure 6B). In those areas, colocalization of CHTRC1$^+$ CAFs and SPP1$^+$ TAMs was also observed (Figure 6C).

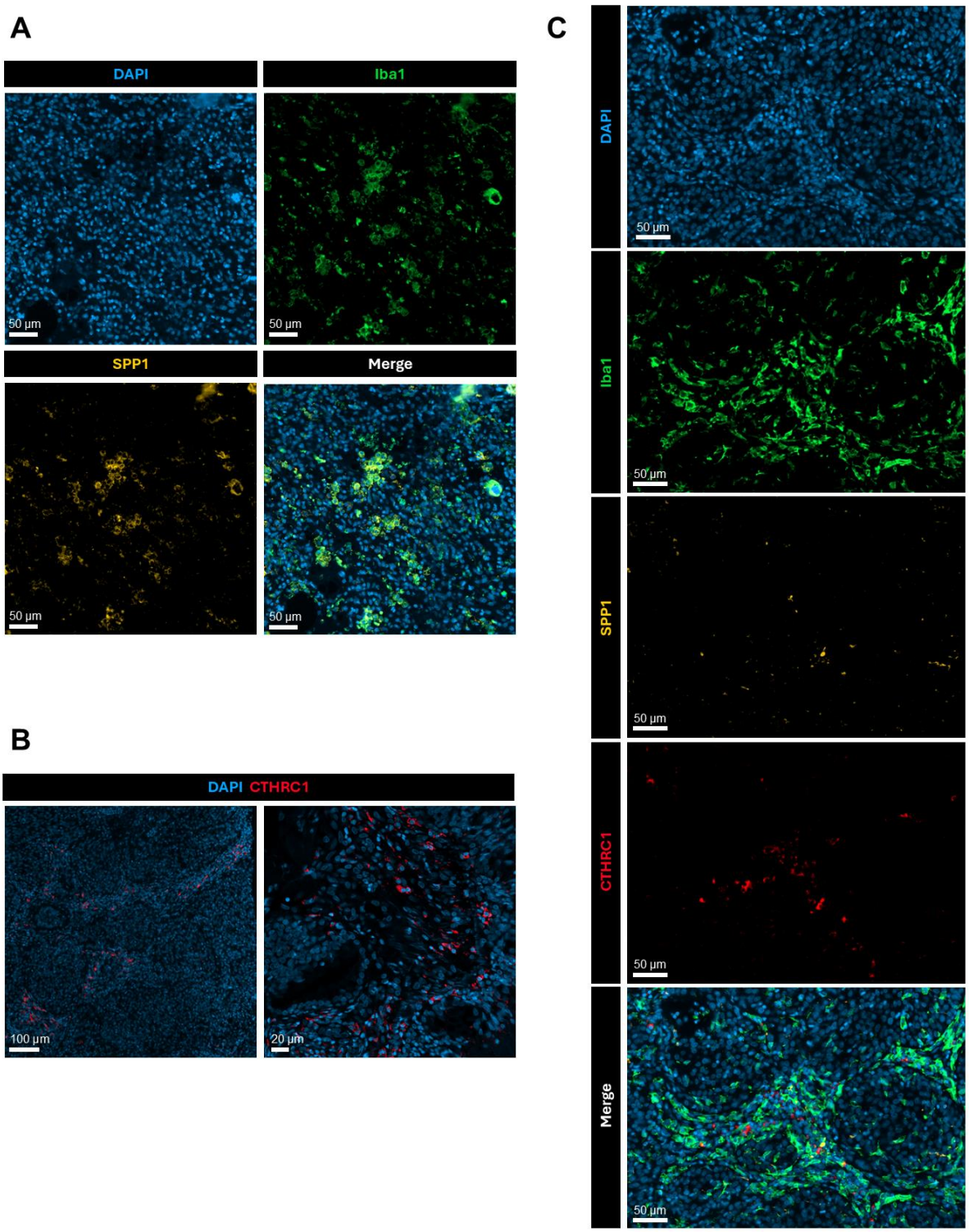

Figure 6. In-situ validation of CTHRC1 and SPP1 through immunofluorescence microscopy. (A) Visualization of co-expression of Iba1 (green), a pan-myeloid marker, and SPP1 (orange), a tumor-associated macrophage (TAM) marker in peritumoral stromal areas. (B) Visualization of CTHRC1 expression (red) by fibroblast-shaped cells, cancer-associated fibroblasts (CAFs), in tumor stroma. (C) Colocalization of CTHRC1^{+} CAFs and SPP1^{+} TAMs in tumor stroma.

Discussion

This study increases knowledge of the canine pulmonary adenocarcinoma microenvironment at single-cell level. It identified an altered cancer-associated fibroblast gene expression profile, especially in myofibroblasts. This study also identified a modification in macrophages/monocytes gene expression profiles, including an overexpression of *SPP1*. Alterations in plasma cells, muscle cells and endothelial cells were also notable. Finally, the transcriptomes of cancer cells from three distinct pulmonary adenocarcinomas were sequenced.

This study confirmed fibroblast activation protein (*FAP*) as a marker of CAFs in PAC, as already shown by immunohistochemistry (Rizzoli et al., 2024). Collagen triple helix repeat containing 1 (*CTHRC1*) appeared as a specific marker of CAFs, more precisely myofibroblastic CAFs in canine pulmonary carcinoma. In human NSCLC, *CTHRC1* was significantly overexpressed and associated with a more aggressive tumor behavior and a worse prognosis (Ke et al., 2014; Y.-J. Liu et al., 2023; Singh et al., 2024). In human NSCLC, $POSTN^+$/$CTHRC1^+$/FAP^+ CAFs correlated with immune suppression and tumor progression (Chen et al., 2023). Interestingly, *CTHRC1* overexpression was the highest in PAC3, which exhibited the most aggressive histological growth patterns. In humans, tumor growth patterns convey prognostic values, as acinar and squamous differentiation are associated with worse prognosis than lepidic patterns (Travis et al., 2013, 2011; Wilson, 2016). Even though canine pulmonary carcinomas display histological features similar to human carcinomas, it is not known whether this classification scheme has a prognostic value in dogs (McPhetridge et al., 2021; Wilson, 2016).

Osteopontin (*SPP1*) was identified as a marker of TAMs in canine PAC. In dogs, *SPP1* was shown to be overexpressed in canine idiopathic pulmonary fibrosis (Fastrès et al., 2023, 2020b). In human NSCLC, *SPP1* was already shown to be highly expressed and to facilitate migration, invasion, progression and drug resistance, and $SPP1^+$ TAMs were shown to promote EMT and facilitate immune escape (Zhang et al., 2017; Leader et al., 2021; Yan et al., 2023). One possible mechanism of immune escape could be the upregulation of immune checkpoint PD-L1 (Zhang et al., 2017).

In this study, PD-L1 and PD-1 were overexpressed mainly in one PAC sample (PAC3), but not statistically significantly overexpressed in all PAC samples. This may be due to low statistical power due to small sample size, low sequencing saturation or inter-tumor expression variability. The expression of immune checkpoint in canine PAC thus requires further investigation. In humans, immune checkpoint inhibitors have been developed and approved for the treatment of NSCLC. PD-1/PD-L1 blockade therapy has been shown to significantly enhance response rates and extend long-

term survival in a subset of patients with advanced NSCLC (Xia et al., 2019). Interestingly, the expression of *CTHRC1* and *SPP1* was positively correlated with the expression of immune checkpoint genes in patients with lung adenocarcinoma and may predict response to immunotherapy (J. Yang et al., 2023).

This study included a spatial dimension with immunofluorescence microscopy, showing that CTHRC1$^+$ CAFs clustered around or adjacent to tumor nests, in proximity with SPP1$^+$ TAMs. Such proximity of CTHRC1$^+$ CAFs and SPP1$^+$ TAMs was also demonstrated in human NSCLC, contributing to extracellular remodeling and immune suppression (Chen et al., 2023). Similarly, studies in human pancreatic ductal adenocarcinoma and colorectal cancer demonstrated that CAFs and SPP1$^+$ TAMs colocalized, promoted a pro-tumorigenic immune-suppressive tumor microenvironment and correlated with worse prognosis (Li et al., 2024; Qi et al., 2022).

This study thus highlight potential new diagnostic and prognostic biomarkers as well as novel therapeutic strategies, such as FAP$^+$ CAFs depletion (Lee et al., 2022), CHTRC1 regulation or inhibition (Singh et al., 2024), targeting SPP1-related signaling pathways (Matsubara et al., 2023) including immune checkpoint inhibitors, which are already under development in veterinary medicine (Igase et al., 2020; Yoshimoto et al., 2023).

Differences in plasma cells populations were identified in this study, such as the overrepresentation of IgKC$^+$ plasma cells. In human lung adenocarcinoma, IgKC was previously reported to be expressed in stroma-infiltrating plasma cells and to serve as a positive prognostic marker (Lohr et al., 2013). However, the present results should be confirmed with in situ validation techniques, such as immunostaining, in a larger number of samples.

This study may also suggest alterations within neutrophils population. Notably, a subset of neutrophils originating from PAC3 appeared to cluster with a population of SPP1$^+$ monocytes. On HE staining, PAC3 exhibited marked neutrophilic infiltration and potentially the most aggressive growth pattern. The role of this neutrophil population in PAC pathogenesis warrants further investigation in larger studies. In NSCLC, distinct subsets of neutrophils exhibit anti-tumor and pro-tumor phenotypes, including SPP1 signaling, and carry a prognostic value (Pang et al., 2022; Peng et al., 2023; Salcher et al., 2022).

This study has several limitations. The sample size was small, due to the high cost of scRNA-seq, resulting in limited statistical power to detect differences in cell type proportions. This limitation was taken into account when setting the p-value threshold for statistical significance;

however, the results should still be interpreted with caution. The small number of samples may also have reduced the power of pseudo-bulk differential expression analyses, potentially leading to missed detection of some overexpressed genes. Additionally, the low sequencing depth, particularly in sample PAC1, may have resulted in underestimated transcript levels for certain genes.

In conclusion, this study provides a single-cell resolution overview of the transcriptional landscape of canine pulmonary adenocarcinoma. It reveals alterations in the tumor microenvironment, particularly in fibroblasts and macrophages, which may contribute to tumor progression and immune evasion. These findings open new avenues for the development of novel therapeutic strategies, particularly for advanced cancer stages.

Acknowledgments

The authors thank the Surgical Oncology unit of the Companion Animal Hospital of the University of Liège for giving access to tumor surgical specimens; the GIGA Genomics and Bioinformatics platform, especially D. Stern and A. Lavergne for their guidance in script writing and data analysis, and L. Karim and her team for their availability for processing scRNA-seq samples within short notice; J.M. Collard for his guidance with immunofluorescence microscopy. Elodie Rizzoli is a Research Fellow of the Fonds de la Recherche Scientifique – FNRS and this study was funded by the 'Fonds Spéciaux de la Recherche' of the University of Liège.

References

Ammons, D.T., Hopkins, L.S., Cronise, K.E., Kurihara, J., Regan, D.P., Dow, S., 2024. Single-cell RNA sequencing reveals the cellular and molecular heterogeneity of treatment-naïve primary osteosarcoma in dogs. Commun Biol 7, 1–18. https://doi.org/10.1038/s42003-024-06182-w

Beck, J., Miller, M.A., Frank, C., DuSold, D., Ramos-Vara, J.A., 2017. Surfactant Protein A and Napsin A in the Immunohistochemical Characterization of Canine Pulmonary Carcinomas: Comparison With Thyroid Transcription Factor-1. Vet Pathol 54, 767–774. https://doi.org/10.1177/0300985817712559

Bettini, G., Marconato, L., Morini, M., Ferrari, F., 2009. Thyroid transcription factor-1 immunohistochemistry: diagnostic tool and malignancy marker in canine malignant lung tumours. Veterinary and Comparative Oncology 7, 28–37. https://doi.org/10.1111/j.1476-5829.2008.00166.x

Bettini, G., Morini, M., Marconato, L., Marcato, P.S., Zini, E., 2010. Association between environmental dust exposure and lung cancer in dogs. The Veterinary Journal 186, 364–369. https://doi.org/10.1016/j.tvjl.2009.09.004

Chen, C., Guo, Q., Liu, Y., Hou, Q., Liao, M., Guo, Y., Zang, Y., Wang, F., Liu, Huanyu, Luan, X., Liang, Y., Guan, Z., Li, Y., Liu, Haozhen, Dong, X., Zhang, X., Liu, J., Xu, Q., 2023. Single-cell and spatial transcriptomics reveal POSTN+ cancer-associated fibroblasts correlated with immune suppression and tumour progression in non-small cell lung cancer. Clin Transl Med 13, e1515. https://doi.org/10.1002/ctm2.1515

Denisenko, E., Guo, B.B., Jones, M., Hou, R., de Kock, L., Lassmann, T., Poppe, D., Clément, O., Simmons, R.K., Lister, R., Forrest, A.R.R., 2020. Systematic assessment of tissue dissociation and storage biases in single-cell and single-nucleus RNA-seq workflows. Genome Biology 21, 130. https://doi.org/10.1186/s13059-020-02048-6

Dow, S., 2019. A Role for Dogs in Advancing Cancer Immunotherapy Research. Front Immunol 10, 2935. https://doi.org/10.3389/fimmu.2019.02935

Fastrès, A., Pirottin, D., Fievez, L., Marichal, T., Desmet, C.J., Bureau, F., Clercx, C., 2020a. Characterization of the Bronchoalveolar Lavage Fluid by Single Cell Gene Expression Analysis in Healthy Dogs: A Promising Technique. Front Immunol 11, 1707. https://doi.org/10.3389/fimmu.2020.01707

Fastrès, A., Pirottin, D., Fievez, L., Tutunaru, A.-C., Bolen, G., Merveille, A.-C., Marichal, T., Desmet, C.J., Bureau, F., Clercx, C., 2020b. Identification of Pro-Fibrotic Macrophage Populations by

Single-Cell Transcriptomic Analysis in West Highland White Terriers Affected With Canine Idiopathic Pulmonary Fibrosis. Front Immunol 11, 611749. https://doi.org/10.3389/fimmu.2020.611749

Fastrès, A., Roels, E., Tutunaru, A.C., Bolen, G., Merveille, A.-C., Day, M.J., Garigliany, M.-M., Antoine, N., Clercx, C., 2023. Osteopontin and fibronectin in lung tissue, serum, and bronchoalveolar lavage fluid of dogs with idiopathic pulmonary fibrosis and control dogs. J Vet Intern Med 37, 2468–2477. https://doi.org/10.1111/jvim.16870

Hao, Y., Hao, S., Andersen-Nissen, E., Mauck, W.M., Zheng, S., Butler, A., Lee, M.J., Wilk, A.J., Darby, C., Zager, M., Hoffman, P., Stoeckius, M., Papalexi, E., Mimitou, E.P., Jain, J., Srivastava, A., Stuart, T., Fleming, L.M., Yeung, B., Rogers, A.J., McElrath, J.M., Blish, C.A., Gottardo, R., Smibert, P., Satija, R., 2021. Integrated analysis of multimodal single-cell data. Cell 184, 3573-3587.e29. https://doi.org/10.1016/j.cell.2021.04.048

Igase, M., Nemoto, Y., Itamoto, K., Tani, K., Nakaichi, M., Sakurai, M., Sakai, Y., Noguchi, S., Kato, M., Tsukui, T., Mizuno, T., 2020. A pilot clinical study of the therapeutic antibody against canine PD-1 for advanced spontaneous cancers in dogs. Sci Rep 10, 18311. https://doi.org/10.1038/s41598-020-75533-4

Ke, Z., He, W., Lai, Y., Guo, X., Chen, S., Li, S., Wang, Y., Wang, L., 2014. Overexpression of Collagen Triple Helix Repeat Containing 1 (CTHRC1) is associated with tumour aggressiveness and poor prognosis in human non-small cell lung cancer. Oncotarget 5, 9410–9424. https://doi.org/10.18632/oncotarget.2421

Leader, A.M., Grout, J.A., Maier, B.B., Nabet, B.Y., Park, M.D., Tabachnikova, A., Chang, C., Walker, L., Lansky, A., Le Berichel, J., Troncoso, L., Malissen, N., Davila, M., Martin, J.C., Magri, G., Tuballes, K., Zhao, Z., Petralia, F., Samstein, R., D'Amore, N.R., Thurston, G., Kamphorst, A.O., Wolf, A., Flores, R., Wang, P., Müller, S., Mellman, I., Beasley, M.B., Salmon, H., Rahman, A.H., Marron, T.U., Kenigsberg, E., Merad, M., 2021. Single-cell analysis of human non-small cell lung cancer lesions refines tumor classification and patient stratification. Cancer Cell 39, 1594-1609.e12. https://doi.org/10.1016/j.ccell.2021.10.009

Lee, B.M., Clarke, D., Watson, M., Laver, T., 2020. Retrospective evaluation of a modified human lung cancer stage classification in dogs with surgically excised primary pulmonary carcinomas. Veterinary and Comparative Oncology 18, 590–598. https://doi.org/10.1111/vco.12582

Lee, I.K., Noguera-Ortega, E., Xiao, Z., Todd, L., Scholler, J., Song, D., Liousia, M., Lohith, K., Xu, K., Edwards, K.J., Farwell, M.D., June, C.H., Albelda, S.M., Puré, E., Sellmyer, M.A., 2022.

Monitoring Therapeutic Response to Anti-FAP CAR T Cells Using [18F]AlF-FAPI-74. Clin Cancer Res 28, 5330–5342. https://doi.org/10.1158/1078-0432.CCR-22-1379

Li, E., Cheung, H.C. (Zoey), Ma, S., 2024. CTHRC1+ fibroblasts and SPP1+ macrophages synergistically contribute to pro-tumorigenic tumor microenvironment in pancreatic ductal adenocarcinoma. Sci Rep 14, 17412. https://doi.org/10.1038/s41598-024-68109-z

Liu, Y.-J., Du, J., Li, J., Tan, X.-P., Zhang, Q., 2023. CTHRC1, a novel gene with multiple functions in physiology, disease and solid tumors (Review). Oncol Lett 25, 266. https://doi.org/10.3892/ol.2023.13852

Lohr, M., Edlund, K., Botling, J., Hammad, S., Hellwig, B., Othman, A., Berglund, A., Lambe, M., Holmberg, L., Ekman, S., Bergqvist, M., Pontén, F., Cadenas, C., Marchan, R., Hengstler, J.G., Rahnenführer, J., Micke, P., 2013. The prognostic relevance of tumour-infiltrating plasma cells and immunoglobulin kappa C indicates an important role of the humoral immune response in non-small cell lung cancer. Cancer Lett 333, 222–228. https://doi.org/10.1016/j.canlet.2013.01.036

Love, M.I., Huber, W., Anders, S., 2014. Moderated estimation of fold change and dispersion for RNA-seq data with DESeq2. Genome Biol 15, 550. https://doi.org/10.1186/s13059-014-0550-8

Matsubara, E., Yano, H., Pan, C., Komohara, Y., Fujiwara, Y., Zhao, S., Shinchi, Y., Kurotaki, D., Suzuki, M., 2023. The Significance of SPP1 in Lung Cancers and Its Impact as a Marker for Protumor Tumor-Associated Macrophages. Cancers (Basel) 15, 2250. https://doi.org/10.3390/cancers15082250

McPhetridge, J.B., Scharf, V.F., Regier, P.J., Toth, D., Lorange, M., Tremolada, G., Dornbusch, J.A., Selmic, L.E., Bae, S., Townsend, K.L., McAdoo, J.C., Thieman, K.M., Solari, F., Walton, R.A., Romeiser, J., Tuohy, J.L., Oblak, M.L., 2021. Distribution of histopathologic types of primary pulmonary neoplasia in dogs and outcome of affected dogs: 340 cases (2010-2019). J Am Vet Med Assoc 260, 234–243. https://doi.org/10.2460/javma.20.12.0698

Ogilvie, G.K., Haschek, W.M., Withrow, S.J., Richardson, R.C., Harvey, H.J., Henderson, R.A., Fowler, J.D., Norris, A.M., Tomlinson, J., McCaw, D., 1989. Classification of primary lung tumors in dogs: 210 cases (1975-1985). J Am Vet Med Assoc 195, 106–108.

Pang, J., Yu, Q., Chen, Y., Yuan, H., Sheng, M., Tang, W., 2022. Integrating Single-cell RNA-seq to construct a Neutrophil prognostic model for predicting immune responses in non-small cell lung cancer. J Transl Med 20, 531. https://doi.org/10.1186/s12967-022-03723-x

Peng, H., Wu, X., Liu, S., He, M., Xie, C., Zhong, R., Liu, J., Tang, C., Li, C., Xiong, S., Zheng, H., He, J., Lu, X., Liang, W., 2023. Multiplex immunofluorescence and single-cell transcriptomic profiling reveal the spatial cell interaction networks in the non-small cell lung cancer microenvironment. Clin Transl Med 13, e1155. https://doi.org/10.1002/ctm2.1155

Qi, J., Sun, H., Zhang, Y., Wang, Z., Xun, Z., Li, Z., Ding, X., Bao, R., Hong, L., Jia, W., Fang, F., Liu, H., Chen, L., Zhong, J., Zou, D., Liu, L., Han, L., Ginhoux, F., Liu, Y., Ye, Y., Su, B., 2022. Single-cell and spatial analysis reveal interaction of FAP+ fibroblasts and SPP1+ macrophages in colorectal cancer. Nat Commun 13, 1742. https://doi.org/10.1038/s41467-022-29366-6

Ramos-Vara, J.A., Miller, M.A., Johnson, G.C., 2005. Usefulness of Thyroid Transcription Factor-1 Immunohistochemical Staining in the Differential Diagnosis of Primary Pulmonary Tumors of Dogs. Vet Pathol 42, 315–320. https://doi.org/10.1354/vp.42-3-315

Rebhun, R.B., Culp, W.T.N., 2020. Tumors of the respiratory system, section D: pulmonary neoplasia, in: Withrow and MacEwen's Small Animal Clinical Oncology, 6th Edition. Elsevier, St. Louis, pp. 507–515.

Rizzoli, E., de Meeûs d'Argenteuil, C., Fastrès, A., Roels, E., Janssen, P., Puré, E., Garigliany, M.-M., Marichal, T., Clercx, C., 2024. Fibroblast activation protein is a cellular marker of fibrotic activity in canine idiopathic pulmonary fibrosis. Front Vet Sci 11, 1416124. https://doi.org/10.3389/fvets.2024.1416124

Rizzoli, E., Fievez, L., Fastrès, A., Roels, E., Marichal, T., Clercx, C., 2025. A single-cell RNA sequencing atlas of the healthy canine lung: a foundation for comparative studies. Front Immunol 16, 1501603. https://doi.org/10.3389/fimmu.2025.1501603

Rose, R.J., Worley, D.R., 2020. A Contemporary Retrospective Study of Survival in Dogs With Primary Lung Tumors: 40 Cases (2005–2017). Front. Vet. Sci. 7. https://doi.org/10.3389/fvets.2020.519703

Salcher, S., Sturm, G., Horvath, L., Untergasser, G., Kuempers, C., Fotakis, G., Panizzolo, E., Martowicz, A., Trebo, M., Pall, G., Gamerith, G., Sykora, M., Augustin, F., Schmitz, K., Finotello, F., Rieder, D., Perner, S., Sopper, S., Wolf, D., Pircher, A., Trajanoski, Z., 2022. High-resolution single-cell atlas reveals diversity and plasticity of tissue-resident neutrophils in non-small cell lung cancer. Cancer Cell 40, 1503-1520.e8. https://doi.org/10.1016/j.ccell.2022.10.008

Shiota, Y., Elbadawy, M., Suzuki, K., Tsunedomi, R., Nagano, H., Ishihara, Y., Yamamoto, H., Azakami, D., Uchide, T., Fukushima, R., Tanaka, R., Yoshida, T., Mori, T., Abugomaa, A., Kaneda, M.,

Yamawaki, H., Shinohara, Y., Aboubakr, M., El-Asrag, M.E., Usui, T., Sasaki, K., 2023. Derivation of a new model of lung adenocarcinoma using canine lung cancer organoids for translational research in pulmonary medicine. Biomedicine & Pharmacotherapy 165, 115079. https://doi.org/10.1016/j.biopha.2023.115079

Siegel, R.L., Giaquinto, A.N., Jemal, A., 2024. Cancer statistics, 2024. CA: A Cancer Journal for Clinicians 74, 12–49. https://doi.org/10.3322/caac.21820

Singh, C.K., Fernandez, S., Chhabra, G., Zaemisch, G.R., Nihal, A., Swanlund, J., Ansari, N., Said, Z., Chang, H., Ahmad, N., 2024. The role of collagen triple helix repeat containing 1 (CTHRC1) in cancer development and progression. Expert Opinion on Therapeutic Targets 28, 419–435. https://doi.org/10.1080/14728222.2024.2349686

Subramanian, A., Tamayo, P., Mootha, V.K., Mukherjee, S., Ebert, B.L., Gillette, M.A., Paulovich, A., Pomeroy, S.L., Golub, T.R., Lander, E.S., Mesirov, J.P., 2005. Gene set enrichment analysis: A knowledge-based approach for interpreting genome-wide expression profiles. Proceedings of the National Academy of Sciences 102, 15545–15550. https://doi.org/10.1073/pnas.0506580102

Tietscher, S., Wagner, J., Anzeneder, T., Langwieder, C., Rees, M., Sobottka, B., de Souza, N., Bodenmiller, B., 2023. A comprehensive single-cell map of T cell exhaustion-associated immune environments in human breast cancer. Nat Commun 14, 98. https://doi.org/10.1038/s41467-022-35238-w

Travis, W.D., Brambilla, E., Noguchi, M., Nicholson, A.G., Geisinger, K., Yatabe, Y., Ishikawa, Y., Wistuba, I., Flieder, D.B., Franklin, W., Gazdar, A., Hasleton, P.S., Henderson, D.W., Kerr, K.M., Petersen, I., Roggli, V., Thunnissen, E., Tsao, M., 2013. Diagnosis of lung cancer in small biopsies and cytology: implications of the 2011 International Association for the Study of Lung Cancer/American Thoracic Society/European Respiratory Society classification. Arch Pathol Lab Med 137, 668–684. https://doi.org/10.5858/arpa.2012-0263-RA

Travis, W.D., Brambilla, E., Noguchi, M., Nicholson, A.G., Geisinger, K.R., Yatabe, Y., Beer, D.G., Powell, C.A., Riely, G.J., Van Schil, P.E., Garg, K., Austin, J.H.M., Asamura, H., Rusch, V.W., Hirsch, F.R., Scagliotti, G., Mitsudomi, T., Huber, R.M., Ishikawa, Y., Jett, J., Sanchez-Cespedes, M., Sculier, J.-P., Takahashi, T., Tsuboi, M., Vansteenkiste, J., Wistuba, I., Yang, P.-C., Aberle, D., Brambilla, C., Flieder, D., Franklin, W., Gazdar, A., Gould, M., Hasleton, P., Henderson, D., Johnson, B., Johnson, D., Kerr, K., Kuriyama, K., Lee, J.S., Miller, V.A., Petersen, I., Roggli, V., Rosell, R., Saijo, N., Thunnissen, E., Tsao, M., Yankelewitz, D., 2011. International Association for the Study of Lung Cancer/American Thoracic

Society/European Respiratory Society International Multidisciplinary Classification of Lung Adenocarcinoma. Journal of Thoracic Oncology 6, 244–285. https://doi.org/10.1097/JTO.0b013e318206a221

Treggiari, E., Romanelli, G., Valenti, P., Montinaro, V., Rossanese, M., 2025. Evaluation of lung lobectomy and adjuvant treatment for primary pulmonary carcinoma in dogs: 89 cases (2005-2022). J Small Anim Pract. https://doi.org/10.1111/jsap.13874

Wilson, D.W., 2016. Tumors of the Respiratory Tract, in: Tumors in Domestic Animals. John Wiley & Sons, Ltd, pp. 467–498. https://doi.org/10.1002/9781119181200.ch12

Wu, T., Hu, E., Xu, S., Chen, M., Guo, P., Dai, Z., Feng, T., Zhou, L., Tang, W., Zhan, L., Fu, X., Liu, S., Bo, X., Yu, G., 2021. clusterProfiler 4.0: A universal enrichment tool for interpreting omics data. The Innovation 2, 100141. https://doi.org/10.1016/j.xinn.2021.100141

Xia, L., Liu, Y., Wang, Y., 2019. PD-1/PD-L1 Blockade Therapy in Advanced Non-Small-Cell Lung Cancer: Current Status and Future Directions. Oncologist 24, S31–S41. https://doi.org/10.1634/theoncologist.2019-IO-S1-s05

Yan, Z., Hu, X., Tang, B., Deng, F., 2023. Role of osteopontin in cancer development and treatment. Heliyon 9, e21055. https://doi.org/10.1016/j.heliyon.2023.e21055

Yang, J., Liu, K., Yang, L., Ji, J., Qin, J., Deng, H., Wang, Z., 2023. Identification and validation of a novel cuproptosis-related stemness signature to predict prognosis and immune landscape in lung adenocarcinoma by integrating single-cell and bulk RNA-sequencing. Front Immunol 14, 1174762. https://doi.org/10.3389/fimmu.2023.1174762

Yoshimoto, S., Chester, N., Xiong, A., Radaelli, E., Wang, H., Brillantes, M., Gulendran, G., Glassman, P., Siegel, D.L., Mason, N.J., 2023. Development and pharmacokinetic assessment of a fully canine anti-PD-1 monoclonal antibody for comparative translational research in dogs with spontaneous tumors. MAbs 15, 2287250. https://doi.org/10.1080/19420862.2023.2287250

Zappia, L., Oshlack, A., 2018. Clustering trees: a visualization for evaluating clusterings at multiple resolutions. GigaScience 7, giy083. https://doi.org/10.1093/gigascience/giy083

Zhang, Y., Du, W., Chen, Z., Xiang, C., 2017. Upregulation of PD-L1 by SPP1 mediates macrophage polarization and facilitates immune escape in lung adenocarcinoma. Exp Cell Res 359, 449–457. https://doi.org/10.1016/j.yexcr.2017.08.028

Supplemental material

Supplementary tables

Supplementary Table 1: Antibodies used for immunofluorescence studies

Primary antibody				Secondary antibodies				
Target	Host species	Manufacturer	Catalog #	Target	Fluorochrome	Host species	Manufacturer	Catalog #
CTHRC1	Mouse	Invitrogen	MA5-34885	Mouse IgG	Alexa Fluor 647	Donkey	Invitrogen	A31571
Iba1	Goat	Abcam	ab5076	Goat IgG	Alexa Fluor 488	Donkey	Invitrogen	A11055
SPP1	Rabbit	Abcam	ab8448	Rabbit IgG	Alexa Fluor 568	Donkey	Invitrogen	A10042

Supplementary Table 2: Summary of sequencing and mapping quality control metrics

	Estimated number of cells	Sequencing saturation, %	Reads mapped confidently to	Reads mapped confidently to transcriptome, %	Mean reads/cell	Median unique molecular identifier	Median genes/cell	Total genes detected
PAC 1	27,418	16.4	83.1	56.7	8,415	2,020	1,032	18,078
PAC 2	6,521	45.5	87.9	60.6	24,620	3,880	1,520	17,082
PAC 3	5,080	51.0	87.7	60.3	36,940	4,243	1,642	16,991
Lung 1	10,487	34.1	83.6	56.8	15,057	2,710	1,368	17,455
Lung 2	8,571	55.0	79.5	48.4	20,043	1,479	873	16,872
Lung 3	8,584	46.8	81.8	52.2	18,085	2,880	1,362	17,019
Lung 4	5,296	52.8	88.1	60.0	35,083	6,871	2,296	16,835

Supplementary Table 3: Top 5 overexpressed genes by each cell cluster compared to all other clusters, generated with the FindMarkers function

Cell cluster	Average log2 fold change	Fraction of cells expressing the gene within this cluster	Fraction of cells expressing the gene within all other cells	Adjusted p-value	Gene
Aerocytes	2.301	0.924	0.169	0	CALCRL
Aerocytes	2.265	0.879	0.267	0	EMP2
Aerocytes	2.207	0.891	0.252	0	CFI
Aerocytes	2.110	0.925	0.3	0	CAV1
Aerocytes	2.097	0.808	0.096	0	KDR
Alveolar fibroblasts	2.920	0.957	0.548	0	ARHGAP45
Alveolar fibroblasts	2.656	0.764	0.152	0	MACROD2
Alveolar fibroblasts	2.649	0.781	0.179	0	CDO1
Alveolar fibroblasts	2.570	0.813	0.176	0	LIMCH1
Alveolar fibroblasts	2.455	0.683	0.045	0	CADM2
Alveolar macrophages	3.666	0.992	0.149	0	CHI3L1
Alveolar macrophages	3.474	0.996	0.219	0	BPI
Alveolar macrophages	2.679	0.838	0.063	0	MARCO
Alveolar macrophages	2.440	0.999	0.688	0	DLA-DRA
Alveolar macrophages	2.397	0.915	0.189	0	CPNE6
Arterial endothelial cells	2.631	0.956	0.189	0	CALCRL
Arterial endothelial cells	2.382	0.974	0.199	0	LDB2
Arterial endothelial cells	2.022	0.958	0.29	0	PTPRG
Arterial endothelial cells	1.963	0.918	0.169	0	PTPRB
Arterial endothelial cells	1.875	0.698	0.035	0	BMPER
Airway smooth muscle cells	3.982	0.856	0.111	0	DGUOK
Airway smooth muscle cells	3.299	0.864	0.028	0	PRUNE2
Airway smooth muscle cells	3.183	0.907	0.099	0	ACTA2
Airway smooth muscle cells	2.976	0.778	0.013	0	HPSE2
Airway smooth muscle cells	2.927	0.926	0.15	0	MYH11
Alveolar Type 1 cells	3.251	0.861	0.162	0	AGER
Alveolar Type 1 cells	2.721	0.92	0.346	0	TSPAN8
Alveolar Type 1 cells	2.354	0.824	0.182	0	CES5A
Alveolar Type 1 cells	2.140	0.854	0.129	0	LMO7
Alveolar Type 1 cells	2.050	0.636	0.026	0	SEMA3E
Alveolar Type 2 cells	6.238	0.994	0.707	0	SFTPC
Alveolar Type 2 cells	3.561	0.951	0.131	0	NAPSA
Alveolar Type 2 cells	3.439	0.862	0.055	0	SLC34A2
Alveolar Type 2 cells	3.343	0.948	0.071	0	C5
Alveolar Type 2 cells	3.138	0.872	0.299	0	WFDC2
B cells	1.917	0.708	0.082	0	LTB

B cells	1.340	0.629	0.103	0	SP140
B cells	1.326	0.592	0.048	0	TNFRSF13C
B cells	1.041	0.489	0.057	0	RALGPS2
B cells	0.856	0.408	0.036	0	BCL11A
C1Q+ Alveolar macrophages	3.470	0.996	0.165	0	CHI3L1
C1Q+ Alveolar macrophages	3.354	1	0.083	0	C1QB
C1Q+ Alveolar macrophages	3.260	1	0.233	0	BPI
C1Q+ Alveolar macrophages	3.008	0.998	0.085	0	C1QA
C1Q+ Alveolar macrophages	2.704	0.996	0.08	0	C1QC
Cancer Cells 2	2.411	0.931	0.137	0	ANK3
Cancer Cells 2	2.147	0.946	0.287	0	MECOM
Cancer Cells 2	2.041	0.893	0.4	0	PDE4D
Cancer Cells 2	1.895	0.897	0.264	0	MCU
Cancer Cells 2	1.657	0.832	0.219	0	CYP7B1
Cancer Cells 3	2.178	0.997	0.435	0	KRT14
Cancer Cells 3	1.992	0.943	0.175	0	CES5A
Cancer Cells 3	1.963	0.892	0.157	0	AGER
Cancer Cells 3	1.807	0.969	0.454	0	METTL7A
Cancer Cells 3	1.613	0.862	0.147	0	CLIC3
CCL13+ Macrophages	2.969	0.789	0.056	0	C1QB
CCL13+ Macrophages	2.879	0.803	0.053	0	C1QC
CCL13+ Macrophages	2.808	0.82	0.057	0	C1QA
CCL13+ Macrophages	2.340	0.851	0.164	0	MRC1
CCL13+ Macrophages	2.166	0.997	0.681	0	DLA-DRA
CCL19+ Adventitial fibroblasts	4.666	0.717	0.031	0	CCL19
CCL19+ Adventitial fibroblasts	2.399	0.941	0.169	0	C1S
CCL19+ Adventitial fibroblasts	2.357	0.703	0.102	0	PRG4
CCL19+ Adventitial fibroblasts	2.149	0.524	0.03	0	ADAMDEC1
CCL19+ Adventitial fibroblasts	1.987	0.857	0.119	0	C1R
CCN3+ Adventitial fibroblasts	4.526	0.873	0.145	0	PI3
CCN3+ Adventitial fibroblasts	4.024	0.985	0.225	0	IGFBP6
CCN3+ Adventitial fibroblasts	3.780	1	0.259	0	DCN
CCN3+ Adventitial fibroblasts	2.856	0.796	0.102	0	PRG4
CCN3+ Adventitial fibroblasts	2.815	0.964	0.1	0	FBLN1
CD4 T cells	1.768	0.604	0.036	0	ICOS
CD4 T cells	1.748	0.619	0.07	0	IL7R
CD4 T cells	1.662	0.675	0.062	0	SKAP1
CD4 T cells	1.644	0.875	0.354	0	PTPRC
CD4 T cells	1.586	0.799	0.276	0	ARHGAP15
CD8 T cells	5.377	0.866	0.057	0	CCL5
CD8 T cells	3.813	0.928	0.145	0	CCL4
CD8 T cells	2.742	0.553	0.013	0	GZMK
CD8 T cells	2.293	0.9	0.271	0	CORO1B
CD8 T cells	2.140	0.826	0.074	0	CD3E
Myeloid/conventional DC 1	2.887	0.963	0.14	0	WDFY4

Myeloid/conventional DC 1	1.672	0.863	0.113	0	SHTN1
Myeloid/conventional DC 1	1.549	0.799	0.068	0	BATF3
Myeloid/conventional DC 1	1.493	0.716	0.052	0	ECM1
Myeloid/conventional DC 1	1.380	0.765	0.103	0	PKIB
Myeloid/conventional DC 2	2.963	0.998	0.966	0	TMSB10
Myeloid/conventional DC 2	2.413	0.958	0.249	0	IFI30
Myeloid/conventional DC 2	2.362	0.998	0.559	0	HLA-DQB2
Myeloid/conventional DC 2	2.277	0.919	0.082	0	PKIB
Myeloid/conventional DC 2	2.271	0.999	0.687	0	DLA-DRA
Ciliated cells	3.425	0.984	0.008	0	LRRIQ1
Ciliated cells	2.936	0.952	0.007	0	DNAH11
Ciliated cells	2.570	0.952	0.026	0	PACRG
Ciliated cells	2.380	0.887	0.021	0	CFAP54
Ciliated cells	2.256	0.839	0.005	0	FGF14
COL23A1+ Adventitial fibroblasts	3.085	0.929	0.217	0	IGFBP6
COL23A1+ Adventitial fibroblasts	3.063	0.948	0.329	0	GSN
COL23A1+ Adventitial fibroblasts	2.940	0.975	0.25	0	DCN
COL23A1+ Adventitial fibroblasts	2.806	0.991	0.45	0	MGP
COL23A1+ Adventitial fibroblasts	2.330	0.909	0.09	0	FBLN1
Cycling epithelial cells	1.525	0.84	0.185	0	STMN1
Cycling epithelial cells	1.525	0.642	0.032	0	TOP2A
Cycling epithelial cells	1.362	0.565	0.025	0	CENPF
Cycling epithelial cells	1.344	0.668	0.103	0	PTTG1 (ENSCAFG00000017264)
Cycling epithelial cells	1.273	0.627	0.027	0	CDC20
Cycling macrophages	1.888	0.948	0.185	0	STMN1
Cycling macrophages	1.780	0.745	0.033	0	TOP2A
Cycling macrophages	1.652	0.717	0.025	0	CENPF
Cycling macrophages	1.335	0.819	0.142	0	PYCARD
Cycling macrophages	1.273	0.581	0.074	0	TENM3
Cycling T cells	1.790	0.865	0.081	0	CD3E
Cycling T cells	1.648	0.49	0.027	0	TNFRSF4
Cycling T cells	1.589	0.646	0.036	0	TOP2A
Cycling T cells	1.584	0.62	0.028	0	CENPF
Cycling T cells	1.491	0.651	0.026	0	MKI67
FN1+ monocytes	2.990	0.883	0.357	0	APOC1
FN1+ monocytes	2.607	0.956	0.223	0	BPI
FN1+ monocytes	2.505	0.946	0.295	0	LYZ
FN1+ monocytes	2.415	0.999	0.689	0	DLA-DRA
FN1+ monocytes	2.239	0.981	0.302	0	CTSS
γδ T cells	1.716	0.732	0.038	0	CRLF2
γδ T cells	1.253	0.331	0.009	1.82E-299	CSF2
γδ T cells	1.018	0.457	0.017	9.11E-299	IL17RB
γδ T cells	1.152	0.535	0.024	7.88E-294	IL2RA
γδ T cells	1.556	0.598	0.034	1.14E-264	ESYT3
General capillary endothelial cells	2.378	0.868	0.114	0	LDB2

General capillary endothelial cells	2.367	0.774	0.077	0	LYVE1
General capillary endothelial cells	2.247	0.867	0.216	0	PTPRG
General capillary endothelial cells	2.126	0.761	0.118	0	CALCRL
General capillary endothelial cells	1.828	0.774	0.093	0	PTPRB
Giant cells	4.766	0.926	0.02	0	MMP9
Giant cells	1.801	0.721	0.013	0	MMP1
Giant cells	1.793	0.838	0.033	0	DPP4
Giant cells	1.562	0.721	0.023	0	NYAP2
Giant cells	1.495	0.662	0.002	0	SLC9B2
Stressed T cells	1.692	0.774	0.083	7.77E-112	CD3E
Stressed T cells	1.504	0.738	0.089	5.03E-95	SKAP1
Stressed T cells	1.623	0.595	0.061	4.65E-88	ICOS
Stressed T cells	1.438	0.702	0.086	5.50E-86	CD3D
Stressed T cells	0.764	0.488	0.045	7.79E-80	CD3G
IFN T cells	1.822	0.764	0.083	6.64E-73	CD3E
IFN T cells	2.787	0.945	0.153	1.37E-72	ISG15
IFN T cells	1.893	0.636	0.062	3.87E-68	ICOS
IFN T cells	2.062	0.873	0.124	1.95E-67	ISG20
IFN T cells	1.991	0.745	0.088	5.90E-66	LTB
IgA+ plasma cells	7.565	0.998	0.35	0	IGHA2(ENSCAFG00000032358)
IgA+ plasma cells	5.092	0.994	0.051	0	JCHAIN
IgA+ plasma cells	2.525	0.903	0.02	0	MZB1
IgA+ plasma cells	2.219	0.958	0.402	0	SEC11C
IgA+ plasma cells	1.951	0.848	0.205	0	PRDX4
IgKC+ plasma cells	8.238	0.906	0.117	0	IGKC
IgKC+ plasma cells	3.935	0.996	0.056	0	JCHAIN
IgKC+ plasma cells	2.381	0.884	0.024	0	MZB1
IgKC+ plasma cells	1.333	0.736	0.028	0	DERL3
IgKC+ plasma cells	1.270	0.726	0.024	0	POU2AF1
IL1B+ monocytes	3.175	0.951	0.286	0	LYZ
IL1B+ monocytes	2.919	0.775	0.045	0	IL1B
IL1B+ monocytes	2.491	0.689	0.128	0	VCAN
IL1B+ monocytes	2.326	0.386	0.017	0	SERPINB2
IL1B+ monocytes	2.192	0.576	0.074	0	PTGS2
Lymphatic endothelial cells	2.724	0.932	0.053	0	FLT4
Lymphatic endothelial cells	2.654	0.839	0.099	0	RHOJ
Lymphatic endothelial cells	2.486	0.767	0.004	0	RELN
Lymphatic endothelial cells	2.114	0.785	0.104	0	STOX2
Lymphatic endothelial cells	1.910	0.803	0.075	0	APOD
Mast cells	5.133	0.894	0.038	0	TRYM (ENSCAFG00000019593)
Mast cells	3.640	0.864	0.018	0	TPSAB1 (ENSCAFG00000031939)
Mast cells	3.135	0.833	0.014	0	CPA3
Mast cells	2.222	0.753	0.026	0	MS4A2
Mast cells	2.081	0.693	0.018	0	CMA1
Mature DC	2.627	0.732	0.13	0	IDO1

Mature DC	2.494	0.845	0.016	0	CCR7
Mature DC	2.435	0.842	0.129	0	TBC1D4
Mature DC	2.168	0.941	0.162	0	SAMSN1
Mature DC	2.159	0.897	0.223	0	BMP2K
MMP12+ monocytes	2.716	0.865	0.076	0	CCL3
MMP12+ monocytes	2.501	0.891	0.149	0	CCL4
MMP12+ monocytes	2.240	0.533	0.034	0	MMP12
MMP12+ monocytes	2.006	0.881	0.168	0	CD83
MMP12+ monocytes	1.881	0.814	0.172	0	CCL23 (ENSCAFG00000031869)
Myofibroblasts	2.418	0.817	0.168	0	TPM2
Myofibroblasts	2.171	0.831	0.097	0	ACTA2
Myofibroblasts	1.339	0.634	0.076	0	TAGLN
Myofibroblasts	0.929	0.362	0.024	0	TFPI2
Myofibroblasts	2.742	0.711	0.132	1.08E-299	COL1A1
Neutrophils	4.593	0.946	0.303	0	CXCL8
Neutrophils	4.555	0.821	0.046	0	S100A12
Neutrophils	4.213	0.8	0.082	0	S100A9 (ENSCAFG00000029470)
Neutrophils	4.021	0.972	0.618	0	SAT1
Neutrophils	3.747	0.902	0.348	0	SOD2
Natural killer cells	2.258	0.819	0.03	0	CD96
Natural killer cells	2.101	0.629	0.021	0	IL12RB2
Natural killer cells	1.558	0.647	0.008	0	KLRB1
Natural killer cells	1.437	0.698	0.017	0	CTSW
Natural killer cells	1.314	0.534	0.011	0	CLNK
Natural killer T cells	4.095	0.642	0.064	0	CCL5
Natural killer T cells	3.950	0.92	0.149	0	CCL4
Natural killer T cells	2.698	0.794	0.009	0	GZMB
Natural killer T cells	2.047	0.746	0.017	0	IL12RB2
Natural killer T cells	2.015	0.768	0.158	0	STAT4
Plasmacytoid dentritic cell	2.672	0.897	0.048	0	PLAC8
Plasmacytoid dentritic cell	2.238	0.751	0.085	0	LTB
Plasmacytoid dentritic cell	1.630	0.725	0.036	0	BCL11A
Plasmacytoid dentritic cell	1.509	0.718	0.056	0	IRAG2
Plasmacytoid dentritic cell	1.373	0.689	0.006	0	RYR1
Plasma cells	4.041	0.975	0.05	0	JCHAIN
Plasma cells	2.426	0.843	0.019	0	MZB1
Plasma cells	2.243	0.933	0.402	0	SEC11C
Plasma cells	2.154	0.886	0.204	0	PRDX4
Plasma cells	1.719	0.766	0.024	0	DERL3
PRG4+ fibroblasts	2.797	0.605	0.089	0	PRG4
PRG4+ fibroblasts	2.333	0.91	0.234	0	COL3A1
PRG4+ fibroblasts	2.324	0.841	0.516	0	TIMP1
PRG4+ fibroblasts	2.315	0.983	0.442	0	MGP
PRG4+ fibroblasts	2.284	0.918	0.213	0	COL1A2
Pulmonary pericytes	3.314	0.908	0.081	0	POSTN

Pulmonary pericytes	3.141	0.97	0.227	0	PRKG1
Pulmonary pericytes	3.123	0.936	0.123	0	GUCY1A2
Pulmonary pericytes	2.771	0.92	0.274	0	ARHGAP42
Pulmonary pericytes	2.678	0.78	0.035	0	COX4I2
Regulatory T cells	2.388	0.748	0.037	0	TNFRSF18
Regulatory T cells	2.275	0.678	0.018	0	TNFRSF4
Regulatory T cells	2.257	0.961	0.41	0	S100A5
Regulatory T cells	2.081	0.831	0.074	0	CD3D
Regulatory T cells	1.997	0.846	0.071	0	CD3E
Secretory/Cancer Cells 1	2.905	0.988	0.426	0	KRT14
Secretory/Cancer Cells 1	2.481	0.905	0.204	0	KRT 86 (ENSCAFG00000007293)
Secretory/Cancer Cells 1	2.253	0.817	0.302	0	WFDC2
Secretory/Cancer Cells 1	2.244	0.947	0.269	0	KRT3
Secretory/Cancer Cells 1	2.217	0.933	0.406	0	KRT18
SPP1+ monocytes/neutrophils	3.319	1	0.948	0	FTL
SPP1+ monocytes/neutrophils	2.595	0.997	0.772	0	CSTB
SPP1+ monocytes/neutrophils	2.139	0.978	0.399	0	BCL2A1
SPP1+ monocytes/neutrophils	2.102	0.789	0.179	0	CDA
SPP1+ monocytes/neutrophils	2.059	1	0.988	0	FTH1.1
Systemic pericytes	2.482	0.386	0.004	0	APOA1
Systemic pericytes	2.470	0.901	0.096	0	ACTA2
Systemic pericytes	2.329	0.82	0.062	0	ADGRL3
Systemic pericytes	2.164	0.97	0.307	0	CALD1
Systemic pericytes	2.095	0.764	0.104	0	RASL11A
Th17-like T cells	1.627	0.338	0.001	0	IL17A
Th17-like T cells	1.535	0.74	0.003	0	IL23R
Th17-like T cells	1.521	0.649	0.02	0	CD52
Th17-like T cells	1.296	0.623	0.009	0	KLRB1
Th17-like T cells	0.819	0.416	0.017	9.88E-154	SYNDIG1
Venous endothelial cells	2.820	0.89	0.105	0	ACKR1
Venous endothelial cells	2.200	0.88	0.118	0	VWF
Venous endothelial cells	2.015	0.964	0.349	0	RAMP2 (ENSCAFG00000014799)
Venous endothelial cells	1.882	0.882	0.2	0	LDB2
Venous endothelial cells	1.869	0.932	0.29	0	PTPRG
Vascular smooth muscle cells	4.368	0.98	0.082	0	ACTA2
Vascular smooth muscle cells	3.610	0.961	0.154	0	TPM2
Vascular smooth muscle cells	3.452	0.896	0.045	0	MUSTN1 (ENSCAFG00000028930)
Vascular smooth muscle cells	3.213	0.953	0.134	0	MYH11
Vascular smooth muscle cells	3.103	0.873	0.096	0	DGUOK

Supplementary Table 4: Cell type distribution comparison between healthy lungs and pulmonary adenocarcinoma

Cell cluster	Median percentages (range) HEALTHY	PAC	P-value *Two-sided Wilcoxon rank sum exact test*	Effect size *Rank-biserial correlation*
Endothelial	**27.5 (12.9-34.2)**	**7.7 (5.5-13.5)**	**0.114**	**0.7**
Aerocytes	23.8 (11.3-26.0)	12.3 (7.3-14.8)	0.229	0.5
General capillary endothelial cell	62.4 (53.4-70)	75.5 (71.9-75.6)	0.057	0.8
Arterial endothelial cell	6.5 (3.8-7.9)	4.5 (3.1-5.4)	0.229	0.5
Venous endothelial cell	6.9 (3.7-9.2)	8.9 (5.9-9.0)	0.857	0.1
Lymphatic endothelial cell	4.0 (1.6-5.7)	1.7 (1.2-2.9)	0.400	0.4
Epithelial	**7.1 (3.1-14.5)**	**20.5 (10.7-27.9)**	**0.114**	**0.7**
Secretory/Cancer Cells 1	21.8 (7.5-32.1)	26.3 (24.8-38.5)	0.629	0.3
Cancer Cells 2	8.2 (5.8-17.8)	21.6 (16.3-26.3)	0.114	0.7
Cancer Cells 3	4.0 (3.0-5.0)	10.0 (2.3-19.5)	0.629	0.3
Cycling epithelial cells	2.0 (1.2-2.7)	8.5 (5.8-10.5)	0.057	0.8
Alveolar type 1 cells	10.1 (4.2-29.8)	5.8 (5.2-14.8)	0.857	0.1
Alveolar type 2 cells	44.5 (28-71.8)	20.5 (13.1-28.1)	0.114	0.7
Ciliated cells	1.0 (0.0-8.0)	0.4 (0.3-1.4)	1.000	0.0
Mesenchymal	**34.0 (31.0-37.4)**	**14.6 (14.4-18.0)**	**0.057**	**0.8**
Fibroblasts	**75.5 (63.9-76.7)**	**72.2 (70.8-75.2)**	**0.629**	**0.3**
Alveolar fibroblasts	44.5 (37.4-55.5)	39.2 (35.0-43.6)	0.629	0.3
PRG4+ fibroblasts	11.4 (7.6-15.9)	17.1 (7.4-21)	0.629	0.3
CCL19+ Adventitial fibroblasts	2.4 (2.1-3.6)	3.0 (2.0-3.0)	1.000	0.0
CCN3+ Adventitial fibroblasts	3.4 (2.2-3.8)	2.2 (0.9-3.1)	0.229	0.5
COL23A1AdvFib	7.7 (4.7-12.1)	6.1 (6.1-8.5)	1.000	0.0
Myofibroblasts	1.9 (1.4-2.6)	5.0 (4.9-10.0)	0.057	0.8
Muscle cells	**24.5 (23.3-36.1)**	**27.8 (24.8-29.2)**	**0.629**	**0.3**
Airway smooth muscle cells	1.7 (1.2-2.7)	1.1 (0.6-2.3)	0.400	0.4
Vascular smooth muscle cells	10.4 (7.9-14.1)	8.5 (6.9-8.7)	0.400	0.4
Systemic pericytes	2.9 (1.1-3.7)	5.1 (4.6-7.5)	0.057	0.8
Pulmonary pericytes	11.5 (7.7-17.2)	12.1 (10.5-13.9)	0.857	0.1
Immune	**31.3 (28.1-39.2)**	**51.9 (51.6-63.5)**	**0.057**	**0.8**
Myeloid	**68.6 (58.0-88.7)**	**71.5 (49.1-76.4)**	**0.629**	**0.3**
Alveolar macrophages	9.1 (1.9-15.9)	2.0 (1.6-6.0)	0.400	0.4
C1Q+ Alveolar macrophages	2.4 (0.3-4.9)	1.2 (0.4-2.1)	0.857	0.1
CCL13+ Macrophages	10.0 (4.7-19.5)	8.8 (6.3-12.7)	0.857	0.1
FN1+ monocytes	4.4 (3.7-15.0)	2.3 (2.0-6.4)	0.400	0.4
SPP1+ monocytes/neutrophils	1.0 (0.6-3.7)	5.3 (2.6-8.4)	0.114	0.7
MMP12+ monocytes	2.3 (1.1-2.8)	1.4 (1.3-2.4)	0.857	0.1
IL1B+ monocytes	6.8 (5.7-11.4)	7.8 (4.8-9.8)	1.000	0.0
Cycling macrophages	0.7 (0.4-1.0)	1.8 (1.0-2.6)	0.114	0.7
Neutrophils	15.0 (10.5-21.3)	20.3 (5.5-39.9)	0.857	0.1
Mast cells	1.6 (0.5-14.3)	0.6 (0.4-3.0)	0.629	0.3
Giant cells	0 (0)	0.1 (0-0.6)	0.078	0.7
Myeloid/conventional DC 1	0.9 (0.8-1.0)	1.1 (0.8-1.9)	0.400	0.4
Myeloid/conventional DC 2	6.1 (5.4-12.9)	2.8 (2.2-8.6)	0.400	0.4

Mature DC	0.7 (0.6-1.0)	1.5 (1.1-2.5)	0.057	0.8
Plasmacytoid dentritic cell	0.3 (0.1-0.4)	0.7 (0.3-2.0)	0.400	0.4
Lymphoid	**31.4 (11.3-42.0)**	**28.5 (23.6-50.9)**	**0.629**	**0.3**
CD4 T cells	14.0 (4.6-20.0)	9.1 (5.7-15.1)	0.629	0.3
CD8 T cells	3.7 (1.5-4.5)	4.0 (2.0-6.1)	0.857	0.1
Natural killer T cells	3.0 (0.6-5.7)	0.8 (0.7-4.5)	0.857	0.1
Natural killer cells	0.4 (0.2-0.9)	0.3 (0.3-1.5)	0.629	0.3
Cycling T cells	0.3 (0.2-1.2)	0.9 (0.8-1.4)	0.229	0.5
Regulatory T cells	3.0 (0.9-4.5)	4.3 (3.6-4.9)	0.229	0.5
γδ T cells	1.0 (0.2-1.7)	0.3 (0.2-0.3)	0.400	0.4
Stressed T cells	0.6 (0.0-1.3)	0.4 (0.1-0.5)	0.857	0.1
IFN T cells	0.1 (0.0-0.3)	0.2 (0.1-1.0)	0.285	0.4
Th17-like T cells	0.6 (0.1-1.4)	0.1 (0.1-0.2)	0.400	0.4
B cells	1.2 (0.1-2.6)	2.3 (2.1-8.3)	0.229	0.5
Plasma cells	1.6 (0.7-1.9)	3.0 (2.2-3.6)	0.057	0.8
IgA+ plasma cells	0.4 (0.2-0.9)	3.2 (2.3-3.2)	0.057	0.8
IgKC+ plasma cells	0.1 (0.0-0.2)	0.5 (0.5-2.2)	0.057	0.8

Supplementary Table 5: List of overrepresented biological processes in canine pulmonary adenocarcinoma, sorted by cell type.

Cell type	Biological process enriched in pulmonary adenocarcinoma	P-value	Adjusted p-value	Q-value	Overexpressed genes from gene set
All fibroblasts	Epithelial-to-mesenchymal transition	3.90E-22	1.95E-20	1.40E-20	MMP3/IGFBP2/COL11A1/COL7A1/EDIL3/FBN2/CRLF1/INHBA/CTHRC1/TFPI2/COL8A2/ACTA2/LOXL2/TIMP1/SERPINE1/PLAUR/LAMA3/WNT5A/SPP1/PDLIM4/THBS2/CAPG/ADAM12/ITGB3/COL12A1/GJA1/ANPEP/COMP/BASP1/BMP1/PMEPA1/COL1A1/HTRA1/QSOX1/MSX1/FAP/TNFRSF12A/POSTN/DKK1/TNFAIP3/TPM2/SPARC/ITGB5/FAS/COL5A1/TGFBI/MGP/SERPINE2/VCAN/CXCL8/DPYSL3/PTHLH/NID2/MMP14/MXRA5/BGN/ENO2/SDC1/COL4A1/TPM1/ITGA5/SERPINH1/FBLN1/IL15/LAMA2/VEGFA/VCAM1/CALD1/PRRX1/COL4A2
	G2M checkpoint	1.38E-05	3.46E-04	2.48E-04	CENPA/TOP2A/CENPF/CCNB2/UBE2C/BUB1/MKI67/CDK1/MYBL2/KIF23/CDC20/TROAP/TTK/KIF11/KNL1/EXO1/RACGAP1/PRC1/HMGA1/TPX2/TACC3/CCNA2/NDC80/PBK/ESPL1/CDKN3/KIF4A/H2AZ1/UBE2S/PLK1/SMC4/NUSAP1/E2F3/CHAF1A/DDX39A/EFNA5/HIF1A/SMARCC1/H2AZ2/CDC6/CENPE
	Allograft rejection	7.96E-05	1.33E-03	9.49E-04	MMP9/INHBA/CCL5/HDAC9/ST8SIA4/CD7/TIMP1/LYN/LTB/MAP4K1/CAPG/IL2RA/CD3E/CD3G/CD3D/GALNT1/ITK/TPD52/CD2/FAS/CD40/PTPRC/BCAT1/PSMB10/ETS1/F2R/CD74/IL12A/B2M/IL16/HIF1A/WARS1/IL15/RIPK2/DYRK3/CSK/LIF
	Hypoxia	2.27E-04	2.84E-03	2.03E-03	ISG20/CA12/SLC2A1/SERPINE1/PLAUR/FBP1/TIPARP/PFKP/SLC6A6/PFKFB3/STC1/CDKN1A/GPC4/TNFAIP3/PGK1/TPD52/TPBG/COL5A1/F3/TGFBI/IER3/CXCR4/HK2/TPST2/GCNT2/GAPDH/MYH9/ET

					S1/ATF3/BGN/ENO2/TPI1/PAM/VEGFA/CHST3/XPNPEP1/FAM162A
	Mitotic spindle	4.31E-04	4.00E-03	2.86E-03	TOP2A/CENPF/CCNB2/BUB1/CDK1/ANLN/KIF23/DLGAP5/TTK/KIF11/FARP1/RACGAP1/PRC1/TPX2/ECT2/NDC80/FLNB/ESPL1/SORBS2/MYO1E/STK38L/KIF4A/ABR/PLK1/BIN1/BCAR1/SMC4/ACTN4/NUSAP1/MYH9/PDLIM5/SHROOM2/RASA2/FSCN1/NCK2/SEPTIN9/CENPE
	KRAS signaling	4.80E-04	4.00E-03	2.86E-03	MMP9/PRDM1/INHBA/MMP11/GALNT3/RELN/HDAC9/KCNN4/ETV4/GUCY1A1/PLAUR/TNNT2/ADGRL4/SPP1/MAP4K1/PLAU/ANO1/LY96/ALDH1A2/MMD/ADAMDEC1/CA2/NR1H4/IKZF1/TNFAIP3/IL7R/GPNMB/CXCR4/SATB1/ANKH/ETS1/RBP4/LCP1/ST6GAL1/PRRX1/LIF
	E2F targets	8.78E-04	6.27E-03	4.49E-03	TOP2A/DEPDC1/CCNB2/TK1/CDCA3/MKI67/CDK1/MYBL2/DLGAP5/CDC20/SPAG5/DIAPH3/RACGAP1/CIT/RRM2/CDCA8/HMGA1/SPC24/TACC3/ESPL1/CDKN1A/CDKN3/KIF4A/BUB1B/H2AZ1/UBE2S/PLK1/RAD51AP1/SMC4/DDX39A/MELK/ATAD2/WDR90/PRDX4/PHF5A/CENPE
	Angiogenesis	1.81E-03	1.13E-02	8.11E-03	PGLYRP1/TIMP1/SPP1/PDGFA/STC1/MSX1/POSTN/VCAN/JAG1/VEGFA
	Inflammatory response	2.33E-03	1.29E-02	9.25E-03	CCL17/RGS1/INHBA/CCL5/TIMP1/SERPINE1/PLAUR/LYN/TNFSF15/TNFAIP6/SELL/ITGB3/AHR/IL18R1/CDKN1A/PDE4B/IL1RL1/IL7R/CD40/TPBG/F3/PDPN/PTPRE/C5AR1/CXCL8/MET/MMP14/HIF1A/ITGA5/IL15/RIPK2/ABCA1/IL1R1/LIF
	Glycolysis	3.70E-03	1.85E-02	1.33E-02	CENPA/DEPDC1/CDK1/ISG20/PKP2/FBP2/PFKP/TGFA/EGLN3/STC1/GPC4/QSOX1/PGK1/TPBG/COL5A1/TGFBI/GALE/VCAN/IER3/CXCR4/HK2/MET/NDST3/ENO2/SDC1/PC/PGLS/TPI1/PAM/VEGFA/B4GALT7/NDUFV3/FAM162A
	TNFα signaling via NF-κB	4.93E-03	2.24E-02	1.60E-02	INHBA/CCL5/DUSP5/SERPINE1/PLAUR/TNFAIP6/PLAU/TIPARP/PFKFB3/BCL2A1/PMEPA1/CDKN1A/PDE4B/TNFAIP3/IL7R/NR4A2/DUSP4/F3/PHLDA1/IER3/PTPRE/PLK2/SPSB1/REL/ATF3/PDLIM5/JAG1/VEGFA/RIPK2/ABCA1/DRAM1/LIF
	TGBβ signaling	7.92E-03	3.30E-02	2.36E-02	SERPINE1/ID1/PMEPA1/LTBP2/ID3/CTNNB1/RAB31/FKBP1A/SMURF2/TGFBR1/HDAC1/NCOR2
Myofibroblasts	Epithelial-to-mesenchymal transition	7.37E-35	3.32E-33	2.87E-33	IGFBP2/TFPI2/CTHRC1/PLAUR/INHBA/IL6/ADAM12/THBS2/COL7A1/COL1A1/FAP/DPYSL3/COL5A1/TIMP1/EDIL3/COL8A2/FBLN1/VCAN/HTRA1/SPARC/COL12A1/CRLF1/CAPG/QSOX1/MXRA5/BMP1/LUM/POSTN/MGP/BGN/PRRX1/CDH11/COL4A1/LAMA2/COL3A1/PLOD2/SERPINH1/TPM1/ITGB5/COL5A2/PMEPA1/CALD1
	Angiogenesis	4.40E-05	9.89E-04	8.56E-04	TIMP1/VCAN/LUM/POSTN/COL3A1/COL5A2
All muscle cells	Epithelial-to-mesenchymal transition	8.93E-13	4.20E-11	3.66E-11	TFPI2/CTHRC1/INHBA/COL7A1/THBS2/SPP1/FAP/TIMP1/IL15/ADAM12/IL6/ITGB3/COL1A1/MXRA5/CDH11/VCAN/SERPINE2/WNT5A/CAPG/LOXL2/COL12A1/COL1A2/BMP1/COL3A1/MSX1/IGFBP4/PMEPA1/ITGB5/FBN1/COL4A1/SPARC/GLIPR1/GADD45A
	E2F targets	1.36E-06	3.19E-05	2.79E-05	CDK1/TK1/DLGAP5/TOP2A/CCNB2/MYBL2/CDC20/CDCA3/RAD51AP1/SPC24/RACGAP1/RRM2/TACC3/CDKN2C/CDKN3/ATAD2/BUB1B/DCTPP1/PRDX4/STMN1/DUT/DDX39A/HUS1/PHF5A
	G2M checkpoint	1.39E-05	2.18E-04	1.90E-04	CDK1/UBE2C/TOP2A/CCNB2/MYBL2/CDC20/RACGAP1/KIF11/PRC1/KNL1/TACC3/NUSAP1/SLC7A1

					/CDKN2C/CDKN3/NDC80/KIF23/E2F3/SMAD3/STMN1/DDX39A/HUS1
	Inflammatory response	2.49E-03	2.92E-02	2.55E-02	CCL17/CXCL10/INHBA/HPN/TIMP1/IL15/IL6/ITGB3/RGS1/IL15RA/SLC7A1/SLC1A2/CD48/LYN/SPHK1/TNFSF15/ATP2B1
All macrophages and monocytes	E2F targets	3.29E-16	1.45E-14	1.32E-14	KIF18B/KIF22/SPAG5/MYBL2/CDCA3/PLK1/E2F8/CCNB2/DIAPH3/SPC24/CDK1/ORC6/TK1/CDC20/DLGAP5/HMGB3/MELK/CENPM/POLE/STMN1/RACGAP1/BUB1B/SPC25/PRDX4/BRCA1/DCTPP1/AURKA/H2AZ1/DUT/NCAPD2/MCM3/WDR90/PA2G4/LIG1
	G2M checkpoint	3.80E-12	8.37E-11	7.60E-11	CENPA/KIF22/PBK/MYBL2/UBE2C/CCNA2/TROAP/PRC1/PLK1/CCNB2/TPX2/CDK1/ORC6/KIF23/CENPF/CDC20/HMGB3/NUSAP1/POLE/STMN1/RACGAP1/NDC80/POLQ/CDC45/AURKA/SMC2/CHAF1A/H2AZ1/MCM3
	Epithelial-to-mesenchymal transition	6.67E-04	9.19E-03	8.36E-03	MMP1/IGFBP2/WNT5A/CRLF1/THBS2/CADM1/SPP1/COL1A1/LAMA3/COL12A1/PRRX1/FBLN1/ITGB5/MGP/SERPINH1/COL1A2
	Mitotic spindle	8.36E-04	9.19E-03	8.36E-03	KIF22/PRC1/PLK1/CCNB2/ANLN/TPX2/CDK1/KIF23/CENPF/DLGAP5/ECT2/NUSAP1/RACGAP1/NDC80/DOCK4/AURKA
SPP1+ monocytes /neutrophils	Hypoxia	1.33E-05	4.25E-04	3.78E-04	F3/ACKR3/PGF/PDK1/FAM162A/GAPDH/GPI/TPI1
	mTORC1 signaing	9.87E-04	1.58E-02	1.40E-02	EGLN3/PDK1/SLC7A11/GAPDH/GPI/TPI1
All endothelial cells	Epithelial-to-mesenchymal transition	4.50E-11	1.58E-09	1.26E-09	IGFBP2/COL12A1/ANPEP/SPP1/IL6/IGFBP3/LAMC2/COL1A1/ITGB3/TFPI2/COL7A1/CXCL12/SAT1/FBLN2/SNTB1/BASP1/THBS1/COL5A1/FAP/PLAUR/PMEPA1/CXCL8/VEGFA/COL1A2/TNC/PRRX1/VEGFC/FBN1/LOXL2/COL4A1/LAMC1/TNFAIP3/MGP/NID2/FN1/COL4A2/FBLN1/GJA1/ITGA2/CD59/MMP14/ITGAV/CCN1
	G2M checkpoint	6.45E-11	1.58E-09	1.26E-09	CENPA/CCNB2/UBE2C/KIF23/PBK/CDC20/TOP2A/PRC1/CCNA2/MKI67/NDC80/KNL1/TPX2/CDK1/RACGAP1/TROAP/PLK1/KIF22/NUSAP1/KIF11/E2F3/CDKN3/KIF4A/ESPL1/ORC6/TACC3/SMAD3/STMN1/SLC7A1/CENPE/KIF15/EFNA5/SLC7A5/CKS1B/RPS6KA5/TLE3/AURKB/HIF1A/SMC4/UBE2S/DDX39A/SLC12A2/H2AZ1
	E2F targets	4.35E-09	7.11E-08	5.65E-08	CCNB2/CDCA3/DLGAP5/CDC20/TOP2A/DEPDC1/SPC24/SPAG5/MKI67/CDK1/RACGAP1/DIAPH3/TK1/PLK1/KIF22/CDCA8/CDKN3/RRM2/KIF4A/ESPL1/BUB1B/ORC6/CIT/TACC3/STMN1/CENPE/RAD51AP1/CKS1B/HELLS/MELK/CTPS1/ATAD2/GINS1/AURKB/SMC4/NCAPD2/UBE2S/DUT/DDX39A/H2AZ1
	Complement	5.01E-06	5.14E-05	4.09E-05	CA2/CCL5/IL6/LGALS3/GNG2/F3/PIK3CG/TFPI2/GZMK/CTSC/PLA2G7/PLEK/PLAUR/OLR1/LCP2/FCER1G/CTSH/DOCK10/SERPINA1/TNFAIP3/CDH13/ME1/FN1/COL4A2/GPD2/CD59/MMP14/PRCP/CASP3/APOC1/PREP/CTSB
	KRAS signaling up	5.25E-06	5.14E-05	4.09E-05	SLPI/MMP9/SCG5/CA2/SPP1/KCNN4/IGFBP3/ADAMDEC1/MAP4K1/LY96/IL33/IKZF1/PLAUR/LCP1/TMEM176A/PLAU/FCER1G/LAPTM5/PRRX1/PRDM1/CD37/ABCB1/TNFAIP3/GLRX/ITGA2/GUCY1A1/TRIB1/ETV5/CAB39L/ST6GAL1/CXCR4/HDAC9/ADGRL4
	TNFα signaling via NF-κB	3.71E-04	3.03E-03	2.41E-03	CCL5/IL6/F3/SAT1/PTGER4/PLEK/PLAUR/PMEPA1/BCL6/OLR1/BCL2A1/VEGFA/SMAD3/PLAU/TNC/ABCA1/TIPARP/REL/NAMPT/TNFAIP3/MAP2K3/ZFP36/TRIB1/FOSL2/TANK/CCN1/PFKFB3/ETS2

	Inflammatory response	2.91E-03	2.04E-02	1.62E-02	CCL17/CCL5/IL6/OSM/PCDH7/ITGB3/F3/PTGER4/LPAR1/RGS1/SLC1A2/PLAUR/OLR1/CXCL8/LCP2/ABCA1/SELL/CCL7/SLC7A1/CD48/NAMPT/SLC11A2/SELE/MMP14/HIF1A/IL1R1
	Coagulation	4.29E-03	2.63E-02	2.09E-02	MMP9/APOA1/ITGB3/F3/TFPI2/THBS1/PLEK/OLR1/PLAU/FBN1/CTSH/SERPINA1/FN1/ITGA2/MMP14/VWF/APOC1/PREP/CTSB
	Mitotic spindle	7.63E-03	4.15E-02	3.30E-02	CCNB2/DLGAP5/KIF23/TOP2A/PRC1/NDC80/TPX2/CDK1/RACGAP1/ANLN/PLK1/KIF22/NUSAP1/KIF11/KIF4A/ESPL1/ECT2/CENPE/KIF15/MYO1E/SORBS2/SMC4/KIF3C/CD2AP/BIN1
All T cells	G2M checkpoint	6.81E-11	3.00E-09	2.94E-09	PLK1/TTK/CDC20/CENPF/KIF23/UBE2C/TOP2A/CDKN3/MYBL2/HMMR/TPX2/CDK1/BUB1/MKI67/HMGB3/KIF11/AURKA/RACGAP1/CKS1B/KIF20B/KNL1/DHDDS/H2AZ2/H2AZ1
	E2F targets	4.75E-07	1.04E-05	1.02E-05	PLK1/CDCA3/CDC20/DLGAP5/SPC24/TOP2A/CDCA8/CDKN3/MYBL2/HMMR/CDK1/MKI67/HMGB3/BUB1B/DIAPH3/AURKA/RACGAP1/CKS1B/H2AZ1
	Mitotic spindle	3.84E-05	5.64E-04	5.53E-04	PLK1/TTK/DLGAP5/CENPF/KIF23/TOP2A/CTTN/TPX2/CDK1/BUB1/KIF11/AURKA/ECT2/ANLN/RACGAP1/KIF20B
General capillary endothelial cells	Epithelial-to-mesenchymal transition	4.24E-14	2.08E-12	1.56E-12	IGFBP2/CRLF1/SPP1/SNTB1/ANPEP/COL12A1/COL1A1/IGFBP3/GJA1/TFPI2/IL6/ITGB3/PLAUR/THY1/PRRX1/LAMC2/SAT1/COL5A1/VEGFC/CXCL12/VCAN/MGP/VEGFA/CXCL8/THBS1/BASP1/PMEPA1/ADAM12/TNC/TNFAIP3/FAP/CD59/COL1A2/FBN1/LOXL2/CTHRC1/FBLN1/NID2/FN1/LAMC1/MMP14/SLIT2/COL4A1/COL4A2/TIMP1/ITGAV/IGFBP4/DST
	G2M checkpoint	4.28E-08	1.05E-06	7.89E-07	UBE2C/CCNB2/CENPA/KIF23/TOP2A/ESPL1/CDC20/CDK1/PBK/EFNA5/PRC1/CCNA2/TPX2/MKI67/RACGAP1/NDC80/NUSAP1/KNL1/PLK1/KIF22/CENPF/KIF11/TACC3/KIF4A/E2F3/CDKN3/CENPE/SLC7A1/STMN1/SMAD3/KIF15/CKS1B/AURKB/HIF1A/RPS6KA5/UBE2S/ORC5/SMC4
	E2F targets	5.40E-07	8.21E-06	6.17E-06	DLGAP5/CCNB2/CDCA3/SPC24/TOP2A/DEPDC1/ESPL1/CDC20/CDK1/TK1/RRM2/MKI67/RACGAP1/DIAPH3/SPAG5/PLK1/KIF22/TACC3/KIF4A/CDCA8/CDKN3/BUB1B/CENPE/CIT/STMN1/MELK/CKS1B/RAD51AP1/CTPS1/AURKB/HELLS/ATAD2/NCAPD2/DUT/UBE2S/SMC4
	Complement	6.70E-07	8.21E-06	6.17E-06	CCL5/GNG2/PLA2G7/TFPI2/IL6/CA2/F3/LGALS3/GZMK/PLAUR/PIK3CG/CTSC/PLEK/CDH13/OLR1/TNFAIP3/CD59/DOCK10/SERPINA1/ME1/CTSH/FN1/MMP14/GPD2/LCP2/COL4A2/CASP3/PRCP/ZFPM2/APOC1/TIMP1/CTSB/PREP/EHD1
	TNFα signaling via NF-κB	1.74E-04	1.71E-03	1.29E-03	CCL5/IL6/F3/PLAUR/SAT1/VEGFA/BCL2A1/PLEK/PMEPA1/BCL6/TNC/OLR1/REL/SPSB1/TNFAIP3/SMAD3/ABCA1/PTGER4/PLAU/TIPARP/NAMPT/TRIB1/MAP2K3/PFKFB3/TANK/ZFP36/PLPP3/EHD1/ATP2B1
	KRAS signaling up	2.54E-04	2.08E-03	1.56E-03	SLPI/MMP9/SCG5/KCNN4/SPP1/IGFBP3/TNNT2/CA2/PLAUR/LY96/PRRX1/ADAMDEC1/IL33/KIF5C/IKZF1/LCP1/MAP4K1/TNFAIP3/GLRX/PRDM1/TMEM176A/LAPTM5/ALDH1A2/PLAU/ABCB1/TRIB1/ST6GAL1/CAB39L/HDAC9
	Mitotic spindle	9.67E-04	6.77E-03	5.09E-03	DLGAP5/CCNB2/KIF23/TOP2A/ESPL1/CDK1/PRC1/TPX2/RACGAP1/NDC80/ANLN/NUSAP1/PLK1/KIF22/CENPF/KIF11/KIF4A/CENPE/KIF15/BIN1/ECT2/MYH10/MID1/SORBS2/MYO1E/CD2AP/SMC4/DST

	Inflammatory response	1.52E-03	9.29E-03	6.99E-03	CCL17/CCL5/OSM/IL6/PCDH7/F3/ITGB3/PLAUR/SELL/LPAR1/RGS1/CXCL8/OLR1/AQP9/SLC7A1/ABCA1/PTGER4/CCL7/NAMPT/SLC11A2/CD48/MMP14/LCP2/HIF1A/SGMS2/TIMP1/ATP2B1
	Coagulation	4.59E-03	2.50E-02	1.88E-02	MMP9/APOA1/TFPI2/F3/ITGB3/THBS1/PLEK/OLR1/SERPINA1/FBN1/CTSH/PLAU/FN1/MMP14/APOC1/TIMP1/VWF/CTSB/PREP
	Allograft rejection	5.95E-03	2.92E-02	2.19E-02	MMP9/CCL5/CD7/LTB/IL6/BCAT1/THY1/CD4/CD2/CD3E/HCLS1/TPD52/MAP4K1/CD86/PRKCB/CCL7/PTPRC/FYB1/LCP2/HIF1A/HDAC9/EIF4G3/TIMP1/STAT4
	Hypoxia	1.08E-02	4.25E-02	3.19E-02	IGFBP3/IL6/F3/SLC2A1/PLAUR/FBP1/COL5A1/VEGFA/TPD52/PDK3/TNFAIP3/GLRX/GPC4/NOCT/TIPARP/RRAGD/STBD1/PRKCA/STC1/PFKFB3/RORA/ZFP36/EXT1/PFKP
	Angiogenesis	1.13E-02	4.25E-02	3.19E-02	SPP1/VCAN/VEGFA/OLR1/STC1/TIMP1/ITGAV
Secretory /Cancer Cells 1	Hypoxia	1.06E-06	4.76E-05	3.79E-05	STC1/SULT2B1/COL5A1/PFKP/NDRG1/SLC2A1/PGF/ERO1A/ALDOC/GAPDH/PFKFB3/PGK1/TPI1/F3/P4HA1/SLC6A6/LXN/FAM162A/HK1
	Interferon gamma response	4.06E-04	7.73E-03	6.14E-03	PFKP/PDE4B/DDX60/OAS3/MX2/IFI30/B2M/LY6E/PSMB9/PLSCR1/PML/ISG15/GCH1/PSME2
	Interferon alpha response	5.15E-04	7.73E-03	6.14E-03	DDX60/IFI30/B2M/LY6E/PSMB9/PLSCR1/ISG15/OAS1/PSME2
	Epithelial-to-mesenchymal transition	9.19E-04	1.03E-02	8.23E-03	GEM/TIMP1/LAMC2/EDIL3/SPP1/COL5A1/PMEPA1/FN1/GJA1/GADD45A/ITGA2/SAT1/CAPG/PLOD2
	Cholesterol homeostasis	3.83E-03	3.44E-02	2.74E-02	CLU/ALDOC/ANTXR2/LGALS3/PLSCR1/CTNNB1/GPX8
Cancer Cells 2	G2M checkpoint	1.26E-08	5.65E-07	4.23E-07	TOP2A/TTK/CENPF/CDKN3/MKI67/KIF11/TPX2/KNL1/CDC20/CCNB2/PRC1/CENPE/KIF4A/NUSAP1/MEIS2/E2F3/PML/KIF20B/H2AZ1
	Epithelial-to-mesenchymal transition	6.46E-08	1.45E-06	1.09E-06	GEM/TIMP1/EDIL3/AREG/FN1/LAMC2/COL5A1/CXCL8/PLAUR/PMEPA1/LOXL1/SPARC/GJA1/SAT1/ITGA2/TNFRSF12A/VEGFA/ITGAV
	Interferon gamma response	3.45E-06	5.18E-05	3.88E-05	ISG20/CXCL10/PFKP/IL18BP/PDE4B/PML/IFI30/OAS2/B2M/MX2/GCH1/ISG15/PSMA2/PSME2/PSMB2
	Mitotic spindle	5.33E-05	6.00E-04	4.49E-04	TOP2A/TTK/CENPF/KIF11/TPX2/FSCN1/DLGAP5/CCNB2/PRC1/CENPE/KIF4A/ECT2/NUSAP1/KIF20B
	E2F targets	2.15E-04	1.94E-03	1.45E-03	TOP2A/CDKN3/BUB1B/MKI67/DLGAP5/CDC20/CCNB2/CENPE/SPC24/KIF4A/MMS22L/H2AZ1/DUT
	TNFα signaling via NF-κB	1.77E-03	1.33E-02	9.95E-03	GEM/CXCL10/PLAU/AREG/PLAUR/PMEPA1/PDE4B/SAT1/F3/VEGFA/GCH1
	Coagulation	5.85E-03	3.73E-02	2.79E-02	PRSS23/PLAU/TIMP1/FN1/SPARC/CLU/ITGA2/F3
	Hypoxia	6.63E-03	3.73E-02	2.79E-02	ISG20/PFKP/COL5A1/PLAUR/GAPDH/F3/TPI1/P4HA1/VEGFA/PGK1
	Interferon alpha response	8.29E-03	4.14E-02	3.10E-02	ISG20/CXCL10/IFI30/B2M/ISG15/PSME2

Supplementary figures

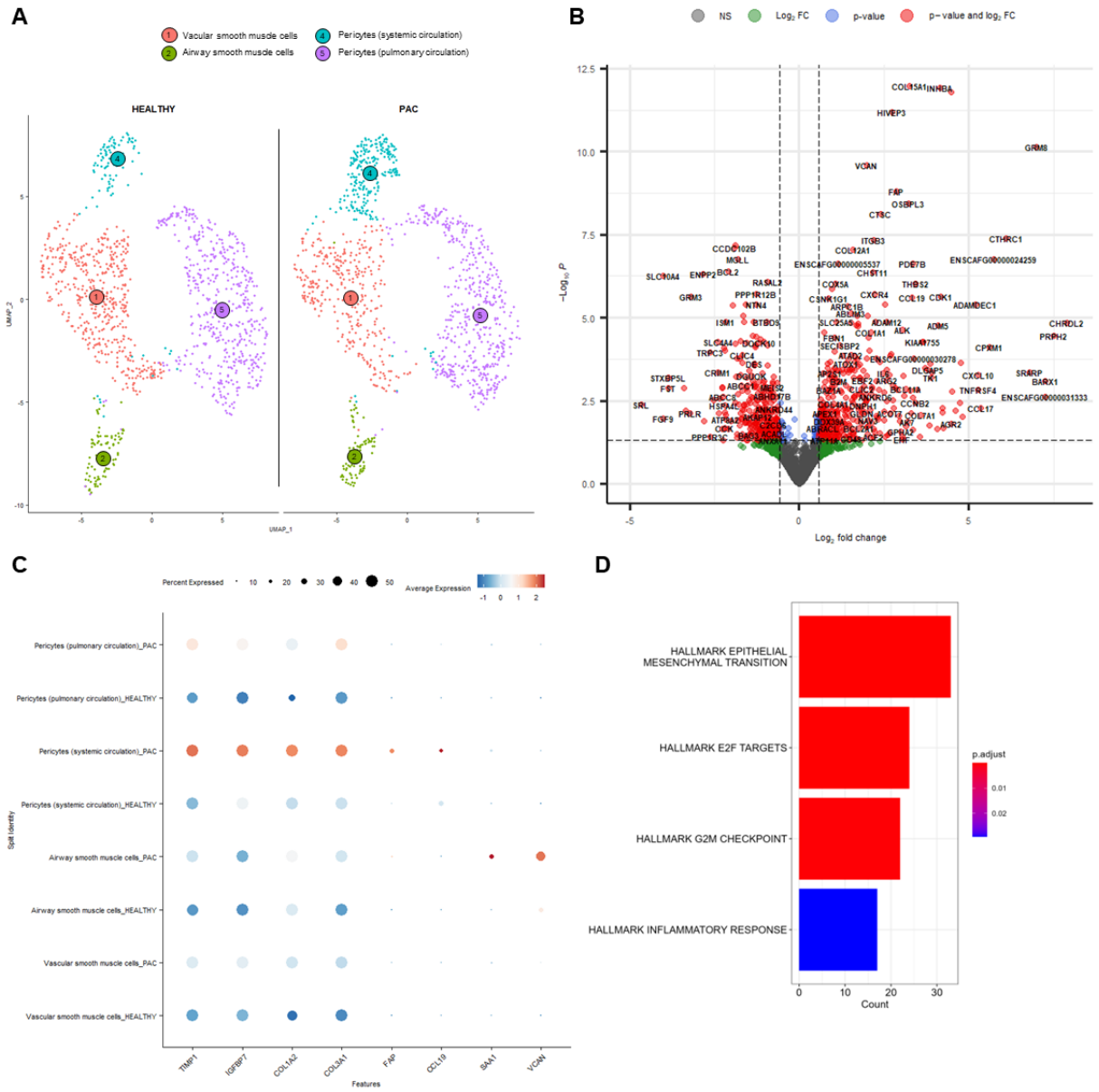

Supplementary Figure 1. Cancer-associated changes in muscle cells. (A) Split UMAP plot representing muscle cell clusters in healthy lungs and in PAC samples. (B) Volcano plot representing differentially expressed genes between all PAC and all healthy lung muscle cells. (C) Split dot plot representing the normalized expression of genes in PAC and healthy lung muscle cell clusters. (D) Bar plot illustrating overrepresented biological processes in all PAC muscle cells. UMAP: Uniform Manifold Approximation and Projection; PAC: pulmonary adenocarcinoma.

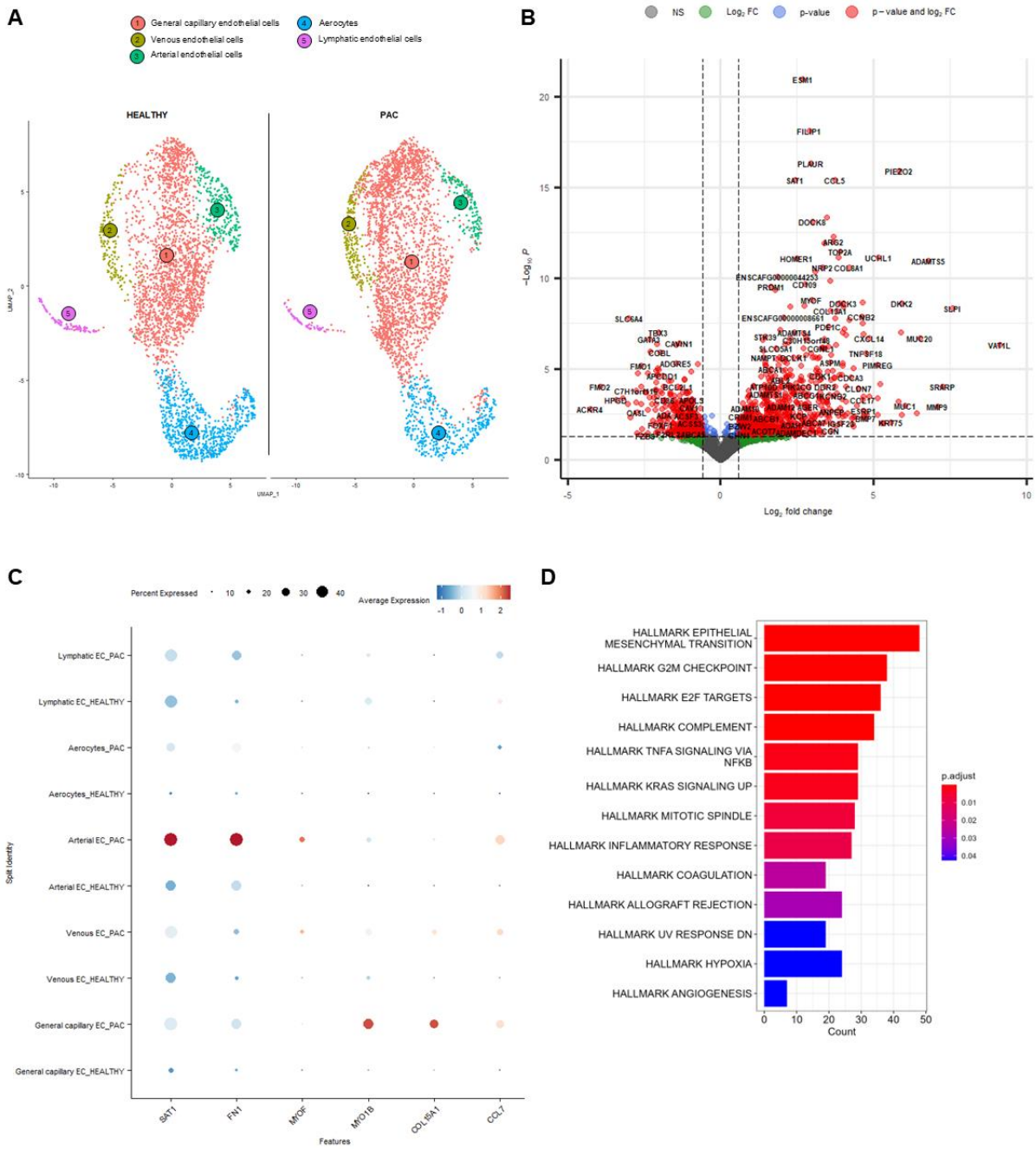

Supplementary Figure 2. Cancer-associated changes in endothelial cells. (A) Split UMAP plot representing endothelial cell clusters in healthy lungs and in PAC samples. (B) Volcano plot representing differentially expressed genes in PAC general capillary endothelial cells compared with general capillary endothelial cells from healthy lungs. (C) Split dot plot representing the normalized expression of genes in PAC and healthy lung endothelial cell clusters. (D) Bar plot illustrating overrepresented biological processes in PAC general capillary endothelial cells. UMAP: Uniform Manifold Approximation and Projection; PAC: pulmonary adenocarcinoma.

Experimental section

Study 3:

Preliminary investigation of molecular disruptions in canine idiopathic pulmonary fibrosis using single-cell RNA sequencing

Preamble

CIPF is characterized by extensive collagen deposition in the lung interstitium, leading to irreversible respiratory decline. It remains poorly understood, with no effective treatments or reliable diagnostic biomarkers currently available. Given its clinical and pathological similarities to human IPF, CIPF is considered a valuable spontaneous model for studying fibrotic lung diseases. To gain deeper insight into the cellular and molecular alterations underlying CIPF, this study applied scRNA-seq to post-mortem lung tissue biopsies from affected dogs and integrated the resulting datasets with our data from healthy canine lungs. The analysis included 11,286 cells from two CIPF-affected dogs and 26,278 cells from four healthy controls, revealing 20 distinct cell types across immune, mesenchymal, epithelial, and endothelial compartments.

Despite the limited sample size, notable transcriptional differences were identified. In CIPF fibroblasts, genes such as *FAP*, *ADAM12*, and *VCAN* were upregulated, suggesting activation of profibrotic pathways. Additionally, *SPP1* was overexpressed in macrophages and monocytes, consistent with previous findings in BALF and serum from CIPF-affected dogs, further supporting its role in disease pathogenesis. Changes were also observed across other cell types, including increased inflammatory signaling in immune cells and stress response pathways in epithelial and endothelial populations. These findings provide the first single-cell transcriptomic map of CIPF lung tissue and lay the groundwork for identifying novel biomarkers and potential therapeutic targets. Further studies with larger cohorts are needed to validate and expand upon these preliminary observations.

Experimental section

Study 3:

Preliminary investigation of molecular disruptions in canine idiopathic pulmonary fibrosis using single-cell RNA sequencing

Preliminary results

Elodie Rizzoli, Aline Fastrès, Laurence Fievez, Elodie Roels, Mutien-Marie Garigliany, Géraldine Bolen, Alexandru Tutunaru, Anne-Christine Merveille, Thomas Marichal, Cécile Clercx

Abstract

Canine idiopathic pulmonary fibrosis (CIPF) is a progressive and fatal interstitial lung disease of unknown origin that primarily affects senior West Highland white terriers (WHWTs). Characterized by excessive collagen deposition in the lung interstitium, CIPF leads to irreversible respiratory decline. Diagnosis remains difficult due to the lack of specific biomarkers and the need to exclude other conditions that can also coexist. The pathogenesis of CIPF is poorly understood, and no effective treatments exist. Single-cell RNA sequencing (scRNA-seq) offers a powerful tool to investigate disease mechanisms by identifying altered cell populations and gene expression changes. While previous scRNA-seq studies in BALF identified pro-fibrotic immune cells, fibroblasts were not assessed. This study aimed to apply scRNA-seq to whole lung tissue biopsies from WHWTs with CIPF to comprehensively characterize cellular and transcriptomic alterations compared to healthy controls.

Fresh post-mortem lung biopsies samples were obtained from CIPF-affected WHWTs and processed for single-cell RNA sequencing. CIPF was confirmed by histopathological evaluation. Datasets from CIPF samples were integrated with published datasets from healthy lung samples before clustering and differential gene expression analysis.

Two CIPF-affected WHWTs were already included in this study and were used to generate preliminary results. A total of 11,286 cells from two CIPF samples were compared with 26,278 cells from four healthy lung samples and sequenced to an average depth of 19,064 reads per cell. Final clustering provided 20 distinct cell types, including 8 immune, 6 mesenchymal, 4 epithelial, and 2 endothelial cell populations. Despite the small sample size, interesting and promising results could be obtained, such as the overexpression of fibroblast activation protein (*FAP*) by fibroblasts, or the overexpression of osteopontin (*SPP1*) by macrophages in CIPF, compared with healthy lungs.

This preliminary study provides the first single-cell transcriptomic overview of CIPF-affected lung tissue, revealing potential molecular targets. Expanding the sample size will be crucial to validate these findings and identify additional disease-relevant alterations, supporting the development of new diagnostic and therapeutic approaches.

Introduction

Canine idiopathic pulmonary fibrosis (CIPF) is progressive interstitial lung disease of unknown etiology that predominantly affects senior West Highland white terriers (WHWTs) (Clercx et al., 2018; Laurila and Rajamäki, 2020a). It consists of an aberrant deposition of collagen in the lung interstitium, leading to progressive respiratory failure and ultimately resulting in death or euthanasia (Heikkilä et al., 2011). In humans, idiopathic pulmonary fibrosis (IPF) also describes one subset of progressive fibrotic interstitial lung disease of unknown cause, which affects older adults, leads to respiratory insufficiency, and carries a poor prognosis (Raghu et al., 2022a). Although computed tomography (CT) and histopathological features are not identical, CIPF shares many similarities with IPF, including clinical features and environmental conditions, and is considered as a suitable animal model to better understand the human disease (Clercx et al., 2018; Barnes et al., 2019). Due to the absence of reliable biomarkers and the need to exclude differential diagnoses and comorbidities, diagnosing CIPF remains a challenge. At present, diagnostic confirmation relies on imaging through CT, histopathological examination of lung tissue, or a combination of both (Clercx et al., 2018; Laurila and Rajamäki, 2020a). To date, its underlying pathobiological mechanisms are not yet fully elucidated, and no curative therapies have been identified (Clercx et al., 2018; Laurila and Rajamäki, 2020a). Thus, prognosis remains poor, with median survival times between 7 and 11 months from diagnosis and survival times highly varying among individuals (Corcoran et al., 1999a; L. I. O. Lilja-Maula et al., 2014; Thierry et al., 2017).

Single-cell RNA sequencing (scRNA-seq) is an emerging high-throughput technology that enables transcriptomic profiling at single-cell resolution (Hedlund and Deng, 2018; Salomon et al., 2019). This approach allows the unbiased identification of altered cell populations and differentially expressed genes in diseased conditions, offering potential insights into new biomarkers and new therapeutic targets (Hedlund and Deng, 2018; Salomon et al., 2019). In humans and mice models, scRNA-seq has been extensively used to decipher the cellular and molecular heterogeneity in healthy lungs and in IPF and altered cell populations were identified, including among macrophage, fibroblast and epithelial populations (Xie et al., 2018; Reyfman et al., 2019; Aran et al., 2019; Peyser et al., 2019; Morse et al., 2019; Tsukui et al., 2020; Travaglini et al., 2020). In dogs, scRNA-seq has been validated and was able to identify pro-fibrotic monocytes and monocytes-derived macrophages in the bronchoalveolar lavage fluid (BALF) from WHWTs affected with CIPF, compared with healthy WHWTs (Fastrès et al., 2020a, 2020b). However, BALF captures only a subset of lung cells and does not reflect the full cellular heterogeneity of the lung. Fibroblasts, which were missing from the

previous study, are key cell types known to be implicated the pathogenesis of IPF (Tsukui et al., 2020).

Therefore, the aim of this study was to use scRNA-seq to characterize changes in cellular composition and gene expression profiles in whole lung tissue biopsies from WHWTs affected by CIPF, in comparison to healthy controls.

Material and methods

1. Sample collection

Post-mortem lung biopsies were collected from client-owned WHWTs affected with CIPF. WHWTs were recruited in the frame of a prospective longitudinal study (Animals Ethics Committee approval n°20-2245) and were diagnosed with CIPF based on the results of a 6-minute walk test, hematology and serum biochemistry, arterial blood gas analysis, cardiac ultrasound, thoracic CT, and endoscopy with bronchoalveolar lavage (Clercx et al., 2018; Laurila and Rajamäki, 2020a). Dogs were followed until their end of life, and with owner written informed consent, lung biopsies were collected immediately after euthanasia. In each dog, biopsies were obtained from each lung lobe, fixed in 10% neutral buffered formalin and embedded in paraffin for histopathological evaluation. An additional biopsy of CIPF-affected lung tissue, as indicated by CT and gross evaluation, was taken from the cranioventral portion of the right caudal lobe and was immediately processed for scRNA-seq analysis.

As controls, four healthy lung samples used to generate a scRNA-seq atlas of the healthy canine lung were included (Rizzoli et al., 2025). Those four samples were collected from client-owned dogs, either post-mortem (n=2) or from non-involved lung adjacent to solitary lung tumors (n=2). All samples, including controls, were processed in the same manner.

2. Histopathology

Formalin-fixed, paraffin-embedded biopsies were cut into 5-µm sections and routinely processed for histopathological evaluation using hematoxylin and eosin staining.

3. Single-cell RNA sequencing

a. Sample preparation, library preparation and sequencing

For scRNA-seq analysis, CIPF biopsies were processed following the procedure used for healthy lungs (Rizzoli et al., 2025). Briefly, fresh biopsies were transported in Hank's Balanced Salt solution (Gibco) containing 5% v/v of fetal bovine serum (Gibco) on ice for immediate processing. Each sample underwent mechanical and chemical dissociation until obtention of a suspension of single cells. Approximately 10,000 cells per sample were processed and sequenced using the 10x Genomics Chromium platform and Illumina NextSeq500, as previously described (Rizzoli et al.,

2025). Sequencing reads were aligned to the dog reference transcriptome (CanFam3.1) and gene-barcode matrices were generated using Cell Ranger v9.0.0 (10x Genomics).

b. Data filtering, integration and clustering

Filtered gene expression matrices were analyzed using Seurat R package (v4.3.0) (Hao et al., 2021). Each sample underwent individual quality control to remove doublets, low-quality or dying cells. Genes expressed in fewer than 10 cells were excluded, along with cells expressing under 200 genes or over 20% mitochondrial reads. Clusters co-expressing markers from multiple tissue compartments were also identified as doublets and removed. Datasets from CIPF samples were integrated with datasets from four healthy lung samples (Rizzoli et al., 2025) after SCTransform normalization, regressing out the effects of the percentage of mitochondrial reads, and canonical correlation analysis integration, using the top 3000 variable genes as integration anchors. Principal component analysis was used for linear dimensionality reduction, and an elbow plot guided the selection of principal components. Clustering was visualized using uniform manifold approximation and projection (UMAP), and optimal resolution was determined with the clustree package (Zappia and Oshlack, 2018).

c. Cell classification and differential expression analysis

Each cluster was assigned to a tissue compartment using their expression of canonical marker genes (*EPCAM* for epithelial, *PTPRC* for immune, *PECAM1* for endothelial cells, the rest being mesenchymal cells) and previously assigned healthy lung cell identities. Cell cluster identities were determined based on previously assigned healthy lung cell identities, and the expression of known marker genes from the literature. Unsupervised cluster-derived cell types were then grouped into biologically relevant subtypes. Differential gene expression analysis between different cell clusters and between CIPF and healthy cell types was performed using the FindMarkers function. Genes with an adjusted P value less than 0.05 were considered significantly differentially expressed.

d. Feature visualization

Gene expression was visualized using feature plots, violin plots and dot plots using SCTransform normalized counts. When split UMAP plots were used to visualize gene expression between conditions, the sample with the highest number of cells was randomly downsampled to depict equal cell numbers per condition.

Preliminary results

For this preliminary study, two dogs affected by CIPF were included. CIPF had been diagnosed 46 and 12 months before death and both WHWTs were euthanized due to terminal stage chronic kidney disease. Table 1 compares clinical data relative to the cases used in the present study.

Table 1. Summary of clinical data from CIPF and healthy lung cases.

Sample	Age	Breed	Weight (kg)	Gender	Lung lobe	Histopathological diagnosis
CIPF1	14	WHWT	10.2	M	Right caudal	CIPF
CIPF2	15	WHWT	7.5	F	Right caudal	CIPF
LUNG1	10	Beagle crossbreed	12.5	F	Right caudal	Healthy
LUNG2	5	Pointer	25	M	Right caudal	Healthy
LUNG3	6	Pointer	30	M	Right caudal	Healthy
LUNG4	8	Cocker	12	F	Right cranial	Healthy

Controls used in this study were used in previously published atlas of the healthy canine lung (Rizzoli et al., 2025)*. F: female; M: male; CIPF: canine idiopathic pulmonary fibrosis.*

A summary of metrics from Cell Ranger filtering are provided in Table 2. Following quality control, we obtained 26,278 cells from four healthy lung samples and 11,286 cells from two CIPF samples, sequenced to an average depth of 19,064 reads per cell. The final analysis identified 20 distinct cell types, including 8 immune, 6 mesenchymal, 4 epithelial, and 2 endothelial populations (Figure 1). The top 15 marker genes for each cell type are summarized in Supplementary Table 1.

Table 2. Summary of sequencing and mapping quality control metrics for each sample

Sample	Estimated number of cells	Sequencing saturation, %	Reads mapped confidently to genome, %	Reads mapped confidently to transcriptome, %	Mean reads /cell	Median unique molecular	Median genes /cell	Total genes detected
CIPF1	8,440	33.7	85.6	56.6	14,279	3,812	1,501	16,539
CIPF2	5,192	56.7	84.1	53.6	24,307	2,452	1,214	16,644
LUNG1	10,487	34.1	83.6	56.8	15,057	2,710	1,368	17,455
LUNG2	8,571	55.0	79.5	48.4	20,043	1,479	873	16,872
LUNG3	8,584	46.8	81.8	52.2	18,085	2,880	1,362	17,019
LUNG4	5,296	52.8	88.1	60.0	35,083	6,871	2,296	16,835

Controls used in this study were used in previously published atlas of the healthy canine lung (Rizzoli et al., 2025). *CIPF: canine idiopathic pulmonary fibrosis.*

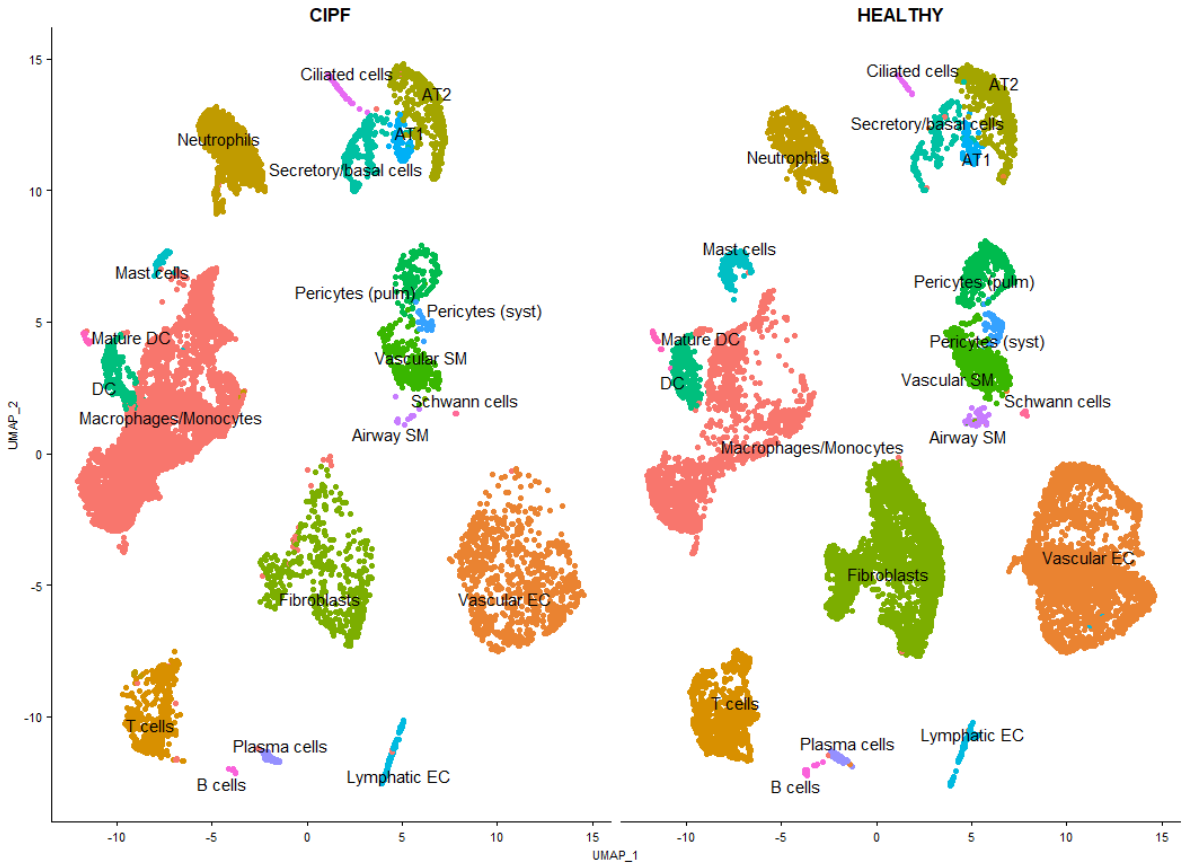

Figure 1. Split uniform manifold approximation and projection (UMAP) representing the different cell types identified in canine idiopathic pulmonary fibrosis (CIPF) and in healthy lung samples. AT1: Alveolar type 1 cells; AT2: Alveolar type 2 cells; DC: dendritic cells; EC: endothelial cells; SM: smooth muscle cells.

In fibroblasts from CIPF lungs, genes such as *ADAMDEC1*, *SAA1*, *VCAN*, *ADAM12*, and *FAP* (Figure 2) were notably overexpressed compared to healthy controls. Compared with healthy clusters, CIPF muscle cells showed higher expression of *IGFBP2*, *NRP1*, *PDE1A*, *NTRK2*, and *LTBP1*. Macrophage and monocyte clusters in CIPF samples overexpressed *VCAN*, *IL1A*, *IL1B*, *EREG*, *IGF1R*, and *SPP1* (Figure 2). In neutrophils, changes involved increased expression of mitochondrial and heat shock protein genes. T cells from CIPF lungs displayed elevated levels of *FKBP5*, *BPI*, *TEX14*, *BTBD11*, *REEP6*, and *CXCL8*. Among epithelial cells, genes such as *REEP6*, *MEOX1*, *MBNL1*, *MAP3K5*, and *MYO1B* were overexpressed in CIPF samples. Finally, endothelial cells from CIPF lungs showed upregulation of *CDH13*, *VWF*, *TSHZ2*, *BTNL9*, *BNC2*, *ADAMTS9*, along with several mitochondrial genes.

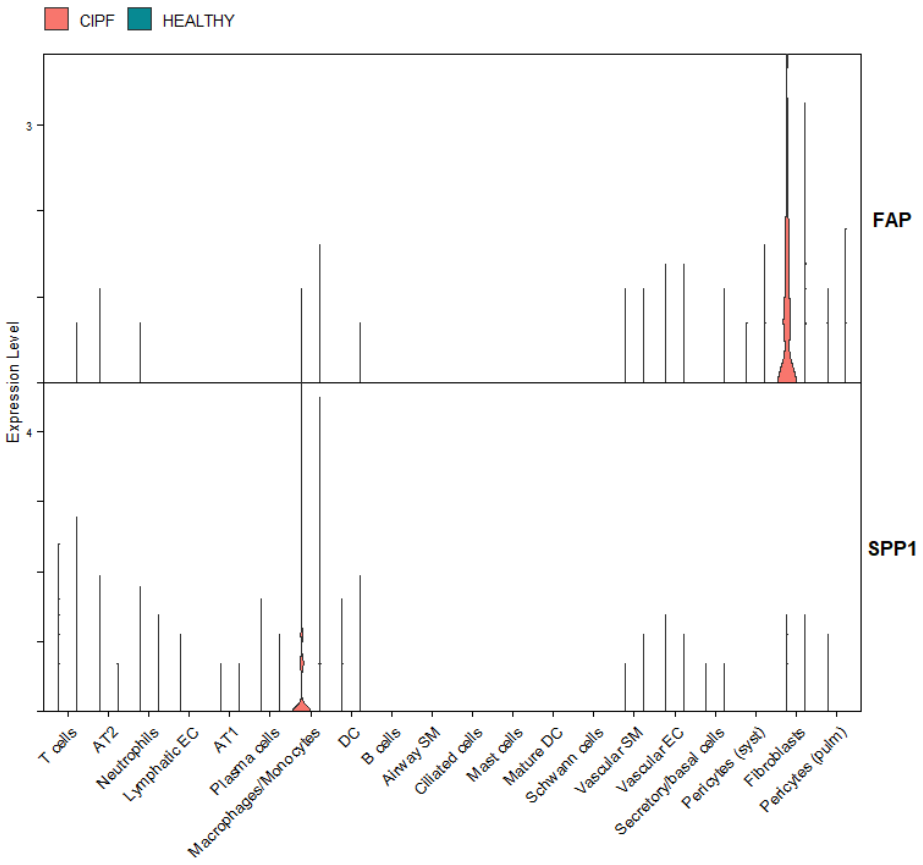

Figure 2. Stacked violin plot showing overexpression of *FAP* in fibroblasts and *SPP1* in macrophages/monocytes from CIPF lung biopsies (left, red violins) compared with healthy lung tissue (right, blue violins). Each violin (or line, when expression is low) represents the gene expression in a specific cell type.

Discussion

This study presents preliminary findings from the analysis of gene expression alterations in lung tissue cells affected by CIPF. We have already identified changes in gene expression profiles in fibroblasts from CIPF lung biopsies. Interestingly, some markers (*FAP, ADAM12, ADAMDEC1*) are common with markers of cancer-associated fibroblasts in a recent scRNA-seq analysis of canine pulmonary adenocarcinoma (unpublished). Fibroblast activation protein (*FAP*) expression has previously been observed by immunohistochemistry in fibroblasts located in areas of active fibrosis in CIPF, as well as in cancer-associated fibroblasts in lung carcinoma biopsies (Rizzoli et al., 2024). In human idiopathic pulmonary fibrosis, FAP is also known to be overexpressed (Acharya et al., 2006). Radiotracers targeting FAP for nuclear imaging are under development, with the aim of aiding diagnosis and predicting disease progression (Röhrich et al., 2022; Mori et al., 2024). FAP has already been investigated as a therapeutic target in malignant diseases (Fu et al., 2022; Lee et al., 2022), and could represent a promising therapeutic target for CIPF as well.

In this study, osteopontin (*SPP1*) was also found to be overexpressed in macrophages and monocytes from CIPF-affected lungs. In prior scRNA-seq studies conducted by our team, SPP1 was similarly overexpressed in monocyte-derived macrophages obtained from BALF of WHWTs affected by CIPF (Fastrès et al., 2020b). Additionally, serum concentrations of SPP1 were higher in WHWTs with CIPF compared to control WHWTs, and also higher in control WHWTs than in other terrier breeds, suggesting a possible contribution of SPP1 to CIPF pathogenesis (Fastrès et al., 2023). Furthermore, SPP1 was shown to be overexpressed in tumor-associated macrophages in canine pulmonary adenocarcinoma (unpublished).

It is important to note that the sample size in this preliminary study was limited, due to challenges in obtaining high-quality lung tissue and the high cost of scRNA-seq. Therefore, these early findings should be interpreted with caution until validated by larger datasets. Furthermore, the case and control groups were not age and breed matched.

In conclusion, this preliminary study offers an initial glimpse into the transcriptional landscape of CIPF-affected lung tissue at single-cell resolution. The current findings already highlight potentially relevant molecular targets. The inclusion of additional samples in future studies will not only be essential to validate these results but may also uncover more diverse and biologically significant alterations, ultimately paving the way for the development of novel therapeutic strategies.

Acknowledgments

The authors thank the GIGA Genomics and Bioinformatics platform, especially D. Stern and A. Lavergne for their guidance in script writing and data analysis, and L. Karim and her team for their availability for processing scRNA-seq samples within short notice. Elodie Rizzoli is a Research Fellow of the Fonds de la Recherche Scientifique – FNRS and this study was funded by the University of Liège.

References

Acharya, P.S., Zukas, A., Chandan, V., Katzenstein, A.-L.A., Puré, E., 2006. Fibroblast activation protein: a serine protease expressed at the remodeling interface in idiopathic pulmonary fibrosis. Hum Pathol 37, 352–360. https://doi.org/10.1016/j.humpath.2005.11.020

Aran, D., Looney, A.P., Liu, L., Wu, E., Fong, V., Hsu, A., Chak, S., Naikawadi, R.P., Wolters, P.J., Abate, A.R., Butte, A.J., Bhattacharya, M., 2019. Reference-based analysis of lung single-cell sequencing reveals a transitional profibrotic macrophage. Nat Immunol 20, 163–172. https://doi.org/10.1038/s41590-018-0276-y

Barnes, T., Brown, K.K., Corcoran, B., Glassberg, M.K., Kervitsky, D.J., Limper, A.H., McGuire, K., Williams, K., Roman, J., Comparative Biology of Pulmonary Fibrosis Group, 2019. Research in Pulmonary Fibrosis Across Species: Unleashing Discovery Through Comparative Biology. Am J Med Sci 357, 399–404. https://doi.org/10.1016/j.amjms.2019.02.005

Clercx, C., Fastrès, A., Roels, E., 2018. Idiopathic pulmonary fibrosis in West Highland white terriers: An update. The Veterinary Journal 242, 53–58. https://doi.org/10.1016/j.tvjl.2018.10.007

Corcoran, B.M., Cobb, M., Martin, M.W., Dukes-McEwan, J., French, A., Fuentes, V.L., Boswood, A., Rhind, S., 1999. Chronic pulmonary disease in West Highland white terriers. Vet Rec 144, 611–616. https://doi.org/10.1136/vr.144.22.611

Fastrès, A., Pirottin, D., Fievez, L., Marichal, T., Desmet, C.J., Bureau, F., Clercx, C., 2020a. Characterization of the Bronchoalveolar Lavage Fluid by Single Cell Gene Expression Analysis in Healthy Dogs: A Promising Technique. Front Immunol 11, 1707. https://doi.org/10.3389/fimmu.2020.01707

Fastrès, A., Pirottin, D., Fievez, L., Tutunaru, A.-C., Bolen, G., Merveille, A.-C., Marichal, T., Desmet, C.J., Bureau, F., Clercx, C., 2020b. Identification of Pro-Fibrotic Macrophage Populations by Single-Cell Transcriptomic Analysis in West Highland White Terriers Affected With Canine Idiopathic Pulmonary Fibrosis. Front Immunol 11, 611749. https://doi.org/10.3389/fimmu.2020.611749

Fastrès, A., Roels, E., Tutunaru, A.C., Bolen, G., Merveille, A.-C., Day, M.J., Garigliany, M.-M., Antoine, N., Clercx, C., 2023. Osteopontin and fibronectin in lung tissue, serum, and bronchoalveolar lavage fluid of dogs with idiopathic pulmonary fibrosis and control dogs. J Vet Intern Med 37, 2468–2477. https://doi.org/10.1111/jvim.16870

Fu, K., Pang, Y., Zhao, L., Lin, L., Wu, H., Sun, L., Lin, Q., Chen, H., 2022. FAP-targeted radionuclide therapy with [177Lu]Lu-FAPI-46 in metastatic nasopharyngeal carcinoma. Eur J Nucl Med Mol Imaging 49, 1767–1769. https://doi.org/10.1007/s00259-021-05634-3

Hao, Y., Hao, S., Andersen-Nissen, E., Mauck, W.M., Zheng, S., Butler, A., Lee, M.J., Wilk, A.J., Darby, C., Zager, M., Hoffman, P., Stoeckius, M., Papalexi, E., Mimitou, E.P., Jain, J., Srivastava, A., Stuart, T., Fleming, L.M., Yeung, B., Rogers, A.J., McElrath, J.M., Blish, C.A., Gottardo, R., Smibert, P., Satija, R., 2021. Integrated analysis of multimodal single-cell data. Cell 184, 3573-3587.e29. https://doi.org/10.1016/j.cell.2021.04.048

Hedlund, E., Deng, Q., 2018. Single-cell RNA sequencing: Technical advancements and biological applications. Mol Aspects Med 59, 36–46. https://doi.org/10.1016/j.mam.2017.07.003

Heikkilä, H. p., Lappalainen, A. k., Day, M. j., Clercx, C., Rajamäki, M. m., 2011. Clinical, Bronchoscopic, Histopathologic, Diagnostic Imaging, and Arterial Oxygenation Findings in West Highland White Terriers with Idiopathic Pulmonary Fibrosis. Journal of Veterinary Internal Medicine 25, 433–439. https://doi.org/10.1111/j.1939-1676.2011.0694.x

Laurila, H.P., Rajamäki, M.M., 2020. Update on Canine Idiopathic Pulmonary Fibrosis in West Highland White Terriers. Vet Clin North Am Small Anim Pract 50, 431–446. https://doi.org/10.1016/j.cvsm.2019.11.004

Lee, I.K., Noguera-Ortega, E., Xiao, Z., Todd, L., Scholler, J., Song, D., Liousia, M., Lohith, K., Xu, K., Edwards, K.J., Farwell, M.D., June, C.H., Albelda, S.M., Puré, E., Sellmyer, M.A., 2022. Monitoring Therapeutic Response to Anti-FAP CAR T Cells Using [18F]AlF-FAPI-74. Clin Cancer Res 28, 5330–5342. https://doi.org/10.1158/1078-0432.CCR-22-1379

Lilja-Maula, L.I.O., Laurila, H.P., Syrjä, P., Lappalainen, A.K., Krafft, E., Clercx, C., Rajamäki, M.M., 2014. Long-term outcome and use of 6-minute walk test in West Highland White Terriers with idiopathic pulmonary fibrosis. J Vet Intern Med 28, 379–385. https://doi.org/10.1111/jvim.12281

Mori, Y., Kramer, V., Novruzov, E., Mamlins, E., Röhrich, M., Fernández, R., Amaral, H., Soza-Ried, C., Monje, B., Sabbagh, E., Florenzano, M., Giesel, F.L., Undurraga, Á., 2024. Initial results with [18F]FAPI-74 PET/CT in idiopathic pulmonary fibrosis. Eur J Nucl Med Mol Imaging 51, 1605–1611. https://doi.org/10.1007/s00259-023-06564-y

Morse, C., Tabib, T., Sembrat, J., Buschur, K.L., Bittar, H.T., Valenzi, E., Jiang, Y., Kass, D.J., Gibson, K., Chen, W., Mora, A., Benos, P.V., Rojas, M., Lafyatis, R., 2019. Proliferating SPP1/MERTK-

expressing macrophages in idiopathic pulmonary fibrosis. European Respiratory Journal 54. https://doi.org/10.1183/13993003.02441-2018

Peyser, R., MacDonnell, S., Gao, Y., Cheng, L., Kim, Y., Kaplan, T., Ruan, Q., Wei, Y., Ni, M., Adler, C., Zhang, W., Devalaraja-Narashimha, K., Grindley, J., Halasz, G., Morton, L., 2019. Defining the Activated Fibroblast Population in Lung Fibrosis Using Single-Cell Sequencing. Am J Respir Cell Mol Biol 61, 74–85. https://doi.org/10.1165/rcmb.2018-0313OC

Raghu, G., Remy-Jardin, M., Richeldi, L., Thomson, C.C., Inoue, Y., Johkoh, T., Kreuter, M., Lynch, D.A., Maher, T.M., Martinez, F.J., Molina-Molina, M., Myers, J.L., Nicholson, A.G., Ryerson, C.J., Strek, M.E., Troy, L.K., Wijsenbeek, M., Mammen, M.J., Hossain, T., Bissell, B.D., Herman, D.D., Hon, S.M., Kheir, F., Khor, Y.H., Macrea, M., Antoniou, K.M., Bouros, D., Buendia-Roldan, I., Caro, F., Crestani, B., Ho, L., Morisset, J., Olson, A.L., Podolanczuk, A., Poletti, V., Selman, M., Ewing, T., Jones, S., Knight, S.L., Ghazipura, M., Wilson, K.C., 2022. Idiopathic Pulmonary Fibrosis (an Update) and Progressive Pulmonary Fibrosis in Adults: An Official ATS/ERS/JRS/ALAT Clinical Practice Guideline. Am J Respir Crit Care Med 205, e18–e47. https://doi.org/10.1164/rccm.202202-0399ST

Reyfman, P.A., Walter, J.M., Joshi, N., Anekalla, K.R., McQuattie-Pimentel, A.C., Chiu, S., Fernandez, R., Akbarpour, M., Chen, C.-I., Ren, Z., Verma, R., Abdala-Valencia, H., Nam, K., Chi, M., Han, S., Gonzalez-Gonzalez, F.J., Soberanes, S., Watanabe, S., Williams, K.J.N., Flozak, A.S., Nicholson, T.T., Morgan, V.K., Winter, D.R., Hinchcliff, M., Hrusch, C.L., Guzy, R.D., Bonham, C.A., Sperling, A.I., Bag, R., Hamanaka, R.B., Mutlu, G.M., Yeldandi, A.V., Marshall, S.A., Shilatifard, A., Amaral, L.A.N., Perlman, H., Sznajder, J.I., Argento, A.C., Gillespie, C.T., Dematte, J., Jain, M., Singer, B.D., Ridge, K.M., Lam, A.P., Bharat, A., Bhorade, S.M., Gottardi, C.J., Budinger, G.R.S., Misharin, A.V., 2019. Single-Cell Transcriptomic Analysis of Human Lung Provides Insights into the Pathobiology of Pulmonary Fibrosis. Am J Respir Crit Care Med 199, 1517–1536. https://doi.org/10.1164/rccm.201712-2410OC

Rizzoli, E., de Meeûs d'Argenteuil, C., Fastrès, A., Roels, E., Janssen, P., Puré, E., Garigliany, M.-M., Marichal, T., Clercx, C., 2024. Fibroblast activation protein is a cellular marker of fibrotic activity in canine idiopathic pulmonary fibrosis. Front Vet Sci 11, 1416124. https://doi.org/10.3389/fvets.2024.1416124

Rizzoli, E., de Meeûs d'Argenteuil, C., Fastrès, A., Roels, E., Janssen, P., Puré, E., Garigliany, M.-M., Marichal, T., Clercx, C., 2024. Fibroblast activation protein is a cellular marker of fibrotic activity in canine idiopathic pulmonary fibrosis. Front. Vet. Sci. 11. https://doi.org/10.3389/fvets.2024.1416124

Rizzoli, E., Fievez, L., Fastrès, A., Roels, E., Marichal, T., Clercx, C., 2025. A single-cell RNA sequencing atlas of the healthy canine lung: a foundation for comparative studies. Front Immunol 16, 1501603. https://doi.org/10.3389/fimmu.2025.1501603

Röhrich, M., Leitz, D., Glatting, F.M., Wefers, A.K., Weinheimer, O., Flechsig, P., Kahn, N., Mall, M.A., Giesel, F.L., Kratochwil, C., Huber, P.E., Deimling, A. von, Heußel, C.P., Kauczor, H.U., Kreuter, M., Haberkorn, U., 2022. Fibroblast Activation Protein-Specific PET/CT Imaging in Fibrotic Interstitial Lung Diseases and Lung Cancer: A Translational Exploratory Study. J Nucl Med 63, 127–133. https://doi.org/10.2967/jnumed.121.261925

Salomon, R., Kaczorowski, D., Valdes-Mora, F., Nordon, R.E., Neild, A., Farbehi, N., Bartonicek, N., Gallego-Ortega, D., 2019. Droplet-based single cell RNAseq tools: a practical guide. Lab Chip 19, 1706–1727. https://doi.org/10.1039/c8lc01239c

Thierry, F., Handel, I., Hammond, G., King, L.G., Corcoran, B.M., Schwarz, T., 2017. Further characterization of computed tomographic and clinical features for staging and prognosis of idiopathic pulmonary fibrosis in West Highland white terriers. Vet Radiol Ultrasound 58, 381–388. https://doi.org/10.1111/vru.12491

Travaglini, K.J., Nabhan, A.N., Penland, L., Sinha, R., Gillich, A., Sit, R.V., Chang, S., Conley, S.D., Mori, Y., Seita, J., Berry, G.J., Shrager, J.B., Metzger, R.J., Kuo, C.S., Neff, N., Weissman, I.L., Quake, S.R., Krasnow, M.A., 2020. A molecular cell atlas of the human lung from single-cell RNA sequencing. Nature 587, 619–625. https://doi.org/10.1038/s41586-020-2922-4

Tsukui, T., Sun, K.-H., Wetter, J.B., Wilson-Kanamori, J.R., Hazelwood, L.A., Henderson, N.C., Adams, T.S., Schupp, J.C., Poli, S.D., Rosas, I.O., Kaminski, N., Matthay, M.A., Wolters, P.J., Sheppard, D., 2020. Collagen-producing lung cell atlas identifies multiple subsets with distinct localization and relevance to fibrosis. Nat Commun 11, 1920. https://doi.org/10.1038/s41467-020-15647-5

Xie, T., Wang, Y., Deng, N., Huang, G., Taghavifar, F., Geng, Y., Liu, N., Kulur, V., Yao, C., Chen, P., Liu, Z., Stripp, B., Tang, J., Liang, J., Noble, P.W., Jiang, D., 2018. Single-Cell Deconvolution of Fibroblast Heterogeneity in Mouse Pulmonary Fibrosis. Cell Reports 22, 3625–3640. https://doi.org/10.1016/j.celrep.2018.03.010

Zappia, L., Oshlack, A., 2018. Clustering trees: a visualization for evaluating clusterings at multiple resolutions. GigaScience 7, giy083. https://doi.org/10.1093/gigascience/giy083

Supplemental material

Supplementary Table 1. Top 15 overexpressed genes by each cell cluster compared to all other clusters, generated with the FindMarkers function

Cell cluster	Average log2 fold change	Fraction of cells expressing the gene within this cluster	Fraction of cells expressing the gene within all other cells	Adjusted p-value	Gene
Fibroblasts	3.90068439	0.962	0.135	0	DCN
Fibroblasts	3.35889449	0.942	0.265	0	MGP
Fibroblasts	3.30401377	0.558	0.041	0	PRG4
Fibroblasts	3.15330079	0.836	0.092	0	CDO1
Fibroblasts	3.11087285	0.888	0.073	0	COL1A2
Fibroblasts	3.04482537	0.915	0.047	0	ENSCAFG00000010290
Fibroblasts	3.04274385	0.992	0.656	0	ARHGAP45
Fibroblasts	2.91885106	0.813	0.041	0	DPT
Fibroblasts	2.90497491	0.92	0.073	0	C7
Fibroblasts	2.85138937	0.81	0.045	0	OGN
Fibroblasts	2.82632957	0.848	0.114	0	LIMCH1
Fibroblasts	2.74639864	0.841	0.102	0	COL3A1
Fibroblasts	2.70967224	0.759	0.117	0	MACROD2
Fibroblasts	2.49240679	0.658	0.017	0	CADM2
Fibroblasts	2.46180754	0.871	0.231	0	GSN
Fibroblasts	2.43603744	0.731	0.121	0	IGFBP6
Macrophages/Monocytes	3.51220014	0.937	0.167	0	BPI
Macrophages/Monocytes	3.30440502	0.984	0.615	0	DLA-DRA
Macrophages/Monocytes	3.27815594	0.907	0.227	0	LYZ
Macrophages/Monocytes	2.76725672	0.933	0.199	0	CTSS
Macrophages/Monocytes	2.73846155	0.788	0.111	0	ENSCAFG00000031869
Macrophages/Monocytes	2.63086056	0.951	0.287	0	CD74
Macrophages/Monocytes	2.62217672	0.768	0.138	0	MRC1
Macrophages/Monocytes	2.59908917	0.953	0.402	0	HLA-DQB2
Macrophages/Monocytes	2.56966499	0.928	0.409	0	LGALS3
Macrophages/Monocytes	2.52297408	0.619	0.101	0	MARCO
Macrophages/Monocytes	2.51652639	0.439	0.078	0	CHI3L1
Macrophages/Monocytes	2.21666169	0.834	0.189	0	BLOC1S6
Macrophages/Monocytes	2.17644942	0.846	0.194	0	GLRX
Macrophages/Monocytes	2.12302377	0.986	0.93	0	FTL
Macrophages/Monocytes	2.119958	0.639	0.252	0	ENSCAFG00000005494
Neutrophils	5.03452607	0.917	0.054	0	S100A12
Neutrophils	4.62587828	0.928	0.084	0	ENSCAFG00000029470
Neutrophils	4.1765822	0.852	0.059	0	SLC7A11
Neutrophils	3.9116103	0.981	0.307	0	CXCL8
Neutrophils	3.61846943	0.99	0.444	0	SOD2
Neutrophils	3.57880304	0.992	0.625	0	SAT1
Neutrophils	3.17577432	0.933	0.178	0	ENSCAFG00000013713
Neutrophils	3.13213095	0.91	0.298	0	C30H15orf48
Neutrophils	3.03719788	0.659	0.121	0	IL18BP
Neutrophils	2.90479314	0.903	0.176	0	PLAUR
Neutrophils	2.81013485	0.761	0.152	0	SAMSN1
Neutrophils	2.78894213	0.979	0.293	0	PLEK
Neutrophils	2.57738248	0.883	0.349	0	ZFAND5
Neutrophils	2.49088309	0.721	0.129	0	IL1R2
Neutrophils	2.46671611	0.941	0.26	0	SRGN
Dendritic cells (DC)	3.56023274	1	0.924	0	TMSB10
Dendritic cells (DC)	2.66441354	0.987	0.31	0	IFI30
Dendritic cells (DC)	2.46173454	0.908	0.088	0	PKIB
Dendritic cells (DC)	2.45761441	1	0.535	0	HLA-DQB2
Dendritic cells (DC)	2.37853074	0.804	0.119	0	NR4A3
Dendritic cells (DC)	2.33662239	0.906	0.272	0	REL
Dendritic cells (DC)	2.26555464	0.89	0.17	0	WDFY4
Dendritic cells (DC)	2.19996784	1	0.705	0	DLA-DRA
Dendritic cells (DC)	2.01331974	0.95	0.271	0	ENSCAFG00000018277

Dendritic cells (DC)	1.9935706	0.893	0.238	0	ENSCAFG00000023735
Dendritic cells (DC)	1.98446726	1	0.906	0	ENSCAFG00000028765
Dendritic cells (DC)	1.72540799	0.998	0.448	0	CD74
Dendritic cells (DC)	1.7005953	0.978	0.31	0	DLA-DQA1
Dendritic cells (DC)	1.66031164	0.743	0.081	0	CSF2RA
Dendritic cells (DC)	1.57814205	0.924	0.272	0	LSP1
Mature DC	3.32730972	0.887	0.011	0	CCR7
Mature DC	2.83339283	0.915	0.01	0	DSCAML1
Mature DC	0.75122984	0.437	0.004	0	LAD1
Mature DC	0.96057543	0.507	0.012	5.23E-287	IL21R
Mature DC	1.79841911	0.803	0.037	1.63E-254	SLC9A7
Mature DC	1.8596563	0.718	0.031	3.68E-238	FLT3
Mature DC	0.79142528	0.366	0.009	5.23E-211	SLCO5A1
Mature DC	2.32850298	0.845	0.059	1.71E-183	IL4I1
Mature DC	0.67230816	0.423	0.014	2.05E-181	NUAK2
Mature DC	0.9153414	0.394	0.014	2.61E-159	ENPP3
Mature DC	1.53496657	0.676	0.044	1.59E-148	GPR155
Mature DC	2.00168949	0.817	0.068	9.61E-139	SLC22A23
Mature DC	0.59284118	0.254	0.007	7.04E-134	NETO2
Mature DC	0.61630114	0.507	0.028	5.63E-126	JAK3
Mature DC	1.02685631	0.535	0.032	2.03E-121	RASGRP1
Mast cells	5.31392247	0.884	0.022	0	ENSCAFG00000019593
Mast cells	4.00642709	0.867	0.012	0	ENSCAFG00000031939
Mast cells	3.34307627	0.828	0.009	0	CPA3
Mast cells	2.52226583	0.785	0.019	0	MS4A2
Mast cells	2.25555007	0.677	0.014	0	CMA1
Mast cells	2.20053031	0.752	0.043	0	KIT
Mast cells	2.01278503	0.81	0.194	0	MAGI2
Mast cells	1.94299092	0.633	0.011	0	FCER1A
Mast cells	1.85240805	0.657	0.062	0	SYTL3
Mast cells	1.70330622	0.696	0.131	0	VWA5A
Mast cells	1.70129517	0.633	0.002	0	ENSCAFG00000030195
Mast cells	1.49734736	0.668	0.035	0	HPGDS
Mast cells	1.305446	0.582	0.065	0	CYP4F22
Mast cells	1.3013315	0.563	0.053	0	GPM6A
Mast cells	1.11931164	0.48	0.052	0	ABCC4
T cells	2.59205376	0.356	0.117	0	CCL4
T cells	2.44202743	0.733	0.03	0	ENSCAFG00000006485
T cells	2.43701677	0.797	0.011	0	ENSCAFG00000014478
T cells	2.31145996	0.635	0.011	0	ENSCAFG00000046009
T cells	1.94604317	0.792	0.014	0	SKAP1
T cells	1.94423939	0.623	0.005	0	ICOS
T cells	1.94276404	0.698	0.108	0	STAT4
T cells	1.8627093	0.608	0.023	0	IL7R
T cells	1.85996656	0.798	0.223	0	CORO1B
T cells	1.76452061	0.884	0.219	0	ETS1
T cells	1.7142131	0.733	0.004	0	CD3E
T cells	1.68339416	0.974	0.411	0	PTPRC
T cells	1.65059153	0.783	0.207	0	SLC9A9
T cells	1.62108923	0.738	0.129	0	RIPOR2
T cells	1.60608903	0.665	0.008	0	CD3D
Plasma cells	9.18796948	0.873	0.125	0	ENSCAFG00000031806
Plasma cells	9.01206162	0.952	0.106	0	ENSCAFG00000030258
Plasma cells	7.44948872	0.487	0.024	0	ENSCAFG00000047066
Plasma cells	5.74362107	0.987	0.022	0	JCHAIN
Plasma cells	3.37843782	0.39	0.001	0	ENSCAFG00000014139
Plasma cells	2.57376003	0.82	0.002	0	MZB1
Plasma cells	2.56775204	0.842	0.035	0	TXNDC5
Plasma cells	2.14153767	0.439	0.002	0	ENSCAFG00000028509
Plasma cells	1.6452432	0.851	0.002	0	POU2AF1
Plasma cells	1.62385466	0.697	0.006	0	DERL3
Plasma cells	1.21100186	0.627	0	0	TNFRSF17
Plasma cells	1.10738879	0.588	0.033	0	CLEC2D
Plasma cells	0.69315799	0.417	0.001	0	TNFRSF13B
Plasma cells	1.3439008	0.61	0.055	4.34E-280	DOCK3
Plasma cells	2.37978716	0.925	0.159	3.05E-278	PRDX4

B cells	1.43229473	0.703	0.029	0	TNFRSF13C
B cells	1.00446273	0.441	0.011	0	CCR7
B cells	1.93795397	0.694	0.044	2.20E-237	LTB
B cells	1.81679076	0.829	0.079	4.65E-180	ENSCAFG00000006485
B cells	0.81485252	0.45	0.027	2.14E-154	BCL11A
B cells	1.11026442	0.577	0.052	3.82E-133	RALGPS2
B cells	0.59079691	0.342	0.019	1.50E-127	ENSCAFG00000050027
B cells	1.14588757	0.595	0.07	5.01E-102	RRAS2
B cells	0.70272824	0.423	0.037	4.90E-97	SLC9A7
B cells	1.6245817	0.964	0.263	4.29E-82	CORO1B
B cells	0.6398451	0.369	0.035	2.44E-75	CLEC2D
B cells	1.0954971	0.64	0.112	1.41E-70	SP140
B cells	1.02198219	0.342	0.036	2.58E-62	PLAC8
B cells	1.39845131	0.874	0.252	3.50E-58	MEF2C
B cells	1.13284733	0.631	0.14	4.34E-52	ENSCAFG00000025115
Vascular smooth muscle	4.44939598	0.971	0.063	0	ACTA2
Vascular smooth muscle	3.70934257	0.941	0.142	0	TPM2
Vascular smooth muscle	3.44816432	0.845	0.043	0	ENSCAFG00000028930
Vascular smooth muscle	3.25655581	0.962	0.173	0	MYH11
Vascular smooth muscle	3.04233684	0.874	0.099	0	DGUOK
Vascular smooth muscle	3.02578141	0.908	0.152	0	MYL9
Vascular smooth muscle	2.91951542	0.909	0.321	0	ADIRF
Vascular smooth muscle	2.65033311	0.927	0.136	0	PDE3A
Vascular smooth muscle	2.60265918	0.964	0.233	0	PRKG1
Vascular smooth muscle	2.54679037	0.89	0.173	0	DMD
Vascular smooth muscle	2.53559596	0.905	0.28	0	DSTN
Vascular smooth muscle	2.43772482	0.85	0.047	0	SYNPO2
Vascular smooth muscle	2.28730836	0.966	0.302	0	CALD1
Vascular smooth muscle	2.11116432	0.763	0.055	0	TAGLN
Vascular smooth muscle	2.10192798	0.781	0.111	0	DES
Pericytes (pulmonary)	3.56249676	0.929	0.061	0	POSTN
Pericytes (pulmonary)	3.27425682	0.951	0.13	0	GUCY1A2
Pericytes (pulmonary)	3.11742866	0.943	0.233	0	ARHGAP42
Pericytes (pulmonary)	3.00209748	0.971	0.237	0	PRKG1
Pericytes (pulmonary)	2.82010057	0.826	0.04	0	COX4I2
Pericytes (pulmonary)	2.67458314	0.796	0.018	0	HIGD1B
Pericytes (pulmonary)	2.52702072	0.758	0.011	0	FAM162B
Pericytes (pulmonary)	2.50261495	0.864	0.032	0	TRPC6
Pericytes (pulmonary)	2.4238508	0.898	0.141	0	PDE3A
Pericytes (pulmonary)	2.34280893	0.844	0.031	0	CCDC102B
Pericytes (pulmonary)	2.32815382	0.798	0.027	0	NDUFA4L2
Pericytes (pulmonary)	2.30816296	0.913	0.154	0	PDE5A
Pericytes (pulmonary)	2.29066955	0.733	0.091	0	SLC4A4
Pericytes (pulmonary)	2.15667099	0.756	0.04	0	F3
Pericytes (pulmonary)	2.11438612	0.881	0.26	0	ITGA1
Pericytes (systemic)	2.55746848	0.89	0.049	0	ADGRL3
Pericytes (systemic)	2.52986423	0.922	0.09	0	ACTA2
Pericytes (systemic)	2.36872624	0.522	0.003	0	APOA1
Pericytes (systemic)	2.21509002	0.812	0.095	0	RASL11A
Pericytes (systemic)	2.1151354	0.62	0.052	0	APOLD1
Pericytes (systemic)	2.05015048	0.804	0.059	0	COX4I2
Pericytes (systemic)	1.95955562	0.673	0.02	0	RGS16
Pericytes (systemic)	1.79019764	0.755	0.071	0	SYNPO2
Pericytes (systemic)	1.43257466	0.731	0.069	0	COL12A1
Pericytes (systemic)	1.42394242	0.694	0.047	0	NDUFA4L2
Pericytes (systemic)	0.96046217	0.514	0.018	0	PDE1A
Pericytes (systemic)	0.77122366	0.367	0.008	0	ADRA2A
Pericytes (systemic)	0.74561955	0.408	0.011	0	RGS5
Pericytes (systemic)	0.63271399	0.388	0.008	0	PDE6H
Pericytes (systemic)	0.92820494	0.539	0.043	4.33E-293	MYOM1
Airway smooth muscle	3.62314567	0.905	0.033	0	PRUNE2
Airway smooth muscle	3.35589873	0.847	0.02	0	HPSE2
Airway smooth muscle	3.09018189	0.894	0.092	0	ACTA2
Airway smooth muscle	2.35761248	0.91	0.072	0	SYNPO2
Airway smooth muscle	2.25300411	0.407	0.003	0	ACTC1
Airway smooth muscle	1.65641374	0.746	0.06	0	SEMA3C

Airway smooth muscle	1.59053895	0.646	0.022	0	DGKB
Airway smooth muscle	1.25403759	0.624	0.045	0	PDLIM3
Airway smooth muscle	1.25246582	0.476	0.007	0	SOSTDC1
Airway smooth muscle	1.01756409	0.54	0.029	0	EPHA7
Airway smooth muscle	0.97445334	0.407	0.014	0	GREM2
Airway smooth muscle	0.92407485	0.46	0.013	0	CNN1
Airway smooth muscle	0.73937109	0.339	0.009	0	EDIL3
Airway smooth muscle	0.71825045	0.339	0.012	0	FGF18
Airway smooth muscle	0.70406139	0.471	0.024	0	PTGS1
Schwann cells	4.89076124	0.972	0.013	0	NRXN1
Schwann cells	3.59321768	0.944	0	0	CDH19
Schwann cells	3.31658222	0.944	0.017	0	SLC35F1
Schwann cells	3.1409219	0.944	0	0	SCN7A
Schwann cells	2.70963759	0.75	0.012	0	ADGRB3
Schwann cells	2.51112172	0.972	0.004	0	SNCA
Schwann cells	1.86725985	0.861	0.004	0	NTNG1
Schwann cells	1.82012253	0.889	0.011	0	PPP2R2B
Schwann cells	1.55530694	0.556	0.001	0	IL1RAPL2
Schwann cells	1.23758657	0.694	0.01	0	NCAM1
Schwann cells	1.03703172	0.417	0.001	0	XKR4
Schwann cells	1.01399142	0.611	0.003	0	GRIK2
Schwann cells	0.82984436	0.5	0	0	NRN1
Schwann cells	0.82589077	0.583	0.003	0	SLITRK6
Schwann cells	0.73692715	0.472	0	0	MPZ
Vascular endothelial	3.75195329	0.971	0.251	0	ENSCAFG00000014799
Vascular endothelial	3.13916618	0.909	0.092	0	CALCRL
Vascular endothelial	2.84349549	0.883	0.061	0	LDB2
Vascular endothelial	2.62186643	0.886	0.171	0	PTPRG
Vascular endothelial	2.57696554	0.766	0.039	0	LYVE1
Vascular endothelial	2.47662991	0.926	0.207	0	CAV1
Vascular endothelial	2.4664784	0.893	0.059	0	EGFL7
Vascular endothelial	2.28555887	0.905	0.175	0	ADGRF5
Vascular endothelial	2.1812789	0.639	0.017	0	ACKR1
Vascular endothelial	2.11979674	0.858	0.151	0	PECAM1
Vascular endothelial	2.0875876	0.754	0.045	0	PTPRB
Vascular endothelial	2.03897807	0.961	0.407	0	IGFBP7
Vascular endothelial	2.01545708	0.922	0.441	0	TNFSF10
Vascular endothelial	2.00200914	0.902	0.275	0	PTPRM
Vascular endothelial	1.97350642	0.717	0.017	0	IDO1
Lymphatic endothelial	2.94315271	0.88	0.003	0	RELN
Lymphatic endothelial	2.82908178	0.936	0.058	0	FLT4
Lymphatic endothelial	2.72184635	0.847	0.106	0	KALRN
Lymphatic endothelial	2.63512291	0.885	0.11	0	RHOJ
Lymphatic endothelial	2.61605226	0.885	0.12	0	TSHZ2
Lymphatic endothelial	2.19973673	0.816	0.088	0	STOX2
Lymphatic endothelial	2.18264196	0.806	0.082	0	PIEZO2
Lymphatic endothelial	2.16982151	0.87	0.184	0	ITGA9
Lymphatic endothelial	2.04813037	0.74	0.066	0	CDH13
Lymphatic endothelial	1.94703063	0.855	0.146	0	PPFIBP1
Lymphatic endothelial	1.94073258	0.742	0.052	0	NTN1
Lymphatic endothelial	1.91223856	0.793	0.071	0	APOD
Lymphatic endothelial	1.85912003	0.809	0.12	0	SMAD1
Lymphatic endothelial	1.84105898	0.821	0.137	0	ABI3BP
Lymphatic endothelial	1.76502232	0.768	0.081	0	ZNF521
Alveolar type 2	7.39006218	0.994	0.61	0	SFTPC
Alveolar type 2	6.31675762	0.988	0.244	0	ENSCAFG00000015754
Alveolar type 2	4.15108819	0.965	0.07	0	NAPSA
Alveolar type 2	4.00225369	0.88	0.028	0	SLC34A2
Alveolar type 2	3.95068684	0.964	0.036	0	C5
Alveolar type 2	3.87306041	0.94	0.087	0	WFDC2
Alveolar type 2	3.5128077	0.954	0.329	0	PDE4D
Alveolar type 2	3.47093978	0.96	0.177	0	ENSCAFG00000003331
Alveolar type 2	3.45863947	0.968	0.551	0	NPC2
Alveolar type 2	3.38566665	0.904	0.055	0	ENSCAFG00000049417
Alveolar type 2	3.03976449	0.927	0.048	0	ACOXL
Alveolar type 2	2.76864533	0.932	0.021	0	SFTPD

Alveolar type 2	2.61956538	0.923	0.173	0	LRRK2
Alveolar type 2	2.5035114	0.911	0.009	0	SFTPB
Alveolar type 2	2.49615093	0.92	0.063	0	KRT3
Secretory/basal cells	4.26002445	0.582	0.037	0	ENSCAFG00000045599
Secretory/basal cells	4.04701519	0.934	0.088	0	KRT14
Secretory/basal cells	2.70848749	0.776	0.079	0	ENSCAFG00000049417
Secretory/basal cells	2.31895375	0.825	0.11	0	WFDC2
Secretory/basal cells	2.16644727	0.811	0.087	0	KRT3
Secretory/basal cells	2.05849868	0.892	0.231	0	MECOM
Secretory/basal cells	2.05441311	0.476	0.036	0	GPC5
Secretory/basal cells	2.04704786	0.837	0.06	0	ANK3
Secretory/basal cells	1.84617354	0.68	0.035	0	FXYD3
Secretory/basal cells	1.83974141	0.476	0.006	0	GPX2
Secretory/basal cells	1.78213166	0.566	0.01	0	ENSCAFG00000001854
Secretory/basal cells	1.57764403	0.576	0.071	0	CES5A
Secretory/basal cells	1.46072653	0.727	0.171	0	PTPRK
Secretory/basal cells	1.42923367	0.663	0.073	0	PCDH7
Secretory/basal cells	1.42517202	0.577	0.084	0	GLIS3
Alveolar type 1	3.49496115	0.862	0.053	0	AGER
Alveolar type 1	3.46638895	0.955	0.198	0	TSPAN8
Alveolar type 1	2.84299324	0.865	0.074	0	CES5A
Alveolar type 1	2.68301429	0.768	0.095	0	KRT3
Alveolar type 1	2.62540958	0.782	0.069	0	ENSCAFG00000007293
Alveolar type 1	2.50540281	0.858	0.072	0	LMO7
Alveolar type 1	2.43080054	0.785	0.099	0	KRT14
Alveolar type 1	2.03067034	0.699	0.048	0	CLIC3
Alveolar type 1	1.90881535	0.623	0.012	0	SEMA3E
Alveolar type 1	1.83667175	0.768	0.039	0	CLDN18
Alveolar type 1	1.77504822	0.702	0.067	0	SCD5
Alveolar type 1	1.69420764	0.723	0.037	0	SUSD2
Alveolar type 1	1.64711164	0.543	0.009	0	RTKN2
Alveolar type 1	1.58876342	0.702	0.085	0	CXADR
Alveolar type 1	1.52679218	0.55	0.039	0	ITGB6
Ciliated cells	3.85121351	0.975	0.055	0	AGBL4
Ciliated cells	3.69080776	0.987	0.006	0	DNAH11
Ciliated cells	3.68182969	0.987	0.004	0	ENSCAFG00000024088
Ciliated cells	3.61683126	1	0.007	0	LRRIQ1
Ciliated cells	3.26656205	0.969	0.006	0	FGF14
Ciliated cells	3.04538068	0.981	0.008	0	MUC13
Ciliated cells	2.88370712	0.981	0.009	0	SPEF2
Ciliated cells	2.88166004	0.956	0.031	0	PACRG
Ciliated cells	2.81348964	0.937	0.003	0	DCDC1
Ciliated cells	2.79527468	0.969	0.029	0	CFAP54
Ciliated cells	2.79488932	0.981	0.071	0	ANK3
Ciliated cells	2.70647772	0.95	0.019	0	TMEM232
Ciliated cells	2.67988707	0.893	0.077	0	CES5A
Ciliated cells	2.61567471	0.969	0.009	0	HYDIN
Ciliated cells	2.59396635	0.969	0.002	0	DNAH5

Experimental section

Study 4:

Fibroblast activation protein is a cellular marker of fibrotic activity in canine idiopathic pulmonary fibrosis

Preamble

Currently, there is a lack of effective diagnostic markers or therapeutic strategies for CIPF. FAP is a membrane-bound serine protease known for its role in extracellular matrix remodeling, particularly through its ability to cleave denatured collagen. While FAP is nearly absent in healthy tissues, it is strongly upregulated in pathological contexts involving active tissue remodeling, such as wound healing, organ fibrosis, and in the stroma of many cancers. In human IPF, FAP is highly expressed in fibroblast foci and its expression correlates with disease severity and progression. The present study evaluated FAP expression in lung tissues from WHWTs with CIPF to determine whether FAP could serve as a marker of fibrotic activity and a candidate for future diagnostic and therapeutic applications.

Using a novel histological scoring system, lung biopsies from 22 WHWTs with CIPF were classified by severity and fibrosis activity. Anti-FAP IHC revealed FAP expression in fibroblasts in 20 of the 22 CIPF samples, with no expression in healthy controls. FAP expression levels correlated strongly with fibrosis activity, but only weakly with fibrosis severity. Digital image analysis confirmed that FAP-positive cells were predominantly localized in regions of active, immature fibrosis, and were sparse within mature collagen-rich fibrotic areas, reinforcing the value of FAP expression as a marker of active fibrogenesis. In addition, FAP expression was assessed in six primary pulmonary adenocarcinomas and one mammary carcinoma metastasis. Strong FAP immunoreactivity was observed in cancer-associated fibroblasts in all tumors.

Interestingly, while FAP was upregulated in fibrotic and neoplastic lung tissues, plasma levels of soluble FAP were significantly lower in WHWTs with CIPF compared to healthy dogs. This echoes observations in certain human pathologies, though the mechanisms remain unclear. As a result, circulating FAP appears insufficiently specific or consistent to serve as a diagnostic biomarker for CIPF.

In conclusion, this study identifies tissue FAP as a marker of fibrotic activity in CIPF and an indicator of tumor stroma activation in canine lung cancers. Its restricted expression to active fibroblastic regions, combined with the emergence of FAP-targeted imaging and therapeutics, positions FAP as a promising candidate for future diagnostic and therapeutic strategies.

Experimental section

Study 4:

Fibroblast activation protein is a cellular marker of fibrotic activity in canine idiopathic pulmonary fibrosis

Frontiers in Veterinary Science *11:1416124*

Elodie Rizzoli, Constance de Meeûs d'Argenteuil, Aline Fastrès, Elodie Roels, Pierre Janssen, Ellen Puré, Mutien-Marie Garigliany, Thomas Marichal, Cécile Clercx

Abstract

Canine idiopathic pulmonary fibrosis (CIPF) is a progressive fibrotic interstitial lung disease of unknown etiology, afflicting aging West Highland white terriers (WHWTs) and leading to progressive respiratory failure. Fibroblast activation protein (FAP), a protease overexpressed in many cancers, is upregulated in idiopathic pulmonary fibrosis in humans. The aim of this study was to investigate FAP as a marker of active fibrosis in lung biopsies from WHWTs affected with CIPF, as well as the potential of plasmatic FAP as a biomarker. After establishing a scoring system to evaluate the severity and activity of fibrosis on histopathological lung sections, anti-FAP immunohistochemistry was performed on healthy and CIPF samples. FAP expression was characterized using both visual and digital quantitative pathology software analyses and then correlated to fibrosis severity and activity. Levels of plasmatic FAP in WHWTs affected with CIPF were measured by enzyme-linked immunosorbent assay and compared with healthy dogs. Lung samples from 22 WHWTs affected with CIPF were collected. According to the fibrosis scoring system, they were classified as cases of mild (5), moderate (9) and severe (8) fibrosis and were attributed scores of fibrosis activity. Fifteen healthy lung samples were classified as non-fibrotic. Healthy lung samples were FAP-negative, whereas fibroblasts were FAP-positive in 20 CIPF samples. FAP immunohistochemical expression correlated mildly with fibrosis severity ($p < 0.05$; $R^2 = 0.22$) but highly with fibrosis activity scores ($p < 0.001$; $R^2 = 0.68$). Digital image analysis detected a higher percentage of FAP-positive cells in areas of active fibrosis ($p < 0.001$) and FAP-positive cells were distributed outside mature fibrosis lesions, clustered in active fibrosis areas or scattered within alveolar septa. On the other hand, plasmatic FAP was significantly lower in dogs affected with CIPF compared with healthy dogs ($p < 0.01$). In conclusion, this study provides a valuable histological scoring system to assess the severity and activity of fibrosis in CIPF. It demonstrates that FAP is a good cellular marker of fibrotic activity in CIPF, and thus constitutes a promising target to be exploited for diagnostic and therapeutic applications. Additionally, it suggests that plasmatic FAP, although non-specific, could be altered in CIPF.

Introduction

Canine idiopathic pulmonary fibrosis (CIPF) is a progressive fibrotic interstitial lung disease of unknown etiology, affecting the West Highland white terrier (WHWT) breed leading to progressive respiratory insufficiency, mimicking idiopathic pulmonary fibrosis (IPF) in humans (Clercx et al., 2018; Laurila and Rajamäki, 2020b). Currently, there are neither consistent diagnostic or prognostic biomarker nor curative treatment options available for this disease (Clercx et al., 2018; Laurila and Rajamäki, 2020b).

Fibroblast Activation Protein (FAP), also known as seprase, is a cell surface protease which exhibits both dipeptidyl peptidase activity and endopeptidase activity (Christiansen et al., 2007). Among substrates of the endopeptidase activity, FAP cleaves denatured type 1 collagen, thus participating in extracellular matrix remodeling (Christiansen et al., 2007). The protease also exists as a soluble circulating form called antiplasmin-cleaving enzyme (APCE) (Lee et al., 2004). FAP is specifically expressed in areas of physiological and pathological active tissue remodeling, including wound healing and scar formation in mammals (Fitzgerald and Weiner, 2020). FAP is usually undetectable in normal tissue (Fitzgerald and Weiner, 2020), although low basal levels have been measured in human adipose tissue, liver and plasma (Roberts et al., 2013; Keane et al., 2014).

In human IPF, immunohistochemical studies on lung biopsies showed that FAP is strongly expressed in areas of lung fibrosis, namely in fibroblast foci and interstitium, and is positively correlated with the severity of fibrosis (Acharya et al., 2006; P. Yang et al., 2023). In humans, FAP is also upregulated in other fibrotic diseases (Levy et al., 2002; Dienus et al., 2010; Rovedatti et al., 2011) as well as non-fibrotic diseases (Milner et al., 2006; Tillmanns et al., 2015), and, importantly, in various types of cancers. Indeed, it is expressed in over 90% of carcinomas, including among others non-small-cell lung carcinoma (Liao et al., 2013; Kilvaer et al., 2015; Shi et al., 2020), colorectal (Iwasa et al., 2003; Solano-Iturri et al., 2020a), esophageal (Liao et al., 2017), breast (Ariga et al., 2001; Hua et al., 2011; Jia et al., 2014) and renal (Solano-Iturri et al., 2020b) cancer. The protease is mainly present in cancer associated fibroblasts, but can also be expressed in other cells in the tumor microenvironment (immune (Arnold et al., 2014) cells or endothelial (Iwasa et al., 2003) cells) or in epithelial tumor cells (Iwasa et al., 2003; Shi et al., 2020). In dogs, overexpression of FAP has already been demonstrated in the stroma of mast cell tumors and mammary carcinomas (Giuliano et al., 2017; Ettlin et al., 2017) as well as in the right atrium of beagle dogs with induced atrial fibrillation (Li et al., 2023). Moreover, overexpression of the FAP gene has been observed in post-mortem lung

biopsies from WHWTs affected with CIPF compared with healthy controls based on microarray analysis and quantitative reverse transcriptase polymerase chain reaction (Krafft et al., 2013b).

Recently, FAP-targeted positron emission tomography (PET) imaging using a FAP inhibitor (FAPI) has been described as a non-invasive sensitive tool for advanced tumor staging and monitoring and has a promising potential owing to its ability to accurately depict most malignant tumors (Nakamoto et al., 2024). Beyond its application in neoplastic disorders, there have been encouraging reports suggesting the utility of FAPI PET in non-neoplastic conditions such as respiratory or cardiac diseases including IPF (Röhrich et al., 2022; P. Yang et al., 2023; Lavis et al., 2023; Mori et al., 2023). Indeed, the uptake of FAP-targeted tracers (labeled with either ^{68}Ga or ^{18}F) in IPF patients is higher than in healthy volunteers, and also seems to be positively correlated to the pulmonary function decline (Mori et al., 2023; P. Yang et al., 2023).

Given the potential role of FAP in the pathogenesis of fibrosis and cancer, several therapeutic strategies seek to target this protein, from selective inhibitors (Jung et al., 2021) to anti-FAP chimeric antigen receptor (CAR)-T cells (Lee et al., 2022) or even recent theragnostic ligands (Fu et al., 2022). However, none of these FAP-based therapeutic approaches have been approved in humans yet.

If FAP appears to be a specific marker of active fibrosis in dogs with CIPF, it could represent both an interesting diagnostic and monitoring marker of the disease and importantly, a potential therapeutic target. Therefore, the aim of this study was to gain insight into the implication of FAP in the pathophysiology of CIPF and to confirm its potential as a marker of disease activity. We hypothesized that FAP is expressed in lungs of WHWTs affected with CIPF, as well as in the stroma of canine lung cancers, used as positive controls, but not in healthy lungs. Anti-FAP immunohistochemistry (IHC) staining was thus performed on sections of lung biopsies from WHWTs affected with CIPF, dogs with lung cancer and dogs without pulmonary disease. The pattern of FAP expression was characterized according to the pattern of severity and activity of fibrosis, using both visual and digital quantitative pathology software analyses. Finally, the potential of circulating FAP as a biomarker of CIPF was investigated by measuring the levels of plasmatic FAP in WHWTs affected with CIPF in comparison with healthy dogs.

Material and methods

1. Lung sample collection

For this cross-sectional observational study, lung biopsies were obtained from 22 WHWTs affected with CIPF (median age of 12.4 years; range 10.3 – 15.6; 10 females and 12 males), 15 dogs of various breeds (WHWT (4), Beagle (3), Yorkshire Terrier (3), mixed breed (2), American Staffordshire Terrier, Bull Terrier, Leonberger and Shih Tzu) exempt from lung disease (median age of 13.2 years; range 7.3 – 16.8; 4 females and 11 males) and 7 dogs of different breeds (WHWT (4), mixed breed (2), Weimaraner) with lung neoplasia (median age of 12.0 years; range 8.2 – 14.2; 5 females and 2 males). In WHWTs, CIPF diagnosis was based on clinical signs, physical examination, 6-minute walk test, hematology, serum biochemistry, arterial blood gas analysis, cardiac ultrasonography, thoracic high-resolution computed tomography, bronchoscopy and analysis of bronchoalveolar lavage fluid (Heikkilä et al., 2011; Clercx et al., 2018). CIPF and healthy WHWTs were recruited as part of a longitudinal study conducted at the University of Liège and approved by the Animal Ethics Committee of the University of Liège (approval #20-2245). Healthy controls were euthanized for reasons unrelated to the study and had no respiratory clinical signs and normal lung histopathology. Five post-mortem lung biopsies were collected: one in the periphery of the right cranial and accessory lobes, two in the periphery of the right diaphragmatic lobe – one ventrally and one dorsally – and one centrally in the right middle lobe. Biopsies of pulmonary neoplasia, collected after either lobectomy or necropsy, were also retrieved. All biopsies were fixed in formalin 10% and embedded in paraffin until further use. All samples were obtained with informed owner consent.

2. Histopathology and fibrosis scoring

Formalin-fixed, paraffin-embedded specimens were sliced into 5 µm sections with a motorized microtome (Microm HM355S, Thermo Fisher Scientific). Hematoxylin and eosin (HE) staining was initially performed. All slides were evaluated by the first author and by a diplomate of the European College of Veterinary Pathology (MMG), who were blinded to the clinical records. For each healthy and CIPF case, one representative section was selected and additional serial slides were stained with Masson's trichrome and Picro Sirius red for further use. All sections were digitalized with NDP NanoZoomer (Hamamatsu) and Picro Sirius red slides were additionally digitalized under polarized light with ZEISS Axioscan 7.

For each selected section, a scoring system of fibrosis was applied, based on both HE and Masson's trichrome. For this purpose, a list of criteria was established, as detailed in Table 1, based

on previously reported histopathological examinations of CIPF lung sections (Heikkilä et al., 2011; Syrjä et al., 2013) and the latest consensus for histopathological diagnosis of human IPF (Raghu et al., 2022b). Categories of criteria included the pattern of interstitial fibrosis (evaluating the severity of fibrosis in the subpleural area, in peribronchiolar area as well as within alveolar septa) based on Masson's trichome stained sections, the maturity of fibrosis and its extent over the section (based on HE and Masson's trichrome), and alveolar epithelial and luminal changes (based on HE). Regarding the maturity of fibrosis, each case was assigned a score of active fibrosis from 0 to 3 reflecting the proportion of the section affected by active fibrosis, which was defined as immature, highly cellular, fibroblast-dominant fibrosis (Syrjä et al., 2013). Another score from 0 to 3 was attributed according to the contribution of mature fibrosis, which was defined as inactive fibrosis and characterized by dense collagen deposition and low cellularity consisting of a few fibrocytes (Syrjä et al., 2013). An overall grade of fibrosis severity was attributed according to the total score as follows: 0-3 (non-fibrotic), 4-7 (mild), 8-11 (moderate) and 12-16 (severe). For lung tumor cases, the histopathological diagnosis was established as precisely as possible based on medical records and HE stained slides.

Table 1. Scoring system used to evaluate fibrosis in canine idiopathic pulmonary fibrosis lung biopsies.

Histopathological features	**Criteria**	**Scores**			
		0	**1**	**2**	**3**
Interstitial fibrosis pattern					
Subpleural	Increase in pleural width	0	2x	≥3x	NA
Peribronchiolar fibrous metaplasia	Smooth muscle over lamina propria and adventitia thickness ratio	> 0.34	≤ 0.34	NA	NA
Diffuse	Increase in septa width by fibrosis	0	2x	3-4x	≥ 5x
	Atelectasis, alveolar distortion, consolidation, and/or honeycombing	Absent	NA	NA	Present
Maturity of fibrosis					
Immature, active, cellular, fibroblast-dominant*	Proportion of the section affected by active fibrosis	0%	1-33%	34-66%	≥ 67%
Mature, inactive, fibrous, few fibrocytes*	Proportion of the section affected by mature fibrosis	0%	1-33%	34-66%	≥ 67%
Alveolar epithelial and luminal changes					
Type II pneumocyte hyperplasia/ bronchiolar metaplasia	Alveolar epithelium	Normal	Type II pneumocyte hyperplasia and/or atypia	Pseudo-stratification	NA
Numerous alveolar macrophages	Alveolar macrophages count per alveolar space	1-2	≥ 3	NA	NA

Note: The grade of severity of fibrosis was attributed by calculating the sum of the score attributed for each criteria: 0-3 (non-fibrotic), 4-7 (mild), 8-11 (moderate) and 12-16 (severe). *As the sum of both percentages cannot exceed 100% (whole section), the sum of the scores from these 2 categories is maximum 4.

3. Tissular FAP immunohistochemistry

a. Staining

Anti-FAP IHC was performed on additional serial sections of formalin-fixed, paraffin-embedded biopsies of CIPF, healthy lungs and lung cancers, which were used as positive controls. The slides were deparaffinized in xylene and rehydrated in graded alcohol series. Antigen retrieval was performed using 10 mM sodium citrate buffer for 5 minutes at 100°C. Slides were washed at room temperature and hydrated in Phosphate-Buffered Saline. Endogenous peroxidase activity was blocked with 3% hydrogen peroxide incubation for 30 minutes. Sections were then washed with distilled water. Nonspecific antibody binding was blocked by incubation for 30 minutes in a blocking buffer containing 0.5% blocking reagent provided in the TSA Plus DNP kit (Akoya Biosciences #NEL747A001KT). Sections were incubated overnight at 4°C temperature with rabbit anti-human fibroblast activation protein alpha monoclonal primary antibody (1:100, Abcam #ab207178, RRID:AB_2864720) or with rabbit isotype IgG control antibody (1:1600, Jackson ImmunoResearch Labs #011-000-003, RRID:AB_2337118) to later screen for non-specific staining. Biotinylated goat anti-rabbit secondary antibody (1:1000, Thermo Fisher Scientific #65-6140, RRID:AB_2533969) was

then incubated for 1 hour at room temperature. The slides were incubated for 30 minutes with streptavidin-horseradish peroxidase (Invitrogen #S911), and signal was amplified using a TSA Plus DNP kit (Akoya Biosciences #NEL747A001KT). Signal development was achieved with a metal enhanced diaminobenzidine substrate kit (Thermo Fisher Scientific #34065). Slides were counterstained with hematoxylin for 30 seconds, then dehydrated and mounted. Each slide was digitalized using NDP NanoZoomer (Hamamatsu).

b. Visual assessment of FAP expression

Two independent observers, including the first author and a diplomate of the European College of Veterinary Pathology (MMG), blinded to the histopathological diagnosis, assessed all healthy and CIPF digitalized sections to determine a staining index for the whole section, that represents the expression of FAP. There was 91% agreement between the two observers and the final index was obtained after a consensus was reached. An area of parenchymal lung was identified as FAP-positive if at least 25% of the cells exhibited FAP staining. The FAP expression index (from 0 to 3) was then attributed according to the percentage of the whole section occupied by FAP-positive areas. An index of 0 (no expression) was attributed if less than 1% of the section was occupied by FAP-positive areas, 1 (low expression) if FAP-positive areas occupied from 1 to 10% of the whole section, 2 (intermediate expression) from 11 to 50% and 3 (high expression) for more than 50%. In all CIPF cases, correlation analyses were conducted between the FAP expression index and the fibrosis severity score, as well as with the fibrosis activity score attributed during the scoring of fibrosis.

c. Digital analysis of FAP expression

Whole slide images were analyzed with an open-source automated software analysis program for digital pathology (QuPath version 0.4.3) (Bankhead et al., 2017). Briefly, lesional areas were determined manually on the HE slides and classified into ‘active fibrosis’ or ‘mature fibrosis’. Ten areas of 200,000 μm^2 each representative of active fibrosis or mature fibrosis were selected. Automated tissue detection was performed in the lesional area to correct for alveolar blank spaces. Thereafter, for fibrosis quantification, built-in algorithms for pixel classification of QuPath and machine learning were used on sequential Picro Sirius red slides for measuring collagen content in lesional areas. The accuracy of collagen detection was then verified by assessing the same area digitalized under polarized light. On FAP-stained sections, the percentage of FAP-positive cells within the lung interstitium for the 20 areas was calculated by applying the deep learning algorithm

StarDist method for cell nuclei segmentation and applying a single threshold to the cell detection to obtain positive cell detection. To visualize the spatial distribution of FAP positive cells in fibrotic areas, image superposition of Picro Sirius red slides and FAP-stained slides was done by using the Warpy extension in QuPath.

4. Plasmatic FAP measurement

a. Test samples

For the plasmatic FAP measurement, we used plasma samples from the day of death of 6 WHWTs affected with CIPF for which positive FAP expression in the lungs was confirmed by the methods described above. They had a median age of 12.6 years (range 10.3 – 15.6; 3 females and 3 males). For the control group, we used the plasma leftover from the analysis of blood donations from 9 healthy canine blood donors of various breeds (Border Collie (4), Golden Retriever (3), Akita Inu, Bull Terrier) with a median age of 6.6 years (range 3.9 – 7.3), including 4 females and 5 males. Dogs were considered healthy based on the absence of clinical signs or physical exam abnormalities, a complete blood analysis and a screening for infectious diseases. In all dogs, blood was collected in a citrated tube before being centrifuged and plasma was isolated and stored at -80°C until the day of the experiment. The assay was performed in citrate plasma in all cases because it was the type of plasma that was available for the higher number of cases in our biobank. Plasma samples underwent maximum 2 freeze-thaw cycles before analysis. Plasma samples were diluted in 1% bovine serum albumin (BSA, Sigma #A7906) in Dulbecco's Phosphate-Buffered Saline (DPBS) in four dilutions (1:50, 1:100, 1:200, 1:400) for titration. The reactivity of the assay with canine FAP was verified by using a homogenate of a FAP-rich metastasis of mammary carcinoma as positive control. A snap frozen biopsy of a lung metastasis of a mammary carcinoma that highly overexpressed FAP in IHC was homogenized using a previously described protocol (Vanneste et al., 2023). This canine FAP-containing solution was then diluted 1:5, 1:10, 1,25, 1:50 in 1% BSA DPBS in the assay for titration. Recombinant human FAP (Abcam #ab79623) with known concentration was used as positive control and standard. Negative control was 1% BSA DPBS.

b. Assay

Plasma levels of FAP were measured using a double-antibody sandwich enzyme-linked immunosorbent assay (ELISA). First, 96-well microplates were coated with a mouse IgG monoclonal anti-canine FAP antibody (5.125 µg/mL, Puré lab, University of Pennsylvania, 4G5) that cross-reacts with human FAP (Lee et al., 2022) and incubated overnight at 4°C. The following day, plates were

blocked with 1% BSA in DPBS for 1h before test samples were added in duplicates and incubated overnight at 4°C with agitation. For detection, a biotinylated polyclonal sheep anti-human FAP antibody (0.4 µg/µl, R&D Systems #BAF3715, RRID:AB_2057508) was added and incubated for 90 min. Plates were then incubated with avidin horseradish peroxidase (1:1000 dilution, Thermo Fisher Scientific #18-4100-94) for 30 min, after which 3,3',5,5'-tetramethylbenzidine (TMB, Life Technologies #SB02) was added. After a 10 min-incubation in the dark, reaction was stopped using 50 µL/well of H2SO4 1M. Plates were read by an optical density reader (Multiskan FC, Thermo Fisher Scientific #51119000) set at 450 nm. Between each step until the chromogenic reaction, 3 to 5 rinses were performed with a wash solution of Tween-20 5% (Thermo Fisher Scientific #233360010) in DPBS.

Because of the lack of commercially available purified canine FAP protein to act as standard, the exact amount of soluble FAP in biological samples could not be calculated. Instead, we expressed results in endpoint titers (EPT). Using a plot of the optical density on the log base 2 of the dilutions, we defined the cutoff line at half the optical density of recombinant human FAP at 78.13 ng/mL concentration. The log2 of the endpoint titer was obtained from the point where the linear line crosses the cutoff line.

5. Statistical analysis

Statistical analyses were conducted using the R Commander interface (Fox et al., 2023) to the R statistical software. Normal distribution was assessed using Shapiro-Wilk normality test. For normally distributed data, parametric tests were used and results were expressed in mean and standard deviation. A Fisher test was used to verify homoscedasticity between groups. When variances were significantly different between groups, comparisons of means were performed using a Welsh two sample t-test. For non-normally distributed data, non-parametric tests were employed and results were expressed in median and interquartile range (P25-P75). For correlation analyses of non-normally distributed data, Spearman's rank correlation rho test was used. For the comparison of medians between two groups, a Mann-Whitney test was used. Significance was established at a P-value lower than 0.05.

Results

1. Histopathological analysis

After scoring fibrosis in CIPF sections, five were characterized as mild (scores ranging from to 4 to 7), nine as moderate (scores ranging from 8 to 11) and eight as severe fibrosis (scores ranging from 12 to 16). Control lung sections were attributed scores from 0 to 3 and were considered as non-fibrotic. Seven cases of lung neoplasia, including six primary pulmonary adenocarcinomas and one metastasis of mammary carcinoma, served as positive controls for IHC.

2. Tissular FAP expression

FAP was expressed in cells interpreted as fibroblasts in the lungs of 20 out of 22 WHWTs affected with CIPF. Using a visual semi-quantitative scoring system, an index of high, intermediate, low and zero FAP expression were attributed in respectively 4, 4, 12, and 2 WHWTs. Healthy lung biopsies from WHWTs and other breeds all had an index of zero FAP expression. In primary pulmonary adenocarcinomas and in the metastasis of mammary carcinoma, cancer-associated fibroblasts were strongly FAP-positive. Cancer cells were also FAP-positive in four out of six cases of primary adenocarcinoma. Figure 1 illustrates examples of FAP staining in lung sections. Within CIPF cases, there was a statistically significant but poorly relevant positive correlation ($p < 0.05$; $R^2 = 0.22$) between the FAP expression index and the score of fibrosis severity. However, the index of FAP expression was highly positively correlated to the score of active fibrosis ($p < 0.001$; $R^2 = 0.68$), as illustrated in Figure 2.

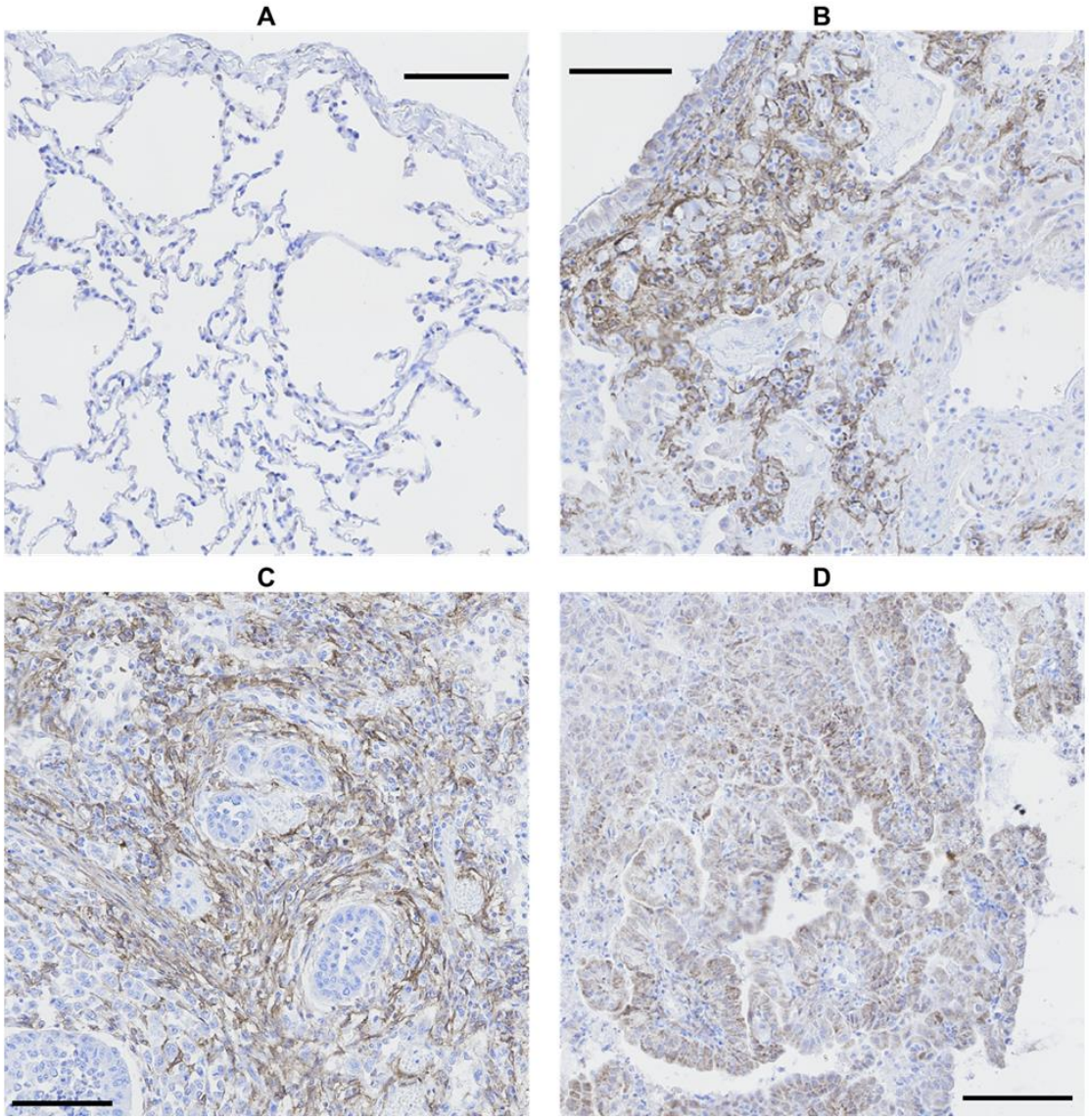

Figure 1. Comparison of FAP immunostaining in canine lung biopsies. No FAP expression in healthy lung (A) and high FAP expression in CIPF (B) and primary pulmonary adenocarcinoma, either in cancer-associated fibroblasts (C) or in cancer cells (D). Immunoperoxidase-diaminobenzidine, hematoxylin counterstain (bar: 100 µm). FAP: fibroblast activation protein, CIPF: canine idiopathic pulmonary fibrosis.

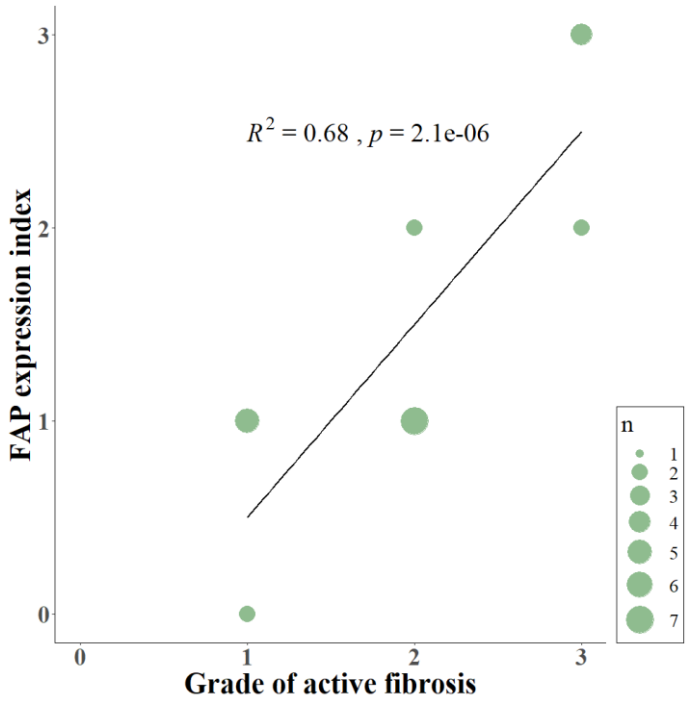

Figure 2. Scatterplot displaying the relationship between the FAP expression index and the grade of active fibrosis. The index of FAP expression (from 0 to 3) is positively correlated ($p < 0.001$; $R^2 = 0.68$) to the score of active fibrosis (from 0 to 3) in lung sections of CIPF. FAP: fibroblast activation protein, CIPF: canine idiopathic pulmonary fibrosis, n: number of cases.

Using quantitative digital analysis, we analyzed 20 areas originating from 11 different cases which were previously attributed with various indices of FAP expression and of fibrosis activity. QuPath automated detection of collagen content in lesional areas accurately reflected the mature collagen fibers visualized by polarized light microscopy (Supplementary Figure 1). The mean collagen content was significantly higher in representative areas of mature fibrosis (32.95 ± 15.28%) than in representative areas of active fibrosis (11.20 ± 7.34%; $p < 0.001$; Figure 3A). This validated our visual, semiquantitative assessment of the maturity of fibrosis. The mean percentage of FAP-positive cells was significantly higher ($p < 0.001$) in representative areas of active (27.73 ± 8.57%) compared with mature fibrosis (9.64 ± 4.02%; Figure 3B). Visual superimposition of serial Picro Sirius red and FAP-stained sections (Figure 4) revealed that FAP-positive cells were rare within highly collagenic mature fibrosis areas (Figure 4A-D). However, FAP-positive cells were clustered in areas of active fibrosis within alveolar septa (Figure 4E-H) or dispersed at the periphery of mature fibrotic lesions, where collagen content is lower (Figure 4I-L).

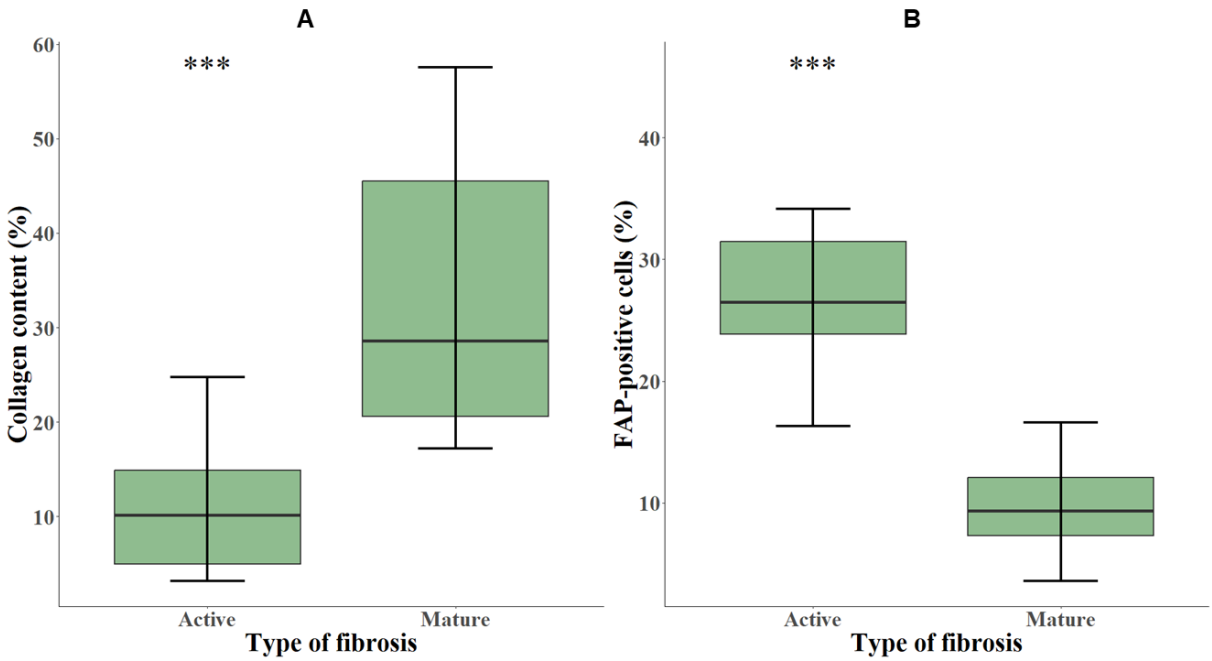

Figure 3. Box-and-whisker plots of collagen content (A) and of FAP-positive cells (B) in areas representing either active (n=10) or mature fibrosis (n=10), calculated with quantitative digital analysis in CIPF lung sections. The box represents the median and interquartile range. The whiskers represent the values within 1.5 times the interquartile range. Significance level: *** indicates a p-value below 0.001. FAP: fibroblast activation protein.

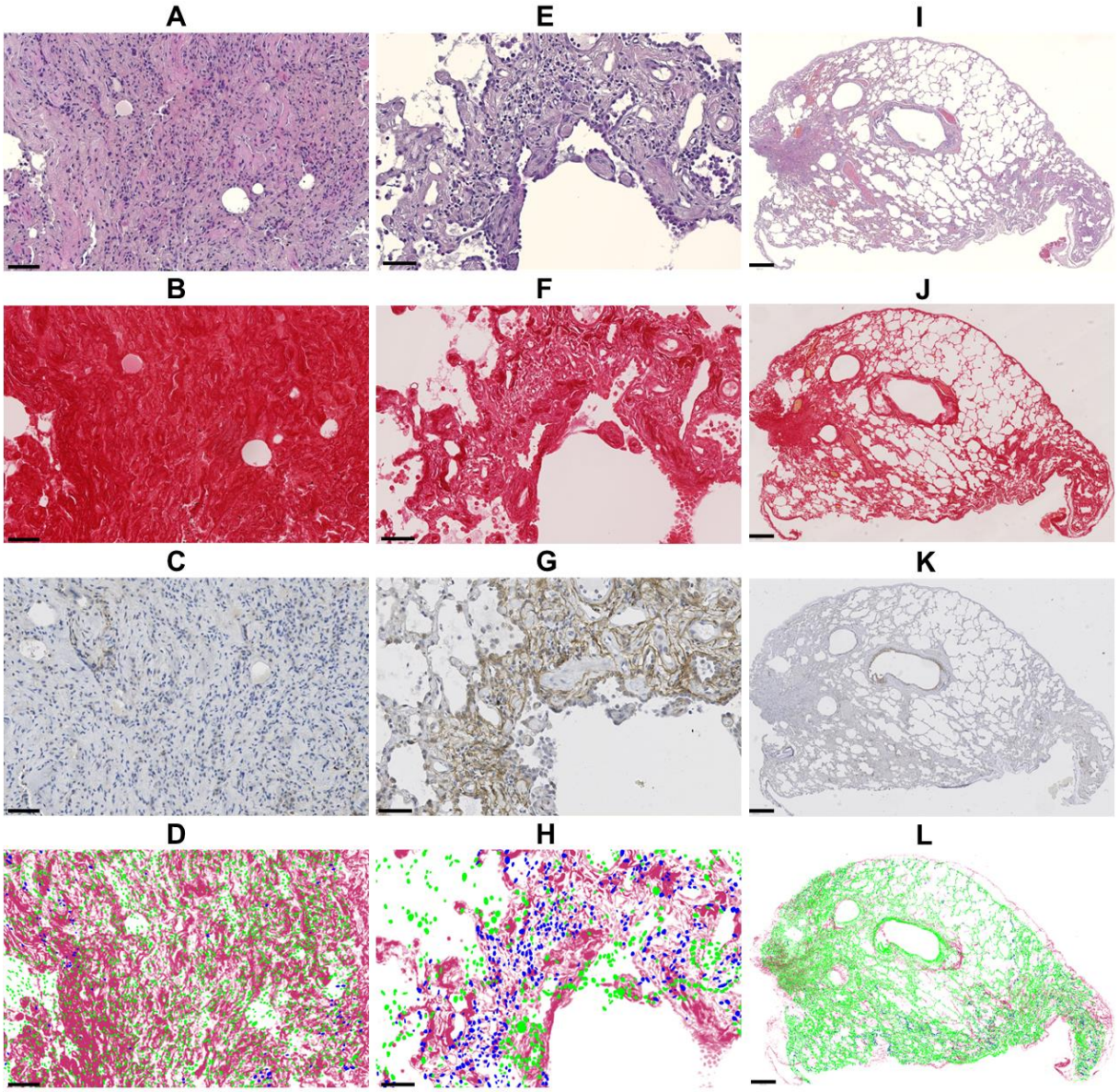

Figure 4. Panel showing sequential sections in HE staining (1st row), Picro Sirus red staining (2nd row), anti-FAP immunohistochemistry staining (3rd row) and the superimposition of cell detections (blue: FAP-positive, green: FAP-negative) based on anti-FAP immunohistochemistry onto Picro Sirus red-stained collagen (4th row). Images A to D show an area of strongly collagenic mature fibrosis with rare FAP-positive cells (bar: 50 µm). Images E to H illustrate an area of active fibrosis with low collagen content and numerous FAP-positive cells (bar: 50 µm). Images I to L show an entire section with mixed fibrosis pattern: few FAP-positive cells within highly collagenic mature fibrosis areas, from which less collagenic, FAP-rich areas extend (bar: 500 µm). FAP: fibroblast activation protein.

3. Plasmatic FAP quantification

The plasmatic levels of soluble FAP, as illustrated in Figure 5, were significantly lower ($p < 0.01$) in WHWTs with CIPF (EPT 0.74 [0.24 – 2.38]) than in healthy dogs (EPT 16.50 [4.78 – 63.84]).

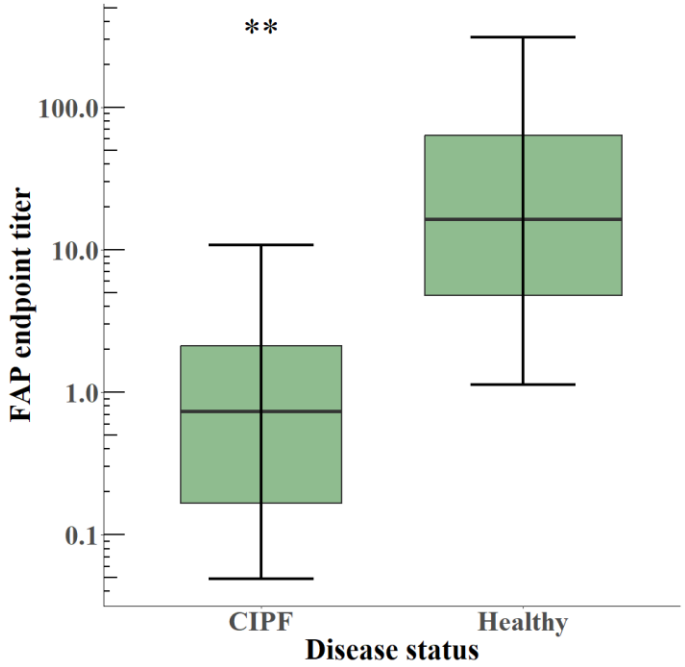

Figure 5. Box-and-whisker plot of plasma levels of soluble FAP in dogs with CIPF (n=6) and in healthy dogs (n=9). The box represents the median and interquartile range, and the whiskers represent the values within 1.5 times the interquartile range. Significance level: ** indicates a p-value below 0.01. FAP: fibroblast activation protein, CIPF: canine idiopathic pulmonary fibrosis.

Discussion

In this study, we established a semiquantitative scoring system destined to evaluate the severity and activity of fibrosis on histopathological sections of CIPF, which in this study exhibited mild to severe fibrosis. As expected, the FAP IHC study revealed that healthy lung sections were FAP-negative, and that cancer-associated fibroblasts from lung tumors were strongly positive. In the majority of CIPF samples, FAP was expressed by cells consistent with fibroblasts at various indices and only 2 samples were negative. FAP expression correlated weakly with fibrosis severity but highly with fibrosis activity. Indeed, automated image analysis detected a higher percentage of FAP-positive cells in areas of active fibrosis. It is also noticeable on superimposition of images that FAP-positive cells are located at the periphery of mature fibrosis lesions and clustered in areas of active fibrosis. Another finding of this study is that plasmatic FAP was significantly lower in WHWTs affected with CIPF compared with healthy dogs.

We established a system of scoring of the histological severity and activity of fibrosis in CIPF. This scoring system aimed to objectively distinguish lung biopsies of old healthy dogs from mild CIPF as well as mild from moderate and severe cases of CIPF. While attributing scores, a particular consideration was given to the distinction between active (immature) and inactive (mature) fibrosis for the purpose of subsequently establishing correlation with FAP IHC analyses. The Ashcroft scoring system (Testa et al., 2021) used for IPF cannot be applied to CIPF as human and canine IPF do not have the same histological pattern. Indeed, in humans, IPF is characterized by usual interstitial pneumonia (UIP) (Hochhegger et al., 2019; Raghu et al., 2022b). UIP diagnosis is based on patchy dense fibrosis accompanied by architectural distortion (with destructive scarring and/or honeycombing) with a predilection for subpleural and paraseptal parenchyma, and the presence of fibroblast foci (Hochhegger et al., 2019; Raghu et al., 2022b). CIPF shares features with UIP but also with non-specific interstitial pneumonia, which is characterized by diffuse interstitial fibrosis (Heikkilä et al., 2011; Syrjä et al., 2013). Indeed, in WHWTs affected with CIPF, histology reveals a mild to moderate diffuse mature interstitial fibrosis with multifocal subpleural or peribronchial areas of accentuation. Besides, no fibroblast foci are described (Heikkilä et al., 2011; Syrjä et al., 2013). The absence of fibroblast foci, as well as the high heterogeneity of fibrosis within a lung biopsy from a CIPF case, also prevented the application of scoring systems used for IHC studies of human IPF sections. This underlines the need for a specific scoring system adapted to dogs, as presented here.

This study confirmed the presence of FAP in lung biopsies from WHWTs affected with CIPF, and its absence in normal lungs, as anticipated from studies of human IPF (Acharya et al., 2006; P.

Yang et al., 2023). Based on the assessment of their morphology and localization, FAP-positive cells appeared as fibroblasts. Nonetheless, the simultaneous expression of other fibroblast markers would be needed to confirm with certainty the precise identity of FAP-positive cells, although previous studies in human IPF reported a FAP expression restricted to activated fibroblasts (Acharya et al., 2006; P. Yang et al., 2023). The majority of cases were assigned a low FAP expression index according to the semiquantitative scoring system. This outcome, which might initially appear disappointing, is actually due to the fact that the scoring system assesses the overall expression across the entire section since CIPF exhibits a more diffuse interstitial fibrosis pattern than UIP (Syrjä et al., 2013). As a whole section of CIPF biopsy can be highly heterogeneous, with varying ratios of mature and active fibrosis, this heterogeneity significantly influences the proportion of the section occupied by FAP-positive areas.

In cases of CIPF, the FAP expression index exhibited a mild correlation with the severity score of fibrosis, aligning with findings from previous studies that have explored the association between FAP expression and fibrosis severity at both histological and clinical level in humans (Acharya et al., 2006; P. Yang et al., 2023). Nevertheless, a good correlation emerged when focused on the activity of fibrosis in lung biopsies. In UIP, the histologic pattern of human IPF, FAP expression is restricted to areas of ongoing tissue injury (Acharya et al., 2006). FAP is indeed strongly expressed in fibroblast foci, which are interstitial clusters of proliferating fibroblasts and myofibroblasts near the injured alveolar epithelium (Acharya et al., 2006). Despite the absence of fibroblast foci in CIPF, it is consistent that FAP is mostly expressed in highly fibroblastic active areas, and not in poorly cellular regions that are consolidated by dense amounts of collagen fibers. The identified positive correlation between FAP expression and fibrosis activity underscores FAP's potential as a promising marker for fibroplasia, providing substantial support for the hypothesis that FAP plays a crucial role in the pathophysiology of the disease.

Automated quantitative image analysis technologies were used to confirm these results with a more sensitive and objective method. Digital image analysis using artificial intelligence solutions is emerging in the field of histopathology and IHC, providing promising techniques for scoring quantification of tissue fibrosis in human IPF or to quantify FAP positivity in IHC images (Testa et al., 2021; P. Yang et al., 2023). Such quantifying tools allowed us to validate our semiquantitative scoring system of fibrosis used to select areas by their representativity of a type of maturity of fibrosis (active or mature) with a precise quantification of the collagen content of the area, which is an established marker of mature fibrosis (Testa et al., 2021). Then, it was confirmed that the proportion of FAP-

positive cells was significantly higher in areas occupied by active fibrosis than in those occupied by mature fibrosis. Digital superimposition of FAP-positive cell detections onto Picro Sirius red stained sections allowed us to witness the spatial distribution of FAP-positive cells in relation to the lesions of fibrosis within the sections. FAP-positive cells, consistent with activated fibroblasts, are sparse within mature lesions and are mainly scattered in alveolar septa that are not yet burdened by large layers of collagen fibers. FAP-positive active fibrosis areas seem to be located in the periphery of mature lesions. In this view, FAP-positive cells appear to play a driving role in fibrosis.

The small cohort of primary pulmonary adenocarcinomas used in this study showed a strong expression of FAP by cancer-associated fibroblasts, and occasionally by cancer cells themselves, aligning with expectations based on both veterinary and human literature (Giuliano et al., 2017; Ettlin et al., 2017; Shi et al., 2020). This provides a foundation for potential extended investigations about the prognostic significance of FAP in lung cancer. Indeed canine lung cancers of advanced stage still carry a poor prognosis and could benefit from novel therapeutic strategies (Lee et al., 2020; McPhetridge et al., 2021).

This analysis revealed lower plasmatic FAP levels in WHWTs affected with CIPF compared with healthy dogs. To date, the variation of plasmatic FAP in humans affected with IPF is not known. However, it has been studied in various other conditions, notably in patients with cancer (Liao et al., 2017; Solano-Iturri et al., 2020a, 2020b), inflammatory bowel disease (Corsi et al., 2021) or acute heart failure (Delgado-Arija et al., 2024), who also exhibited a lower plasmatic FAP concentration compared with healthy volunteers, despite an overexpression of FAP in diseased tissues. The reason for such decrease, as well as the source of the soluble form of FAP, are still unknown, including whether it results from shedding from the cellular membrane or from alternative splicing (Lee et al., 2006; Tillmanns et al., 2013; Keane et al., 2014). Current hypotheses suggest that multiple organs may contribute to a low basal level of circulating FAP, which would decrease due to a systemic reaction to the disease (Javidroozi et al., 2012; Liao et al., 2017; Delgado-Arija et al., 2024). Interestingly, other studies showed an increase of circulating FAP in patients with liver fibrosis and support the hypothesis that the liver constitutes a major source of elevated circulating FAP (Keane et al., 2014; Williams et al., 2015; Uitte De Willige et al., 2017). Further studies on a greater number of cases are thus required to explain why circulating FAP is decreased in CIPF.

This study of plasmatic FAP concentrations is based on a small number of dogs which could expose us to sampling biases. Furthermore, due to the nature of the selection criteria for blood donation (dogs of less than 10 years old and more than 20 kg), the control group is not matched for

age and breed with the study population. Nonetheless, a strong association between age and circulating FAP levels has never been established in existing literature (Lavis et al., 2023). However, it appears that various conditions can influence the level of plasmatic FAP, such as malignant, inflammatory, metabolic, cardiac, or other organs fibrotic conditions (Williams et al., 2015; Uitte De Willige et al., 2017; Solano-Iturri et al., 2020b; Corsi et al., 2021; Delgado-Arija et al., 2024). Although plasmatic FAP appears significantly decreased in dogs with CIPF, we do not believe that it would constitute a useful biomarker of CIPF since it does not seem specific to the disease.

As perspectives, the sensitivity of FAP to identify active fibrosis specifically localized within the lungs in cases of CIPF can be harnessed by FAP-targeted PET examinations. FAPI-based PET/CT are emerging in preclinical and clinical studies on interstitial lung disease (such as IPF) or cancer and are presented as non-invasive tools to monitor disease progression or response to treatment (Rosenkrans et al., 2022; Röhrich et al., 2022). This promising technique would allow to assess FAP expression in dogs in vivo and thus enable an early detection of CIPF and evaluation of progression or response to treatment. In this field, FAP-targeted therapies (such as anti-FAP CAR-T cells or FAPI-based theragnostic) emerge as promising prospects, given the current lack of available treatments for CIPF. Considering that CIPF is regarded as a spontaneous preclinical model of IPF, human patients could also gain advantages from these findings.

In conclusion, this study shows new insights into the pathology of CIPF by describing the cellular expression of FAP in progressing active immature lesions of fibrosis. These findings position tissular FAP – but not plasmatic FAP – as a promising marker of activity of the disease, which could be exploited by multiple diagnostic and therapeutic applications.

Acknowledgments

Preliminary results were partly presented as an abstract at the 32nd congress of the European College of Veterinary Internal Medicine – Companion Animals (ECVIM-CA), Göteborg, Sweden, 1-3 September 2022. We gratefully thank Yue Li, Pranidhi Baddam, and Leslie Hopper for their help with the IHC staining and the management of the slides.

References

Acharya, P.S., Zukas, A., Chandan, V., Katzenstein, A.-L.A., Puré, E., 2006. Fibroblast activation protein: a serine protease expressed at the remodeling interface in idiopathic pulmonary fibrosis. Hum. Pathol. 37, 352–360. https://doi.org/10.1016/j.humpath.2005.11.020

Ariga, N., Sato, E., Ohuchi, N., Nagura, H., Ohtani, H., 2001. Stromal expression of fibroblast activation protein/seprase, a cell membrane serine proteinase and gelatinase, is associated with longer survival in patients with invasive ductal carcinoma of breast. Int. J. Cancer 95, 67–72. https://doi.org/10.1002/1097-0215(20010120)95:1<67::aid-ijc1012>3.0.co;2-u

Arnold, J.N., Magiera, L., Kraman, M., Fearon, D.T., 2014. Tumoral Immune Suppression by Macrophages Expressing Fibroblast Activation Protein-Alpha and Heme Oxygenase-1. Cancer Immunol. Res. 2, 121–126. https://doi.org/10.1158/2326-6066.CIR-13-0150

Bankhead, P., Loughrey, M.B., Fernández, J.A., Dombrowski, Y., McArt, D.G., Dunne, P.D., McQuaid, S., Gray, R.T., Murray, L.J., Coleman, H.G., James, J.A., Salto-Tellez, M., Hamilton, P.W., 2017. QuPath: Open source software for digital pathology image analysis. Sci. Rep. 7, 16878. https://doi.org/10.1038/s41598-017-17204-5

Christiansen, V.J., Jackson, K.W., Lee, K.N., McKee, P.A., 2007. Effect of fibroblast activation protein and α2-antiplasmin cleaving enzyme on collagen Types I, III, and IV. Arch. Biochem. Biophys. 457, 177–186. https://doi.org/10.1016/j.abb.2006.11.006

Clercx, C., Fastrès, A., Roels, E., 2018. Idiopathic pulmonary fibrosis in West Highland white terriers: An update. Vet. J. 242, 53–58. https://doi.org/10.1016/j.tvjl.2018.10.007

Corsi, F., Sorrentino, L., Albasini, S., Colombo, F., Cigognini, M., Massari, A., Morasso, C., Mazzucchelli, S., Piccotti, F., Ardizzone, S., Sampietro, G.M., Truffi, M., 2021. Circulating Fibroblast Activation Protein as Potential Biomarker in Patients With Inflammatory Bowel Disease. Front. Med. 8.

Delgado-Arija, M., Genovés, P., Pérez-Carrillo, L., González-Torrent, I., Giménez-Escamilla, I., Martínez-Dolz, L., Portolés, M., Tarazón, E., Roselló-Lletí, E., 2024. Plasma fibroblast activation protein is decreased in acute heart failure despite cardiac tissue upregulation. J. Transl. Med. 22, 124. https://doi.org/10.1186/s12967-024-04900-w

Dienus, K., Bayat, A., Gilmore, B.F., Seifert, O., 2010. Increased expression of fibroblast activation protein-alpha in keloid fibroblasts: implications for development of a novel treatment option. Arch. Dermatol. Res. 302, 725–731. https://doi.org/10.1007/s00403-010-1084-x

Ettlin, J., Clementi, E., Amini, P., Malbon, A., Markkanen, E., 2017. Analysis of Gene Expression Signatures in Cancer-Associated Stroma from Canine Mammary Tumours Reveals Molecular Homology to Human Breast Carcinomas. Int. J. Mol. Sci. 18, 1101. https://doi.org/10.3390/ijms18051101

Fitzgerald, A.A., Weiner, L.M., 2020. The role of fibroblast activation protein in health and malignancy. Cancer Metastasis Rev. 39, 783–803. https://doi.org/10.1007/s10555-020-09909-3

Fox, J., Munoz Marquez, M., Bouchet-Valat, M., 2023. Rcmdr: R Commander.

Fu, K., Pang, Y., Zhao, L., Lin, L., Wu, H., Sun, L., Lin, Q., Chen, H., 2022. FAP-targeted radionuclide therapy with [177Lu]Lu-FAPI-46 in metastatic nasopharyngeal carcinoma. Eur. J. Nucl. Med. Mol. Imaging 49, 1767–1769. https://doi.org/10.1007/s00259-021-05634-3

Giuliano, A., dos Santos Horta, R., Constantino-Casas, F., Hoather, T., Dobson, J., 2017. Expression of Fibroblast Activating Protein and Correlation with Histological Grade, Mitotic Index and Ki67 Expression in Canine Mast Cell Tumours. J. Comp. Pathol. 156, 14–20. https://doi.org/10.1016/j.jcpa.2016.10.004

Heikkilä, H. p., Lappalainen, A. k., Day, M. j., Clercx, C., Rajamäki, M. m., 2011. Clinical, Bronchoscopic, Histopathologic, Diagnostic Imaging, and Arterial Oxygenation Findings in West Highland White Terriers with Idiopathic Pulmonary Fibrosis. J. Vet. Intern. Med. 25, 433–439. https://doi.org/10.1111/j.1939-1676.2011.0694.x

Hochhegger, B., Marchiori, E., Zanon, M., Rubin, A.S., Fragomeni, R., Altmayer, S., Carvalho, C.R.R., Baldi, B.G., 2019. Imaging in idiopathic pulmonary fibrosis: diagnosis and mimics. Clin. Sao Paulo Braz. 74, e225. https://doi.org/10.6061/clinics/2019/e225

Hua, X., Yu, L., Huang, X., Liao, Z., Xian, Q., 2011. Expression and role of fibroblast activation protein-alpha in microinvasive breast carcinoma. Diagn. Pathol. 6, 111. https://doi.org/10.1186/1746-1596-6-111

Iwasa, S., Jin, X., Okada, K., Mitsumata, M., Ooi, A., 2003. Increased expression of seprase, a membrane-type serine protease, is associated with lymph node metastasis in human colorectal cancer. Cancer Lett. 199, 91–98. https://doi.org/10.1016/S0304-3835(03)00315-X

Javidroozi, M., Zucker, S., Chen, W.-T., 2012. Plasma seprase and DPP4 levels as markers of disease and prognosis in cancer. Dis. Markers 32, 309–320. https://doi.org/10.3233/DMA-2011-0889

Jia, J., Martin, T.A., Ye, L., Jiang, W.G., 2014. FAP-α (Fibroblast activation protein-α) is involved in the control of human breast cancer cell line growth and motility via the FAK pathway. BMC Cell Biol. 15, 16. https://doi.org/10.1186/1471-2121-15-16

Jung, H.J., Nam, E.H., Park, J.Y., Ghosh, P., Kim, I.S., 2021. Identification of BR102910 as a selective fibroblast activation protein (FAP) inhibitor. Bioorg. Med. Chem. Lett. 37, 127846. https://doi.org/10.1016/j.bmcl.2021.127846

Keane, F.M., Yao, T.-W., Seelk, S., Gall, M.G., Chowdhury, S., Poplawski, S.E., Lai, J.H., Li, Y., Wu, W., Farrell, P., Vieira de Ribeiro, A.J., Osborne, B., Yu, D.M.T., Seth, D., Rahman, K., Haber, P., Topaloglu, A.K., Wang, C., Thomson, S., Hennessy, A., Prins, J., Twigg, S.M., McLennan, S.V., McCaughan, G.W., Bachovchin, W.W., Gorrell, M.D., 2014. Quantitation of fibroblast activation protein (FAP)-specific protease activity in mouse, baboon and human fluids and organs. FEBS Open Bio 4, 43–54. https://doi.org/10.1016/j.fob.2013.12.001

Kilvaer, T.K., Khanehkenari, M.R., Hellevik, T., Al-Saad, S., Paulsen, E.-E., Bremnes, R.M., Busund, L.-T., Donnem, T., Martinez, I.Z., 2015. Cancer Associated Fibroblasts in Stage I-IIIA NSCLC: Prognostic Impact and Their Correlations with Tumor Molecular Markers. PLOS ONE 10, e0134965. https://doi.org/10.1371/journal.pone.0134965

Krafft, E., Laurila, H.P., Peters, I.R., Bureau, F., Peeters, D., Day, M.J., Rajamäki, M.M., Clercx, C., 2013. Analysis of gene expression in canine idiopathic pulmonary fibrosis. Vet. J. Lond. Engl. 1997 198, 479–486. https://doi.org/10.1016/j.tvjl.2013.08.018

Laurila, H.P., Rajamäki, M.M., 2020. Update on Canine Idiopathic Pulmonary Fibrosis in West Highland White Terriers. Vet. Clin. North Am. Small Anim. Pract., Canine and Feline Respiratory Medicine: An Update 50, 431–446. https://doi.org/10.1016/j.cvsm.2019.11.004

Lavis, P., Pingitore, J., Doumont, G., Garabet, A., Van Simaeys, G., Lacroix, S., Passon, N., Van Heymbeek, C., De Maeseneire, C., Allard, J., Collin, A., Huaux, F., Decaestecker, C., Salmon, I., Goldman, S., Cardozo, A.K., Bondue, B., 2023. Usefulness of FAPα assessment in bronchoalveolar lavage as a marker of fibrogenesis: results of a preclinical study and first report in patients with idiopathic pulmonary fibrosis. Respir. Res. 24, 254. https://doi.org/10.1186/s12931-023-02556-6

Lee, B.M., Clarke, D., Watson, M., Laver, T., 2020. Retrospective evaluation of a modified human lung cancer stage classification in dogs with surgically excised primary pulmonary carcinomas. Vet. Comp. Oncol. 18, 590–598. https://doi.org/10.1111/vco.12582

Lee, I.K., Noguera-Ortega, E., Xiao, Z., Todd, L., Scholler, J., Song, D., Liousia, M., Lohith, K., Xu, K., Edwards, K.J., Farwell, M.D., June, C.H., Albelda, S.M., Puré, E., Sellmyer, M.A., 2022. Monitoring Therapeutic Response to Anti-FAP CAR T Cells Using [18F]AlF-FAPI-74. Clin. Cancer Res. Off. J. Am. Assoc. Cancer Res. 28, 5330–5342. https://doi.org/10.1158/1078-0432.CCR-22-1379

Lee, K.N., Jackson, K.W., Christiansen, V.J., Chung, K.H., McKee, P.A., 2004. A novel plasma proteinase potentiates α2-antiplasmin inhibition of fibrin digestion. Blood 103, 3783–3788. https://doi.org/10.1182/blood-2003-12-4240

Lee, K.N., Jackson, K.W., Christiansen, V.J., Lee, C.S., Chun, J.-G., McKee, P.A., 2006. Antiplasmin-cleaving enzyme is a soluble form of fibroblast activation protein. Blood 107, 1397–1404. https://doi.org/10.1182/blood-2005-08-3452

Levy, M., McCaughan, G., Marinos, G., Gorrell, M., 2002. Intrahepatic expression of the hepatic stellate cell marker fibroblast activation protein correlates with the degree of fibrosis in hepatitis C virus infection. Liver 22, 93–101. https://doi.org/10.1034/j.1600-0676.2002.01503.x

Li, L., Gao, J., Chen, B.-X., Liu, X., Shi, L., Wang, Yanjiang, Wang, L., Wang, Yidan, Su, P., Yang, M.-F., Xie, B., 2023. Fibroblast activation protein imaging in atrial fibrillation: a proof-of-concept study. J. Nucl. Cardiol. 30, 2712–2720. https://doi.org/10.1007/s12350-023-03352-x

Liao, Y., Ni, Y., He, R., Liu, W., Du, J., 2013. Clinical implications of fibroblast activation protein-α in non-small cell lung cancer after curative resection: a new predictor for prognosis. J. Cancer Res. Clin. Oncol. 139, 1523–1528. https://doi.org/10.1007/s00432-013-1471-8

Liao, Y., Xing, S., Xu, B., Liu, W., Zhang, G., 2017. Evaluation of the circulating level of fibroblast activation protein α for diagnosis of esophageal squamous cell carcinoma. Oncotarget 8, 30050–30062. https://doi.org/10.18632/oncotarget.16274

McPhetridge, J.B., Scharf, V.F., Regier, P.J., Toth, D., Lorange, M., Tremolada, G., Dornbusch, J.A., Selmic, L.E., Bae, S., Townsend, K.L., McAdoo, J.C., Thieman, K.M., Solari, F., Walton, R.A., Romeiser, J., Tuohy, J.L., Oblak, M.L., 2021. Distribution of histopathologic types of primary pulmonary neoplasia in dogs and outcome of affected dogs: 340 cases (2010-2019). J. Am. Vet. Med. Assoc. 260, 234–243. https://doi.org/10.2460/javma.20.12.0698

Milner, J.M., Kevorkian, L., Young, D.A., Jones, D., Wait, R., Donell, S.T., Barksby, E., Patterson, A.M., Middleton, J., Cravatt, B.F., Clark, I.M., Rowan, A.D., Cawston, T.E., 2006. Fibroblast activation protein alpha is expressed by chondrocytes following a pro-inflammatory stimulus and is elevated in osteoarthritis. Arthritis Res. Ther. 8, R23. https://doi.org/10.1186/ar1877

Mori, Y., Kramer, V., Novruzov, E., Mamlins, E., Röhrich, M., Fernández, R., Amaral, H., Soza-Ried, C., Monje, B., Sabbagh, E., Florenzano, M., Giesel, F.L., Undurraga, Á., 2023. Initial results with [18F]FAPI-74 PET/CT in idiopathic pulmonary fibrosis. Eur. J. Nucl. Med. Mol. Imaging. https://doi.org/10.1007/s00259-023-06564-y

Nakamoto, Y., Baba, S., Kaida, H., Manabe, O., Uehara, T., 2024. Recent topics in fibroblast activation protein inhibitor-PET/CT: clinical and pharmacological aspects. Ann. Nucl. Med. 38, 10–19. https://doi.org/10.1007/s12149-023-01873-6

Raghu, G., Remy-Jardin, M., Richeldi, L., Thomson, C.C., Inoue, Y., Johkoh, T., Kreuter, M., Lynch, D.A., Maher, T.M., Martinez, F.J., Molina-Molina, M., Myers, J.L., Nicholson, A.G., Ryerson, C.J., Strek, M.E., Troy, L.K., Wijsenbeek, M., Mammen, M.J., Hossain, T., Bissell, B.D., Herman, D.D., Hon, S.M., Kheir, F., Khor, Y.H., Macrea, M., Antoniou, K.M., Bouros, D., Buendia-Roldan, I., Caro, F., Crestani, B., Ho, L., Morisset, J., Olson, A.L., Podolanczuk, A., Poletti, V., Selman, M., Ewing, T., Jones, S., Knight, S.L., Ghazipura, M., Wilson, K.C., 2022. Idiopathic Pulmonary Fibrosis (an Update) and Progressive Pulmonary Fibrosis in Adults: An Official ATS/ERS/JRS/ALAT Clinical Practice Guideline. Am. J. Respir. Crit. Care Med. 205, e18–e47. https://doi.org/10.1164/rccm.202202-0399ST

Roberts, E.W., Deonarine, A., Jones, J.O., Denton, A.E., Feig, C., Lyons, S.K., Espeli, M., Kraman, M., McKenna, B., Wells, R.J.B., Zhao, Q., Caballero, O.L., Larder, R., Coll, A.P., O'Rahilly, S., Brindle, K.M., Teichmann, S.A., Tuveson, D.A., Fearon, D.T., 2013. Depletion of stromal cells expressing fibroblast activation protein-α from skeletal muscle and bone marrow results in cachexia and anemia. J. Exp. Med. 210, 1137–1151. https://doi.org/10.1084/jem.20122344

Röhrich, M., Leitz, D., Glatting, F.M., Wefers, A.K., Weinheimer, O., Flechsig, P., Kahn, N., Mall, M.A., Giesel, F.L., Kratochwil, C., Huber, P.E., Deimling, A. von, Heußel, C.P., Kauczor, H.U., Kreuter, M., Haberkorn, U., 2022. Fibroblast Activation Protein-Specific PET/CT Imaging in Fibrotic Interstitial Lung Diseases and Lung Cancer: A Translational Exploratory Study. J. Nucl. Med. Off. Publ. Soc. Nucl. Med. 63, 127–133. https://doi.org/10.2967/jnumed.121.261925

Rosenkrans, Z.T., Massey, C.F., Bernau, K., Ferreira, C.A., Jeffery, J.J., Schulte, J.J., Moore, M., Valla, F., Batterton, J.M., Drake, C.R., McMillan, A.B., Sandbo, N., Pirasteh, A., Hernandez, R., 2022. [68 Ga]Ga-FAPI-46 PET for non-invasive detection of pulmonary fibrosis disease activity. Eur. J. Nucl. Med. Mol. Imaging 49, 3705–3716. https://doi.org/10.1007/s00259-022-05814-9

Rovedatti, L., Di Sabatino, A., Knowles, C.H., Sengupta, N., Biancheri, P., Corazza, G.R., MacDonald, T.T., 2011. Fibroblast activation protein expression in Crohn's disease strictures. Inflamm. Bowel Dis. 17, 1251–1253. https://doi.org/10.1002/ibd.21446

Shi, J., Hou, Z., Yan, J., Qiu, W., Liang, L., Meng, M., Li, L., Wang, X., Xie, Y., Jiang, L., Wang, W., 2020. The prognostic significance of fibroblast activation protein-α in human lung adenocarcinoma. Ann. Transl. Med. 8, 224–224. https://doi.org/10.21037/atm.2020.01.82

Solano-Iturri, J.D., Beitia, M., Errarte, P., Calvete-Candenas, J., Etxezarraga, M.C., Loizate, A., Echevarria, E., Badiola, I., Larrinaga, G., 2020a. Altered expression of fibroblast activation protein-α (FAP) in colorectal adenoma-carcinoma sequence and in lymph node and liver metastases. Aging 12, 10337–10358. https://doi.org/10.18632/aging.103261

Solano-Iturri, J.D., Errarte, P., Etxezarraga, M.C., Echevarria, E., Angulo, J., López, J.I., Larrinaga, G., 2020b. Altered Tissue and Plasma Levels of Fibroblast Activation Protein-α (FAP) in Renal Tumours. Cancers 12, E3393. https://doi.org/10.3390/cancers12113393

Syrjä, P., Heikkilä, H.P., Lilja-Maula, L., Krafft, E., Clercx, C., Day, M.J., Rönty, M., Myllärniemi, M., Rajamäki, M.M., 2013. The Histopathology of Idiopathic Pulmonary Fibrosis in West Highland White Terriers Shares Features of Both Non-specific Interstitial Pneumonia and Usual Interstitial Pneumonia in Man. J. Comp. Pathol. 149, 303–313. https://doi.org/10.1016/j.jcpa.2013.03.006

Testa, L.C., Jule, Y., Lundh, L., Bertotti, K., Merideth, M.A., O'Brien, K.J., Nathan, S.D., Venuto, D.C., El-Chemaly, S., Malicdan, M.C.V., Gochuico, B.R., 2021. Automated Digital Quantification of Pulmonary Fibrosis in Human Histopathology Specimens. Front. Med. 8, 607720. https://doi.org/10.3389/fmed.2021.607720

Tillmanns, J., Hoffmann, D., Habbaba, Y., Schmitto, J.D., Sedding, D., Fraccarollo, D., Galuppo, P., Bauersachs, J., 2015. Fibroblast activation protein alpha expression identifies activated fibroblasts after myocardial infarction. J. Mol. Cell. Cardiol. 87, 194–203. https://doi.org/10.1016/j.yjmcc.2015.08.016

Tillmanns, J., Widera, C., Habbaba, Y., Galuppo, P., Kempf, T., Wollert, K.C., Bauersachs, J., 2013. Circulating concentrations of fibroblast activation protein α in apparently healthy individuals and patients with acute coronary syndrome as assessed by sandwich ELISA. Int. J. Cardiol. 168, 3926–3931. https://doi.org/10.1016/j.ijcard.2013.06.061

Uitte De Willige, S., Keane, F.M., Bowen, D.G., Malfliet, J.J.M.C., Zhang, H.E., Maneck, B., McCaughan, G.W., Leebeek, F.W.G., Rijken, D.C., Gorrell, M.D., 2017. Circulating fibroblast activation protein activity and antigen levels correlate strongly when measured in liver disease and coronary heart disease. PLOS ONE 12, e0178987. https://doi.org/10.1371/journal.pone.0178987

Vanneste, D., Bai, Q., Hasan, S., Peng, W., Pirottin, D., Schyns, J., Maréchal, P., Ruscitti, C., Meunier, M., Liu, Z., Legrand, C., Fievez, L., Ginhoux, F., Radermecker, C., Bureau, F., Marichal, T., 2023. MafB-restricted local monocyte proliferation precedes lung interstitial macrophage differentiation. Nat. Immunol. 24, 827–840. https://doi.org/10.1038/s41590-023-01468-3

Williams, K.H., Viera de Ribeiro, A.J., Prakoso, E., Veillard, A.S., Shackel, N.A., Bu, Y., Brooks, B., Cavanagh, E., Raleigh, J., McLennan, S.V., McCaughan, G.W., Bachovchin, W.W., Keane, F.M., Zekry, A., Twigg, S.M., Gorrell, M.D., 2015. Lower serum fibroblast activation protein shows promise in the exclusion of clinically significant liver fibrosis due to non-alcoholic fatty liver disease in diabetes and obesity. Diabetes Res. Clin. Pract. 108, 466–472. https://doi.org/10.1016/j.diabres.2015.02.024

Yang, P., Luo, Q., Wang, X., Fang, Q., Fu, Z., Li, Jia, Lai, Y., Chen, X., Xu, X., Peng, X., Hu, K., Nie, X., Liu, S., Zhang, J., Li, Junqi, Shen, C., Gu, Y., Liu, J., Chen, J., Zhong, N., Su, J., 2023. Comprehensive Analysis of Fibroblast Activation Protein Expression in Interstitial Lung Diseases. Am. J. Respir. Crit. Care Med. 207, 160–172. https://doi.org/10.1164/rccm.202110-2414OC

Supplemental material

The Supplementary material for this article can be found online at:

https://www.frontiersin.org/articles/10.3389/fvets.2024.1416124/full#supplementary-material

Experimental section

Study 5:

Evaluation of [^{18}F]FAPI-74 PET/CT in healthy dogs and in West Highland white terriers with canine idiopathic pulmonary fibrosis: a pilot study

Preamble

Diagnosing and predicting the progression of CIPF remains a clinical challenge. In the previous study, FAP has emerged as a cellular marker of active fibrosis in post-mortem lung tissue of CIPF-affected dogs. In human medicine, PET/CT using FAP inhibitors (FAPI) is emerging as a tool to assess fibrotic activity in interstitial lung diseases such as IPF, offering a promising approach for monitoring disease progression and treatment response. So far, FAP expression was never investigated in canine lungs in vivo.

This exploratory pilot study aimed to evaluate whether [^{18}F]FAPI-74 PET/CT could safely and effectively detect FAP expression in the lungs of CIPF-affected WHWTs. The study involved two healthy senior Beagles and two client-owned WHWTs diagnosed with CIPF. All dogs underwent [^{18}F]FAPI-74 PET/CT imaging, including dynamic thoracic and static abdominal scans, to assess tracer uptake in the lungs and analyze biodistribution patterns.

The findings demonstrated that [^{18}F]FAPI-74 PET/CT imaging was both feasible and safe in all subjects. Significantly increased [^{18}F]FAPI-74 uptake was observed in the lungs of CIPF-affected WHWTs compared to healthy controls, indicating active fibrotic processes. Additionally, the tracer showed urinary and hepatobiliary elimination, with moderate uptake in the gastrointestinal tract.

These results suggest that [^{18}F]FAPI-74 PET/CT provides a valuable, noninvasive method for detecting active pulmonary fibrosis in vivo. This imaging modality holds promise as a clinical tool for early diagnosis, monitoring disease progression, and evaluating therapeutic interventions in dogs with CIPF, potentially improving management of this devastating condition.

Experimental section

Study 5:

Evaluation of [^{18}F]FAPI-74 PET/CT in healthy dogs and in West Highland white terriers with canine idiopathic pulmonary fibrosis: a pilot study

Submitted

Elodie Rizzoli, Mohamed Ali Bahri, Sylvestre Dammicco, Christian Degueldre, Alexandru Tutunaru, Mutien-Marie Garigliany, Mazarine Gérardy, Géraldine Bolen, Nadia Withofs, Thibault Gendron, Cécile Clercx

Abstract

Background – Canine idiopathic pulmonary fibrosis (CIPF) is a fatal disease affecting primarily dogs from the West Highland white terrier (WHWT) breed. CIPF remains challenging to diagnose and to treat and disease progression is difficult to predict. Recently, fibroblast activation protein (FAP) was identified as a cellular marker of active fibrosis in CIPF-affected post-mortem lung biopsies. Therefore, FAP-targeted imaging using FAP inhibitors (FAPI) may be useful for noninvasive assessment of active fibrosis in canine lungs in vivo.

Hypothesis/Objectives – This study aimed to assess whether [^{18}F]FAPI-74 positron emission tomography combined with computed tomography (PET/CT) would allow to safely detect FAP expression in the lungs of CIPF-affected WHWTs.

Animals – This prospective exploratory pilot study included two healthy senior purpose-bred Beagle dogs and two client-owned WHWTs diagnosed with CIPF.

Methods – [^{18}F]FAPI-74 PET/CT was performed in all dogs. Dynamic thoracic and static abdominal PET images were acquired to measure [^{18}F]FAPI-74 lung uptake and collect biodistribution data.

Results – [^{18}F]FAPI-74 PET/CT was feasible and safe in dogs. [^{18}F]FAPI-74 uptake was markedly increased in CIPF-affected lungs compared with healthy lungs. Urinary and hepatobiliary elimination of [^{18}F]FAPI-74 was observed, along with moderate uptake in gastrointestinal organs.

Conclusions and clinical importance – [^{18}F]FAPI-74 PET combined with CT enables in vivo detection of active fibrosis and represents a promising noninvasive tool for detecting and monitoring CIPF, providing new opportunities to evaluate therapeutic strategies for this fatal canine disease.

Introduction

Canine idiopathic pulmonary fibrosis (CIPF) is an interstitial lung disease of unknown etiology that particularly affects senior West Highland White Terriers (WHWTs) (Clercx et al., 2018; Laurila and Rajamäki, 2020a). It leads to progressive respiratory failure, ultimately resulting in death or euthanasia (Heikkilä et al., 2011). Diagnosis is based on the exclusion of other diseases and typically involves a combination of tests, including a 6-minute walk test, arterial blood gas analysis, complete blood analysis, cardiac ultrasound, bronchoscopy with bronchoalveolar lavage, thoracic X-rays, and, most importantly, computed tomography (CT) of the thorax (Heikkilä et al., 2011; L. I. O. Lilja-Maula et al., 2014; Roels et al., 2017; Thierry et al., 2017). A definitive diagnosis requires histopathological examination, which is most often conducted post-mortem (Heikkilä et al., 2011; Syrjä et al., 2013). Given the absence of curative treatment, the prognosis for CIPF remains poor, with median survival times between 7 and 11 months from diagnosis (Corcoran et al., 1999a; L. I. O. Lilja-Maula et al., 2014; Thierry et al., 2017). The variability in disease progression among individuals and the lack of prognostic biomarker make it challenging to predict disease progression (Clercx et al., 2018; Laurila and Rajamäki, 2020a).

Humans can also develop fibrotic interstitial lung diseases of unknown causes, the most frequent being idiopathic pulmonary fibrosis (IPF) (Raghu et al., 2022a). IPF primarily affects older adults, leads to respiratory insufficiency, and carries a poor prognosis (Raghu et al., 2022a). Recently, new techniques have been developed for the noninvasive assessment of fibrotic interstitial lung diseases by targeting in vivo fibroblast activation protein (FAP), a marker of activated fibroblasts (Acharya et al., 2006; P. Yang et al., 2023). FAP inhibitors (FAPI), radiolabeled with ^{68}Ga or ^{18}F, are used as radiotracers for positron emission tomography (PET), often combined with CT (PET/CT) (Röhrich et al., 2022; P. Yang et al., 2023; Mori et al., 2024; Hotta et al., 2024). FAP-targeted PET/CT imaging shows an elevated uptake in IPF, indicating active fibrogenesis, being correlated with CT findings and disease severity, and potentially predicting disease progression (Röhrich et al., 2022; P. Yang et al., 2023; Mori et al., 2024; Hotta et al., 2024).

As in humans, FAP-targeted PET/CT could constitute a new noninvasive diagnostic tool to detect activated fibroblasts in CIPF and potentially predict disease progression or evaluate response to therapy. FAP expression has recently been described in areas of active fibrosis in post-mortem lung biopsies from CIPF-affected dogs (Rizzoli et al., 2024), but has never been investigated in canine lungs in vivo. Furthermore, there is no available data on [^{18}F]FAPI-74 pharmacokinetics in dogs. In veterinary medicine, PET imaging is gaining popularity for clinical and research applications

(LeBlanc and Morandi, 2014; LeBlanc and Peremans, 2014; Randall, 2016). Despite limited PET(/CT) availability in veterinary settings, collaborations with human medical institutions enable imaging of veterinary patients (LeBlanc and Morandi, 2014). Combining the molecular insights of PET with the anatomical precision of CT makes PET/CT a powerful tool for diagnosis and staging (LeBlanc and Peremans, 2014; Randall, 2016; Maitz et al., 2022).

This study aimed to assess the safety and feasibility of [^{18}F]FAPI-74 PET in dogs, and to explore its ability to detect in vivo FAP expression in CIPF-affected versus healthy lungs, hypothesizing increased [^{18}F]FAPI-74 uptake in diseased lungs only.

Material and methods

1. Case selection

This prospective exploratory pilot study included two healthy senior purpose-bred Beagle dogs (Control1 and Control2) with no history of lung disease, no clinical sign, and normal physical examination including cardiorespiratory auscultation. In addition, two client-owned WHWTs previously diagnosed with CIPF (CIPF1 and CIPF2) were included, with owner's written informed consent. CIPF diagnosis was established prior to enrollment, based on a 6-minute walk test, hematology and serum biochemistry, arterial blood gas analysis, cardiac ultrasound, thoracic CT, and endoscopy with bronchoalveolar lavage (Clercx et al., 2018; Laurila and Rajamäki, 2020a).

2. [^{18}F]FAPI-74 production

[^{18}F]FAPI-74 radiotracer was synthesized on an AllInOne synthesizer using production cassette and reagent kit from TRASIS (Ans, Belgium). The precursor and ^{19}F reference were provided by SOFIE iTheranostics (Dulles, VA). The radioactivity of the [^{18}F]FAPI-74 solution was 5.1±0.5 GBq with a decay-corrected yield of 66 ± 7%. The molar activity of 94 ± 20 GBq/µmol was measured after radiosynthesis with a purity of 99.5 ± 0.1%. Final solution was diluted with saline to reach a volume of injection between 2 and 3 mL per dog.

3. [^{18}F]FAPI-74 positron emission tomography

Before PET imaging, the dogs were anesthetized, and a urinary catheter was placed to prevent radioactive contamination. The dogs were positioned in sternal recumbency for the imaging session. PET images were acquired using a Siemens/CTI (Knoxville, TN) ECAT EXACT HR+ scanner with a 15-cm field of view. A cold 10-min transmission scan with ^{68}Ge was performed before radiotracer injection.

The [^{18}F]FAPI-74 radiotracer was injected as an intravenous bolus via the saphenous vein. The median injected activity was 10.3 MBq/kg (8.1–20.6 MBq/kg). Dynamic PET acquisitions of the thorax were performed. The timeframes used were 6x10, 8x30, 5x120 and 15x300 seconds, a scanning time of 90 min. In Control2 and CIPF1, dynamic PET was followed by a static 5-min abdominal scan. Table 1 summarizes patient, injection and acquisition parameters. All PET images were reconstructed using filtered back projection including corrections for measured attenuation, dead time, random events, and scatter using standard software (ECAT 7.1, Siemens/CTI, Knoxville, TN).

Table 1. Patient, injection and acquisition parameters for [^{18}F]FAPI-74 PET

Case	Age, years	Breed	Gender	Weight, kg	Injected activity, MBq/kg	Scanned regions
Control 1	10	Beagle	Intact female	10.7	20.6	Thorax
Control 2	10	Beagle	Intact female	14.1	10.7	Thorax Abdomen
CIPF 1	14	WHWT	Intact male	9.3	9.9	Thorax Abdomen
CIPF 2	10	WHWT	Neutered female	10.0	8.1	Thorax

CIPF: canine idiopathic pulmonary fibrosis; WHWT: West Highland white terrier.

At the end of the procedure, the bladder was emptied, and the urinary catheter was removed once the dogs were awake. The dogs were cleared for the kennel or home when the radioactive dose rate, measured with a Geiger-Müller counter at a 1-meter distance, dropped below 20 µSv/h.

4. Computed tomography

In all dogs, non-enhanced CT was performed with a 64-multislice CT scanner (Somatom Confidence 64, Siemens, Germany). For Beagle dogs, the acquisition parameters were as follows: voltage 100 kV, reference current 212 mA modulated by automatic exposure control (Care Dose, Siemens), pitch 0.8, reconstructed with a 0.75-mm slice thickness. For WHWTs, the acquisition parameters were as follows: voltage 100 kV, reference current 170 mA modulated by automatic exposure control (Care Dose, Siemens), pitch 1.2, reconstructed with a 1-mm slice thickness. CT images were acquired under general anesthesia, except for one case (CIPF1), which was performed under sedation due to a prior CT examination under general anesthesia. In all cases performed under general anesthesia, images obtained during the expiratory pause were selected for analysis.

5. Image analysis

The PET images were co-registered with CT images and analyzed using PMOD software v4.0. The total volume of both lungs (TLV) was segmented semi-automatically based on CT images. Regions of interest (ROIs), represented by 12-mm diameter spheres, were drawn on PET images, under CT images guidance. ROIs were placed over nine standardized lung areas in both lungs: in the periphery of the right cranial lobe (A1) and cranial part of the left cranial lobe (B1); centrally, near the hilum, in the right middle lobe (A2) and in the caudal part of the left cranial lobe (B2); caudo-dorsally (A3 and B3) and ventro-laterally (A4 and B4) in the right and left caudal lobes; and in the periphery of the accessory lobe (A5). Additional ROIs were drawn on other identifiable anatomical structures within the field of view, including thoracic aorta, caudal vena cava, esophagus, right and left ventricles, 5th thoracic vertebra (T5), paravertebral muscle (lateral to T5), cranial and medial liver,

gallbladder, gastric wall and kidneys. Mean (SUV_{mean}) and maximal (SUV_{max}) standardized uptake values were measured for each ROI and TLV. Target-to-background ratios (TBR) were calculated by dividing SUV_{mean} of the ROI by SUV_{mean} of the paravertebral muscle, serving as background reference. Mean Hounsfield units (HU_{mean}) were measured on CT images for lung ROIs and TLV.

To calculate parameters that reflect the tracer distribution pattern, the following approach was adapted from a human patient study (P. Yang et al., 2023). The mediastinal blood pool activity, quantified by the SUV_{mean} of the aorta, was used as an absolute threshold for a threshold-based segmentation within the TLV, defining the total active volume (TAV) (P. Yang et al., 2023). To account for the significant size difference between dog breeds, TAV was expressed as a percentage of TLV (TAV%). Finally, TAV% was multiplied by the SUV_{mean} of TAV to obtain the SUV_{total} (P. Yang et al., 2023).

Due to the small pilot sample, group comparisons are reported descriptively using medians and ranges.

6. Immunohistochemistry

To investigate FAP expression in tissues showing unexpected [^{18}F]FAPI-74 uptake, full thickness gastric wall biopsies were collected post-mortem from the fundus, greater curvature, and antrum of dogs euthanized for unrelated medical reasons, with owner consent. Biopsies were formalin-fixed, paraffin-embedded, and routinely processed for histopathological evaluation using hematoxylin and eosin staining. Adjacent 5-µm sections were deparaffinized, and rehydrated, and subjected to antigen retrieval by Tris-EDTA (10mM Tris, 1mM EDTA, pH 8.5-9.0) incubation in microwave for 15 min at 600W. Endogenous peroxidase activity was blocked with 3% hydrogen peroxide incubation for 30 min. Nonspecific binding was blocked by incubation in blocking buffer (Vector Laboratories #SP-5035-100) for 30 min. Sections were incubated overnight at 4°C with rabbit anti-human FAP monoclonal antibody (Abcam #ab207178, 1:100) validated for dogs (Rizzoli et al., 2024). For specificity control, the primary antibody was substituted with isotype rabbit IgG antibody (Enzo #ENZ-ABS491-0200, 1:200). Sections were incubated with peroxidase-labeled polymer goat anti-rabbit antibody (Dako #K4003) for 30 min at room temperature, followed by AEC (ImmPACT #SK-4205) for 12 min and hematoxylin counterstaining. FAP expression was evaluated subjectively by two observers (including a diplomate of the European College of Veterinary Pathologists) and classified as negative or positive.

Results

1. Clinical data

Both Beagle dogs presented no clinical signs, had normal lung auscultation and showed no abnormalities on CT scans. Clinical parameters of CIPF cases are summarized in Table 2. One year after PET images acquisition, Control1 was euthanized for unrelated medical reasons, which allowed the collection of post-mortem lung biopsies to confirm the absence of lung disease. At the time of writing, other dogs were still alive.

Table 2. Summary of clinical parameters of CIPF cases at diagnosis

Case	Clinical signs	6MWD, m	paO_2, mmHg	Estimated systolic PAP, mmHg	Thoracic CT findings
CIPF 1	Chronic dry cough, dyspnea, syncope, inspiratory lung crackles	308.7	56.6	50	Diffuse ground glass opacities in a mosaic pattern
CIPF 2	Chronic dry cough, dyspnea, exercise intolerance, inspiratory lung crackles	434.7	61.4	47	Diffuse ground glass opacities in a mosaic pattern and parenchymal bands

Systolic PAP was estimated based on the pressure gradient derived from the tricuspid regurgitation velocity measured by cardiac ultrasound, which indicated a high probability of moderate pulmonary hypertension in both cases according to the ACVIM guidelines (Reinero et al., 2020). *CIPF: canine idiopathic pulmonary fibrosis; 6MWD: 6-minute walk distance; paO_2: partial pressures of oxygen in arterial blood; PAP: pulmonary arterial pressure.*

Following the injection of [^{18}F]FAPI-74, no drug-related adverse event was observed. One hour after the injection, the urine collected from Control1 contained 28 MBq of [^{18}F] activity, corresponding to 20% of the injected activity (decay corrected). Control1 remained above the 20 µSv/h dose-rate threshold for 2.5 hours after receiving 220.9 MBq of [^{18}F]FAPI-74. In contrast, Control2, which received 150.4 MBq, fell below 20 µSv/h by the end of the dynamic acquisition and was allowed to return to the kennel immediately upon waking. One hour post-injection of 92 and 81 MBq, respectively, both WHWTs had radioactive dose rates below 20 µSv/h and therefore did not require restricted-area confinement.

2. [^{18}F]FAPI-74 uptake

Figure 1 illustrates the dynamic evolution of lung [^{18}F]FAPI-74 uptake, quantified by SUV_{mean} and TBR, for TLV in all dogs, as well as for standardized lung ROIs in CIPF dogs. Based on this preliminary study, a 60-min uptake time, shown to be optimal for FAP-targeted PET scans in human

patients with IPF (Röhrich et al., 2022; P. Yang et al., 2023; Mori et al., 2024; Hotta et al., 2024), also appears suitable for dogs. This time-point allows for sufficient background signal reduction while preserving adequate uptake. Additionally, a 60-min uptake time is practical for clinical use. In all CIPF lung ROIs, [^{18}F]FAPI-74 uptake was higher than background activity (paravertebral muscle).

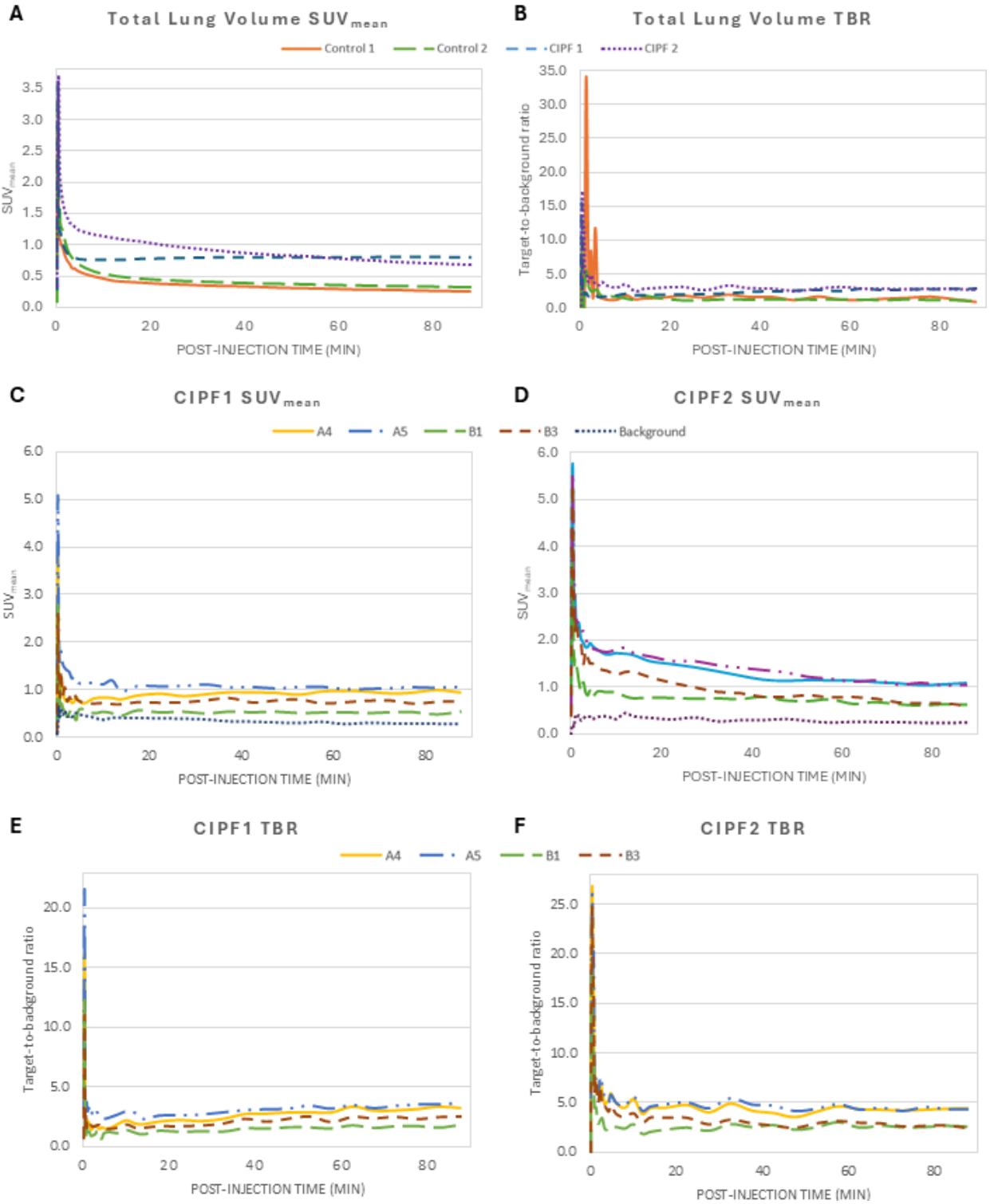

Figure 1. [^{18}F]FAPI-74 lung uptake curves over the dynamic phase of the study (90 min). Evolution of (A) SUV_{mean} and (B) target-to-background ratio (TBR) of total lung volume for the four dogs; evolution of SUV_{mean} (C-D) and TBR (E-F) at standardized lungs areas (A4, A5, B1, B3) within both lungs in CIPF1 and CIPF2. The selected standardized lung areas exhibited the most distinct curves and were located: in the latero-ventral region of the right caudal lobes (A4); in the periphery of the accessory lobe (A5); in the periphery of the cranial part of the

cranial left lobe (B1); in the dorso-caudal region of the left caudal lobe (B3). SUV: standardized uptake values; TBR: target-to-background ratio; CIPF: canine idiopathic pulmonary fibrosis.

Representative images of lung [^{18}F]FAPI-74 uptake 60 min post-injection are shown in Figure 2. All uptake parameters, as well as attenuation values, were higher in CIPF-affected WHWTs compared with control dogs (Table 3).

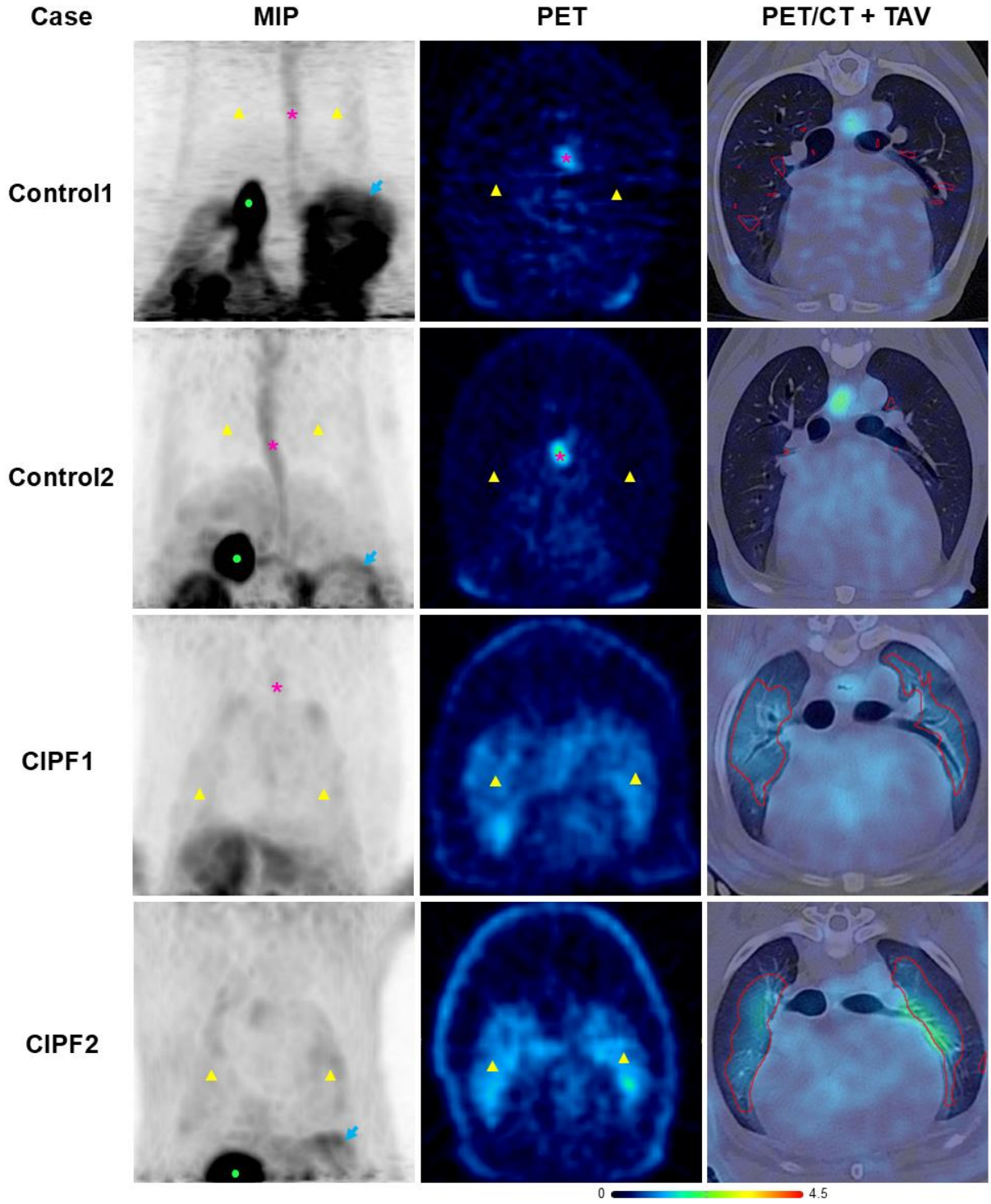

Figure 2. [^{18}F]FAPI-74 lung uptake in healthy dogs (Control1 and Control2) and in CIPF-affected WHWTs (CIPF1 and CIPF2) 60 min after injection. From left to right, the uptake is represented by maximum intensity projection

(MIP) images in dorsal plane, PET images in transverse plane at the level of the 7th thoracic vertebra, PET and CT (pulmonary window) fusion images in transverse plane at the level of the 5th thoracic vertebra, with delineation of the total active volume (red line). MIP images display the highest-intensity signals along each line of sight through the body, providing a 3D-like overview that highlights areas of high tracer uptake. PET images are corrected for attenuation and displayed at a SUV scale of 0-4.5. Yellow triangle: lung; pink star: esophagus; green dot: gallbladder. Of note, Control1 was positioned too cranially, thus a large portion of the cranial abdomen is in the field of view. PET: positron emission tomography; CT: computed tomography.

Table 3. [18F]FAPI-74 lung uptake data 60 min after injection, in control and in CIPF-affected dogs.

	Control dogs (n=2)	CIPF-affected WHWTs (n=2)
Region of interest (ROI) "A4"		
SUV_{mean}	0.3 (0.3 for both)	1.1 (1.0-1.1)
SUV_{max}	0.5 (0.4-0.6)	1.4 (1.1-1.6)
Target-to-background ratio	1.2 (1.1-1.3)	3.8 (3.4-4.3)
Mean attenuation, HU	-754 (-804 to -704)	-591 (-629 to -553)
Total lung volume (TLV), mL	424 (263-585)	223 (202-244)
SUV_{mean}	0.3 (0.3-0.4)	0.8 (0.8 for both)
SUV_{max}	2.2 (1.6-2.8)	2.3 (1.8-2.9)
Target-to-background ratio	0.8 (0.4-1.2)	2.8 (2.8-2.9)
Mean attenuation, HU	-772 (-789 to -756)	-600 (-632 to -568)
Total active volume (TAV), mL	36 (31-41)	110 (88-132)
TAV%	9.4 (7.0-11.9)	48.6 (43.2-54.0)
SUV_{mean}	0.7 (0.5-0.9)	1.0 (1.0 for both)
SUV_{total}	6.2 (6.0-6.4)	48.7 (42.3-55.1)
Mean attenuation, HU	-773 (-773 to -772)	-564 (-604 to -523)

Data are expressed as medians and ranges. In this table, [18F]FAPI-74 lung uptake was illustrated in TLV, TAV and one ROI (A4), positioned ventrolaterally to the right caudal lung lobe in each dog. This ROI was selected due to its sufficient distance from adjacent organs, such as the liver, that could artifactually elevate lung uptake values, particularly SUV_{max} in TLV. Target-to-background ratio was calculated by dividing the SUV_{mean} of TLV by the SUV_{mean} of the paravertebral muscle. TAV% was calculated as the TAV divided by the TLV, expressed as a percentage. SUV_{total} is the multiplication of TAV% by the SUV_{mean} of TAV. CIPF: canine idiopathic pulmonary fibrosis; WHWTs: West Highland white terriers.

In all dogs, the cranial abdomen appeared on thoracic PET images and in one dog per group, abdominal PET images were acquired 90 minutes post-injection. In all dogs, urinary and hepato-biliary elimination of [18F]FAPI-74 were observed, as evidenced by high activity in the urinary bladder (SUV_{mean} 29.6 in CIPF1), the kidneys (SUV_{mean} 6.6 [4.5-6.9] in the right kidney) and the gallbladder (SUV_{mean} 12.0 [11.6-23.6]), along with moderate activity in the liver (SUV_{mean} 1.2 [0.7-2.1]). Unexpectedly, moderate uptake was also detected in the gastrointestinal tract of all dogs,

particularly in the gastric wall (SUV_{mean} 2.3 [0.7-3.1]), the intestines (SUV_{mean} 3.0 [2.9-3.0] in Control2 and CIPF1) and the esophagus (SUV_{mean} 1.1 [0.7-2.1]). The uptake in abdominal organs of CIPF1 is illustrated in Figure 3.

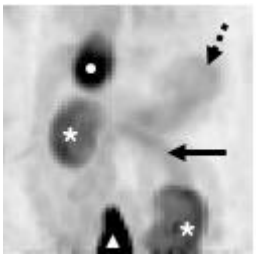

Figure 3. Maximum intensity projection image of the abdominal [^{18}F]FAPI-74 uptake in CIPF1 90 min after injection. Stars: kidneys; triangle: urinary bladder; dot: gallbladder; dotted arrow: stomach; full arrow: intestines.

3. Anti-FAP immunohistochemistry

Table 4 summarizes the clinical and histopathological characteristics of cases assessed for FAP expression via immunohistochemistry on gastric wall biopsies. FAP was expressed by fibroblasts from the lamina propria and muscularis mucosae in dogs with various levels of chronic gastritis, even in the absence of gastrointestinal clinical signs (Figure 4).

Table 4. Summary of cases used for FAP immunohistochemistry on gastric wall biopsies

Case	Age, years	Breed	Gastrointestinal signs	Cause of euthanasia	Histopathological diagnosis	FAP expression
1	12	Hovawart	None	Aspiration pneumonia	Normal	-
2	10	Maltese	None	Mammary cancer	Mild gastric fibrosis	+
3	16	Beagle	None	Severely impaired locomotion	Mild gastric fibrosis	+
4	11	Beagle	Vomiting, melena	Terminal CKD	Chronic lymphoplasmacytic gastritis with severe fibrosis	+
5	14	WHWT	Vomiting	Terminal CKD	Severe gastric fibrosis	+
6	11	Beagle	None	Ulcerated mammary tumor	Severe gastric fibrosis	+

+: positive; -: negative. CKD: chronic kidney disease; FAP: fibroblast activation protein. Case 6 corresponds to Control1, which died a year after the PET study, which allowed post-mortem biopsy collection.

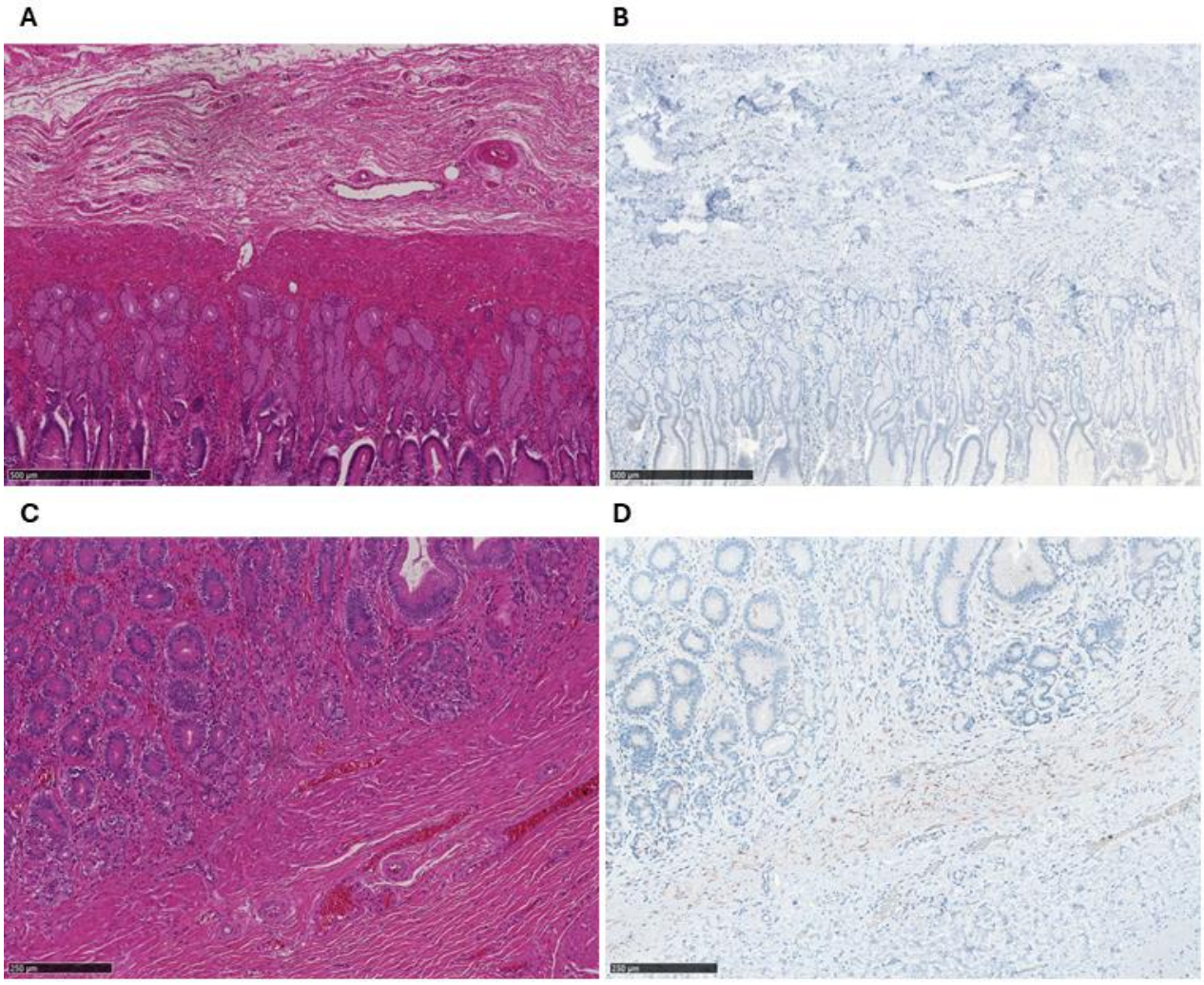

Figure 4. Panel illustrating FAP expression in canine gastric wall biopsies. Healthy gastric wall in hematoxylin and eosin staining (A) with no FAP expression (B). Gastric wall with gastric fibrosis in hematoxylin and eosin staining (C) with FAP expression (in red staining) in the muscularis mucosae (D).

Discussion

[^{18}F]FAPI-74 PET is a safe and feasible technique in dogs. Importantly, after dose adjustment, no confinement was necessary beyond the 60-min uptake time, which appears as an optimal acquisition time-point. [^{18}F]FAPI-74 uptake was markedly increased in CIPF-affected lungs, compared with healthy lungs. Urinary and hepatobiliary elimination of [^{18}F]FAPI-74 was observed, creating a physiological activity in the gallbladder, liver, kidneys and urinary bladder. Additionally, all dogs showed variable moderate uptake in gastrointestinal organs, likely associated with fibrosis based on immunostaining findings.

A marked [^{18}F]FAPI-74 uptake was observed in the lungs of CIPF-affected dogs compared with controls, as seen in human IPF (Röhrich et al., 2022; P. Yang et al., 2023; Mori et al., 2024; Hotta et al., 2024). These findings support the potential of FAP-targeted PET/CT imaging as a noninvasive method to evaluate the abundance and distribution of activated fibroblasts in vivo in dogs, and to potentially aid in predicting disease progression (Röhrich et al., 2022; P. Yang et al., 2023; Mori et al., 2024). It could help diagnose early CIPF cases for which the distinction between inactive and active, progressive fibrosis is challenging. Some experimental studies have found that FAP expression is induced in the early phase of lung fibroblast activation rather than in the late phase of lung fibrosis (P. Yang et al., 2023). [^{18}F]FAPI-74 PET imaging could help in the selection and enrolment of CIPF-affected dogs at an early stage in clinical trials evaluating response to therapy by assessing fibrotic activity (Röhrich et al., 2022). There was no FAPI uptake [^{18}F]FAPI-74 in lungs from control dogs. The low spatial resolution of PET and the impact of respiratory motion tend to artificially elevate the SUV in pulmonary areas adjacent to the diaphragm, thereby leading to an overestimation of SUV, particularly the SUV_{max}, across the total lung volume.

Urinary elimination appeared to be the main route of excretion of [^{18}F]FAPI-74 in dogs, similar to what has been observed in humans (Giesel et al., 2021; Röhrich et al., 2022; P. Yang et al., 2023; Mori et al., 2024). Hepatobiliary elimination of FAPI, although less commonly reported, has been previously reported and is believed to be due to the lipophilicity of the NOTA chelator used for chelation of [^{18}F]AlF (Giesel et al., 2021; Mu et al., 2023; Xu et al., 2024). Unexpectedly, mild to moderate [^{18}F]FAPI-74 uptake was observed in gastrointestinal organs. In a previous [^{18}F]FAPI PET/CT study, esophageal uptake could be seen in at least one control Beagle dog although it was not discussed in the text (Li et al., 2023). Specific gastrointestinal uptake has not been described in [^{18}F]FAPI-74 studies in humans, although intestinal retention is sometimes described (Mu et al., 2023). The suspicion of specific [^{18}F]FAPI-74 uptake was supported by the detection of FAP expression

by immunohistochemistry in a small number of gastric walls presenting a degree of fibrosis, even in dogs without gastrointestinal clinical signs.

This study has limitations. First, due to its exploratory nature, only four dogs were included. Two Beagle dogs were necessary to refine the imaging procedure and adjust the injected dose before testing it in two privately-owned CIPF-affected WHWTs. While this small sample size was sufficient to assess feasibility and demonstrate the potential of this tool to detect active fibrosis in vivo, a larger study, with standardized injected doses, is needed to investigate correlations with disease progression or severity. Another limitation is the 15-cm field of view of the PET scanner used for this study, which restricts imaging in large dogs unless static images are acquired at multiple bed positions. Additionally, the use of a hybrid PET/CT scanner instead of stand-alone PET would improve co-registration of PET and CT images, while also reducing anesthesia duration (LeBlanc and Morandi, 2014).

In conclusion, this study demonstrates that [^{18}F]FAPI-74 uptake is observed in the lungs of CIPF-affected dogs, allowing the detection of active fibrosis in vivo. This finding supports the potential of [^{18}F]FAPI-74 PET/CT as a promising noninvasive tool for diagnosing and monitoring this fatal canine disease.

Acknowledgments

This study was funded by the Special Research Funds of the Faculty of Veterinary Medicine from the University of Liège and Elodie Rizzoli is a research fellow of the fonds National de la Recherche Scientifique – FNRS. The authors gratefully thank Laurie Van Bossuyt, for the technical management of the CT scans; Anne-Christine Merveille and Margaux Legrand for the cardiac ultrasound for CIPF diagnostic work-up; Gaëlle Schils, for her technical assistance for the PET scans.

SOFIE (iTheranostics) graciously provided [^{18}F]FAPI-74 but were not involved in the study design, collection, analysis, interpretation of data and the writing of this article.

This study was approved by the animal ethics committee of the University of Liège (approval number 22-2473).

References

Acharya, P.S., Zukas, A., Chandan, V., Katzenstein, A.-L.A., Puré, E., 2006. Fibroblast activation protein: a serine protease expressed at the remodeling interface in idiopathic pulmonary fibrosis. Hum Pathol 37, 352–360. https://doi.org/10.1016/j.humpath.2005.11.020

Clercx, C., Fastrès, A., Roels, E., 2018. Idiopathic pulmonary fibrosis in West Highland white terriers: An update. The Veterinary Journal 242, 53–58. https://doi.org/10.1016/j.tvjl.2018.10.007

Corcoran, B.M., Cobb, M., Martin, M.W., Dukes-McEwan, J., French, A., Fuentes, V.L., Boswood, A., Rhind, S., 1999. Chronic pulmonary disease in West Highland white terriers. Vet Rec 144, 611–616. https://doi.org/10.1136/vr.144.22.611

Giesel, F.L., Adeberg, S., Syed, M., Lindner, T., Jiménez-Franco, L.D., Mavriopoulou, E., Staudinger, F., Tonndorf-Martini, E., Regnery, S., Rieken, S., El Shafie, R., Röhrich, M., Flechsig, P., Kluge, A., Altmann, A., Debus, J., Haberkorn, U., Kratochwil, C., 2021. FAPI-74 PET/CT Using Either 18F-AlF or Cold-Kit 68Ga Labeling: Biodistribution, Radiation Dosimetry, and Tumor Delineation in Lung Cancer Patients. J Nucl Med 62, 201–207. https://doi.org/10.2967/jnumed.120.245084

Heikkilä, H. p., Lappalainen, A. k., Day, M. j., Clercx, C., Rajamäki, M. m., 2011. Clinical, Bronchoscopic, Histopathologic, Diagnostic Imaging, and Arterial Oxygenation Findings in West Highland White Terriers with Idiopathic Pulmonary Fibrosis. Journal of Veterinary Internal Medicine 25, 433–439. https://doi.org/10.1111/j.1939-1676.2011.0694.x

Hotta, M., Kim, G.H.J., Rerkpichaisuth, V., Teng, P.Y., Armstrong, W.R., Carlucci, G., Dahlbom, M., Abtin, F., Lari, S.M., Fishbein, G.A., Czernin, J., Volkmann, E.R., Weigt, S.S., Calais, J., 2024. Correlation of FAPI PET Uptake with Immunohistochemistry in Explanted Lungs from Patients with Advanced Interstitial Lung Disease. Journal of Nuclear Medicine. https://doi.org/10.2967/jnumed.124.268351

Laurila, H.P., Rajamäki, M.M., 2020. Update on Canine Idiopathic Pulmonary Fibrosis in West Highland White Terriers. Vet Clin North Am Small Anim Pract 50, 431–446. https://doi.org/10.1016/j.cvsm.2019.11.004

LeBlanc, A.K., Morandi, F., 2014. Invited review--Off-site PET imaging programs: challenges and opportunities. Vet Radiol Ultrasound 55, 109–112. https://doi.org/10.1111/vru.12103

LeBlanc, A.K., Peremans, K., 2014. PET and SPECT Imaging in Veterinary Medicine. Seminars in Nuclear Medicine, Veterinary Nuclear Medicine 44, 47–56. https://doi.org/10.1053/j.semnuclmed.2013.08.004

Li, L., Gao, J., Chen, B.-X., Liu, X., Shi, L., Wang, Yanjiang, Wang, L., Wang, Yidan, Su, P., Yang, M.-F., Xie, B., 2023. Fibroblast activation protein imaging in atrial fibrillation: a proof-of-concept study. Journal of Nuclear Cardiology 30, 2712–2720. https://doi.org/10.1007/s12350-023-03352-x

Lilja-Maula, L.I.O., Laurila, H.P., Syrjä, P., Lappalainen, A.K., Krafft, E., Clercx, C., Rajamäki, M.M., 2014. Long-term outcome and use of 6-minute walk test in West Highland White Terriers with idiopathic pulmonary fibrosis. J Vet Intern Med 28, 379–385. https://doi.org/10.1111/jvim.12281

Maitz, C.A., Tate, D., Bechtel, S., Lunceford, J., Henry, C., Flesner, B., Collins, A., Varterasian, M., Tung, D., Zhang, L., Saha, S., Bryan, J.N., 2022. Paired 18F-Fluorodeoxyglucose (18F-FDG), and 64Cu-Copper(II)-diacetyl-bis(N(4)-methylthiosemicarbazone) (64Cu-ATSM) PET Scans in Dogs with Spontaneous Tumors and Evaluation for Hypoxia-Directed Therapy. Radiat Res 197, 253–260. https://doi.org/10.1667/RADE-20-00186.1

Mori, Y., Kramer, V., Novruzov, E., Mamlins, E., Röhrich, M., Fernández, R., Amaral, H., Soza-Ried, C., Monje, B., Sabbagh, E., Florenzano, M., Giesel, F.L., Undurraga, Á., 2024. Initial results with [18F]FAPI-74 PET/CT in idiopathic pulmonary fibrosis. Eur J Nucl Med Mol Imaging 51, 1605–1611. https://doi.org/10.1007/s00259-023-06564-y

Mu, X., Mo, B., Qin, J., Li, Z., Chong, W., Zeng, Y., Lu, L., Zhang, L., Fu, W., 2023. Comparative analysis of two timepoints on [18F]FAPI-42 PET/CT in various cancers. Eur J Hybrid Imaging 7, 27. https://doi.org/10.1186/s41824-023-00186-1

Raghu, G., Remy-Jardin, M., Richeldi, L., Thomson, C.C., Inoue, Y., Johkoh, T., Kreuter, M., Lynch, D.A., Maher, T.M., Martinez, F.J., Molina-Molina, M., Myers, J.L., Nicholson, A.G., Ryerson, C.J., Strek, M.E., Troy, L.K., Wijsenbeek, M., Mammen, M.J., Hossain, T., Bissell, B.D., Herman, D.D., Hon, S.M., Kheir, F., Khor, Y.H., Macrea, M., Antoniou, K.M., Bouros, D., Buendia-Roldan, I., Caro, F., Crestani, B., Ho, L., Morisset, J., Olson, A.L., Podolanczuk, A., Poletti, V., Selman, M., Ewing, T., Jones, S., Knight, S.L., Ghazipura, M., Wilson, K.C., 2022. Idiopathic Pulmonary Fibrosis (an Update) and Progressive Pulmonary Fibrosis in Adults: An Official ATS/ERS/JRS/ALAT Clinical Practice Guideline. Am J Respir Crit Care Med 205, e18–e47. https://doi.org/10.1164/rccm.202202-0399ST

Randall, E.K., 2016. PET-Computed Tomography in Veterinary Medicine. Vet Clin North Am Small Anim Pract 46, 515–533, vi. https://doi.org/10.1016/j.cvsm.2015.12.008

Reinero, C., Visser, L.C., Kellihan, H.B., Masseau, I., Rozanski, E., Clercx, C., Williams, K., Abbott, J., Borgarelli, M., Scansen, B.A., 2020. ACVIM consensus statement guidelines for the diagnosis, classification, treatment, and monitoring of pulmonary hypertension in dogs. Journal of Veterinary Internal Medicine 34, 549–573. https://doi.org/10.1111/jvim.15725

Rizzoli, E., de Meeûs d'Argenteuil, C., Fastrès, A., Roels, E., Janssen, P., Puré, E., Garigliany, M.-M., Marichal, T., Clercx, C., 2024. Fibroblast activation protein is a cellular marker of fibrotic activity in canine idiopathic pulmonary fibrosis. Front Vet Sci 11, 1416124. https://doi.org/10.3389/fvets.2024.1416124

Roels, E., Couvreur, T., Farnir, F., Clercx, C., Verschakelen, J., Bolen, G., 2017. Comparison between sedation and general anesthesia for high resolution computed tomographic characterization of canine idiopathic pulmonary fibrosis in west highland white terriers. Veterinary Radiology and Ultrasound. https://doi.org/10.1111/vru.12481

Röhrich, M., Leitz, D., Glatting, F.M., Wefers, A.K., Weinheimer, O., Flechsig, P., Kahn, N., Mall, M.A., Giesel, F.L., Kratochwil, C., Huber, P.E., Deimling, A. von, Heußel, C.P., Kauczor, H.U., Kreuter, M., Haberkorn, U., 2022. Fibroblast Activation Protein-Specific PET/CT Imaging in Fibrotic Interstitial Lung Diseases and Lung Cancer: A Translational Exploratory Study. J Nucl Med 63, 127–133. https://doi.org/10.2967/jnumed.121.261925

Syrjä, P., Heikkilä, H.P., Lilja-Maula, L., Krafft, E., Clercx, C., Day, M.J., Rönty, M., Myllärniemi, M., Rajamäki, M.M., 2013. The Histopathology of Idiopathic Pulmonary Fibrosis in West Highland White Terriers Shares Features of Both Non-specific Interstitial Pneumonia and Usual Interstitial Pneumonia in Man. Journal of Comparative Pathology 149, 303–313. https://doi.org/10.1016/j.jcpa.2013.03.006

Thierry, F., Handel, I., Hammond, G., King, L.G., Corcoran, B.M., Schwarz, T., 2017. Further characterization of computed tomographic and clinical features for staging and prognosis of idiopathic pulmonary fibrosis in West Highland white terriers. Vet Radiol Ultrasound 58, 381–388. https://doi.org/10.1111/vru.12491

Xu, W., Cai, J., Peng, T., Meng, T., Pang, Y., Sun, L., Wu, H., Zhang, J., Chen, X., Chen, H., 2024. Fibroblast Activation Protein–Targeted PET/CT with 18F-Fibroblast Activation Protein Inhibitor-74 for Evaluation of Gastrointestinal Cancer: Comparison with 18F-FDG PET/CT. Journal of Nuclear Medicine 65, 40–51. https://doi.org/10.2967/jnumed.123.266329

Yang, P., Luo, Q., Wang, X., Fang, Q., Fu, Z., Li, Jia, Lai, Y., Chen, X., Xu, X., Peng, X., Hu, K., Nie, X., Liu, S., Zhang, J., Li, Junqi, Shen, C., Gu, Y., Liu, J., Chen, J., Zhong, N., Su, J., 2023. Comprehensive Analysis of Fibroblast Activation Protein Expression in Interstitial Lung Diseases. Am J Respir Crit Care Med 207, 160–172. https://doi.org/10.1164/rccm.202110-2414OC

Discussion - Perspectives

Discussion and perspectives

The first aim of this work was to establish a comprehensive molecular cell atlas of the healthy canine lung using single-cell RNA sequencing (scRNA-seq), to serve as a reference to investigate cellular and molecular alterations in canine lung diseases, particularly canine idiopathic pulmonary fibrosis (CIPF) and canine pulmonary adenocarcinoma (PAC). In dogs, scRNA-seq has already been used in various samples, such as bronchoalveolar lavage fluid (BALF) cells (Fastrès et al., 2020a, 2020b), blood cells (Ammons et al., 2023; Eschke et al., 2023), osteosarcoma (Ammons et al., 2024), duodenum (Manchester et al., 2024) and iliac and subclavian arteries (Shi et al., 2022), but was never used in canine whole lung tissue. Using scRNA-seq on four healthy lung tissue biopsies, we characterized 46 transcriptionally distinct cell subpopulations across all lung tissue compartments including 23 immune, 13 mesenchymal, 5 epithelial and 5 endothelial cell subpopulations.

In those healthy lungs, six distinct fibroblast clusters were identified, highlighting notable heterogeneity. This diversity may reflect different activation states and functional roles, with some clusters potentially involved in immune regulation. To date, single-cell expression profiles of fibroblast subsets in dogs have not been described in the literature. Existing studies either lack fibroblasts entirely, such as those using BALF samples (Fastrès et al., 2020a, 2020b), or treat them as a single, uniform population (Shi et al., 2022; Ammons et al., 2024; Manchester et al., 2024). Their classification as alveolar or adventitial was based on human and mice markers, so definitive classification should be confirmed by spatial validation in lung biopsies. Some fibroblasts subsets appear promising because they share features with fibroblast subpopulations already described in the healthy human lung, such as CCL19^{+} adventitial fibroblasts that resemble immune-recruiting fibroblasts and COL23A1^{+} adventitial fibroblasts that resemble peribronchial fibroblasts that may be implicated in human lung diseases (Madissoon et al., 2023).

The annotation of monocyte and macrophage clusters remained challenging. Indeed, conventional markers arising from human and mouse studies are sometimes unhelpful for cell identification in dogs, due to incomplete annotation of the canine genome, species differences regarding transcriptome, or occasional low transcript abundance (Ammons et al., 2023). Previous studies on BALF cells allowed the annotation of alveolar macrophages with high confidence (Fastrès et al., 2020a). The cluster annotated as 'FN1^{+} monocytes' shares features with a cluster of 'monocyte-derived macrophages or monocytes' in canine BALF (Fastrès et al., 2020a), and with monocyte-derived macrophages in the human lung (Sikkema et al., 2023). According to recent studies, monocyte-derived macrophages are believed to be involved in the pathogenesis of canine

idiopathic pulmonary fibrosis (Fastrès et al., 2020b, 2023), human COVID-19, pulmonary fibrosis and lung cancer (Sikkema et al., 2023). 'CCL13^{+} macrophages' may be identified as interstitial macrophages based on their expression of markers known in humans (Patel and Metcalf, 2018; Sikkema et al., 2023) and mice (Gibbings et al., 2017; Chakarov et al., 2019; Schyns et al., 2019; Chaudhary et al., 2022), their absence in canine BALF (Fastrès et al., 2020a, 2020b), and their transcriptomic similarity to macrophages from the canine duodenum (Manchester et al., 2024). The latter are expected to exhibit a phenotype close to that of interstitial macrophages, as suggested by mouse studies (Gibbings et al., 2017). However, studies incorporating spatial resolution would be highly valuable to confirm the localization of these cell subpopulations within the tissue.

Additional cell types were identified with high resolution, including rare cell types such as γδ T cells and Schwann cells. Unfortunately, mesothelial cells could not be identified in any of the four samples. Possible explanations include the rarity of this cell population, the loss of mesothelial cells during tissue dissociation, the lack annotation in the canine genome of mesothelial cell makers usually used in dogs or lack of expression of mesothelial cell makers usually used in other species. As expected from other scRNA-seq studies, eosinophils were absent from our dataset, likely due to their high RNase content causing rapid mRNA degradation (Fastrès et al., 2020a; Travaglini et al., 2020; Madissoon et al., 2023).

Homology analysis between canine and human lungs revealed a high degree of similarity in lung cell transcriptional profiles, while also uncovering potential species-specific differences. Canine smooth muscle cells, epithelial cells, and endothelial cells were readily identified using human-based classification systems and markers (Travaglini et al., 2020; Schupp et al., 2021; Madissoon et al., 2023; Sikkema et al., 2023). These findings underscore the value of the canine model for advancing our understanding of human lung diseases. In addition to confirming these similarities, this study contributed to the identification of novel, cell type–specific markers in the canine lung, expanding the current repertoire of cellular markers.

In this work, fibroblast activation protein (FAP) was identified as a marker of cancer-associated fibroblasts (CAFs) in canine PAC through both scRNA-seq and immunohistochemistry (IHC) analyses. These findings support the potential application of FAP-targeted nuclear imaging for tumor staging and treatment planning in dogs, paralleling current approaches in human oncology (Giesel et al., 2021; Röhrich et al., 2022). Given the poor prognosis associated with advanced-stage canine lung carcinoma (Lee et al., 2020; McPhetridge et al., 2021), FAP-targeted therapeutic

strategies, such as the selective depletion of FAP-expressing CAFs, may offer clinical benefit (Lee et al., 2022). Notably, in contrast to IHC studies and observations in human non-small cell lung cancer (NSCLC) (Shi et al., 2020), scRNA-seq did not detect FAP expression in malignant epithelial cells. Whether the FAP positivity observed by IHC reflects true protein-level expression in tumor cells undergoing epithelial-to-mesenchymal transition or is attributable to antibody cross-reactivity remains to be determined.

Collagen triple helix repeat containing 1 (CTHRC1) emerged as a specific marker of CAFs in canine PAC through scRNA-seq, while immunofluorescence microscopy further revealed that CTHRC1$^+$ CAFs are predominantly localized around or near tumor nests. In human NSCLC, *CTHRC1* is significantly overexpressed and has been associated with more aggressive tumor behavior and poorer prognosis (Ke et al., 2014; Y.-J. Liu et al., 2023; Singh et al., 2024), while CAFs co-expressing *POSTN*, *CTHRC1*, and *FAP* have been implicated in promoting immunosuppression and tumor progression (Chen et al., 2023). These findings highlight CTHRC1 as a potential therapeutic target in canine PAC, via its inhibition or regulation (Singh et al., 2024).

Osteopontin (SPP1) was identified as a marker of TAMs in canine PAC, with confirmation by immunofluorescence microscopy. In human NSCLC, *SPP1* overexpression has been implicated in tumor progression, epithelial-to-mesenchymal transition, immune evasion, and therapy resistance, with SPP1$^+$ TAMs potentially acting in synergy with CTHRC1$^+$ CAFs (Zhang et al., 2017; Leader et al., 2021; Yan et al., 2023; Chen et al., 2023). These findings underscore the relevance of SPP1 as a potential diagnostic and prognostic biomarker, and targeting SPP1-related signaling pathways may provide therapeutic benefit for canine PAC (Matsubara et al., 2023).

SPP1 may contribute to immune evasion, potentially through the upregulation of immune checkpoint molecules such as PD-L1 (Zhang et al., 2017). In human NSCLC, immune checkpoint inhibitors targeting the PD-1/PD-L1 axis have been developed and approved, significantly improving response rates and long-term survival in patients with advanced disease (Xia et al., 2019). However, clinical benefit is limited to a subset of patients, and the identification of reliable predictive biomarkers remains an active area of research (Xia et al., 2019). In veterinary oncology, immune checkpoint inhibitors are also under development (Igase et al., 2020; Yoshimoto et al., 2023). Although this study did not demonstrate statistically significant overexpression of PD-L1 or PD-1 in canine PAC, the expression of immune checkpoint pathways warrants further investigation in this context.

Other alterations in cell distributions within plasma cells, neutrophils, mature dendritic cells were highlighted and warrant further investigation as they may convey prognostic value, as in humans (Lohr et al., 2013; Pang et al., 2022; Peng et al., 2023). Altered gene expression profiles were identified in additional cell types, such as enrichments in genes involved in EMT, mitosis and inflammatory response in PAC muscle, endothelial and cancer cells.

Preliminary scRNA-seq data from two CIPF-affected lung tissue biopsies revealed notable transcriptional similarities between activated fibroblasts in CIPF and CAFs in canine PAC. In particular, the overexpression of *FAP*, *ADAM12*, and *ADAMDEC1* in CIPF fibroblasts suggests the emergence of a shared profibrotic and potentially pro-tumoral phenotype and may reflect conserved activation pathways in fibroblasts across fibrotic and neoplastic contexts. Interestingly, *CTHRC1*, a marker of CAFs in canine PAC, was not expressed by fibroblasts in CIPF samples. This absence may indicate a degree of specificity of CTHRC1 expression for CAFs. However, in human IPF, CTHRC1-expressing fibroblasts have been localized specifically within fibroblastic foci (Tsukui et al., 2020), a key histopathological feature of IPF that is typically absent in CIPF. The lack of CTHRC1 expression in this study may thus reflect a pathological difference between CIPF and IPF, potentially linked to the absence of fibroblastic foci in the canine disease. Inclusion of additional CIPF samples in future analyses will be essential to confirm whether this observation represents a consistent biological divergence or results from the limited sampling in this preliminary dataset.

In this preliminary study, *SPP1* was found to be overexpressed in macrophages and monocytes from CIPF-affected lungs. This finding is consistent with previous scRNA-seq studies, which reported elevated SPP1 expression in monocyte-derived macrophages isolated from BALF of WHWTs with CIPF (Fastrès et al., 2020b). Moreover, serum concentrations of SPP1 are higher in WHWTs with CIPF compared to healthy controls, and even control WHWTs exhibit higher SPP1 levels than other terrier breeds, suggesting a potential breed- and disease-associated upregulation of SPP1 (Fastrès et al., 2023). Interestingly, SPP1 was also identified as a marker of tumor-associated macrophages in canine PAC, indicating that SPP1-expressing macrophages may play roles in both fibrotic and neoplastic lung conditions. This shared expression pattern raises the possibility of overlapping macrophage activation states or common inflammatory pathways contributing to disease progression in both CIPF and PAC, although further studies are needed to confirm these associations and clarify their functional relevance.

Additional samples will be essential to validate these preliminary findings and enable a more detailed characterization of specific cell subsets, particularly macrophages. Altered gene expression profiles have already been identified in BALF macrophages from dogs affected by CIPF (Fastrès et al., 2020b). However, BALF-derived cells do not include interstitial macrophages (IMs), which reside within the lung interstitium and are thought to exert anti-inflammatory functions (Liegeois et al., 2018; Schyns et al., 2019). In murine models of lung fibrosis, the role of IMs remains controversial: while some studies have shown that they acquire a pro-fibrotic phenotype (Shi et al., 2021), others suggest they play a protective role (Chakarov et al., 2019). Investigating the gene expression profile of IMs in CIPF would provide valuable insights into disease pathobiology and should be complemented by in situ validation to confirm their spatial localization within the interstitial compartment.

With the inclusion of additional samples, further investigation of epithelial cells in CIPF may be particularly informative. In human IPF, a previously unknown population of aberrant basaloid epithelial cells has recently been identified and is absent in commonly used murine models of lung fibrosis (Adams et al., 2020). These cells are characterized by a unique transcriptional profile, co-expressing markers of basal epithelium, mesenchymal transition, senescence, and developmental pathways (Adams et al., 2020). Notably, they are typically found at the edges of fibroblast foci and are considered highly specific to IPF (Adams et al., 2020). The identification of such a population in CIPF could clarify whether similar epithelial responses to chronic lung injury occur in dogs and enhance our understanding of epithelial contributions to disease pathogenesis.

The expression of FAP by fibroblasts in lung biopsies from dogs affected by CIPF was demonstrated using scRNA-seq and IHC, aligning with previous findings in human IPF (Acharya et al., 2006; P. Yang et al., 2023). In human IPF, FAP expression is restricted to areas of ongoing tissue injury, with strong expression observed in fibroblast foci (Acharya et al., 2006). In dogs, FAP expression correlated with fibrosis activity scores in lung biopsies. Despite the absence of fibroblast foci in CIPF, FAP was predominantly expressed in areas of active fibrosis rather than mature fibrotic regions. The positive correlation between FAP expression and fibrosis activity highlights its potential as a promising marker of fibrogenesis, supporting the hypothesis that FAP plays a crucial role in the pathogenesis of the disease.

Interestingly, while FAP was upregulated in fibrotic and neoplastic lung tissues, plasma levels of soluble FAP were significantly lower in WHWTs with CIPF compared to healthy dogs.

Similarly, a recent study has demonstrated that serum levels of soluble FAP were lower in patients with IPF than in healthy controls, but were not associated with disease severity, progression or survival (Prior et al., 2024). Lower soluble FAP has also been identified in various other human pathologies, such as patients with cancer (Liao et al., 2017; Solano-Iturri et al., 2020a, 2020b), though the mechanisms and the source of soluble FAP remain unclear. As a result, circulating FAP appears as an unspecific and insufficiently reliable diagnostic biomarker for CIPF.

Given the current lack of effective treatments for CIPF, targeting FAP presents a promising therapeutic and diagnostic approach. Emerging FAP-targeted therapies, such as FAP-targeted radionuclide therapy (Privé et al., 2023) and FAP-directed chimeric antigen receptor (CAR)-T cell therapy (Lee et al., 2022), offer potential for modulating fibrotic activity in affected dogs. Additionally, FAP-targeted radiotracers for nuclear imaging may help in diagnosing CIPF and predicting disease progression (Röhrich et al., 2022; Mori et al., 2024). As CIPF is considered a spontaneous preclinical model of human IPF, these insights could have translational relevance, potentially benefiting both veterinary and human patients.

FAPI-based PET/CT is increasingly being explored in both preclinical and clinical settings for interstitial lung diseases such as IPF, emerging as a promising non-invasive tool for monitoring disease progression and treatment response (Röhrich et al., 2022; Yang et al., 2023; Hotta et al., 2024; Mori et al., 2024). Regarding human lung cancer, FAP-targeted PET imaging also constitutes a highly promising diagnostic technique for lung cancer staging and treatment planning, offering several advantages over conventional [^{18}F]FDG PET imaging, notably regarding metastasis detection (Giesel et al., 2021; Röhrich et al., 2022; Wei et al., 2022, 2023).

In our pilot study, we demonstrated that [^{18}F]FAPI-74 PET is a safe and feasible imaging modality in dogs. Notably, no confinement beyond the 60-minute uptake period was required, and this time point appeared optimal for image acquisition, supporting the practicality for clinical use. Increased [^{18}F]FAPI-74 uptake was observed in the lungs of CIPF-affected dogs compared to controls, consistent with findings in human IPF (Röhrich et al., 2022; P. Yang et al., 2023; Mori et al., 2024; Hotta et al., 2024). These results support the use of FAP-targeted PET/CT as a noninvasive tool to assess activated fibroblast distribution and fibrotic activity in vivo. This imaging approach may aid in early diagnosis, where distinguishing active from inactive fibrosis may be challenging, and evaluate response to potential antifibrotic therapies (Röhrich et al., 2022).

Limitations

While this study provides novel insights into the pathobiology of CIPF and canine PAC and highlights the utility of advanced molecular and imaging tools, several limitations must be acknowledged to contextualize the findings and guide future research.

A primary limitation of scRNA-seq is the need for fresh tissue samples. This technique requires immediate processing to prevent RNA contamination from dead or lysed cells, which can compromise data quality (Chen et al., 2019). Such constraints may limit the availability and diversity of samples, especially in veterinary studies where access to fresh clinical material is restricted.

Moreover, the high cost of scRNA-seq limited the number of dogs included in the study. The small sample size inherently reduces the statistical power for detecting differences in cell abundance and performing differential gene expression analyses and may introduce sampling bias. Despite these constraints, we were able to identify major cell populations and their associated gene expression profiles, demonstrating the feasibility of this approach in canine lung tissue.

Another challenge relates to the incomplete annotation of the canine genome. At the time of analysis, our study, like most currently published studies, relied on the CanFam3.1 assembly, which has since been updated. The limited gene annotation in earlier genome versions may affect gene identification and the interpretation of transcriptomic data (Fastrès et al., 2020a). Continued improvements in canine genome annotation will enhance the resolution and accuracy of such analyses in future studies.

Technical artifacts introduced during tissue dissociation represent an additional source of bias. The enzymatic digestion required to isolate single cells, typically involving proteolytic enzymes at 37°, can stress sensitive cell types, potentially leading to artificial gene expression changes, such as the upregulation of heat shock proteins (Denisenko et al., 2020). Furthermore, delicate populations like epithelial cells may be partially lost or underrepresented due to their fragility during processing. Rare immune cell types, such as eosinophils, may not be captured without specialized isolation methods (See et al., 2018; Travaglini et al., 2020)

While scRNA-seq excels in revealing cell-type-specific transcriptomes, it inherently lacks spatial resolution. This absence of spatial context limits our ability to precisely localize cell populations within the lung architecture, which is crucial for understanding the lung microenvironment. Ideally, in situ validation techniques such as IHC or spatial transcriptomics

would complement these findings. However, the scarcity of canine-specific reagents, particularly reliable antibodies for flow cytometry or histological validation, remains a significant barrier. The development of such tools is essential for strengthening the biological interpretations derived from single-cell analyses in dogs.

FAPI-based PET imaging, while offering promising translational and diagnostic potential, is still an experimental modality in human and veterinary medicine. The pilot nature of this study, which included only four CIPF-affected dogs, limits the generalizability of the findings. Although the study successfully demonstrated the feasibility and safety of [^{18}F]FAPI-74 PET to detect fibrotic activity in vivo, larger cohorts will be necessary to establish meaningful correlations between FAP uptake, disease severity, and progression.

Additionally, this study employed a stand-alone PET scanner, which lacks the anatomical precision afforded by hybrid PET/CT systems. Co-registration of PET and CT images in a single acquisition would not only enhance anatomical localization of radiotracer uptake but also reduce anesthesia duration (LeBlanc and Morandi, 2014). The incorporation of hybrid imaging in future studies could therefore improve both the accuracy and clinical applicability of [^{18}F]FAPI-74 PET in dogs.

Conclusion

This thesis advances our understanding of the canine lung in both health and disease through the integration of cutting-edge single-cell transcriptomics and molecular imaging. Collectively, the work presented here establishes foundational knowledge, identifies novel biomarkers, and explores innovative diagnostic tools with potential applications in both veterinary and translational pulmonary medicine.

The generation of the first single-cell atlas of the healthy canine lung represents a major contribution to comparative respiratory biology. By revealing the rich cellular heterogeneity and identifying novel markers across diverse lung cell populations, this work not only deepens our molecular understanding of normal lung physiology in dogs but also creates a crucial reference for future studies investigating pulmonary pathologies.

Extending this approach to disease contexts, the single-cell characterization of canine pulmonary adenocarcinoma uncovers profound alterations in the tumor microenvironment, particularly within fibroblast and macrophage populations. These findings provide valuable insight

into mechanisms of tumor progression and immune evasion, and highlight potential targets for therapeutic intervention, particularly in late-stage cancers.

Similarly, the preliminary single-cell analysis of lungs affected by canine idiopathic pulmonary fibrosis offers an initial yet meaningful window into the transcriptional landscape of this poorly understood condition. Despite the limited sample size, the data point to potentially relevant molecular pathways and candidate targets that merit further investigation. As additional samples are included in future research, these findings are expected to expand significantly, paving the way toward the development of more effective therapeutic strategies.

Among the molecular markers explored, FAP emerged as a key indicator of pathological tissue remodeling. Its selective expression in regions of active fibrosis in CIPF and in the stroma of lung tumors suggests a central role in both fibrotic and neoplastic processes. The translational relevance of FAP is further underscored by its compatibility with emerging imaging and therapeutic platforms.

In this context, the feasibility and safety of [^{18}F]FAPI-74 PET/CT imaging in CIPF-affected dogs, demonstrated in a pilot study, opens new possibilities for noninvasively detecting and monitoring fibrotic activity in vivo. This imaging modality holds promise not only for improving disease diagnosis and progression tracking but also for guiding clinical trial inclusion and therapeutic response assessment.

In summary, this body of work highlights the value of the dog as a biologically relevant model for human pulmonary diseases and illustrates the power of combining single-cell transcriptomics with molecular imaging to uncover novel mechanisms, biomarkers, and diagnostic strategies. These findings lay the groundwork for future investigations and contribute to the broader effort of advancing precision medicine in both veterinary and human respiratory health.

References

Acharya, P.S., Zukas, A., Chandan, V., Katzenstein, A.-L.A., Puré, E., 2006. Fibroblast activation protein: a serine protease expressed at the remodeling interface in idiopathic pulmonary fibrosis. Hum Pathol 37, 352–360. https://doi.org/10.1016/j.humpath.2005.11.020

Adams, T.S., Schupp, J.C., Poli, S., Ayaub, E.A., Neumark, N., Ahangari, F., Chu, S.G., Raby, B.A., Deluliis, G., Januszyk, M., Duan, Q., Arnett, H.A., Siddiqui, A., Washko, G.R., Homer, R., Yan, X., Rosas, I.O., Kaminski, N., 2020. Single-cell RNA-seq reveals ectopic and aberrant lung-resident cell populations in idiopathic pulmonary fibrosis. Science Advances 6, eaba1983. https://doi.org/10.1126/sciadv.aba1983

Alexander, K., Joly, H., Blond, L., D'Anjou, M.-A., Nadeau, M.-È., Olive, J., Beauchamp, G., 2012. A Comparison of Computed Tomography, Computed Radiography, and Film-Screen Radiography for the Detection of Canine Pulmonary Nodules. Veterinary Radiology & Ultrasound 53, 258–265. https://doi.org/10.1111/j.1740-8261.2012.01924.x

Alfaro, T.M., Robalo Cordeiro, C., 2020. Comorbidity in idiopathic pulmonary fibrosis - what can biomarkers tell us? Ther Adv Respir Dis 14, 1753466620910092. https://doi.org/10.1177/1753466620910092

Ammons, D.T., Harris, R.A., Hopkins, L.S., Kurihara, J., Weishaar, K., Dow, S., 2023. A single-cell RNA sequencing atlas of circulating leukocytes from healthy and osteosarcoma affected dogs. Front Immunol 14, 1162700. https://doi.org/10.3389/fimmu.2023.1162700

Ammons, D.T., Hopkins, L.S., Cronise, K.E., Kurihara, J., Regan, D.P., Dow, S., 2024. Single-cell RNA sequencing reveals the cellular and molecular heterogeneity of treatment-naïve primary osteosarcoma in dogs. Commun Biol 7, 1–18. https://doi.org/10.1038/s42003-024-06182-w

Aran, D., Looney, A.P., Liu, L., Wu, E., Fong, V., Hsu, A., Chak, S., Naikawadi, R.P., Wolters, P.J., Abate, A.R., Butte, A.J., Bhattacharya, M., 2019. Reference-based analysis of lung single-cell sequencing reveals a transitional profibrotic macrophage. Nat Immunol 20, 163–172. https://doi.org/10.1038/s41590-018-0276-y

Ariga, N., Sato, E., Ohuchi, N., Nagura, H., Ohtani, H., 2001. Stromal expression of fibroblast activation protein/seprase, a cell membrane serine proteinase and gelatinase, is associated with longer survival in patients with invasive ductal carcinoma of breast. Int J Cancer 95, 67–72. https://doi.org/10.1002/1097-0215(20010120)95:1<67::aid-ijc1012>3.0.co;2-u

Armbrust, L.J., Biller, D.S., Bamford, A., Chun, R., Garrett, L.D., Sanderson, M.W., 2012. Comparison of three-view thoracic radiography and computed tomography for detection of pulmonary nodules in dogs with neoplasia. https://doi.org/10.2460/javma.240.9.1088

Arnold, J.N., Magiera, L., Kraman, M., Fearon, D.T., 2014. Tumoral Immune Suppression by Macrophages Expressing Fibroblast Activation Protein-Alpha and Heme Oxygenase-1. Cancer Immunol Res 2, 121–126. https://doi.org/10.1158/2326-6066.CIR-13-0150

Ballegeer, E.A., Adams, W.M., Dubielzig, R.R., Paoloni, M.C., Klauer, J.M., Keuler, N.S., 2010. Computed Tomography Characteristics of Canine Tracheobronchial Lymph Node Metastasis. Veterinary Radiology & Ultrasound 51, 397–403. https://doi.org/10.1111/j.1740-8261.2010.01675.x

Ballester, B., Milara, J., Cortijo, J., 2019. Idiopathic Pulmonary Fibrosis and Lung Cancer: Mechanisms and Molecular Targets. IJMS 20, 593. https://doi.org/10.3390/ijms20030593

Bankhead, P., Loughrey, M.B., Fernández, J.A., Dombrowski, Y., McArt, D.G., Dunne, P.D., McQuaid, S., Gray, R.T., Murray, L.J., Coleman, H.G., James, J.A., Salto-Tellez, M., Hamilton, P.W., 2017. QuPath: Open source software for digital pathology image analysis. Sci Rep 7, 16878. https://doi.org/10.1038/s41598-017-17204-5

Bankier, A.A., MacMahon, H., Colby, T., Gevenois, P.A., Goo, J.M., Leung, A.N.C., Lynch, D.A., Schaefer-Prokop, C.M., Tomiyama, N., Travis, W.D., Verschakelen, J.A., White, C.S., Naidich, D.P., 2024. Fleischner Society: Glossary of Terms for Thoracic Imaging. Radiology 310, e232558. https://doi.org/10.1148/radiol.232558

Barnes, T., Brown, K.K., Corcoran, B., Glassberg, M.K., Kervitsky, D.J., Limper, A.H., McGuire, K., Williams, K., Roman, J., Comparative Biology of Pulmonary Fibrosis Group, 2019. Research in Pulmonary Fibrosis Across Species: Unleashing Discovery Through Comparative Biology. Am J Med Sci 357, 399–404. https://doi.org/10.1016/j.amjms.2019.02.005

Bauer, S., Jendro, M.C., Wadle, A., Kleber, S., Stenner, F., Dinser, R., Reich, A., Faccin, E., Gödde, S., Dinges, H., Müller-Ladner, U., Renner, C., 2006. Fibroblast activation protein is expressed by rheumatoid myofibroblast-like synoviocytes. Arthritis Research & Therapy 8, R171. https://doi.org/10.1186/ar2080

Bauer, T.G., 2000. Lung Biopsy. Veterinary Clinics of North America: Small Animal Practice 30, 1207–1225. https://doi.org/10.1016/S0195-5616(00)06003-4

Beck, J., Miller, M.A., Frank, C., DuSold, D., Ramos-Vara, J.A., 2017. Surfactant Protein A and Napsin A in the Immunohistochemical Characterization of Canine Pulmonary Carcinomas: Comparison With Thyroid Transcription Factor-1. Vet Pathol 54, 767–774. https://doi.org/10.1177/0300985817712559

Bettini, G., Marconato, L., Morini, M., Ferrari, F., 2009. Thyroid transcription factor-1 immunohistochemistry: diagnostic tool and malignancy marker in canine malignant lung tumours. Veterinary and Comparative Oncology 7, 28–37. https://doi.org/10.1111/j.1476-5829.2008.00166.x

Bettini, G., Morini, M., Marconato, L., Marcato, P.S., Zini, E., 2010. Association between environmental dust exposure and lung cancer in dogs. The Veterinary Journal 186, 364–369. https://doi.org/10.1016/j.tvjl.2009.09.004

Bleakley, S., Duncan, C.G., Monnet, E., 2015. Thoracoscopic Lung Lobectomy for Primary Lung Tumors in 13 Dogs. Vet Surg 44, 1029–1035. https://doi.org/10.1111/vsu.12411

Brokopp, C.E., Schoenauer, R., Richards, P., Bauer, S., Lohmann, C., Emmert, M.Y., Weber, B., Winnik, S., Aikawa, E., Graves, K., Genoni, M., Vogt, P., Lüscher, T.F., Renner, C., Hoerstrup, S.P., Matter, C.M., 2011. Fibroblast activation protein is induced by inflammation and degrades type I collagen in thin-cap fibroatheromata. European Heart Journal 32, 2713–2722. https://doi.org/10.1093/eurheartj/ehq519

Brown, A.J., Davison, E., Sleeper, M.M., 2010. Clinical efficacy of sildenafil in treatment of pulmonary arterial hypertension in dogs. J Vet Intern Med 24, 850–854. https://doi.org/10.1111/j.1939-1676.2010.0517.x

Caminati, A., Lonati, C., Cassandro, R., Elia, D., Pelosi, G., Torre, O., Zompatori, M., Uslenghi, E., Harari, S., 2019. Comorbidities in idiopathic pulmonary fibrosis: an underestimated issue. European Respiratory Review 28. https://doi.org/10.1183/16000617.0044-2019

Chakarov, S., Lim, H.Y., Tan, L., Lim, S.Y., See, P., Lum, J., Zhang, X.-M., Foo, S., Nakamizo, S., Duan, K., Kong, W.T., Gentek, R., Balachander, A., Carbajo, D., Bleriot, C., Malleret, B., Tam, J.K.C., Baig, S., Shabeer, M., Toh, S.-A.E.S., Schlitzer, A., Larbi, A., Marichal, T., Malissen, B., Chen, J., Poidinger, M., Kabashima, K., Bajenoff, M., Ng, L.G., Angeli, V., Ginhoux, F., 2019. Two distinct interstitial macrophage populations coexist across tissues in specific subtissular niches. Science 363, eaau0964. https://doi.org/10.1126/science.aau0964

Chaudhary, N., Jayaraman, A., Reinhardt, C., Campbell, J.D., Bosmann, M., 2022. A single-cell lung atlas of complement genes identifies the mesothelium and epithelium as prominent sources of extrahepatic complement proteins. Mucosal Immunol 15, 927–939. https://doi.org/10.1038/s41385-022-00534-7

Chen, C., Guo, Q., Liu, Y., Hou, Q., Liao, M., Guo, Y., Zang, Y., Wang, F., Liu, Huanyu, Luan, X., Liang, Y., Guan, Z., Li, Y., Liu, Haozhen, Dong, X., Zhang, X., Liu, J., Xu, Q., 2023. Single-cell and

spatial transcriptomics reveal POSTN+ cancer-associated fibroblasts correlated with immune suppression and tumour progression in non-small cell lung cancer. Clin Transl Med 13, e1515. https://doi.org/10.1002/ctm2.1515

Chen, G., Ning, B., Shi, T., 2019. Single-Cell RNA-Seq Technologies and Related Computational Data Analysis. Front Genet 10, 317. https://doi.org/10.3389/fgene.2019.00317

Chow, L., Wheat, W., Ramirez, D., Impastato, R., Dow, S., 2024. Direct comparison of canine and human immune responses using transcriptomic and functional analyses. Sci Rep 14, 2207. https://doi.org/10.1038/s41598-023-50340-9

Christiansen, V.J., Jackson, K.W., Lee, K.N., McKee, P.A., 2007. Effect of fibroblast activation protein and α2-antiplasmin cleaving enzyme on collagen Types I, III, and IV. Archives of Biochemistry and Biophysics 457, 177–186. https://doi.org/10.1016/j.abb.2006.11.006

Clercx, C., Fastrès, A., Roels, E., 2018. Idiopathic pulmonary fibrosis in West Highland white terriers: An update. The Veterinary Journal 242, 53–58. https://doi.org/10.1016/j.tvjl.2018.10.007

Cohn, L.A., Norris, C.R., Hawkins, E.C., Dye, J.A., Johnson, C.A., Williams, K.J., 2004. Identification and characterization of an idiopathic pulmonary fibrosis-like condition in cats. J Vet Intern Med 18, 632–641. https://doi.org/10.1111/j.1939-1676.2004.tb02598.x

Collard, H.R., Ryerson, C.J., Corte, T.J., Jenkins, G., Kondoh, Y., Lederer, D.J., Lee, J.S., Maher, T.M., Wells, A.U., Antoniou, K.M., Behr, J., Brown, K.K., Cottin, V., Flaherty, K.R., Fukuoka, J., Hansell, D.M., Johkoh, T., Kaminski, N., Kim, D.S., Kolb, M., Lynch, D.A., Myers, J.L., Raghu, G., Richeldi, L., Taniguchi, H., Martinez, F.J., 2016. Acute Exacerbation of Idiopathic Pulmonary Fibrosis. An International Working Group Report. Am J Respir Crit Care Med 194, 265–275. https://doi.org/10.1164/rccm.201604-0801CI

Corcoran, B.M., Cobb, M., Martin, M.W., Dukes-McEwan, J., French, A., Fuentes, V.L., Boswood, A., Rhind, S., 1999a. Chronic pulmonary disease in West Highland white terriers. Vet Rec 144, 611–616. https://doi.org/10.1136/vr.144.22.611

Corcoran, B.M., Dukes-McEwan, J., Rhind, S., French, A., 1999b. Idiopathic pulmonary fibrosis in a Staffordshire bull terrier with hypothyroidism. J Small Anim Pract 40, 185–188. https://doi.org/10.1111/j.1748-5827.1999.tb03788.x

Corcoran, B.M., King, L.G., Schwarz, T., Hammond, G., Sullivan, M., 2011. Further characterisation of the clinical features of chronic pulmonary disease in West Highland white terriers. Veterinary Record 168, 355–355. https://doi.org/10.1136/vr.c6519

Corsi, F., Sorrentino, L., Albasini, S., Colombo, F., Cigognini, M., Massari, A., Morasso, C., Mazzucchelli, S., Piccotti, F., Ardizzone, S., Sampietro, G.M., Truffi, M., 2021. Circulating Fibroblast Activation Protein as Potential Biomarker in Patients With Inflammatory Bowel Disease. Frontiers in Medicine 8.

Crooks, M.G., Fahim, A., Naseem, K.M., Morice, A.H., Hart, S.P., 2014. Increased platelet reactivity in idiopathic pulmonary fibrosis is mediated by a plasma factor. PLoS One 9, e111347. https://doi.org/10.1371/journal.pone.0111347

Delgado-Arija, M., Genovés, P., Pérez-Carrillo, L., González-Torrent, I., Giménez-Escamilla, I., Martínez-Dolz, L., Portolés, M., Tarazón, E., Roselló-Lletí, E., 2024. Plasma fibroblast activation protein is decreased in acute heart failure despite cardiac tissue upregulation. J Transl Med 22, 124. https://doi.org/10.1186/s12967-024-04900-w

Dendl, K., Koerber, S.A., Kratochwil, C., Cardinale, J., Finck, R., Dabir, M., Novruzov, E., Watabe, T., Kramer, V., Choyke, P.L., Haberkorn, U., Giesel, F.L., 2021. FAP and FAPI-PET/CT in Malignant and Non-Malignant Diseases: A Perfect Symbiosis? Cancers 13, 4946. https://doi.org/10.3390/cancers13194946

Denisenko, E., Guo, B.B., Jones, M., Hou, R., de Kock, L., Lassmann, T., Poppe, D., Clément, O., Simmons, R.K., Lister, R., Forrest, A.R.R., 2020. Systematic assessment of tissue dissociation and storage biases in single-cell and single-nucleus RNA-seq workflows. Genome Biology 21, 130. https://doi.org/10.1186/s13059-020-02048-6

Dienus, K., Bayat, A., Gilmore, B.F., Seifert, O., 2010. Increased expression of fibroblast activation protein-alpha in keloid fibroblasts: implications for development of a novel treatment option. Arch Dermatol Res 302, 725–731. https://doi.org/10.1007/s00403-010-1084-x

Dow, S., 2019. A Role for Dogs in Advancing Cancer Immunotherapy Research. Front Immunol 10, 2935. https://doi.org/10.3389/fimmu.2019.02935

Dunshee, D.R., Bainbridge, T.W., Kljavin, N.M., Zavala-Solorio, J., Schroeder, A.C., Chan, R., Corpuz, R., Wong, M., Zhou, W., Deshmukh, G., Ly, J., Sutherlin, D.P., Ernst, J.A., Sonoda, J., 2016. Fibroblast Activation Protein Cleaves and Inactivates Fibroblast Growth Factor 21*. Journal of Biological Chemistry 291, 5986–5996. https://doi.org/10.1074/jbc.M115.710582

Ellis, P.M., Vandermeer, R., 2011. Delays in the diagnosis of lung cancer. J Thorac Dis 3, 183–188. https://doi.org/10.3978/j.issn.2072-1439.2011.01.01

Eschke, M., Moore, P.F., Chang, H., Alber, G., Keller, S.M., 2023. Canine peripheral blood TCRαβ T cell atlas: Identification of diverse subsets including CD8A+ MAIT-like cells by combined

single-cell transcriptome and V(D)J repertoire analysis. Front Immunol 14, 1123366. https://doi.org/10.3389/fimmu.2023.1123366

Ettlin, J., Clementi, E., Amini, P., Malbon, A., Markkanen, E., 2017. Analysis of Gene Expression Signatures in Cancer-Associated Stroma from Canine Mammary Tumours Reveals Molecular Homology to Human Breast Carcinomas. Int J Mol Sci 18, 1101. https://doi.org/10.3390/ijms18051101

European Medicines Agency, 2015. Ofev : EPAR - Public assessment report.

Fan, X., Zhong, R., Liang, H., Zhong, Q., Huang, H., He, Juan, Chen, Y., Wang, Z., Xie, S., Jiang, Y., Lin, Y., Chen, S., Liang, W., He, Jianxing, 2024. Exhaled VOC detection in lung cancer screening: a comprehensive meta-analysis. BMC Cancer 24, 775. https://doi.org/10.1186/s12885-024-12537-7

Fastrès, A., Pirottin, D., Fievez, L., Marichal, T., Desmet, C.J., Bureau, F., Clercx, C., 2020a. Characterization of the Bronchoalveolar Lavage Fluid by Single Cell Gene Expression Analysis in Healthy Dogs: A Promising Technique. Front Immunol 11, 1707. https://doi.org/10.3389/fimmu.2020.01707

Fastrès, A., Pirottin, D., Fievez, L., Tutunaru, A.-C., Bolen, G., Merveille, A.-C., Marichal, T., Desmet, C.J., Bureau, F., Clercx, C., 2020b. Identification of Pro-Fibrotic Macrophage Populations by Single-Cell Transcriptomic Analysis in West Highland White Terriers Affected With Canine Idiopathic Pulmonary Fibrosis. Front Immunol 11, 611749. https://doi.org/10.3389/fimmu.2020.611749

Fastrès, A., Roels, E., Bolen, G., Tutunaru, A.-C., Antoine, N., Farnir, F., Clercx, C., 2018. Investigation of serum Krebs Von den Lungen 6 concentration as a predisposing factor and in the diagnosis of canine idiopathic pulmonary fibrosis in the West Highland white terrier. Presented at the 28th ECVIM-CA congress.

Fastrès, A., Roels, E., Tutunaru, A.C., Bolen, G., Merveille, A.-C., Day, M.J., Garigliany, M.-M., Antoine, N., Clercx, C., 2023. Osteopontin and fibronectin in lung tissue, serum, and bronchoalveolar lavage fluid of dogs with idiopathic pulmonary fibrosis and control dogs. J Vet Intern Med 37, 2468–2477. https://doi.org/10.1111/jvim.16870

Fastrès, A., Roels, E., Vangrinsven, E., Taminiau, B., Jabri, H., Bolen, G., Merveille, A.-C., Tutunaru, A.-C., Moyse, E., Daube, G., Clercx, C., 2020c. Assessment of the lung microbiota in dogs: influence of the type of breed, living conditions and canine idiopathic pulmonary fibrosis. BMC Microbiology 20, 84. https://doi.org/10.1186/s12866-020-01784-w

Fernández Pérez, E.R., Daniels, C.E., Schroeder, D.R., St Sauver, J., Hartman, T.E., Bartholmai, B.J., Yi, E.S., Ryu, J.H., 2010. Incidence, prevalence, and clinical course of idiopathic pulmonary fibrosis: a population-based study. Chest 137, 129–137. https://doi.org/10.1378/chest.09-1002

Fitzgerald, A.A., Weiner, L.M., 2020. The role of fibroblast activation protein in health and malignancy. Cancer Metastasis Rev 39, 783–803. https://doi.org/10.1007/s10555-020-09909-3

Fox, J., Munoz Marquez, M., Bouchet-Valat, M., 2023. Rcmdr: R Commander.

Fu, K., Pang, Y., Zhao, L., Lin, L., Wu, H., Sun, L., Lin, Q., Chen, H., 2022. FAP-targeted radionuclide therapy with [177Lu]Lu-FAPI-46 in metastatic nasopharyngeal carcinoma. Eur J Nucl Med Mol Imaging 49, 1767–1769. https://doi.org/10.1007/s00259-021-05634-3

Gibbings, S.L., Thomas, S.M., Atif, S.M., McCubbrey, A.L., Desch, A.N., Danhorn, T., Leach, S.M., Bratton, D.L., Henson, P.M., Janssen, W.J., Jakubzick, C.V., 2017. Three Unique Interstitial Macrophages in the Murine Lung at Steady State. American Journal of Respiratory Cell and Molecular Biology 57, 66. https://doi.org/10.1165/rcmb.2016-0361OC

Giesel, F.L., Adeberg, S., Syed, M., Lindner, T., Jiménez-Franco, L.D., Mavriopoulou, E., Staudinger, F., Tonndorf-Martini, E., Regnery, S., Rieken, S., El Shafie, R., Röhrich, M., Flechsig, P., Kluge, A., Altmann, A., Debus, J., Haberkorn, U., Kratochwil, C., 2021. FAPI-74 PET/CT Using Either 18F-AlF or Cold-Kit 68Ga Labeling: Biodistribution, Radiation Dosimetry, and Tumor Delineation in Lung Cancer Patients. J Nucl Med 62, 201–207. https://doi.org/10.2967/jnumed.120.245084

Gingrich, A.A., Reiter, T.E., Judge, S.J., York, D., Yanagisawa, M., Razmara, A., Sturgill, I., Basmaci, U.N., Brady, R.V., Stoffel, K., Murphy, W.J., Rebhun, R.B., Brown, C.T., Canter, R.J., 2021. Comparative Immunogenomics of Canine Natural Killer Cells as Immunotherapy Target. Front Immunol 12, 670309. https://doi.org/10.3389/fimmu.2021.670309

Giuliano, A., dos Santos Horta, R., Constantino-Casas, F., Hoather, T., Dobson, J., 2017. Expression of Fibroblast Activating Protein and Correlation with Histological Grade, Mitotic Index and Ki67 Expression in Canine Mast Cell Tumours. Journal of Comparative Pathology 156, 14–20. https://doi.org/10.1016/j.jcpa.2016.10.004

Glassberg, M.K., 2019. Overview of idiopathic pulmonary fibrosis, evidence-based guidelines, and recent developments in the treatment landscape. Am J Manag Care 25, S195–S203.

Guo, M., Morley, M.P., Jiang, C., Wu, Y., Li, G., Du, Y., Zhao, S., Wagner, A., Cakar, A.C., Kouril, M., Jin, K., Gaddis, N., Kitzmiller, J.A., Stewart, K., Basil, M.C., Lin, S.M., Ying, Y., Babu, A.,

Wikenheiser-Brokamp, K.A., Mun, K.S., Naren, A.P., Clair, G., Adkins, J.N., Pryhuber, G.S., Misra, R.S., Aronow, B.J., Tickle, T.L., Salomonis, N., Sun, X., Morrisey, E.E., Whitsett, J.A., Lin, S., Xu, Y., 2023. Guided construction of single cell reference for human and mouse lung. Nat Commun 14, 4566. https://doi.org/10.1038/s41467-023-40173-5

Habermann, A.C., Gutierrez, A.J., Bui, L.T., Yahn, S.L., Winters, N.I., Calvi, C.L., Peter, L., Chung, M.-I., Taylor, C.J., Jetter, C., Raju, L., Roberson, J., Ding, G., Wood, L., Sucre, J.M.S., Richmond, B.W., Serezani, A.P., McDonnell, W.J., Mallal, S.B., Bacchetta, M.J., Loyd, J.E., Shaver, C.M., Ware, L.B., Bremner, R., Walia, R., Blackwell, T.S., Banovich, N.E., Kropski, J.A., 2020. Single-cell RNA sequencing reveals profibrotic roles of distinct epithelial and mesenchymal lineages in pulmonary fibrosis. Sci Adv 6, eaba1972. https://doi.org/10.1126/sciadv.aba1972

Hamson, E.J., Keane, F.M., Tholen, S., Schilling, O., Gorrell, M.D., 2014. Understanding fibroblast activation protein (FAP): substrates, activities, expression and targeting for cancer therapy. Proteomics Clin Appl 8, 454–463. https://doi.org/10.1002/prca.201300095

Hao, Y., Hao, S., Andersen-Nissen, E., Mauck, W.M., Zheng, S., Butler, A., Lee, M.J., Wilk, A.J., Darby, C., Zager, M., Hoffman, P., Stoeckius, M., Papalexi, E., Mimitou, E.P., Jain, J., Srivastava, A., Stuart, T., Fleming, L.M., Yeung, B., Rogers, A.J., McElrath, J.M., Blish, C.A., Gottardo, R., Smibert, P., Satija, R., 2021. Integrated analysis of multimodal single-cell data. Cell 184, 3573-3587.e29. https://doi.org/10.1016/j.cell.2021.04.048

Hedlund, E., Deng, Q., 2018. Single-cell RNA sequencing: Technical advancements and biological applications. Mol Aspects Med 59, 36–46. https://doi.org/10.1016/j.mam.2017.07.003

Heikkilä, H.P., Krafft, E., Jespers, P., McEntee, K., Rajamäki, M.M., Clercx, C., 2013. Procollagen type III amino terminal propeptide concentrations in dogs with idiopathic pulmonary fibrosis compared with chronic bronchitis and eosinophilic bronchopneumopathy. Vet J 196, 52–56. https://doi.org/10.1016/j.tvjl.2012.07.023

Heikkilä, H.P., Lappalainen, A.K., Day, M.J., Clercx, C., Rajamäki, M.M., 2011. Clinical, bronchoscopic, histopathologic, diagnostic imaging, and arterial oxygenation findings in West Highland White Terriers with idiopathic pulmonary fibrosis. J Vet Intern Med 25, 433–439. https://doi.org/10.1111/j.1939-1676.2011.0694.x

Heikkilä-Laurila, H.P., Rajamäki, M.M., 2014. Idiopathic pulmonary fibrosis in West Highland white terriers. Vet Clin North Am Small Anim Pract 44, 129–142. https://doi.org/10.1016/j.cvsm.2013.08.003

Hochhegger, B., Marchiori, E., Zanon, M., Rubin, A.S., Fragomeni, R., Altmayer, S., Carvalho, C.R.R., Baldi, B.G., 2019. Imaging in idiopathic pulmonary fibrosis: diagnosis and mimics. Clinics (Sao Paulo) 74, e225. https://doi.org/10.6061/clinics/2019/e225

Holopainen, S., Rautala, E., Lilja-Maula, L., Lohi, H., Rajamäki, M.M., Lappalainen, A.K., 2019. Thoracic high resolution CT using the modified VetMousetrap™ device is a feasible method for diagnosing canine idiopathic pulmonary fibrosis in awake West Highland White Terriers. Vet Radiol Ultrasound 60, 525–532. https://doi.org/10.1111/vru.12779

Hotta, M., Kim, G.H.J., Rerkpichaisuth, V., Teng, P.Y., Armstrong, W.R., Carlucci, G., Dahlbom, M., Abtin, F., Lari, S.M., Fishbein, G.A., Czernin, J., Volkmann, E.R., Weigt, S.S., Calais, J., 2024. Correlation of FAPI PET Uptake with Immunohistochemistry in Explanted Lungs from Patients with Advanced Interstitial Lung Disease. J Nucl Med 65, 1789–1794. https://doi.org/10.2967/jnumed.124.268351

Hua, X., Yu, L., Huang, X., Liao, Z., Xian, Q., 2011. Expression and role of fibroblast activation protein-alpha in microinvasive breast carcinoma. Diagnostic Pathology 6, 111. https://doi.org/10.1186/1746-1596-6-111

Huang, Y., Simms, A.E., Mazur, A., Wang, S., León, N.R., Jones, B., Aziz, N., Kelly, T., 2011. Fibroblast activation protein-α promotes tumor growth and invasion of breast cancer cells through non-enzymatic functions. Clin Exp Metastasis 28, 567–579. https://doi.org/10.1007/s10585-011-9392-x

Hwang, B., Lee, J.H., Bang, D., 2018. Single-cell RNA sequencing technologies and bioinformatics pipelines. Exp Mol Med 50, 1–14. https://doi.org/10.1038/s12276-018-0071-8

Hytönen, M.K., Lohi, H., 2016. Canine models of human rare disorders. Rare Dis 4, e1241362. https://doi.org/10.1080/21675511.2016.1241362

Ichimata, M., Kagawa, Y., Namiki, K., Toshima, A., Nakano, Y., Matsuyama, F., Fukazawa, E., Harada, K., Katayama, R., Kobayashi, T., 2023. Prognosis of primary pulmonary adenocarcinoma after surgical resection in small-breed dogs: 52 cases (2005-2021). Journal of Veterinary Internal Medicine 37, 1466–1474. https://doi.org/10.1111/jvim.16739

Igase, M., Nemoto, Y., Itamoto, K., Tani, K., Nakaichi, M., Sakurai, M., Sakai, Y., Noguchi, S., Kato, M., Tsukui, T., Mizuno, T., 2020. A pilot clinical study of the therapeutic antibody against canine PD-1 for advanced spontaneous cancers in dogs. Sci Rep 10, 18311. https://doi.org/10.1038/s41598-020-75533-4

Iwasa, S., Jin, X., Okada, K., Mitsumata, M., Ooi, A., 2003. Increased expression of seprase, a membrane-type serine protease, is associated with lymph node metastasis in human colorectal cancer. Cancer Letters 199, 91–98. https://doi.org/10.1016/S0304-3835(03)00315-X

Jacob, F., 2024. Fluoroscopy-guided fine-needle aspiration of deep-seated pulmonary masses in dogs and cats appears safe and accurate. https://doi.org/10.2460/javma.23.07.0413

Jaffey, J.A., Wiggen, K., Leach, S.B., Masseau, I., Girens, R.E., Reinero, C.R., 2019. Pulmonary hypertension secondary to respiratory disease and/or hypoxia in dogs: Clinical features, diagnostic testing and survival. Vet J 251, 105347. https://doi.org/10.1016/j.tvjl.2019.105347

Javidroozi, M., Zucker, S., Chen, W.-T., 2012. Plasma seprase and DPP4 levels as markers of disease and prognosis in cancer. Dis Markers 32, 309–320. https://doi.org/10.3233/DMA-2011-0889

Jia, J., Martin, T.A., Ye, L., Jiang, W.G., 2014. FAP-α (Fibroblast activation protein-α) is involved in the control of human breast cancer cell line growth and motility via the FAK pathway. BMC Cell Biology 15, 16. https://doi.org/10.1186/1471-2121-15-16

Johnson, L.R., Lappin, M.R., Baker, D.C., 1999. Pulmonary Thromboembolism in 29 Dogs: 1985–1995. J Vet Intern Med 13, 338–345. https://doi.org/10.1111/j.1939-1676.1999.tb02192.x

Johnson, L.R., Stern, J.A., 2020. Clinical features and outcome in 25 dogs with respiratory-associated pulmonary hypertension treated with sildenafil. J Vet Intern Med 34, 65–73. https://doi.org/10.1111/jvim.15679

Johnson, V.S., Corcoran, B.M., Wotton, P.R., Schwarz, T., Sullivan, M., 2005. Thoracic high-resolution computed tomographic findings in dogs with canine idiopathic pulmonary fibrosis. J Small Anim Pract 46, 381–388. https://doi.org/10.1111/j.1748-5827.2005.tb00334.x

Jung, H.J., Nam, E.H., Park, J.Y., Ghosh, P., Kim, I.S., 2021. Identification of BR102910 as a selective fibroblast activation protein (FAP) inhibitor. Bioorg Med Chem Lett 37, 127846. https://doi.org/10.1016/j.bmcl.2021.127846

Kawabe, M., Kitajima, Y., Murakami, M., Iwasaki, R., Goto, S., Sakai, H., Mori, T., 2019. Hypofractionated radiotherapy in nine dogs with unresectable solitary lung adenocarcinoma. Vet Radiol Ultrasound 60, 456–464. https://doi.org/10.1111/vru.12754

Ke, Z., He, W., Lai, Y., Guo, X., Chen, S., Li, S., Wang, Y., Wang, L., 2014. Overexpression of Collagen Triple Helix Repeat Containing 1 (CTHRC1) is associated with tumour aggressiveness

and poor prognosis in human non-small cell lung cancer. Oncotarget 5, 9410–9424. https://doi.org/10.18632/oncotarget.2421

Keane, F.M., Nadvi, N.A., Yao, T.-W., Gorrell, M.D., 2011. Neuropeptide Y, B-type natriuretic peptide, substance P and peptide YY are novel substrates of fibroblast activation protein-α. The FEBS Journal 278, 1316–1332. https://doi.org/10.1111/j.1742-4658.2011.08051.x

Keane, F.M., Yao, T.-W., Seelk, S., Gall, M.G., Chowdhury, S., Poplawski, S.E., Lai, J.H., Li, Y., Wu, W., Farrell, P., Vieira de Ribeiro, A.J., Osborne, B., Yu, D.M.T., Seth, D., Rahman, K., Haber, P., Topaloglu, A.K., Wang, C., Thomson, S., Hennessy, A., Prins, J., Twigg, S.M., McLennan, S.V., McCaughan, G.W., Bachovchin, W.W., Gorrell, M.D., 2014. Quantitation of fibroblast activation protein (FAP)-specific protease activity in mouse, baboon and human fluids and organs. FEBS Open Bio 4, 43–54. https://doi.org/10.1016/j.fob.2013.12.001

Kewalramani, N., Machahua, C., Poletti, V., Cadranel, J., Wells, A.U., Funke-Chambour, M., 2022. Lung cancer in patients with fibrosing interstitial lung diseases: an overview of current knowledge and challenges. ERJ Open Res 8, 00115–02022. https://doi.org/10.1183/23120541.00115-2022

Kilvaer, T.K., Khanehkenari, M.R., Hellevik, T., Al-Saad, S., Paulsen, E.-E., Bremnes, R.M., Busund, L.-T., Donnem, T., Martinez, I.Z., 2015. Cancer Associated Fibroblasts in Stage I-IIIA NSCLC: Prognostic Impact and Their Correlations with Tumor Molecular Markers. PLOS ONE 10, e0134965. https://doi.org/10.1371/journal.pone.0134965

Kim, J., Kwon, S.Y., Cena, R., Park, S., Oh, J., Oui, H., Cho, K.-O., Min, J.-J., Choi, J., 2014. CT and PET-CT of a Dog with Multiple Pulmonary Adenocarcinoma. Journal of Veterinary Medical Science 76, 615–620. https://doi.org/10.1292/jvms.13-0434

Kouki, S., Viitanen, S.J., Koho, N., Laurila, H.P., Lilja-Maula, L., Holopainen, S., Neuvonen, M., Niemi, M., Fastrès, A., Clercx, C., Rajamäki, M.M., 2023. Extraesophageal reflux and reflux aspiration in dogs with respiratory diseases and in healthy dogs. Journal of Veterinary Internal Medicine 37, 268–276. https://doi.org/10.1111/jvim.16622

Krafft, E., Heikkilä, H.P., Jespers, P., Peeters, D., Day, M.J., Rajamäki, M.M., Mc Entee, K., Clercx, C., 2011. Serum and bronchoalveolar lavage fluid endothelin-1 concentrations as diagnostic biomarkers of canine idiopathic pulmonary fibrosis. Journal of Veterinary Internal Medicine. https://doi.org/10.1111/j.1939-1676.2011.0766.x

Krafft, E., Laurila, H.P., Peters, I.R., Bureau, F., Peeters, D., Day, M.J., Rajamäki, M.M., Clercx, C., 2013a. Analysis of gene expression in canine idiopathic pulmonary fibrosis. Vet J 198, 479–486. https://doi.org/10.1016/j.tvjl.2013.08.018

Krafft, E., Laurila, H.P., Peters, I.R., Bureau, F., Peeters, D., Day, M.J., Rajamäki, M.M., Clercx, C., 2013b. Analysis of gene expression in canine idiopathic pulmonary fibrosis. Vet J 198, 479–486. https://doi.org/10.1016/j.tvjl.2013.08.018

Krafft, E., Lybaert, P., Roels, E., Laurila, H.P., Rajamäki, M.M., Farnir, F., Myllärniemi, M., Day, M.J., Mc Entee, K., Clercx, C., 2014. Transforming growth factor beta 1 activation, storage, and signaling pathways in idiopathic pulmonary fibrosis in dogs. J Vet Intern Med 28, 1666–1675. https://doi.org/10.1111/jvim.12432

Kratochwil, C., Flechsig, P., Lindner, T., Abderrahim, L., Altmann, A., Mier, W., Adeberg, S., Rathke, H., Röhrich, M., Winter, H., Plinkert, P.K., Marme, F., Lang, M., Kauczor, H.-U., Jäger, D., Debus, J., Haberkorn, U., Giesel, F.L., 2019. 68Ga-FAPI PET/CT: Tracer Uptake in 28 Different Kinds of Cancer. J Nucl Med 60, 801–805. https://doi.org/10.2967/jnumed.119.227967

Lahiri, A., Maji, A., Potdar, P.D., Singh, N., Parikh, P., Bisht, B., Mukherjee, A., Paul, M.K., 2023. Lung cancer immunotherapy: progress, pitfalls, and promises. Mol Cancer 22, 40. https://doi.org/10.1186/s12943-023-01740-y

Larson, M.M., 2009. Ultrasound of the Thorax (Noncardiac). Veterinary Clinics of North America: Small Animal Practice, New Concepts in Diagnostic Radiology 39, 733–745. https://doi.org/10.1016/j.cvsm.2009.04.006

Laurila, H.P., Rajamäki, M.M., 2020a. Update on Canine Idiopathic Pulmonary Fibrosis in West Highland White Terriers. Vet Clin North Am Small Anim Pract 50, 431–446. https://doi.org/10.1016/j.cvsm.2019.11.004

Laurila, H.P., Rajamäki, M.M., 2020b. Update on Canine Idiopathic Pulmonary Fibrosis in West Highland White Terriers. Veterinary Clinics of North America: Small Animal Practice, Canine and Feline Respiratory Medicine: An Update 50, 431–446. https://doi.org/10.1016/j.cvsm.2019.11.004

Lavis, P., Pingitore, J., Doumont, G., Garabet, A., Van Simaeys, G., Lacroix, S., Passon, N., Van Heymbeek, C., De Maeseneire, C., Allard, J., Collin, A., Huaux, F., Decaestecker, C., Salmon, I., Goldman, S., Cardozo, A.K., Bondue, B., 2023. Usefulness of FAPα assessment in bronchoalveolar lavage as a marker of fibrogenesis: results of a preclinical study and first report

in patients with idiopathic pulmonary fibrosis. Respir Res 24, 254. https://doi.org/10.1186/s12931-023-02556-6

Leader, A.M., Grout, J.A., Maier, B.B., Nabet, B.Y., Park, M.D., Tabachnikova, A., Chang, C., Walker, L., Lansky, A., Le Berichel, J., Troncoso, L., Malissen, N., Davila, M., Martin, J.C., Magri, G., Tuballes, K., Zhao, Z., Petralia, F., Samstein, R., D'Amore, N.R., Thurston, G., Kamphorst, A.O., Wolf, A., Flores, R., Wang, P., Müller, S., Mellman, I., Beasley, M.B., Salmon, H., Rahman, A.H., Marron, T.U., Kenigsberg, E., Merad, M., 2021. Single-cell analysis of human non-small cell lung cancer lesions refines tumor classification and patient stratification. Cancer Cell 39, 1594-1609.e12. https://doi.org/10.1016/j.ccell.2021.10.009

LeBlanc, A.K., Morandi, F., 2014. Invited review--Off-site PET imaging programs: challenges and opportunities. Vet Radiol Ultrasound 55, 109–112. https://doi.org/10.1111/vru.12103

LeBlanc, A.K., Peremans, K., 2014. PET and SPECT Imaging in Veterinary Medicine. Seminars in Nuclear Medicine, Veterinary Nuclear Medicine 44, 47–56. https://doi.org/10.1053/j.semnuclmed.2013.08.004

Lee, B.M., Clarke, D., Watson, M., Laver, T., 2020. Retrospective evaluation of a modified human lung cancer stage classification in dogs with surgically excised primary pulmonary carcinomas. Veterinary and Comparative Oncology 18, 590–598. https://doi.org/10.1111/vco.12582

Lee, I.K., Noguera-Ortega, E., Xiao, Z., Todd, L., Scholler, J., Song, D., Liousia, M., Lohith, K., Xu, K., Edwards, K.J., Farwell, M.D., June, C.H., Albelda, S.M., Puré, E., Sellmyer, M.A., 2022. Monitoring Therapeutic Response to Anti-FAP CAR T Cells Using [18F]AlF-FAPI-74. Clin Cancer Res 28, 5330–5342. https://doi.org/10.1158/1078-0432.CCR-22-1379

Lee, K.N., Jackson, K.W., Christiansen, V.J., Chung, K.H., McKee, P.A., 2004. A novel plasma proteinase potentiates α2-antiplasmin inhibition of fibrin digestion. Blood 103, 3783–3788. https://doi.org/10.1182/blood-2003-12-4240

Lee, K.N., Jackson, K.W., Christiansen, V.J., Lee, C.S., Chun, J.-G., McKee, P.A., 2006. Antiplasmin-cleaving enzyme is a soluble form of fibroblast activation protein. Blood 107, 1397–1404. https://doi.org/10.1182/blood-2005-08-3452

Levy, M., McCaughan, G., Marinos, G., Gorrell, M., 2002. Intrahepatic expression of the hepatic stellate cell marker fibroblast activation protein correlates with the degree of fibrosis in hepatitis C virus infection. Liver 22, 93–101. https://doi.org/10.1034/j.1600-0676.2002.01503.x

Li, E., Cheung, H.C. (Zoey), Ma, S., 2024. CTHRC1+ fibroblasts and SPP1+ macrophages synergistically contribute to pro-tumorigenic tumor microenvironment in pancreatic ductal adenocarcinoma. Sci Rep 14, 17412. https://doi.org/10.1038/s41598-024-68109-z

Li, L., Gao, J., Chen, B.-X., Liu, X., Shi, L., Wang, Yanjiang, Wang, L., Wang, Yidan, Su, P., Yang, M.-F., Xie, B., 2023. Fibroblast activation protein imaging in atrial fibrillation: a proof-of-concept study. Journal of Nuclear Cardiology 30, 2712–2720. https://doi.org/10.1007/s12350-023-03352-x

Liao, Y., Ni, Y., He, R., Liu, W., Du, J., 2013. Clinical implications of fibroblast activation protein-α in non-small cell lung cancer after curative resection: a new predictor for prognosis. J Cancer Res Clin Oncol 139, 1523–1528. https://doi.org/10.1007/s00432-013-1471-8

Liao, Y., Xing, S., Xu, B., Liu, W., Zhang, G., 2017. Evaluation of the circulating level of fibroblast activation protein α for diagnosis of esophageal squamous cell carcinoma. Oncotarget 8, 30050–30062. https://doi.org/10.18632/oncotarget.16274

Liegeois, M., Legrand, C., Desmet, C.J., Marichal, T., Bureau, F., 2018. The interstitial macrophage: A long-neglected piece in the puzzle of lung immunity. Cellular Immunology, Special Issue: A Tissue Macrophage Compendium 330, 91–96. https://doi.org/10.1016/j.cellimm.2018.02.001

Lilja-Maula, L., Syrjä, P., Laurila, H.P., Sutinen, E., Palviainen, M., Ritvos, O., Koli, K., Rajamäki, M.M., Myllärniemi, M., 2015. Upregulation of alveolar levels of activin B, but not activin A, in lungs of west highland white terriers with idiopathic pulmonary fibrosis and diffuse alveolar damage. J Comp Pathol 152, 192–200. https://doi.org/10.1016/j.jcpa.2014.11.006

Lilja-Maula, L., Syrjä, P., Laurila, H.P., Sutinen, E., Rönty, M., Koli, K., Rajamäki, M.M., Myllärniemi, M., 2014. Comparative study of transforming growth factor-β signalling and regulatory molecules in human and canine idiopathic pulmonary fibrosis. J Comp Pathol 150, 399–407. https://doi.org/10.1016/j.jcpa.2013.12.001

Lilja-Maula, L.I.O., Laurila, H.P., Syrjä, P., Lappalainen, A.K., Krafft, E., Clercx, C., Rajamäki, M.M., 2014. Long-term outcome and use of 6-minute walk test in West Highland White Terriers with idiopathic pulmonary fibrosis. J Vet Intern Med 28, 379–385. https://doi.org/10.1111/jvim.12281

Liu, F., Qi, L., Liu, B., Liu, J., Zhang, H., Che, D., Cao, J., Shen, J., Geng, J., Bi, Y., Ye, L., Pan, B., Yu, Y., 2015. Fibroblast Activation Protein Overexpression and Clinical Implications in Solid Tumors: A Meta-Analysis. PLoS One 10, e0116683. https://doi.org/10.1371/journal.pone.0116683

Liu, S., Liu, C., Wang, Q., Liu, Suosi, Min, J., 2023. CC Chemokines in Idiopathic Pulmonary Fibrosis: Pathogenic Role and Therapeutic Potential. Biomolecules 13, 333. https://doi.org/10.3390/biom13020333

Liu, Y., Chen, P., Wang, H., Wu, S., Zhao, S., He, Y., Zhou, C., Hirsch, F.R., 2021. The landscape of immune checkpoints expression in non-small cell lung cancer: a narrative review. Transl Lung Cancer Res 10, 1029–1038. https://doi.org/10.21037/tlcr-20-1019

Liu, Y.-J., Du, J., Li, J., Tan, X.-P., Zhang, Q., 2023. CTHRC1, a novel gene with multiple functions in physiology, disease and solid tumors (Review). Oncol Lett 25, 266. https://doi.org/10.3892/ol.2023.13852

Lobetti, R.G., Milner, R., Lane, E., 2001. Chronic idiopathic pulmonary fibrosis in five dogs. J Am Anim Hosp Assoc 37, 119–127. https://doi.org/10.5326/15473317-37-2-119

Lohr, M., Edlund, K., Botling, J., Hammad, S., Hellwig, B., Othman, A., Berglund, A., Lambe, M., Holmberg, L., Ekman, S., Bergqvist, M., Pontén, F., Cadenas, C., Marchan, R., Hengstler, J.G., Rahnenführer, J., Micke, P., 2013. The prognostic relevance of tumour-infiltrating plasma cells and immunoglobulin kappa C indicates an important role of the humoral immune response in non-small cell lung cancer. Cancer Lett 333, 222–228. https://doi.org/10.1016/j.canlet.2013.01.036

LoPiccolo, J., Gusev, A., Christiani, D.C., Jänne, P.A., 2024. Lung cancer in patients who have never smoked - an emerging disease. Nat Rev Clin Oncol 21, 121–146. https://doi.org/10.1038/s41571-023-00844-0

Lorch, G., Sivaprakasam, K., Zismann, V., Perdigones, N., Contente-Cuomo, T., Nazareno, A., Facista, S., Wong, S., Drenner, K., Liang, W.S., Amann, J.M., Sinicropi-Yao, S.L., Koenig, M.J., La Perle, K., Whitsett, T.G., Murtaza, M., Trent, J.M., Carbone, D.P., Hendricks, W.P.D., 2019. Identification of Recurrent Activating HER2 Mutations in Primary Canine Pulmonary Adenocarcinoma. Clinical Cancer Research 25, 5866–5877. https://doi.org/10.1158/1078-0432.CCR-19-1145

Love, M.I., Huber, W., Anders, S., 2014. Moderated estimation of fold change and dispersion for RNA-seq data with DESeq2. Genome Biol 15, 550. https://doi.org/10.1186/s13059-014-0550-8

Lv, B., Xie, F., Zhao, P., Ma, X., Jiang, W.G., Yu, J., Zhang, X., Jia, J., 2016. Promotion of Cellular Growth and Motility Is Independent of Enzymatic Activity of Fibroblast Activation Protein-α. Cancer Genomics Proteomics 13, 201–208.

Määttä, M., Laurila, H.P., Holopainen, S., Aaltonen, K., Lilja-Maula, L., Viitanen, S., Rajamäki, M.M., 2021. Matrix metalloproteinase-2, -7, and -9 activities in dogs with idiopathic pulmonary fibrosis compared to healthy dogs and dogs with other respiratory diseases. J Vet Intern Med 35, 462–471. https://doi.org/10.1111/jvim.15970

Määttä, O.L.M., Laurila, H.P., Holopainen, S., Lilja-Maula, L., Melamies, M., Viitanen, S.J., Johnson, L.R., Koho, N., Neuvonen, M., Niemi, M., Rajamäki, M.M., 2018. Reflux aspiration in lungs of dogs with respiratory disease and in healthy West Highland White Terriers. J Vet Intern Med 32, 2074–2081. https://doi.org/10.1111/jvim.15321

Macosko, E.Z., Basu, A., Satija, R., Nemesh, J., Shekhar, K., Goldman, M., Tirosh, I., Bialas, A.R., Kamitaki, N., Martersteck, E.M., Trombetta, J.J., Weitz, D.A., Sanes, J.R., Shalek, A.K., Regev, A., McCarroll, S.A., 2015. Highly Parallel Genome-wide Expression Profiling of Individual Cells Using Nanoliter Droplets. Cell 161, 1202–1214. https://doi.org/10.1016/j.cell.2015.05.002

Madissoon, E., Oliver, A.J., Kleshchevnikov, V., Wilbrey-Clark, A., Polanski, K., Richoz, N., Ribeiro Orsi, A., Mamanova, L., Bolt, L., Elmentaite, R., Pett, J.P., Huang, N., Xu, C., He, P., Dabrowska, M., Pritchard, S., Tuck, L., Prigmore, E., Perera, S., Knights, A., Oszlanczi, A., Hunter, A., Vieira, S.F., Patel, M., Lindeboom, R.G.H., Campos, L.S., Matsuo, K., Nakayama, T., Yoshida, M., Worlock, K.B., Nikolić, M.Z., Georgakopoulos, N., Mahbubani, K.T., Saeb-Parsy, K., Bayraktar, O.A., Clatworthy, M.R., Stegle, O., Kumasaka, N., Teichmann, S.A., Meyer, K.B., 2023. A spatially resolved atlas of the human lung characterizes a gland-associated immune niche. Nat Genet 55, 66–77. https://doi.org/10.1038/s41588-022-01243-4

Maher, R.E., Määttä, M., Beynon, R.J., Laurila, H.P., McNamara, P.S., Rajamäki, M.M., 2022. Quantitative proteomic analysis of bronchoalveolar lavage fluid in West Highland white terriers with canine idiopathic pulmonary fibrosis. BMC Vet Res 18, 121. https://doi.org/10.1186/s12917-022-03202-x

Maitz, C.A., Tate, D., Bechtel, S., Lunceford, J., Henry, C., Flesner, B., Collins, A., Varterasian, M., Tung, D., Zhang, L., Saha, S., Bryan, J.N., 2022. Paired 18F-Fluorodeoxyglucose (18F-FDG), and 64Cu-Copper(II)-diacetyl-bis(N(4)-methylthiosemicarbazone) (64Cu-ATSM) PET Scans in Dogs with Spontaneous Tumors and Evaluation for Hypoxia-Directed Therapy. Radiat Res 197, 253–260. https://doi.org/10.1667/RADE-20-00186.1

Malhotra, J., Malvezzi, M., Negri, E., Vecchia, C.L., Boffetta, P., 2016. Risk factors for lung cancer worldwide. European Respiratory Journal 48, 889–902. https://doi.org/10.1183/13993003.00359-2016

Manchester, A.C., Ammons, D.T., Lappin, M.R., Dow, S., 2024. Single cell transcriptomic analysis of the canine duodenum in chronic inflammatory enteropathy and health. Front Immunol 15, 1397590. https://doi.org/10.3389/fimmu.2024.1397590

Marcinowska, A., Horta, R.D.S., Queiroga, F., Giuliano, A., 2025. Canine lung carcinoma—A descriptive review. Front. Vet. Sci. 11. https://doi.org/10.3389/fvets.2024.1464659

Mariotti, E.T., Premanandan, C., Lorch, G., 2014. Canine pulmonary adenocarcinoma tyrosine kinase receptor expression and phosphorylation. BMC Veterinary Research 10, 19. https://doi.org/10.1186/1746-6148-10-19

Marlowe, K.W., Robat, C.S., Clarke, D.M., Taylor, A., Touret, M., Husbands, B.D., Vail, D.M., 2018. Primary pulmonary histiocytic sarcoma in dogs: A retrospective analysis of 37 cases (2000-2015). Vet Comp Oncol 16, 658–663. https://doi.org/10.1111/vco.12437

Marolf, A.J., Gibbons, D.S., Podell, B.K., Park, R.D., 2011. Computed tomographic appearance of primary lung tumors in dogs. Veterinary Radiology & Ultrasound 52, 168–172. https://doi.org/10.1111/j.1740-8261.2010.01759.x

Martin, T.W., LaRue, S.M., Griffin, L., Leary, D., Boss, M.-K., 2023. Retrospective study evaluating the efficacy of stereotactic body radiation therapy for the treatment of confirmed or suspected primary pulmonary carcinomas in dogs. Veterinary and Comparative Oncology 21, 656–664. https://doi.org/10.1111/vco.12928

Matsubara, E., Yano, H., Pan, C., Komohara, Y., Fujiwara, Y., Zhao, S., Shinchi, Y., Kurotaki, D., Suzuki, M., 2023. The Significance of SPP1 in Lung Cancers and Its Impact as a Marker for Protumor Tumor-Associated Macrophages. Cancers (Basel) 15, 2250. https://doi.org/10.3390/cancers15082250

Mayhew, P.D., Hunt, G.B., Steffey, M.A., Culp, W.T.N., Mayhew, K.N., Fuller, M., Johnson, L.R., Pascoe, P.J., 2013. Evaluation of short-term outcome after lung lobectomy for resection of primary lung tumors via video-assisted thoracoscopic surgery or open thoracotomy in medium- to large-breed dogs. J Am Vet Med Assoc 243, 681–688. https://doi.org/10.2460/javma.243.5.681

McNiel, E.A., Ogilvie, G.K., Powers, B.E., Hutchison, J.M., Salman, M.D., Withrow, S.J., 1997. Evaluation of prognostic factors for dogs with primary lung tumors: 67 cases (1985-1992). J Am Vet Med Assoc 211, 1422–1427.

McPhetridge, J.B., Scharf, V.F., Regier, P.J., Toth, D., Lorange, M., Tremolada, G., Dornbusch, J.A., Selmic, L.E., Bae, S., Townsend, K.L., McAdoo, J.C., Thieman, K.M., Solari, F., Walton, R.A., Romeiser, J., Tuohy, J.L., Oblak, M.L., 2021. Distribution of histopathologic types of primary

pulmonary neoplasia in dogs and outcome of affected dogs: 340 cases (2010-2019). J Am Vet Med Assoc 260, 234–243. https://doi.org/10.2460/javma.20.12.0698

Mercier, E., Bolognin, M., Hoffmann, A.C., Tual, C., Day, M.J., Clercx, C., 2011. Influence of age on bronchoscopic findings in healthy beagle dogs. The Veterinary Journal 187, 225–228. https://doi.org/10.1016/j.tvjl.2009.12.007

Meyer, M.-L., Fitzgerald, B.G., Paz-Ares, L., Cappuzzo, F., Jänne, P.A., Peters, S., Hirsch, F.R., 2024. New promises and challenges in the treatment of advanced non-small-cell lung cancer. Lancet 404, 803–822. https://doi.org/10.1016/S0140-6736(24)01029-8

Milner, J.M., Kevorkian, L., Young, D.A., Jones, D., Wait, R., Donell, S.T., Barksby, E., Patterson, A.M., Middleton, J., Cravatt, B.F., Clark, I.M., Rowan, A.D., Cawston, T.E., 2006. Fibroblast activation protein alpha is expressed by chondrocytes following a pro-inflammatory stimulus and is elevated in osteoarthritis. Arthritis Research & Therapy 8, R23. https://doi.org/10.1186/ar1877

Mori, Y., Kramer, V., Novruzov, E., Mamlins, E., Röhrich, M., Fernández, R., Amaral, H., Soza-Ried, C., Monje, B., Sabbagh, E., Florenzano, M., Giesel, F.L., Undurraga, Á., 2024. Initial results with [18F]FAPI-74 PET/CT in idiopathic pulmonary fibrosis. Eur J Nucl Med Mol Imaging 51, 1605–1611. https://doi.org/10.1007/s00259-023-06564-y

Mori, Y., Kramer, V., Novruzov, E., Mamlins, E., Röhrich, M., Fernández, R., Amaral, H., Soza-Ried, C., Monje, B., Sabbagh, E., Florenzano, M., Giesel, F.L., Undurraga, Á., 2023. Initial results with [18F]FAPI-74 PET/CT in idiopathic pulmonary fibrosis. Eur J Nucl Med Mol Imaging. https://doi.org/10.1007/s00259-023-06564-y

Morse, C., Tabib, T., Sembrat, J., Buschur, K.L., Bittar, H.T., Valenzi, E., Jiang, Y., Kass, D.J., Gibson, K., Chen, W., Mora, A., Benos, P.V., Rojas, M., Lafyatis, R., 2019. Proliferating SPP1/MERTK-expressing macrophages in idiopathic pulmonary fibrosis. European Respiratory Journal 54. https://doi.org/10.1183/13993003.02441-2018

Mu, X., Mo, B., Qin, J., Li, Z., Chong, W., Zeng, Y., Lu, L., Zhang, L., Fu, W., 2023. Comparative analysis of two timepoints on [18F]FAPI-42 PET/CT in various cancers. Eur J Hybrid Imaging 7, 27. https://doi.org/10.1186/s41824-023-00186-1

Nakamoto, Y., Baba, S., Kaida, H., Manabe, O., Uehara, T., 2024. Recent topics in fibroblast activation protein inhibitor-PET/CT: clinical and pharmacological aspects. Ann Nucl Med 38, 10–19. https://doi.org/10.1007/s12149-023-01873-6

Narvaez Del Pilar, O., Gacha Garay, M.J., Chen, J., 2022. Three-axis classification of mouse lung mesenchymal cells reveals two populations of myofibroblasts. Development 149, dev200081. https://doi.org/10.1242/dev.200081

Nemanic, S., London, C.A., Wisner, E.R., 2006. Comparison of Thoracic Radiographs and Single Breath-Hold Helical CT for Detection of Pulmonary Nodules in Dogs with Metastatic Neoplasia. Journal of Veterinary Internal Medicine 20, 508–515. https://doi.org/10.1111/j.1939-1676.2006.tb02889.x

Niinikoski, I., Kouki, S., Koho, N., Aromaa, M., Holopainen, S., Laurila, H.P., Fastrès, A., Clercx, C., Lilja-Maula, L., Rajamäki, M.M., 2022. Evaluation of VEGF-A and CCL2 in dogs with brachycephalic obstructive airway syndrome or canine idiopathic pulmonary fibrosis and in normocephalic dogs. Research in Veterinary Science 152. https://doi.org/10.1016/j.rvsc.2022.09.022

Norris, A.J., Naydan, D.K., Wilson, D.W., 2005. Interstitial lung disease in West Highland White Terriers. Vet Pathol 42, 35–41. https://doi.org/10.1354/vp.42-1-35

Norris, C.R., Griffey, S.M., Walsh, P., 2002. Use of keyhole lung biopsy for diagnosis of interstitial lung diseases in dogs and cats: 13 cases (1998-2001). J Am Vet Med Assoc 221, 1453–1459. https://doi.org/10.2460/javma.2002.221.1453

Ogilvie, G.K., Haschek, W.M., Withrow, S.J., Richardson, R.C., Harvey, H.J., Henderson, R.A., Fowler, J.D., Norris, A.M., Tomlinson, J., McCaw, D., 1989. Classification of primary lung tumors in dogs: 210 cases (1975-1985). J Am Vet Med Assoc 195, 106–108.

O'Neill, D.G., Ballantyne, Z.F., Hendricks, A., Church, D.B., Brodbelt, D.C., Pegram, C., 2019. West Highland White Terriers under primary veterinary care in the UK in 2016: demography, mortality and disorders. Canine Genetics and Epidemiology 6, 7. https://doi.org/10.1186/s40575-019-0075-2

Pacholec, C., Lisciandro, G.R., Masseau, I., Donnelly, L., DeClue, A., Reinero, C.R., 2021. Lung ultrasound nodule sign for detection of pulmonary nodule lesions in dogs: Comparison to thoracic radiography using computed tomography as the criterion standard. The Veterinary Journal 275, 105727. https://doi.org/10.1016/j.tvjl.2021.105727

Pang, J., Yu, Q., Chen, Y., Yuan, H., Sheng, M., Tang, W., 2022. Integrating Single-cell RNA-seq to construct a Neutrophil prognostic model for predicting immune responses in non-small cell lung cancer. J Transl Med 20, 531. https://doi.org/10.1186/s12967-022-03723-x

Paoloni, M., Khanna, C., 2008. Translation of new cancer treatments from pet dogs to humans. Nat Rev Cancer 8, 147–156. https://doi.org/10.1038/nrc2273

Paoloni, M.C., Adams, W.M., Dubielzig, R.R., Kurzman, I., Vail, D.M., Hardie, R.J., 2006. Comparison of results of computed tomography and radiography with histopathologic findings in tracheobronchial lymph nodes in dogs with primary lung tumors: 14 cases (1999-2002). J Am Vet Med Assoc 228, 1718–1722. https://doi.org/10.2460/javma.228.11.1718

Paoloni, M.C., Khanna, C., 2007. Comparative Oncology Today. Veterinary Clinics of North America: Small Animal Practice, State of the Art Veterinary Oncology 37, 1023–1032. https://doi.org/10.1016/j.cvsm.2007.08.003

Papalexi, E., Satija, R., 2018. Single-cell RNA sequencing to explore immune cell heterogeneity. Nat Rev Immunol 18, 35–45. https://doi.org/10.1038/nri.2017.76

Park, Y., Ahn, C., Kim, T.-H., 2021. Occupational and environmental risk factors of idiopathic pulmonary fibrosis: a systematic review and meta-analyses. Sci Rep 11, 4318. https://doi.org/10.1038/s41598-021-81591-z

Patel, V.I., Metcalf, J.P., 2018. Airway Macrophage and Dendritic Cell Subsets in the Resting Human Lung. Crit Rev Immunol 38, 303–331. https://doi.org/10.1615/CritRevImmunol.2018026459

Pelosof, L., Ahn, C., Gao, A., Horn, L., Madrigales, A., Cox, J., McGavic, D., Minna, J.D., Gazdar, A.F., Schiller, J., 2017. Proportion of Never-Smoker Non-Small Cell Lung Cancer Patients at Three Diverse Institutions. J Natl Cancer Inst 109, djw295. https://doi.org/10.1093/jnci/djw295

Peng, H., Wu, X., Liu, S., He, M., Xie, C., Zhong, R., Liu, J., Tang, C., Li, C., Xiong, S., Zheng, H., He, J., Lu, X., Liang, W., 2023. Multiplex immunofluorescence and single-cell transcriptomic profiling reveal the spatial cell interaction networks in the non-small cell lung cancer microenvironment. Clin Transl Med 13, e1155. https://doi.org/10.1002/ctm2.1155

Peyser, R., MacDonnell, S., Gao, Y., Cheng, L., Kim, Y., Kaplan, T., Ruan, Q., Wei, Y., Ni, M., Adler, C., Zhang, W., Devalaraja-Narashimha, K., Grindley, J., Halasz, G., Morton, L., 2019. Defining the Activated Fibroblast Population in Lung Fibrosis Using Single-Cell Sequencing. Am J Respir Cell Mol Biol 61, 74–85. https://doi.org/10.1165/rcmb.2018-0313OC

Piras, I.S., Bleul, C., Siniard, A., Wolfe, A.J., De Both, M.D., Hernandez, A.G., Huentelman, M.J., 2020. Association of Common Genetic Variants in the CPSF7 and SDHAF2 Genes with Canine Idiopathic Pulmonary Fibrosis in the West Highland White Terrier. Genes (Basel) 11, 609. https://doi.org/10.3390/genes11060609

Polton, G., Finotello, R., Sabattini, S., Rossi, F., Laganga, P., Vasconi, M.E., Barbanera, A., Stiborova, K., Rohrer Bley, C., Marconato, L., 2018. Survival analysis of dogs with advanced primary lung carcinoma treated by metronomic cyclophosphamide, piroxicam and thalidomide. Veterinary and Comparative Oncology 16, 399–408. https://doi.org/10.1111/vco.12393

Prior, T.S., Hoyer, N., Davidsen, J.R., Shaker, S.B., Hundahl, M.P., Lomholt, S., Deleuran, B.W., Bendstrup, E., Kragstrup, T.W., 2024. Fibroblast activation protein and disease severity, progression, and survival in idiopathic pulmonary fibrosis. Scand J Immunol 100, e13392. https://doi.org/10.1111/sji.13392

Privé, B.M., Boussihmad, M.A., Timmermans, B., van Gemert, W.A., Peters, S.M.B., Derks, Y.H.W., van Lith, S.A.M., Mehra, N., Nagarajah, J., Heskamp, S., Westdorp, H., 2023. Fibroblast activation protein-targeted radionuclide therapy: background, opportunities, and challenges of first (pre)clinical studies. Eur J Nucl Med Mol Imaging 50, 1906–1918. https://doi.org/10.1007/s00259-023-06144-0

Puré, E., Blomberg, R., 2018. Pro-tumorigenic roles of fibroblast activation protein in cancer: back to the basics. Oncogene 37, 4343–4357. https://doi.org/10.1038/s41388-018-0275-3

Qi, J., Sun, H., Zhang, Y., Wang, Z., Xun, Z., Li, Z., Ding, X., Bao, R., Hong, L., Jia, W., Fang, F., Liu, H., Chen, L., Zhong, J., Zou, D., Liu, L., Han, L., Ginhoux, F., Liu, Y., Ye, Y., Su, B., 2022. Single-cell and spatial analysis reveal interaction of FAP+ fibroblasts and SPP1+ macrophages in colorectal cancer. Nat Commun 13, 1742. https://doi.org/10.1038/s41467-022-29366-6

Raghu, G., Remy-Jardin, M., Richeldi, L., Thomson, C.C., Inoue, Y., Johkoh, T., Kreuter, M., Lynch, D.A., Maher, T.M., Martinez, F.J., Molina-Molina, M., Myers, J.L., Nicholson, A.G., Ryerson, C.J., Strek, M.E., Troy, L.K., Wijsenbeek, M., Mammen, M.J., Hossain, T., Bissell, B.D., Herman, D.D., Hon, S.M., Kheir, F., Khor, Y.H., Macrea, M., Antoniou, K.M., Bouros, D., Buendia-Roldan, I., Caro, F., Crestani, B., Ho, L., Morisset, J., Olson, A.L., Podolanczuk, A., Poletti, V., Selman, M., Ewing, T., Jones, S., Knight, S.L., Ghazipura, M., Wilson, K.C., 2022a. Idiopathic Pulmonary Fibrosis (an Update) and Progressive Pulmonary Fibrosis in Adults: An Official ATS/ERS/JRS/ALAT Clinical Practice Guideline. Am J Respir Crit Care Med 205, e18–e47. https://doi.org/10.1164/rccm.202202-0399ST

Raghu, G., Remy-Jardin, M., Richeldi, L., Thomson, C.C., Inoue, Y., Johkoh, T., Kreuter, M., Lynch, D.A., Maher, T.M., Martinez, F.J., Molina-Molina, M., Myers, J.L., Nicholson, A.G., Ryerson, C.J., Strek, M.E., Troy, L.K., Wijsenbeek, M., Mammen, M.J., Hossain, T., Bissell, B.D., Herman, D.D., Hon, S.M., Kheir, F., Khor, Y.H., Macrea, M., Antoniou, K.M., Bouros, D., Buendia-Roldan, I.,

Caro, F., Crestani, B., Ho, L., Morisset, J., Olson, A.L., Podolanczuk, A., Poletti, V., Selman, M., Ewing, T., Jones, S., Knight, S.L., Ghazipura, M., Wilson, K.C., 2022b. Idiopathic Pulmonary Fibrosis (an Update) and Progressive Pulmonary Fibrosis in Adults: An Official ATS/ERS/JRS/ALAT Clinical Practice Guideline. Am J Respir Crit Care Med 205, e18–e47. https://doi.org/10.1164/rccm.202202-0399ST

Ramos-Vara, J.A., Miller, M.A., Johnson, G.C., 2005. Usefulness of Thyroid Transcription Factor-1 Immunohistochemical Staining in the Differential Diagnosis of Primary Pulmonary Tumors of Dogs. Vet Pathol 42, 315–320. https://doi.org/10.1354/vp.42-3-315

Randall, E.K., 2016. PET-Computed Tomography in Veterinary Medicine. Vet Clin North Am Small Anim Pract 46, 515–533, vi. https://doi.org/10.1016/j.cvsm.2015.12.008

Rebhun, R.B., Culp, W.T.N., 2020. Tumors of the respiratory system, section D: pulmonary neoplasia, in: Withrow and MacEwen's Small Animal Clinical Oncology, 6th Edition. Elsevier, St. Louis, pp. 507–515.

Reck, M., Remon, J., Hellmann, M.D., 2022. First-Line Immunotherapy for Non-Small-Cell Lung Cancer. J Clin Oncol 40, 586–597. https://doi.org/10.1200/JCO.21.01497

Reichle, J.K., Wisner, E.R., 2000. Non-Cardiac Thoracic Ultrasound in 75 Feline and Canine Patients. Veterinary Radiology & Ultrasound 41, 154–162. https://doi.org/10.1111/j.1740-8261.2000.tb01470.x

Reif, J.S., Dunn, K., Ogilvie, G.K., Harris, C.K., 1992. Passive Smoking and Canine Lung Cancer Risk. American Journal of Epidemiology 135, 234–239. https://doi.org/10.1093/oxfordjournals.aje.a116276

Reinero, C., 2019a. Interstitial lung diseases in dogs and cats part I: The idiopathic interstitial pneumonias. The Veterinary Journal 243, 48–54. https://doi.org/10.1016/j.tvjl.2018.11.010

Reinero, C., 2019b. Interstitial lung diseases in dogs and cats part II: Known cause and other discrete forms. Vet J 243, 55–64. https://doi.org/10.1016/j.tvjl.2018.11.011

Reinero, C., Visser, L.C., Kellihan, H.B., Masseau, I., Rozanski, E., Clercx, C., Williams, K., Abbott, J., Borgarelli, M., Scansen, B.A., 2020. ACVIM consensus statement guidelines for the diagnosis, classification, treatment, and monitoring of pulmonary hypertension in dogs. Journal of Veterinary Internal Medicine 34, 549–573. https://doi.org/10.1111/jvim.15725

Remon, J., Soria, J.-C., Peters, S., ESMO Guidelines Committee. Electronic address: clinicalguidelines@esmo.org, 2021. Early and locally advanced non-small-cell lung cancer: an

update of the ESMO Clinical Practice Guidelines focusing on diagnosis, staging, systemic and local therapy. Ann Oncol 32, 1637–1642. https://doi.org/10.1016/j.annonc.2021.08.1994

Reyfman, P.A., Walter, J.M., Joshi, N., Anekalla, K.R., McQuattie-Pimentel, A.C., Chiu, S., Fernandez, R., Akbarpour, M., Chen, C.-I., Ren, Z., Verma, R., Abdala-Valencia, H., Nam, K., Chi, M., Han, S., Gonzalez-Gonzalez, F.J., Soberanes, S., Watanabe, S., Williams, K.J.N., Flozak, A.S., Nicholson, T.T., Morgan, V.K., Winter, D.R., Hinchcliff, M., Hrusch, C.L., Guzy, R.D., Bonham, C.A., Sperling, A.I., Bag, R., Hamanaka, R.B., Mutlu, G.M., Yeldandi, A.V., Marshall, S.A., Shilatifard, A., Amaral, L.A.N., Perlman, H., Sznajder, J.I., Argento, A.C., Gillespie, C.T., Dematte, J., Jain, M., Singer, B.D., Ridge, K.M., Lam, A.P., Bharat, A., Bhorade, S.M., Gottardi, C.J., Budinger, G.R.S., Misharin, A.V., 2019. Single-Cell Transcriptomic Analysis of Human Lung Provides Insights into the Pathobiology of Pulmonary Fibrosis. Am J Respir Crit Care Med 199, 1517–1536. https://doi.org/10.1164/rccm.201712-2410OC

Rick, T., Kleiter, M., Schwendenwein, I., Ludewig, E., Reifinger, M., Hittmair, K.M., 2019. Contrast-enhanced ultrasonography characteristics of intrathoracic mass lesions in 36 dogs and 24 cats. Veterinary Radiology & Ultrasound 60, 56–64. https://doi.org/10.1111/vru.12698

Rinaldi, V., Finotello, R., Boari, A., Cabibbo, E., Crisi, P.E., 2023. Vinorelbine as First-Line Treatment in Stage IV Canine Primary Pulmonary Carcinoma. Vet Sci 10, 664. https://doi.org/10.3390/vetsci10120664

Rizzoli, E., de Meeûs d'Argenteuil, C., Fastrès, A., Roels, E., Janssen, P., Puré, E., Garigliany, M.-M., Marichal, T., Clercx, C., 2024. Fibroblast activation protein is a cellular marker of fibrotic activity in canine idiopathic pulmonary fibrosis. Front Vet Sci 11, 1416124. https://doi.org/10.3389/fvets.2024.1416124

Rizzoli, E., Fievez, L., Fastrès, A., Roels, E., Marichal, T., Clercx, C., 2025. A single-cell RNA sequencing atlas of the healthy canine lung: a foundation for comparative studies. Front Immunol 16, 1501603. https://doi.org/10.3389/fimmu.2025.1501603

Roberts, E.W., Deonarine, A., Jones, J.O., Denton, A.E., Feig, C., Lyons, S.K., Espeli, M., Kraman, M., McKenna, B., Wells, R.J.B., Zhao, Q., Caballero, O.L., Larder, R., Coll, A.P., O'Rahilly, S., Brindle, K.M., Teichmann, S.A., Tuveson, D.A., Fearon, D.T., 2013. Depletion of stromal cells expressing fibroblast activation protein-α from skeletal muscle and bone marrow results in cachexia and anemia. Journal of Experimental Medicine 210, 1137–1151. https://doi.org/10.1084/jem.20122344

Roels, E., Bauer, N., Lecut, C., Moritz, A., Gothot, A., Clercx, C., 2019. Haemostatic, fibrinolytic and inflammatory profiles in West Highland white terriers with canine idiopathic

pulmonary fibrosis and controls. BMC Vet Res 15, 379. https://doi.org/10.1186/s12917-019-2134-z

Roels, E., Coralie, B., Laurence, M., Minna, R., Jessica, T., Vanessa, B., Clercx, C., 2022. Pan-Fungal Polymerase Chain Reaction and Fungal Precipitins Assays in West Highland White Terriers with Canine Idiopathic Pulmonary Fibrosis. Journal of Veterinary Medicine and Animal Sciences 5.

Roels, E., Couvreur, T., Farnir, F., Clercx, C., Verschakelen, J., Bolen, G., 2017. Comparison Between Sedation and General Anesthesia for High Resolution Computed Tomographic Characterization of Canine Idiopathic Pulmonary Fibrosis in West Highland White Terriers. Veterinary Radiology & Ultrasound 58, 284–294. https://doi.org/10.1111/vru.12481

Roels, E., Dourcy, M., Holopainen, S., Rajamäki, M.M., Gillet, L., Ehlers, B., Clercx, C., 2016. No Evidence of Herpesvirus Infection in West Highland White Terriers With Canine Idiopathic Pulmonary Fibrosis. Vet Pathol 53, 1210–1212. https://doi.org/10.1177/0300985816641991

Roels, E., Fastrès, A., McGeown, Gommeren, K., Saegerman, C., Clercx, C., 2018. A questionnaire-based survey of owner-reported environment and care of West Highland white Terrier with or without idiopathic pulmonary fibrosis. Presented at the 28th ECVIM-CA congress.

Roels, E., Fastrès, A., Merveille, A.-C., Bolen, G., Teske, E., Clercx, C., Mc Entee, K., 2021. The prevalence of pulmonary hypertension assessed using the pulmonary vein-to-right pulmonary artery ratio and its association with survival in West Highland white terriers with canine idiopathic pulmonary fibrosis. BMC Veterinary Research 17, 171. https://doi.org/10.1186/s12917-021-02879-w

Roels, E., Fastrès, A., Rizzoli, E., Clercx, C., Merveille, A.-C., 2024. Observational Longitudinal Study of Pulmonary Hypertension in West Highland White Terriers Affected With Canine Idiopathic Pulmonary Fibrosis, in: Journal of Veterinary Internal Medicine. Presented at the 34th Annual ECVIM-CA Congress.

Roels, Elodie, Holopainen, S., Teske, E., Allerton, F., Bomassi, E., Damoiseaux, C., De Lorenzi, D., Fisher, A., Muller, N., Hendrickx, T., Vrancken, A., Rajamäki, M.M., Clercx, C., 2015a. Chemokine (CC-motif) ligand 2 as a prognostic serum marker in canine idiopathic pulmonary fibrosis. Presented at the ECVIM-CA Congress 2015.

Roels, E., Krafft, E., Antoine, N., Farnir, F., Laurila, H.P., Holopainen, S., Rajamäki, M.M., Clercx, C., 2015. Evaluation of chemokines CXCL8 and CCL2, serotonin, and vascular endothelial growth factor serum concentrations in healthy dogs from seven breeds with variable

predisposition for canine idiopathic pulmonary fibrosis. Res Vet Sci 101, 57–62. https://doi.org/10.1016/j.rvsc.2015.05.020

Roels, Elodie, Krafft, E., Farnir, F., Holopainen, S., Laurila, H.P., Rajamäki, M.M., Day, M.J., Antoine, N., Pirottin, D., Clercx, C., 2015b. Assessment of CCL2 and CXCL8 chemokines in serum, bronchoalveolar lavage fluid and lung tissue samples from dogs affected with canine idiopathic pulmonary fibrosis. The Veterinary Journal 206, 75–82. https://doi.org/10.1016/j.tvjl.2015.06.001

Röhrich, M., Leitz, D., Glatting, F.M., Wefers, A.K., Weinheimer, O., Flechsig, P., Kahn, N., Mall, M.A., Giesel, F.L., Kratochwil, C., Huber, P.E., Deimling, A. von, Heußel, C.P., Kauczor, H.U., Kreuter, M., Haberkorn, U., 2022. Fibroblast Activation Protein-Specific PET/CT Imaging in Fibrotic Interstitial Lung Diseases and Lung Cancer: A Translational Exploratory Study. J Nucl Med 63, 127–133. https://doi.org/10.2967/jnumed.121.261925

Rose, R.J., Worley, D.R., 2020. A Contemporary Retrospective Study of Survival in Dogs With Primary Lung Tumors: 40 Cases (2005–2017). Front. Vet. Sci. 7. https://doi.org/10.3389/fvets.2020.519703

Rosenkrans, Z.T., Massey, C.F., Bernau, K., Ferreira, C.A., Jeffery, J.J., Schulte, J.J., Moore, M., Valla, F., Batterton, J.M., Drake, C.R., McMillan, A.B., Sandbo, N., Pirasteh, A., Hernandez, R., 2022. [68 Ga]Ga-FAPI-46 PET for non-invasive detection of pulmonary fibrosis disease activity. Eur J Nucl Med Mol Imaging 49, 3705–3716. https://doi.org/10.1007/s00259-022-05814-9

Rovedatti, L., Di Sabatino, A., Knowles, C.H., Sengupta, N., Biancheri, P., Corazza, G.R., MacDonald, T.T., 2011. Fibroblast activation protein expression in Crohn's disease strictures. Inflammatory Bowel Diseases 17, 1251–1253. https://doi.org/10.1002/ibd.21446

Roza, M.R., Viegas, C.A.A., 2007. The Dog as a Passive Smoker: Effects of Exposure to Environmental Cigarette Smoke on Domestic Dogs. Nicotine & Tobacco Research 9, 1171–1176. https://doi.org/10.1080/14622200701648391

Ruby, J., Secrest, S., Sharma, A., 2020. Radiographic differentiation of mediastinal versus pulmonary masses in dogs and cats can be challenging. Veterinary Radiology & Ultrasound 61, 385–393. https://doi.org/10.1111/vru.12859

Sabattini, S., Mancini, F.R., Marconato, L., Bacci, B., Rossi, F., Vignoli, M., Bettini, G., 2014. EGFR overexpression in canine primary lung cancer: pathogenetic implications and impact on survival. Vet Comp Oncol 12, 237–248. https://doi.org/10.1111/vco.12002

Salcher, S., Sturm, G., Horvath, L., Untergasser, G., Kuempers, C., Fotakis, G., Panizzolo, E., Martowicz, A., Trebo, M., Pall, G., Gamerith, G., Sykora, M., Augustin, F., Schmitz, K., Finotello, F.,

Rieder, D., Perner, S., Sopper, S., Wolf, D., Pircher, A., Trajanoski, Z., 2022. High-resolution single-cell atlas reveals diversity and plasticity of tissue-resident neutrophils in non-small cell lung cancer. Cancer Cell 40, 1503-1520.e8. https://doi.org/10.1016/j.ccell.2022.10.008

Salisbury, M.L., Tolle, L.B., Xia, M., Murray, S., Tayob, N., Nambiar, A.M., Schmidt, S.L., Lagstein, A., Myers, J.L., Gross, B.H., Kazerooni, E.A., Sundaram, B., Chughtai, A.R., Martinez, F.J., Flaherty, K.R., 2017. Possible UIP pattern on high-resolution computed tomography is associated with better survival than definite UIP in IPF patients. Respir Med 131, 229–235. https://doi.org/10.1016/j.rmed.2017.08.025

Salomon, R., Kaczorowski, D., Valdes-Mora, F., Nordon, R.E., Neild, A., Farbehi, N., Bartonicek, N., Gallego-Ortega, D., 2019. Droplet-based single cell RNAseq tools: a practical guide. Lab Chip 19, 1706–1727. https://doi.org/10.1039/c8lc01239c

Schilder, B., Skene, N., 2022. orthogene: an R package for easy mapping of orthologous genes across hundreds of species. Bioconductor.

Schober, K.E., Baade, H., 2006. Doppler Echocardiographic Prediction of Pulmonary Hypertension in West Highland White Terriers with Chronic Pulmonary Disease. Journal of Veterinary Internal Medicine 20, 912–920. https://doi.org/10.1111/j.1939-1676.2006.tb01805.x

Schupp, J.C., Adams, T.S., Cosme, C., Raredon, M.S.B., Yuan, Y., Omote, N., Poli, S., Chioccioli, M., Rose, K.-A., Manning, E.P., Sauler, M., DeIuliis, G., Ahangari, F., Neumark, N., Habermann, A.C., Gutierrez, A.J., Bui, L.T., Lafyatis, R., Pierce, R.W., Meyer, K.B., Nawijn, M.C., Teichmann, S.A., Banovich, N.E., Kropski, J.A., Niklason, L.E., Pe'er, D., Yan, X., Homer, R.J., Rosas, I.O., Kaminski, N., 2021. Integrated Single-Cell Atlas of Endothelial Cells of the Human Lung. Circulation 144, 286–302. https://doi.org/10.1161/CIRCULATIONAHA.120.052318

Schyns, J., Bai, Q., Ruscitti, C., Radermecker, C., De Schepper, S., Chakarov, S., Farnir, F., Pirottin, D., Ginhoux, F., Boeckxstaens, G., Bureau, F., Marichal, T., 2019. Non-classical tissue monocytes and two functionally distinct populations of interstitial macrophages populate the mouse lung. Nat Commun 10, 3964. https://doi.org/10.1038/s41467-019-11843-0

See, P., Lum, J., Chen, J., Ginhoux, F., 2018. A Single-Cell Sequencing Guide for Immunologists. Front Immunol 9, 2425. https://doi.org/10.3389/fimmu.2018.02425

Seiler, S.M.F., Baumgartner, C., Hirschberger, J., Beer, A.J., Brühschwein, A., Kreutzmann, N., Laberke, S., Wergin, M.C., Meyer-Lindenberg, A., Brandl, J., Thaden, A.-K. von, Farrell, E., Schwaiger, M., 2015. Comparative Oncology: Evaluation of 2-Deoxy-2-[18F]fluoro-D-glucose

(FDG) Positron Emission Tomography/Computed Tomography (PET/CT) for the Staging of Dogs with Malignant Tumors. PLOS ONE 10, e0127800. https://doi.org/10.1371/journal.pone.0127800

Selman, M., Pardo, A., 2020. The leading role of epithelial cells in the pathogenesis of idiopathic pulmonary fibrosis. Cell Signal 66, 109482. https://doi.org/10.1016/j.cellsig.2019.109482

Sgalla, G., Iovene, B., Calvello, M., Ori, M., Varone, F., Richeldi, L., 2018. Idiopathic pulmonary fibrosis: pathogenesis and management. Respir Res 19, 32. https://doi.org/10.1186/s12931-018-0730-2

She, Y.X., Yu, Q.Y., Tang, X.X., 2021. Role of interleukins in the pathogenesis of pulmonary fibrosis. Cell Death Discov. 7, 1–10. https://doi.org/10.1038/s41420-021-00437-9

Shi, J., Hou, Z., Yan, J., Qiu, W., Liang, L., Meng, M., Li, L., Wang, X., Xie, Y., Jiang, L., Wang, W., 2020. The prognostic significance of fibroblast activation protein-α in human lung adenocarcinoma. Ann Transl Med 8, 224–224. https://doi.org/10.21037/atm.2020.01.82

Shi, T., Denney, L., An, H., Ho, L.-P., Zheng, Y., 2021. Alveolar and lung interstitial macrophages: Definitions, functions, and roles in lung fibrosis. Journal of Leukocyte Biology 110, 107–114. https://doi.org/10.1002/JLB.3RU0720-418R

Shi, X., Zhu, S., Liu, M., Stone, S.S., Rong, Y., Mao, K., Xu, X., Ma, C., Jiang, Z., Zha, Y., Yan, C., Yu, X., Wu, D., Liu, G., Mi, J., Zhao, J., Li, Y., Ding, Y., Wang, X., Zhang, Y.-B., Ji, X., 2022. Single-Cell RNA-Seq Reveals a Population of Smooth Muscle Cells Responsible for Atherogenesis. Aging Dis 13, 1939–1953. https://doi.org/10.14336/AD.2022.0313

Shiota, Y., Elbadawy, M., Suzuki, K., Tsunedomi, R., Nagano, H., Ishihara, Y., Yamamoto, H., Azakami, D., Uchide, T., Fukushima, R., Tanaka, R., Yoshida, T., Mori, T., Abugomaa, A., Kaneda, M., Yamawaki, H., Shinohara, Y., Aboubakr, M., El-Asrag, M.E., Usui, T., Sasaki, K., 2023. Derivation of a new model of lung adenocarcinoma using canine lung cancer organoids for translational research in pulmonary medicine. Biomedicine & Pharmacotherapy 165, 115079. https://doi.org/10.1016/j.biopha.2023.115079

Siegel, R.L., Giaquinto, A.N., Jemal, A., 2024. Cancer statistics, 2024. CA: A Cancer Journal for Clinicians 74, 12–49. https://doi.org/10.3322/caac.21820

Siegel, R.L., Miller, K.D., Wagle, N.S., Jemal, A., 2023. Cancer statistics, 2023. CA Cancer J Clin 73, 17–48. https://doi.org/10.3322/caac.21763

Sikkema, L., Ramírez-Suástegui, C., Strobl, D.C., Gillett, T.E., Zappia, L., Madissoon, E., Markov, N.S., Zaragosi, L.-E., Ji, Y., Ansari, M., Arguel, M.-J., Apperloo, L., Banchero, M., Bécavin,

C., Berg, M., Chichelnitskiy, E., Chung, M., Collin, A., Gay, A.C.A., Gote-Schniering, J., Hooshiar Kashani, B., Inecik, K., Jain, M., Kapellos, T.S., Kole, T.M., Leroy, S., Mayr, C.H., Oliver, A.J., von Papen, M., Peter, L., Taylor, C.J., Walzthoeni, T., Xu, C., Bui, L.T., De Donno, C., Dony, L., Faiz, A., Guo, M., Gutierrez, A.J., Heumos, L., Huang, N., Ibarra, I.L., Jackson, N.D., Kadur Lakshminarasimha Murthy, P., Lotfollahi, M., Tabib, T., Talavera-López, C., Travaglini, K.J., Wilbrey-Clark, A., Worlock, K.B., Yoshida, M., van den Berge, M., Bossé, Y., Desai, T.J., Eickelberg, O., Kaminski, N., Krasnow, M.A., Lafyatis, R., Nikolic, M.Z., Powell, J.E., Rajagopal, J., Rojas, M., Rozenblatt-Rosen, O., Seibold, M.A., Sheppard, D., Shepherd, D.P., Sin, D.D., Timens, W., Tsankov, A.M., Whitsett, J., Xu, Y., Banovich, N.E., Barbry, P., Duong, T.E., Falk, C.S., Meyer, K.B., Kropski, J.A., Pe'er, D., Schiller, H.B., Tata, P.R., Schultze, J.L., Teichmann, S.A., Misharin, A.V., Nawijn, M.C., Luecken, M.D., Theis, F.J., 2023. An integrated cell atlas of the lung in health and disease. Nat Med 29, 1563–1577. https://doi.org/10.1038/s41591-023-02327-2

Singh, C.K., Fernandez, S., Chhabra, G., Zaemisch, G.R., Nihal, A., Swanlund, J., Ansari, N., Said, Z., Chang, H., Ahmad, N., 2024. The role of collagen triple helix repeat containing 1 (CTHRC1) in cancer development and progression. Expert Opinion on Therapeutic Targets 28, 419–435. https://doi.org/10.1080/14728222.2024.2349686

Solano-Iturri, J.D., Beitia, M., Errarte, P., Calvete-Candenas, J., Etxezarraga, M.C., Loizate, A., Echevarria, E., Badiola, I., Larrinaga, G., 2020a. Altered expression of fibroblast activation protein-α (FAP) in colorectal adenoma-carcinoma sequence and in lymph node and liver metastases. Aging (Albany NY) 12, 10337–10358. https://doi.org/10.18632/aging.103261

Solano-Iturri, J.D., Errarte, P., Etxezarraga, M.C., Echevarria, E., Angulo, J., López, J.I., Larrinaga, G., 2020b. Altered Tissue and Plasma Levels of Fibroblast Activation Protein-α (FAP) in Renal Tumours. Cancers (Basel) 12, E3393. https://doi.org/10.3390/cancers12113393

Soliveres, E., Mc Entee, K., Couvreur, T., Fastrès, A., Roels, E., Merveille, A.-C., Tutunaru, A.-C., Clercx, C., Bolen, G., 2021. Utility of Computed Tomographic Angiography for Pulmonary Hypertension Assessment in a Cohort of West Highland White Terriers With or Without Canine Idiopathic Pulmonary Fibrosis. Front. Vet. Sci. 8, 732133. https://doi.org/10.3389/fvets.2021.732133

Stuart, T., Satija, R., 2019. Integrative single-cell analysis. Nat Rev Genet 20, 257–272. https://doi.org/10.1038/s41576-019-0093-7

Subramanian, A., Tamayo, P., Mootha, V.K., Mukherjee, S., Ebert, B.L., Gillette, M.A., Paulovich, A., Pomeroy, S.L., Golub, T.R., Lander, E.S., Mesirov, J.P., 2005. Gene set enrichment analysis: A knowledge-based approach for interpreting genome-wide expression profiles.

Proceedings of the National Academy of Sciences 102, 15545–15550. https://doi.org/10.1073/pnas.0506580102

Syrjä, P., Heikkilä, H.P., Lilja-Maula, L., Krafft, E., Clercx, C., Day, M.J., Rönty, M., Myllärniemi, M., Rajamäki, M.M., 2013. The Histopathology of Idiopathic Pulmonary Fibrosis in West Highland White Terriers Shares Features of Both Non-specific Interstitial Pneumonia and Usual Interstitial Pneumonia in Man. Journal of Comparative Pathology 149, 303–313. https://doi.org/10.1016/j.jcpa.2013.03.006

Testa, L.C., Jule, Y., Lundh, L., Bertotti, K., Merideth, M.A., O'Brien, K.J., Nathan, S.D., Venuto, D.C., El-Chemaly, S., Malicdan, M.C.V., Gochuico, B.R., 2021. Automated Digital Quantification of Pulmonary Fibrosis in Human Histopathology Specimens. Front Med (Lausanne) 8, 607720. https://doi.org/10.3389/fmed.2021.607720

Thierry, F., Handel, I., Hammond, G., King, L.G., Corcoran, B.M., Schwarz, T., 2017. Further characterization of computed tomographic and clinical features for staging and prognosis of idiopathic pulmonary fibrosis in West Highland white terriers. Vet Radiol Ultrasound 58, 381–388. https://doi.org/10.1111/vru.12491

Tietscher, S., Wagner, J., Anzeneder, T., Langwieder, C., Rees, M., Sobottka, B., de Souza, N., Bodenmiller, B., 2023. A comprehensive single-cell map of T cell exhaustion-associated immune environments in human breast cancer. Nat Commun 14, 98. https://doi.org/10.1038/s41467-022-35238-w

Tillmanns, J., Hoffmann, D., Habbaba, Y., Schmitto, J.D., Sedding, D., Fraccarollo, D., Galuppo, P., Bauersachs, J., 2015. Fibroblast activation protein alpha expression identifies activated fibroblasts after myocardial infarction. Journal of Molecular and Cellular Cardiology 87, 194–203. https://doi.org/10.1016/j.yjmcc.2015.08.016

Tillmanns, J., Widera, C., Habbaba, Y., Galuppo, P., Kempf, T., Wollert, K.C., Bauersachs, J., 2013. Circulating concentrations of fibroblast activation protein α in apparently healthy individuals and patients with acute coronary syndrome as assessed by sandwich ELISA. International Journal of Cardiology 168, 3926–3931. https://doi.org/10.1016/j.ijcard.2013.06.061

Tomassetti, S., Gurioli, C., Ryu, J.H., Decker, P.A., Ravaglia, C., Tantalocco, P., Buccioli, M., Piciucchi, S., Sverzellati, N., Dubini, A., Gavelli, G., Chilosi, M., Poletti, V., 2015. The impact of lung cancer on survival of idiopathic pulmonary fibrosis. Chest 147, 157–164. https://doi.org/10.1378/chest.14-0359

Travaglini, K.J., Nabhan, A.N., Penland, L., Sinha, R., Gillich, A., Sit, R.V., Chang, S., Conley, S.D., Mori, Y., Seita, J., Berry, G.J., Shrager, J.B., Metzger, R.J., Kuo, C.S., Neff, N., Weissman, I.L., Quake, S.R., Krasnow, M.A., 2020. A molecular cell atlas of the human lung from single-cell RNA sequencing. Nature 587, 619–625. https://doi.org/10.1038/s41586-020-2922-4

Travis, W.D., Brambilla, E., Noguchi, M., Nicholson, A.G., Geisinger, K., Yatabe, Y., Ishikawa, Y., Wistuba, I., Flieder, D.B., Franklin, W., Gazdar, A., Hasleton, P.S., Henderson, D.W., Kerr, K.M., Petersen, I., Roggli, V., Thunnissen, E., Tsao, M., 2013. Diagnosis of lung cancer in small biopsies and cytology: implications of the 2011 International Association for the Study of Lung Cancer/American Thoracic Society/European Respiratory Society classification. Arch Pathol Lab Med 137, 668–684. https://doi.org/10.5858/arpa.2012-0263-RA

Travis, W.D., Brambilla, E., Noguchi, M., Nicholson, A.G., Geisinger, K.R., Yatabe, Y., Beer, D.G., Powell, C.A., Riely, G.J., Van Schil, P.E., Garg, K., Austin, J.H.M., Asamura, H., Rusch, V.W., Hirsch, F.R., Scagliotti, G., Mitsudomi, T., Huber, R.M., Ishikawa, Y., Jett, J., Sanchez-Cespedes, M., Sculier, J.-P., Takahashi, T., Tsuboi, M., Vansteenkiste, J., Wistuba, I., Yang, P.-C., Aberle, D., Brambilla, C., Flieder, D., Franklin, W., Gazdar, A., Gould, M., Hasleton, P., Henderson, D., Johnson, B., Johnson, D., Kerr, K., Kuriyama, K., Lee, J.S., Miller, V.A., Petersen, I., Roggli, V., Rosell, R., Saijo, N., Thunnissen, E., Tsao, M., Yankelewitz, D., 2011. International Association for the Study of Lung Cancer/American Thoracic Society/European Respiratory Society International Multidisciplinary Classification of Lung Adenocarcinoma. Journal of Thoracic Oncology 6, 244–285. https://doi.org/10.1097/JTO.0b013e318206a221

Treggiari, E., Romanelli, G., Valenti, P., Montinaro, V., Rossanese, M., 2025. Evaluation of lung lobectomy and adjuvant treatment for primary pulmonary carcinoma in dogs: 89 cases (2005-2022). J Small Anim Pract. https://doi.org/10.1111/jsap.13874

Tsukui, T., Sun, K.-H., Wetter, J.B., Wilson-Kanamori, J.R., Hazelwood, L.A., Henderson, N.C., Adams, T.S., Schupp, J.C., Poli, S.D., Rosas, I.O., Kaminski, N., Matthay, M.A., Wolters, P.J., Sheppard, D., 2020. Collagen-producing lung cell atlas identifies multiple subsets with distinct localization and relevance to fibrosis. Nat Commun 11, 1920. https://doi.org/10.1038/s41467-020-15647-5

Uitte De Willige, S., Keane, F.M., Bowen, D.G., Malfliet, J.J.M.C., Zhang, H.E., Maneck, B., McCaughan, G.W., Leebeek, F.W.G., Rijken, D.C., Gorrell, M.D., 2017. Circulating fibroblast activation protein activity and antigen levels correlate strongly when measured in liver disease and coronary heart disease. PLoS ONE 12, e0178987. https://doi.org/10.1371/journal.pone.0178987

Vanneste, D., Bai, Q., Hasan, S., Peng, W., Pirottin, D., Schyns, J., Maréchal, P., Ruscitti, C., Meunier, M., Liu, Z., Legrand, C., Fievez, L., Ginhoux, F., Radermecker, C., Bureau, F., Marichal, T., 2023. MafB-restricted local monocyte proliferation precedes lung interstitial macrophage differentiation. Nat Immunol 24, 827–840. https://doi.org/10.1038/s41590-023-01468-3

Webb, J.A., Armstrong, J., 2002. Chronic idiopathic pulmonary fibrosis in a West Highland white terrier. Can Vet J 43, 703–705.

Wei, Y., Ma, L., Li, P., Lu, J., Ren, J., Yan, S., Wu, H., Yuan, S., Fu, Z., Yu, J., 2023. FAPI Compared with FDG PET/CT for Diagnosis of Primary and Metastatic Lung Cancer. Radiology 308, e222785. https://doi.org/10.1148/radiol.222785

Wei, Y., Zheng, J., Ma, L., Liu, X., Xu, S., Wang, S., Pei, J., Cheng, K., Yuan, S., Yu, J., 2022. [18F]AlF-NOTA-FAPI-04: FAP-targeting specificity, biodistribution, and PET/CT imaging of various cancers. Eur J Nucl Med Mol Imaging 49, 2761–2773. https://doi.org/10.1007/s00259-022-05758-0

Williams, K.H., Viera de Ribeiro, A.J., Prakoso, E., Veillard, A.S., Shackel, N.A., Bu, Y., Brooks, B., Cavanagh, E., Raleigh, J., McLennan, S.V., McCaughan, G.W., Bachovchin, W.W., Keane, F.M., Zekry, A., Twigg, S.M., Gorrell, M.D., 2015. Lower serum fibroblast activation protein shows promise in the exclusion of clinically significant liver fibrosis due to non-alcoholic fatty liver disease in diabetes and obesity. Diabetes Research and Clinical Practice 108, 466–472. https://doi.org/10.1016/j.diabres.2015.02.024

Williams, K.J., 2014. Gammaherpesviruses and pulmonary fibrosis: evidence from humans, horses, and rodents. Vet Pathol 51, 372–384. https://doi.org/10.1177/0300985814521838

Wilson, D.W., 2016. Tumors of the Respiratory Tract, in: Tumors in Domestic Animals. John Wiley & Sons, Ltd, pp. 467–498. https://doi.org/10.1002/9781119181200.ch12

Wood, E.F., O'Brien, R.T., Young, K.M., 1998. Ultrasound-Guided Fine-Needle Aspiration of Focal Parenchymal Lesions of the Lung in Dogs and Cats. Journal of Veterinary Internal Medicine 12, 338–342. https://doi.org/10.1111/j.1939-1676.1998.tb02132.x

Wormser, C., Singhal, S., Holt, D.E., Runge, J.J., 2014. Thoracoscopic-assisted pulmonary surgery for partial and complete lung lobectomy in dogs and cats: 11 cases (2008–2013). https://doi.org/10.2460/javma.245.9.1036

Wu, T., Hu, E., Xu, S., Chen, M., Guo, P., Dai, Z., Feng, T., Zhou, L., Tang, W., Zhan, L., Fu, X., Liu, S., Bo, X., Yu, G., 2021. clusterProfiler 4.0: A universal enrichment tool for interpreting omics data. The Innovation 2, 100141. https://doi.org/10.1016/j.xinn.2021.100141

Xia, L., Liu, Y., Wang, Y., 2019. PD-1/PD-L1 Blockade Therapy in Advanced Non-Small-Cell Lung Cancer: Current Status and Future Directions. Oncologist 24, S31–S41. https://doi.org/10.1634/theoncologist.2019-IO-S1-s05

Xie, T., Wang, Y., Deng, N., Huang, G., Taghavifar, F., Geng, Y., Liu, N., Kulur, V., Yao, C., Chen, P., Liu, Z., Stripp, B., Tang, J., Liang, J., Noble, P.W., Jiang, D., 2018. Single-Cell Deconvolution of Fibroblast Heterogeneity in Mouse Pulmonary Fibrosis. Cell Reports 22, 3625–3640. https://doi.org/10.1016/j.celrep.2018.03.010

Xu, W., Cai, J., Peng, T., Meng, T., Pang, Y., Sun, L., Wu, H., Zhang, J., Chen, X., Chen, H., 2024. Fibroblast Activation Protein–Targeted PET/CT with 18F-Fibroblast Activation Protein Inhibitor-74 for Evaluation of Gastrointestinal Cancer: Comparison with 18F-FDG PET/CT. Journal of Nuclear Medicine 65, 40–51. https://doi.org/10.2967/jnumed.123.266329

Yamazaki, H., Tanaka, T., Mie, K., Nishida, H., Miura, N., Akiyoshi, H., 2020. Assessment of postoperative adjuvant treatment using toceranib phosphate against adenocarcinoma in dogs. J Vet Intern Med 34, 1272–1281. https://doi.org/10.1111/jvim.15768

Yan, Z., Hu, X., Tang, B., Deng, F., 2023. Role of osteopontin in cancer development and treatment. Heliyon 9, e21055. https://doi.org/10.1016/j.heliyon.2023.e21055

Yang, J., Liu, K., Yang, L., Ji, J., Qin, J., Deng, H., Wang, Z., 2023. Identification and validation of a novel cuproptosis-related stemness signature to predict prognosis and immune landscape in lung adenocarcinoma by integrating single-cell and bulk RNA-sequencing. Front Immunol 14, 1174762. https://doi.org/10.3389/fimmu.2023.1174762

Yang, L., Herrera, J., Gilbertsen, A., Xia, H., Smith, K., Benyumov, A., Bitterman, P.B., Henke, C.A., 2018. IL-8 mediates idiopathic pulmonary fibrosis mesenchymal progenitor cell fibrogenicity. Am J Physiol Lung Cell Mol Physiol 314, L127–L136. https://doi.org/10.1152/ajplung.00200.2017

Yang, P., Luo, Q., Wang, X., Fang, Q., Fu, Z., Li, Jia, Lai, Y., Chen, X., Xu, X., Peng, X., Hu, K., Nie, X., Liu, S., Zhang, J., Li, Junqi, Shen, C., Gu, Y., Liu, J., Chen, J., Zhong, N., Su, J., 2023. Comprehensive Analysis of Fibroblast Activation Protein Expression in Interstitial Lung Diseases. Am J Respir Crit Care Med 207, 160–172. https://doi.org/10.1164/rccm.202110-2414OC

Yokota, S., Kaji, K., Yonezawa, T., Momoi, Y., Maeda, S., 2023. $CD204^{+}$ tumor-associated macrophages are associated with clinical outcome in canine pulmonary adenocarcinoma and transitional cell carcinoma. Vet J 296–297, 105992. https://doi.org/10.1016/j.tvjl.2023.105992

Yoshimoto, S., Chester, N., Xiong, A., Radaelli, E., Wang, H., Brillantes, M., Gulendran, G., Glassman, P., Siegel, D.L., Mason, N.J., 2023. Development and pharmacokinetic assessment of a fully canine anti-PD-1 monoclonal antibody for comparative translational research in dogs with spontaneous tumors. MAbs 15, 2287250. https://doi.org/10.1080/19420862.2023.2287250

Yoshimoto, S., Kato, D., Kamoto, S., Yamamoto, K., Tsuboi, M., Shinada, M., Ikeda, N., Tanaka, Y., Yoshitake, R., Eto, S., Saeki, K., Chambers, J., Hashimoto, Y., Uchida, K., Nishimura, R., Nakagawa, T., 2020. Overexpression of human epidermal growth factor receptor 2 in canine primary lung cancer. Journal of Veterinary Medical Science 82, 804–808. https://doi.org/10.1292/jvms.20-0026

Zappia, L., Oshlack, A., 2018. Clustering trees: a visualization for evaluating clusterings at multiple resolutions. GigaScience 7, giy083. https://doi.org/10.1093/gigascience/giy083

Zekas, L.J., Crawford, J.T., O'Brien, R.T., 2005. Computed Tomography-Guided Fine-Needle Aspirate and Tissue-Core Biopsy of Intrathoracic Lesions in Thirty Dogs and Cats. Veterinary Radiology & Ultrasound 46, 200–204. https://doi.org/10.1111/j.1740-8261.2005.00043.x

Zhang, Y., Du, W., Chen, Z., Xiang, C., 2017. Upregulation of PD-L1 by SPP1 mediates macrophage polarization and facilitates immune escape in lung adenocarcinoma. Exp Cell Res 359, 449–457. https://doi.org/10.1016/j.yexcr.2017.08.028

Zhen, E.Y., Jin, Z., Ackermann, B.L., Thomas, M.K., Gutierrez, J.A., 2016. Circulating FGF21 proteolytic processing mediated by fibroblast activation protein. Biochemical Journal 473, 605–614. https://doi.org/10.1042/BJ20151085

Zheng, G.X.Y., Terry, J.M., Belgrader, P., Ryvkin, P., Bent, Z.W., Wilson, R., Ziraldo, S.B., Wheeler, T.D., McDermott, G.P., Zhu, J., Gregory, M.T., Shuga, J., Montesclaros, L., Underwood, J.G., Masquelier, D.A., Nishimura, S.Y., Schnall-Levin, M., Wyatt, P.W., Hindson, C.M., Bharadwaj, R., Wong, A., Ness, K.D., Beppu, L.W., Deeg, H.J., McFarland, C., Loeb, K.R., Valente, W.J., Ericson, N.G., Stevens, E.A., Radich, J.P., Mikkelsen, T.S., Hindson, B.J., Bielas, J.H., 2017. Massively parallel digital transcriptional profiling of single cells. Nat Commun 8, 14049. https://doi.org/10.1038/ncomms14049

Zilionis, R., Engblom, C., Pfirschke, C., Savova, V., Zemmour, D., Saatcioglu, H.D., Krishnan, I., Maroni, G., Meyerovitz, C.V., Kerwin, C.M., Choi, S., Richards, W.G., De Rienzo, A., Tenen, D.G., Bueno, R., Levantini, E., Pittet, M.J., Klein, A.M., 2019. Single-Cell Transcriptomics of Human and Mouse Lung Cancers Reveals Conserved Myeloid Populations across Individuals and Species. Immunity 50, 1317-1334.e10. https://doi.org/10.1016/j.immuni.2019.03.009

Presses de la Faculté de Médecine vétérinaire de l'Université de Liège

4000 Liège (Belgique)

D/2025/0480/11

ISBN 978-2-87543-239-1